Modelling the stratospheric residual circulation under historical and future climates

Andreas Chrysanthou

School of Earth and Environment

University of Leeds

A thesis submitted for the degree of

Doctor of Philosophy

September 2020

Declaration

I confirm that the work submitted in this thesis is my own, except where work which has formed part of jointly-authored publications has been included. My contributions to jointly-authored papers and that of the other authors is explicitly indicated below. I confirm also that appropriate credit has been given within this thesis where reference has been made to the work of others.

The majority of the research included in the thesis, in Chapters 2 and 3, has been peer-reviewed and published. The remaining research in Chapter 4 has been prepared for submission to a peer-reviewed journal. This thesis is published using the University of Leeds alternative thesis format, which allows the research within it to be readily identified and accessed.

Chapter 2 has been published as the following:

Chrysanthou, A., Maycock, A. C., Chipperfield, M. P., Dhomse, S., Garny, H., Kinnison, D., Akiyoshi, H., Deushi, M., Garcia, R. R., Jöckel, P., Kirner, O., Pitari, G., Plummer, D. A., Revell, L., Rozanov, E., Stenke, A., Tanaka, T. Y., Visioni, D., & Yamashita, Y. (2019). The effect of atmospheric nudging on the stratospheric residual circulation in chemistry-climate models. *Atmospheric Chemistry and Physics*, 19(17), 11559-11586. https://doi.org/10.5194/acp-19-11559-2019

The author contributions to this work are:

I performed the analysis and wrote the article. Amanda C. Maycock and Martyn P. Chipperfield designed the study and made substantial contributions to the interpretation of the data. Moreover, they participated in drafting and revising the paper. Hella Garny provided the correctly calculated EMAC data, and Sandip Dhomse contributed to the discussion of the content. Andrea Stenke provided the SOCOL REF-C1SD data. The other coauthors contributed information pertaining to their individual models and helped edit the paper.

Chapter 3 has been published as the following:

Chrysanthou, A., Maycock, A. C., & Chipperfield, M. P. (2020). Decomposing the response of the stratospheric Brewer-Dobson circulation to an abrupt quadrupling in CO_2. *Weather and Climate Dynamics*, 1(1), 155-174. https://doi.org/10.5194/wcd-1-155-2020

The author contributions to this work are:

I and Amanda C. Maycock designed the study. I ran the model simulations and analysed the data. I and Amanda C. Maycock interpreted the data and wrote the article with input from Martyn P. Chipperfield.

The work in **Chapter 4** of the thesis is prepared as a manuscript to be submitted in *Atmospheric Science Letters* as follows: Chrysanthou, A.; Maycock, A. C., & Chipperfield, M. P. . The utility of indirect measures of the stratospheric residual circulation.

The author contributions to this work are:

I and Amanda C. Maycock designed the study. I processed and analysed the data and wrote the first draft of the article. I and Amanda C. Maycock interpreted the data. Amanda C. Maycock made substantial contributions in editing the article with input from Martyn P. Chipperfield.

Acknowledgements

First and foremost, a massive thank you to my supervisors: Amanda Maycock and Martyn Chipperfield, for all your guidance and support over the past four years. Your ethos (*ήθος*) as human beings and scientists has taught me a lot. Thank you for encouraging and pushing me over the line at times when some doubts started to creep in. Thank you both for showing me the way robust research should be conducted and the benefits of a meticulous approach in science. Amanda, thank you for showing me that if you work hard enough, you can achieve pretty much everything you set out to do. Thank you for introducing me to the stratospheric community, priming me to be involved in international projects and for providing financial support beyond my scholarship funding. Martyn, thank you for being so insightful with my work, your eagerness to give advice on PhD-related issues as well as my personal development. It was a pleasure being part of your group, albeit always late by five minutes. You both welcomed me to Leeds and now Leeds feels like extended family. I hope I can repay you both sometime (probably with Greek cheese, olives and honey).

I would like to thank all my office mates both at SEE building and Priestley Centre, especially to Giannis for all the office discussions. A special thank you to Richard Rigby for supporting me on various technical issues throughout my time in Leeds. Chris Smith, thanks for guiding me in setting up my HadGEM3 simulations. I would also like to thank my colleagues in both Physical Climate Change and Atmospheric Chemistry groups for their feedback over the past years. Paloma, Sandip and Wuhu thanks for being my smoking buddies, a very unhealthy but welcome (at the time) break. An extra special thank you to my Leeds friends over the past years. Allan, thanks for being such a good friend in a such a short space of time, we got

to know Leeds together. Adriano, thanks for always winding me up to play football together and drink on every occasion, I really wonder how managed to finish your PhD. Alex, a YNWA will not suffice. Thanks for always coming round to watch the Mighty Reds no matter the weather, for all the beers, food and the interesting chats. Manolis, I really miss our κουτσομπολιό accompanied by coffee every single day before leaving for Uni. Thanks also to Dimitra and Luis, I really enjoyed all the food and chats we had together.

Thank you to my Greek friends Μαρία and Χάρη, for being there on every occasion, good or bad, being my gig mates over the past four years, hosting me at every opportunity and taking my mind away from the PhD with whisky drinking. Special thanks for their remote support over the years to my oldest and closest group of friends Άιλς, Κόβα και Μάρκ as well as to Θανάση, Μιχάλη, Παναγιώτη, Στάυρο, Στέφανο, Χρυσάνθη και Χρήστο. A massive thanks to Μίτς (Lord Gegen) as well as to Αργύρη (High Gegen) for all the venting alongside gegen throughout the years, this might be the reason I am still sane. A huge thank you to Έλενα for her love and support during my PhD, you were always caring, understanding and easing my mind; your help has been invaluable.

Τέλος, θα ήθελα να ευχαριστήσω την οικογένεια μου για την συνεισφορά τους στο πως έχω εξελιχθεί ως άνθρωπος και πιο συγκεκριμμένα, την μητέρα μου Μερόπη, τον πατέρα μου Κώστα, τα αδέρφια μου Άκη και Αργύρη, τα ξάδερφια μου Λεωνίδα και Φρόσω, τον θείο μου Μανώλη και την θεία μου Μαίρη. Δεν θα μπορούσα να τα καταφέρω χωρίς εσάς.

Abstract

This thesis deals with the advective part of the global Brewer-Dobson circulation (BDC), also known as the stratospheric residual circulation. The residual circulation cannot be directly measured and is relatively poorly constrained in observations and models. While the processes that drive the residual circulation are relatively well understood, our knowledge of how these processes can manifest in response to an evolving climate state is insufficient. This research addresses several topics related to the representation of the stratospheric residual circulation in models under historical and future climates. The residual circulation is evaluated in a suite of "specified dynamics or nudged" chemistry-climate simulations relaxed towards reanalysis data. It is found that nudging does not constrain the mean strength of the residual circulation while it does tightly constrain the interannual variability in the lower stratosphere. To investigate climate change effects on the residual circulation, model simulations are performed using a $4\times CO_2$ experiment separated into three components: a rapid adjustment due to the radiative effects of CO_2; a global mean sea surface temperature (SST) response; and the local deviations of SST from the global mean. It is shown that the global SST explains most of the increased in circulation in the lower stratosphere, while both the rapid adjustment and global SST are important in the upper stratosphere. This means there are two characteristic timescales in the response of the residual circulation to increased CO_2, with the relative importance of each timescale being height dependent. Lastly, the utility of different observational-based indirect proxy measures for the residual circulation in the tropical lower stratosphere are evaluated within a chemistry-climate model framework. It is shown that a temperature-based measure captures variability in the residual circulation on interannual timescales, whereas tropical mean ozone concentrations, when lagged, exhibit a close out-of-phase relationship with tropical upwelling across seasonal, interannual and multi-decadal timescales. Overall, this work has progressed our understanding pertaining to mechanistic and diagnostic processes related to the stratospheric residual circulation in numerical simulations.

Abbreviations

ACCMIP	Atmospheric Chemistry and Climate Model Intercomparison Project
AoA	Age of Air
BDC	Brewer-Dobson circulation
CCM	Chemistry climate model
CCMI	Chemistry Climate Model Initiative
CCMVal	Chemistry Climate Model Validation activity
CFCs	Chlorofluorocarbons
CMIP	Coupled Model Intercomparison Project
CO_2	Carbon dioxide
CTM	Chemical transport model
EESC	Equivalent effective stratospheric chlorine
ENSO	El Niño Southern Oscillation
GCM	General circulation model
GHGs	Greenhouse gases
GSAT	Global surface air temperature
O	Oxygen atom
O_2	Molecular oxygen
O_3	Ozone
ODSs	Ozone depleting substances
QBO	Quasi-Biennial Oscillation
RCP	Representative Concentration Pathway
SAD	Surface area density
SF_6	Sulphur hexafluoride
SIC	Sea ice concentration
SPARC	Stratosphere-troposphere Processes And their Role in Climate
SST	Sea surface temperature
STE	Stratosphere-troposphere exchange
TTL	Tropical tropopause layer
UNFCCC	United Nations Framework Convention on Climate Change
UTLS	Upper troposphere/lower stratosphere
UV	Ultraviolet
WCRP	World Climate Research Programme
WMO	World Meteorological Organisation

Contents

List of Figures

List of Tables

Chapter 1

Introduction

1.1 Atmosphere in layers

Earth's atmosphere can be partitioned into different layers broadly characterised by the vertical profile of temperature, which leads to distinct physical and dynamical properties of each layer. Starting from the surface, the lowest layer is the troposphere which spans up to around 10 km where the temperature decreases with height at an average rate of ~ 6.5 K km^{-1}. Separated by a thin transitional layer called the tropopause with a lapse rate of ~ 2 K km^{-1}, the stratosphere extends from around 10 km to around 50 km, exhibiting increasing temperatures with height hence explaining its strong stratification. Above this lies the mesosphere between $50 - 80$ km, where the temperature again decreases with height, and the thermosphere between 80 and ~ 500 km where temperature increases dramatically with height due to the fact that molecular processes dominate over eddy mixing in this region. Together the stratosphere and mesosphere are often referred to as the "middle atmosphere" (Andrews et al., 1987).

In the troposphere, latent heating processes associated with phase changes of water and cloud radiative effects have a presiding role, particularly in the tropics associated with moist convection, while in the extratropics baroclinic eddies are a dominant feature of the general circulation. These processes mean that in the troposphere the vertical advection of air typically occurs on timescales of hours to days. In contrast, the stratosphere is very dry owing to the freeze-drying of the air as it ascends through the cold tropical tropopause layer, as deduced from observations as early as the late 1940s

(Brewer, 1949). The stratospheric temperature distribution is strongly modulated by ozone, which is photochemically produced in the middle stratosphere (∼35 km) and absorbs incoming solar ultraviolet (UV) radiation, underscoring its importance as the major contributor to the radiative heat input throughout the depth of stratosphere and mesosphere (Kiehl and Solomon, 1986). The strong stable stratification of the stratosphere means that parcels of air are transported upwards with timescales that range from months to years (Holton et al., 1995). Although the global mean temperature distribution of the stratosphere can be mainly explained in terms of radiative heating and cooling processes (Andrews et al., 1987), dynamical processes regulate local temperatures via adiabatic heating and cooling.

Despite their distinct physical characteristics, the troposphere and stratosphere are intricately entangled through dynamical, radiative and chemical processes. For example: a) stratospheric ozone affects the tropospheric chemical balance through stratosphere-troposphere exchange (STE; Holton et al., 1995); b) stratospheric composition affects the radiative balance of the troposphere via ozone (e.g. Ramaswamy et al., 1992; Forster and Shine, 1997) and water vapour (e.g. Forster and Shine, 1999, 2002) radiative effects; and c) dynamical coupling operates in both directions, with the troposphere being the source of planetary Rossby waves and gravity waves that drive the stratospheric circulation (see Section 1.2.2), and stratospheric conditions affecting tropospheric weather and climate (Haynes, 2005) e.g., via coupling with the dominant modes of variability in the troposphere, the Southern Hemisphere and Northern Hemisphere annular modes (Thompson and Wallace, 2000).

1.2 The Brewer-Dobson circulation

1.2.1 Historical overview

The physical concept that broadly describes the stratospheric mean mass transport was first proposed independently by Dobson and Brewer in order to explain the observed ozone (Dobson et al., 1929; Dobson, 1956) and water vapour (Brewer, 1949) distributions in the stratosphere. Although at the time a theoretical explanation was lacking, they suggested a model for the global circulation that entails air originating in the troposphere, ascending into the stratosphere in the tropics, and subsequently moving upward

and poleward before descending back into the troposphere at extratropical latitudes. Further stratospheric transport studies based on atmospheric nuclear tests in the late 1950s conducted by the USA, USSR and UK (e.g. Telegadas, 1967, 1971; Telegadas et al., 1972; Kinnison et al., 1994) corroborated the theory that the radioactive tracers would follow the global mass circulation. Moreover, the transport characteristics of the radioactive fallout, as well as aerosols from tropical volcanic eruptions (Dyer and Hicks, 1968), provided evidence of the existence of subtropical transport barriers due to the persistence of their tropical maxima. The proposed concept based on tracer transport into and out of the stratosphere agreed quantitatively with the estimate of a diabatic stratospheric meridional circulation, which indicated ascent at the tropical tropopause and descent across the extratropical tropopause along with mesospheric meridional flow (Murgatroyd and Singleton, 1961). However, Murgatroyd and Singleton (1961) also found that since they had neglected eddy processes, their model did not conserve angular momentum, highlighting the importance of accounting for eddy forces within the mean meridional circulation. In an effort to account for the missing eddy forcing, Vincent (1968) utilised the Eulerian-mean approach and deduced that two circulation cells are at play instead of a single hemispheric cell suggested by previous studies, with a reverse cell that had rising motion in the polar latitudes and descending motion in the middle latitudes.

The physical inconsistency of the two-cell Eulerian mean circulation (Vincent, 1968) with the observed mass transport circulation, was almost equally insufficient with the diabatic circulation that which had better agreement with the observed mass transport but lacked conservation of angular momentum (Murgatroyd and Singleton, 1961). Rectifying these discrepancies was only made possible by using the generalised Lagrangian mean formulation (Andrews and McIntyre, 1978a) along with the theoretical advances under the transformed Eulerian mean (TEM) framework by Andrews and McIntyre (1976, 1978b). The principal notion of a dynamically-consistent definition of the Brewer-Dobson circulation (BDC) was first derived by Dunkerton (1978) and is the same theoretical framework that is now widely used to define the mean meridional circulation (Plumb, 2002). Kida (1983) later confirmed this picture by studying the trajectories of advected air parcels. The underlying mechanisms that force the BDC through extratropical wave driving and breaking in the stratosphere create a mid-latitude "surf-zone"

(McIntyre and Palmer, 1984) due to the existence of an "extratropical pump" (Holton et al., 1995). These mechanisms were unravelled through the formulation of the "downward control principle" (Haynes and McIntyre, 1987; Haynes et al., 1991) built on the TEM approaches of Andrews and McIntyre (1976, 1978b). Different types of waves contribute to driving the mean meridional circulation of the middle atmosphere, with synoptic scale waves reaching the lowermost stratosphere, planetary-scale Rossby waves penetrating higher into the winter hemisphere stratosphere, and gravity waves driving the circulation higher up in the mesosphere (Plumb, 2002), as shown in Figure 1.1.

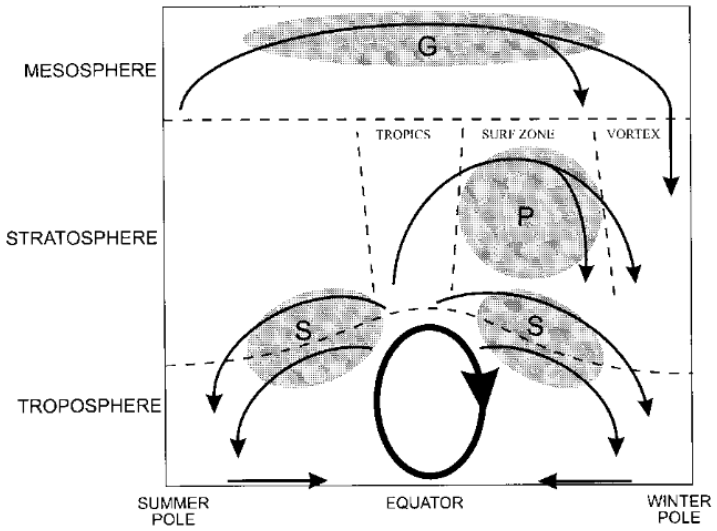

Figure 1.1: Illustration of the mean meridional circulation in the atmosphere. The tropical Hadley cell of the circulation in the troposphere is shown by the thick ellipse in black. The synoptic- (S), planetary-scale (P) and gravity (G) wave driving regions that force the mean meridional circulation in the stratosphere and mesosphere are shown by the shaded areas. Taken from Plumb (2002).

More recently, Birner and Bönisch (2011) and Bönisch et al. (2011) deduced that the BDC can be separated into two different branches, the shallow and the deep, which have their own distinct characteristics. In the lower stratosphere, ascending air in the tropics and descending air in the subtropical and middle latitudes constitutes the shallow branch, while the deep branch entails ascending air that extends upwards into the upper stratosphere with descending branches that reach into the high latitudes, shown

schematically in Figure 1.2. A model study of the residual circulation transit times (RCTT; the time taken for an air parcel that enters into the stratosphere through the tropical tropopause to reach a given location) between the two branches of the BDC revealed that a differentiating factor is the longer transit times characterising the deep branch along with lower amounts of mass flux reaching those heights (Birner and Bönisch, 2011). As different types of waves propagate into different parts of the stratosphere (Fig. 1.1) depositing their momentum and altering the flow, it follows that different types of waves force the shallow and deep branches of the BDC (see Section 1.2.2).

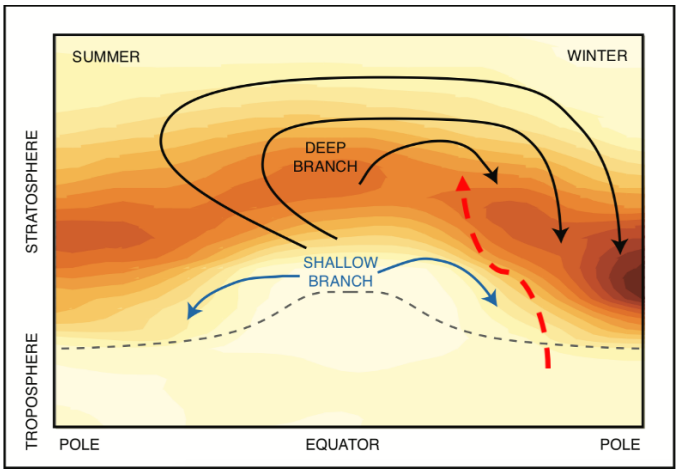

Figure 1.2: Latitude-height cross-section of the atmosphere showing ozone density based on the Northern hemisphere wintertime climatology (colour shading, with darker shades indicating larger ozone concentrations). The arrow streamlines depict the different spatial characteristics of the shallow and deep branches of the Brewer-Dobson circulation at solstices. The dashed line indicates the approximate location of the tropopause and the red dashed arrow represents planetary wave activity propagating into the stratosphere. Adapted from Figure 4-7 in WMO (2014).

In addition to the advective part of the BDC (defined as the zonal-mean residual circulation) considered so far, to fully describe the stratospheric transport circulation the component of the two-way exchange of air masses needs to be accounted for as well. The breaking of planetary waves in the stratosphere leads to quasi-horizontal mixing as the

air masses are stirred over thousands of kilometres (McIntyre and Palmer, 1984) with a rapid rate compared to the slow advective component of the BDC (Plumb, 2007). The diagnostic of mean age of stratospheric air (AoA) captures the combined effects of the advective part of the BDC and mixing on stratospheric tracer transport. It is defined as the time that has elapsed since a parcel of air entered the stratosphere through the tropical tropopause at a given location (Kida, 1983; Hall and Plumb, 1994; Waugh and Hall, 2002). It can be indirectly inferred from observations of long-lived quasi-passive tracers with an approximately constant atmospheric growth rate (including sources and sinks) corrected for non-linearities such as SF_6 and CO_2, among others. Theoretical model studies of this idealised tracer such as the "tropical-leaky pipe" conceptual model by Neu and Plumb (1999), revealed that two-way mixing between the tropics and extratropics has a global impact on AoA leading to a net increase. Since both the advective part of the BDC and mixing processes are incorporated by definition into this measure, AoA can be separated into the RCTT (Birner and Bönisch, 2011) that quantifies the residual circulation and the ageing by mixing (Garny et al., 2014), as presented in Figure 1.3.

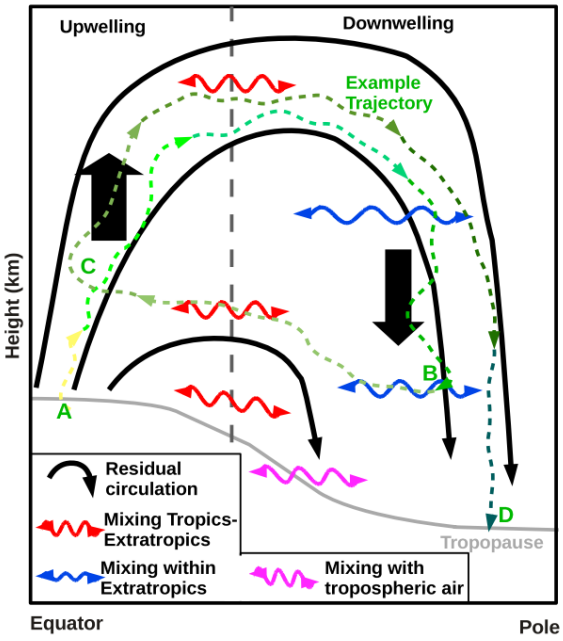

Figure 1.3: Illustration of the advective and mixing transport processes in the stratosphere. Taken from Garny et al. (2014).

Investigation of these combined effects highlight the areas where the overturning residual circulation dominates and regions where quasi-isentropic mixing has a substantial contribution via re-circulation of air parcels, resulting in an increase of AoA throughout the depth of the stratosphere (Garny et al., 2014; WMO, 2018) (Fig. 1.3). As this thesis focuses on the advective part of the BDC, the literature review that follows omits a comprehensive consideration of studies that analyse AoA where the effects of mixing and stirring are included, except when discussing observational evidence for past changes in the BDC.

1.2.2 Driving mechanisms

The residual circulation in the stratosphere is often termed the "extratropical pump" (Holton et al., 1995) or "Rossby-wave" pump (Plumb, 2002). The stratosphere is forced away from radiative equilibrium via the effects of upward-propagating planetary-scale Rossby waves emanating from the troposphere which amplify and break, dissipating their momentum and energy into the stratosphere. In the winter extratropical stratosphere where solar heating is absent, the temperature gradient is equatorward (cold pole) forcing a strong westerly flow in the extratropics and around the pole (polar vortex), an essential characteristic that allows for planetary-scale Rossby wave propagation (Charney and Drazin, 1961). As the zonal phase speed of planetary-scale Rossby waves can only be westward, their deposited wave drag with respect to the wave-mean flow can only be westward (easterly). The westward drag is partly balanced by the Coriolis force through an one-way pump that acts to draw air poleward (due to the Earth's rotation) in order to conserve angular momentum, known as "gyroscopic pumping" (McIntyre, 1998), accounting for the ever-present poleward mass flow in the middle and upper winter stratosphere. Subsequently, for the steady-state limit, this poleward flow is compensated by tropical air drawn up into the stratosphere and pushed down at extratropical latitudes into the troposphere to close the circulation through mass continuity.

As shown in Section 1.2.1, the differentiation between the shallow and the deep branch of the BDC (Birner and Bönisch, 2011) reveals distinct characteristics of the wave driving that influences the two branches. In the shallow branch in the subtropical lowermost stratosphere, synoptic-scale wave driving dominates throughout the year (Fig. 1.1)

while in the deep branch, planetary-scale waves drive the wintertime circulation. The marked differences of the mesospheric component of the BDC manifested as a single cell with flow from the summer to the winter pole (Fig. 1.1) are due to the effect of upward-propagating gravity waves, selectively filtered by stratospheric winds causing an eastward (westward) drag and an equatorward (poleward) pumping in the summer (winter) hemisphere Plumb (2002).

In addition to the important role of extratropical wave forcing, the literature has also addressed whether tropical wave forcing can have a significant impact in driving the residual circulation (e.g., Plumb and Eluszkiewicz, 1999). Multiple studies have investigated the potential mechanisms associated with the tropical wave forcing contributing to driving the BDC (e.g. Semeniuk and Shepherd, 2001; Boehm and Lee, 2003; Kerr-Munslow and Norton, 2006; Randel et al., 2008; Calvo and Garcia, 2009; Garny et al., 2011). Randel et al. (2008) found that the tropical wave forcing is both due to an equatorward propagation of extratropical waves as well as latent heat generated tropical planetary waves associated with deep convection processes (Gill, 1980). On the other hand, Calvo and Garcia (2009) pinpointed tropical quasi-stationary waves as the dominant cause of the tropical wave forcing in the upper troposphere and lower stratosphere. Moreover, the tropical wave forcing has been shown to be due to both extratropical transient synoptic-scale waves refracted equatorward and tropical stationary planetary waves in Garny et al. (2011). However, there is no consensus regarding the underlying mechanism of the tropical wave forcing due to the notoriously difficult task of disentangling a cause and effect relationship between zonal winds modulated by wave dissipation (Andrews et al., 1987) in the deep tropics.

There is a strong seasonality in the strength of the BDC that is related to the hemispheric and height-dependent asymmetry in the two branches of the circulation (Rosenlof, 1995). Due to the asymmetries in the land-sea distribution between hemispheres, stronger planetary wave forcing during Northern hemisphere (NH) winter drives a stronger circulation in December, January, February (DJF) than in June, July, August (JJA) during Southern hemisphere (SH) winter (Rosenlof, 1995). Furthermore, the seasonal cycle is also reflected in the boundaries between the regions of tropical upwelling and extratropical downwelling termed as “turnaround latitudes” (Rosenlof,

1995), as their position follows the seasonal movement of the circulation cells.

In the tropics, the picture is somewhat more complex as the wave forcing alone cannot account for the characteristics of the BDC as seen by the observed upwelling rates in this region (e.g. upwelling maximum in summer side of the equator; Plumb and Eluszkiewicz, 1999). In order to untangle this apparent discrepancy, the diabatic heating processes need to be taken into account since they force a strong seasonal cycle in the tropical lower stratospheric upwelling (Plumb and Eluszkiewicz, 1999). The role of diabatic heating for the residual circulation in the tropics has been also considered in the context of the latitudinal distribution of the time-averaged upwelling in the tropical lower stratosphere. Specifically, the double-peaked structure in upwelling with maxima $\sim \pm 20^{\circ}$ may be considered as being forced by the distribution of radiative heating associated with ozone and water vapour, with the wave forcing adjusting to the imposed heating to maintain angular momentum conservation (Ming et al., 2016). However, there are multiple implications and caveats when considering the complex interplay between wave forcing changes on the mean flow and a potential partly thermally driven circulation in the deep tropics as discussed by Haynes (2005).

1.2.3 Diagnostics and mathematical formulations

The effort to address the discrepancies between the diabatic and Eulerian-mean circulations associated with the eddy transport introducing the Stokes drift (Dunkerton, 1978) feeding back to the mean transport, was key in the transformation of the Eulerian-mean equations to the TEM framework (Andrews and McIntyre, 1976, 1978b). Consequently, the TEM formulation incorporates the eddy and mean transport contributions into an approximated single quantity that can be applied in a wide range of circumstances (Butchart, 2014). The meridional and vertical components of the residual circulation ($\overline{v}^*$, $\overline{w}^*$) in the TEM framework are given in equations 1.1 and 1.2:

$$\overline{v}^* = -\frac{1}{\rho_0 \alpha \cos\phi} \frac{\partial \overline{\Psi}^*}{\partial z} \tag{1.1}$$

$$\overline{w}^* = \frac{1}{\rho_0 \alpha \cos\phi} \frac{\partial \overline{\Psi}^*}{\partial \phi}, \tag{1.2}$$

where z is the log-pressure height, $\overline{\Psi}^*(\phi, z)$ is the residual meridional mass streamfunction, ρ_0 is log-pressure density, α is Earth's radius, and ϕ is latitude.

The "downward control principle" (DCP) formulated by Haynes et al. (1991) based on the TEM framework (Andrews and McIntyre, 1976, 1978b), is often employed to quantify the wave driving of the BDC. A major advantage of using the DCP is that a measure of the mass flow can be deduced entirely by determining the remote zonal-mean forcing $\overline{F}$ that acts above a given height z over a sufficiently long timescales and large horizontal scales (steady-state assumption; e.g. seasonal mean Rosenlof, 1995). In the quasi-geostrophic limit, $\overline{m}_\phi \approx -2\Omega\alpha^2 \sin\phi\cos\phi$, the DCP formulation for the residual circulation is given via equation 1.3:

$$\overline{w}^*(\phi, z) = \frac{1}{\rho_0 \cos\phi} \frac{\partial}{\partial\phi} \int_z^\infty \left\{ \frac{\rho_0 \alpha^2 \overline{F} \cos^2\phi}{\overline{m}_\phi} \right\}_{\phi=\phi(z')} dz', \tag{1.3}$$

It should be noted that this formulation holds along lines of constant angular momentum ($\overline{m} = \alpha\cos\phi(\overline{u} + \alpha\Omega\cos\phi)$ where $\overline{u}$ is the zonal mean zonal wind and Ω is Earth's rotation rate), which in the extratropics can be approximated as lines of constant latitude, but this breaks down in the deep tropics ($< \pm 15°$) where angular momentum surfaces are curved, hence for simplicity this approach is usually applied in the extratropics. Nevertheless, through mass continuity the DCP can be straightforwardly applied to infer the total tropical upward mass flux across a pressure surface as the sum of the extratropical downward mass flux in each hemisphere (Rosenlof and Holton, 1993; Rosenlof, 1995), without needing to compute the residual vertical velocity $\overline{w}^*$ within the deep tropics. In climate models, $\overline{F}$ has contributions from explicitly resolved planetary and synoptic-scale Rossby waves and from sub-grid parameterised gravity waves that originate from orographic sources, convection and frontal instabilities (non-orographic).

Evaluation of the the residual circulation in general circulation models (GCMs) and chemistry-climate models (CCMs) commonly employs the TEM formulation as it can be straightforwardly calculated using model fields (e.g. SPARC, 2010; Butchart and

Scaife, 2001; Butchart et al., 2006, 2010, 2011; Hardiman et al., 2014). Apart from the implementation of the DCP to partition the contribution of the different components of the wave forcing in modelling studies, Rosenlof (1995); Rosenlof and Holton (1993) established the use of the net upward mass flux across a given pressure level and this has become a widely used benchmark metric to quantify the strength of the residual circulation (Butchart, 2014).

1.3 Diagnosing the residual circulation

1.3.1 Age of air and distinguishing effects of mixing

Different observational estimates of AoA diagnostics from satellite (Mahieu et al., 2014) and Lagrangian models driven by reanalysis studies (e.g. Ploeger et al., 2015a,b; Ploeger and Birner, 2016), as well as observationally constrained estimates of the meridional overturning diabatic circulation (more closely related to the residual circulation) (e.g. Linz et al., 2017, 2019), can also provide a measure of the overall strength of the mass transport in the stratosphere. However, as AoA can only be quantified through long-lived tracer measurements based on certain assumptions and approximations, the effects of mixing and the residual circulation are entangled (see Fig. 1.3) and cannot be separated in a straightforward way. Deriving observationally-based BDC trends through AoA has an inherent uncertainty due to the limited observations across spatial and temporal scales (e.g. Garcia et al., 2011) as well as the large internal variability (e.g. Hardiman et al., 2017b). Recently, Engel et al. (2017) updated the results of Engel et al. (2009) which, based on balloon measurements, reported a small increase of AoA in the NH mid-latitudes between 1985 and 2005, albeit not statistically significant, consistent with those derived by different observational datasets in Stiller et al. (2012) and Haenel et al. (2015). Reconciling this finding with the modelled negative trends of AoA indicating a strengthening of the BDC (e.g. Waugh, 2009), motivated studies that derived long-term AoA trends by combining observations with a hierarchy of models (e.g. "tropical-leaky pipe"; Neu and Plumb, 1999) in order to address this discrepancy (e.g. Hegglin et al., 2014; Ray et al., 2014). Application of this method yielded successful results as the hybrid model-observations estimate (Ray et al., 2014) converged to the observations made by Engel et al. (2009) and corroborated by the more recently updated study Engel et al. (2017). Ray et al. (2014) results exhibited younger AoA in the lower

stratosphere consistent with enhanced tropical upwelling seen in modelling studies and older AoA with increasing height in the NH mid-latitudes where observations and models still exhibit significant discrepancies (Figure 5 – 9 in WMO, 2018). Offline Lagrangian transport models driven by reanalysis exhibit a decrease in AoA in the NH mid-latitude lower stratosphere associated with a strengthened residual circulation but older AoA in the high-latitude middle to upper stratosphere (Diallo et al., 2012). However, there are distinct structural (latitude and altitude dependent) differences in the behaviour of the slower residual circulation and the faster mixing processes making up the distribution of the mean AoA trends. The aforementioned differences can be attributed to the net effect of ageing by mixing processes both in comprehensive climate models (Garny et al., 2014) and reanalysis-driven transport models (Ploeger et al., 2015a). Hence, this issue goes beyond the scope of this PhD thesis and will not be discussed further.

1.3.2 Reanalyses and observations

Since it is not possible to directly measure the residual circulation of the stratosphere, inferring the circulation from globally observed meteorological variables was only made possible after the beginning of the satellite era (1979). While the availability of these observations enabled the first studies of the observed stratospheric residual circulation, and led to breakthroughs in tackling the conceptual issues identified by Murgatroyd and Singleton (1961) and Vincent (1968), the estimates of the residual circulation remained quite noisy in most reanalysis products (Iwasaki et al., 2009). However, Rosenlof (1995) found that robust thermodynamic estimates of the residual circulation can be obtained via the method of Murgatroyd and Singleton (1961) with certain approximations that rendered the originally unaccounted for eddy forcing and horizontal advection terms negligible in the tropical lower and middle stratosphere, as well as constraining corrections for the tropics. Holton (1990) developed an additional indirect method to estimate the global mass flux exchange between the troposphere and stratosphere, through the eddy heat and momentum fluxes that were based on meteorological balloon-borne radiosonde observations (Oort and Peixóto, 1983), using a version of the DCP formulation. However, a caveat of this method was highlighted by Rosenlof and Holton (1993), who noted that it requires knowledge of the unresolved gravity-wave induced zonal forcing to reliably estimate the residual circulation.

Advances in the generation of modern reanalysis products, including parameterisations of unresolved processes, further developments in data assimilation and bias correction schemes, have improved their physical consistency leading to a better representation of the overall features of the BDC for specific reanalyses. These include the European Centre for Medium-Range Weather Forecasts (ECMWF) ERA-Interim product (Seviour et al., 2012) and the Japanese Meteorological Agency (JMA) JRA-55 product (Kobayashi and Iwasaki, 2016). These reanalysis products were refined compared to their older respective versions and a reduction in the inter-reanalysis spread was achieved for different measures of the residual circulation. However, other discrepancies were identified; e.g. a substantial spread between different estimates of the BDC, including one based on the residual circulation along with a thermodynamic and a momentum balance estimate (Abalos et al., 2015). Within an internally self-consistent model, estimates from different methods should be approximately identical. Nonetheless, the addition of analysis increments in reanalyses will not necessarily conserve key quantities, e.g. angular momentum (Abalos et al., 2015).

Figure 1.4 presents these metrics from three modern reanalysis products (ERA-Interim, JRA-55 and NASA MERRA) at various pressure levels between $1979-2012$ within the stratosphere as detailed in Abalos et al. (2015). Apart from the standard TEM estimate (dashed lines), a thermodynamic approximation based on the original work of Murgatroyd and Singleton (1961) without accounting for the eddy forcing, as well as a metric based on the momentum balance equation, an expression combined with the DCP calculation (Haynes et al., 1991) are included. Although the estimates look quite similar in terms of their latitudinal structure, there are some notable discrepancies between the estimates, especially in the upper levels (above $\sim$ 20 hPa) where observations are scarce causing discontinuities in the data assimilation of the reanalysis products. The key take-away point is that the differences between these three estimates in each reanalysis are larger than the difference across the three reanalysis for each estimate (Abalos et al., 2015), highlighting a substantial uncertainty ($\sim 40\%$) in the mean magnitude of the climatological residual circulation among reanalyses (Fig. 1.4). In addition, modern reanalyses exhibit a large spread in their long-term residual circulation trends over the historical period, showing $\sim 2-5\%$ decade^{-1} acceleration in lower stratospheric tropical upwelling (Fueglistaler et al., 2014; Abalos et al., 2015; Miyazaki et al., 2016),

highlighting uncertainty in the long-term changes in the BDC deduced from reanalysis datasets.

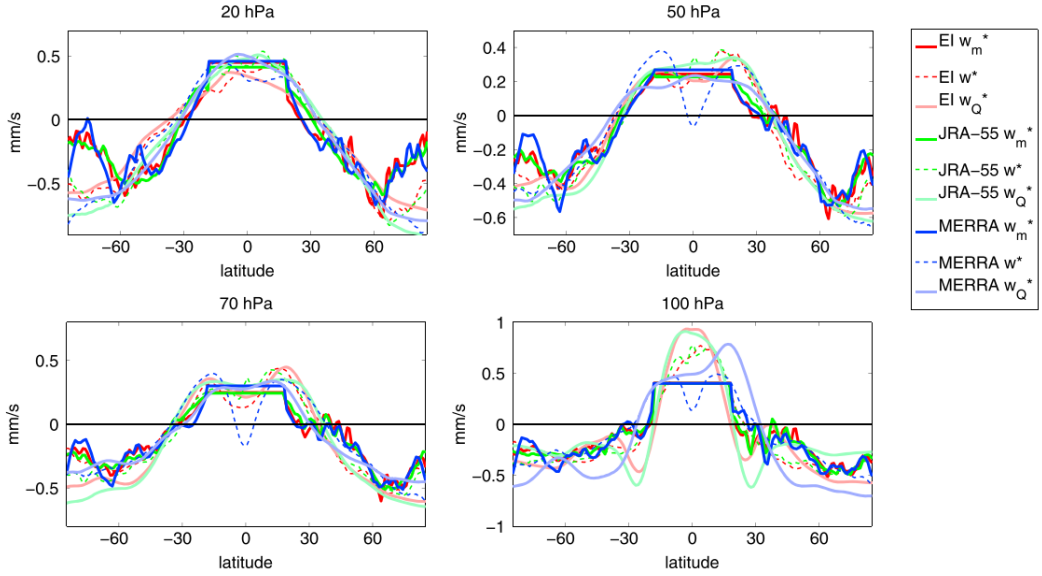

Figure 1.4: Latitudinal structure of the climatological residual circulation on pressure levels near 20, 50, 70, and 100 hPa for the TEM ($\overline{w}^*$), thermodynamic ($\overline{w}^*_q$) and momentum estimate ($\overline{w}^*_m$) in each of the three reanalyses (ERA-I, JRA-55, and MERRA). Taken from Abalos et al. (2015).

Multiple studies utilising satellite and radiosonde (e.g. Microwave Sounding Unit MSU/ AMSU, Stratospheric Sounding Unit SSU) temperature observations in the lower stratosphere have been used to indirectly infer information regarding trends in the residual circulation (e.g. Fu et al., 2010; Young et al., 2012; Ossó et al., 2015; Fu et al., 2015, 2019). It has been shown that temperature variations in this region are closely tied to changes in the residual circulation velocities (Yulaeva et al., 1994; Randel et al., 2006). For an acceleration of the residual circulation, this is manifested as an anomalous cooling of the tropical lower stratosphere and a reverse signature of warming in high latitudes. Indeed, a long-term cooling trend was found in the tropical lower stratospheric temperatures since 1979 (Thompson and Solomon, 2005; Rosenlof and Reid, 2008; Thompson and Solomon, 2009; Thompson et al., 2012) precisely pinpointed over the period of intensive ozone depletion until mid- to late 1990s (Maycock et al., 2018), consistent with

a warming in the high latitude lower stratosphere (Johanson and Fu, 2007; Hu and Fu, 2009; Lin et al., 2009). Along with reanalysis data (e.g. estimates of eddy heat flux), this out-of-phase (anti-correlated) relationship between tropical and extratropical stratospheric temperatures allows for a hemispheric, seasonal and vertically-resolved study of the long-term BDC changes, provided that sources of interannual variability (e.g. El Niño Southern Oscillation, quasi-biennial oscillation, solar and volcanic activity) that can modulate the strength of the BDC can be removed (e.g. Young et al., 2012). Using this methodology, earlier studies found that lower stratospheric upwelling accelerated over the historical period between $1980-2005$, though there was an inconsistent picture of BDC trends in the upper stratosphere (Fu et al., 2010; Young et al., 2012). Subsequent studies, based on the same methodology, estimated a robust 2.1% decade^{-1} acceleration of the lower stratospheric annual mean upwelling (Fu et al., 2015) despite the caveats of the method reported by Ossó et al. (2015). More recently, an updated study by Fu et al. (2019) of BDC changes covering both the stratospheric ozone depletion ($1980-1999$) and recovery periods ($2000-2018$) found that the annual mean tropical lower stratospheric upwelling accelerated over the first period but decelerated over the latter, with most of the changes arising from the SH cell, pointing towards the role of ozone depleting substances (ODS). Over the full period 1980-2018 considered by Fu et al. (2019), the strengthening of the annual mean upwelling in the lower stratosphere was estimated at $\sim 1.7\%$ decade^{-1}, mostly contributed by the SH cell (60%).

Seasonal trace-gas observations within regions where the effects of mixing processes are minimal can be also used to derive quantitative estimates of the residual circulation. Specifically for the tropical lower stratosphere, the method known as the tropical water vapour "tape recorder" developed by Mote et al. (1996) set the scene for multiple subsequent studies (e.g. Niwano et al., 2003; Schoeberl et al., 2008; Schwartz et al., 2008; Flury et al., 2013; Hegglin et al., 2014; Jiang et al., 2015; Minschwaner et al., 2016; Glanville and Birner, 2017; Linz et al., 2019). This method is based on the fact that the water vapour upwelling rates in that vicinity reflect the seasonal cycle of the upwelling via the strong seasonal cycle in tropical tropopause temperatures (e.g. Yulaeva et al., 1994), that imprint an analogous cycle on water vapour entry values in the stratosphere. Quantifying this estimate is achieved through the calculation of the phase-lag between

tape recorder signals across different pressure levels; however, caution must be exercised as these signals are contaminated by the effects of mixing with increasing height, reflected in the decreasing amplitudes of the seasonal cycle with height (Minschwaner et al., 2016).

1.3.3 Modelling studies

The strength of the BDC and its changes over time have been investigated in many studies using GCMs and CCMs (e.g. Butchart and Scaife, 2001; Butchart et al., 2006, 2010, 2011; Garcia and Randel, 2008; Garcia et al., 2007; Calvo and Garcia, 2009; Oman et al., 2009; SPARC, 2010; Lin and Fu, 2013; Oberländer et al., 2013; Hardiman et al., 2014; Oberländer-Hayn et al., 2015, 2016 Polvani et al., 2019, 2017, 2018; Abalos et al., 2019). Model simulations of the historical period generally show climatological features of the stratospheric residual circulation that are in relatively close agreement to reanalysis datasets. This includes models contributing to the Climate Model Intercomparison Project Phase 5 (CMIP5) archive (e.g. Figure 1 in Hardiman et al., 2014) and CCMs that participated in the SPARC Chemistry Climate Model Validation phase 2 activity (CCMVal-2; Butchart et al., 2011). However, it should be noted that upon applying the DCP, substantial intermodel spread is found in the contributions of resolved (i.e. planetary- and synoptic-scale Rossby waves) and parameterised waves (from orographic and non-orographic gravity sources) to the tropical upwelling in the lower stratosphere (Figure 10; Butchart et al., 2011). However, it has been recognised that there may be some compensating effects between different types of wave forcing of the residual circulation (e.g. Cohen et al., 2013; Sigmond and Shepherd, 2014) such that a similar overall circulation is driven by different combinations of wave forcing types.

With respect to long-term changes in the residual circulation, studies typically find that models simulate an increase in tropical upwelling rates over the historical period (e.g. Butchart and Scaife, 2001; Butchart et al., 2006, 2010, 2011; Garcia and Randel, 2008; Li et al., 2008; Calvo and Garcia, 2009; McLandress and Shepherd, 2009; Oman et al., 2009; Garny et al., 2011; Shepherd and McLandress, 2011; Bunzel and Schmidt, 2013; Lin and Fu, 2013; Schmidt et al., 2013). Similarly, for future projections under a scenario for greenhouse gas induced climate change, models consistently simulate a long-term strengthening of the residual circulation by around $2 - 3.2\%$ decade^{-1} (e.g.

Butchart and Scaife, 2001; Butchart et al., 2006, 2010; Garcia and Randel, 2008; Li et al., 2008; Calvo and Garcia, 2009; McLandress and Shepherd, 2009; Oman et al., 2009; Garny et al., 2011 Shepherd and McLandress, 2011; Bunzel and Schmidt, 2013; Lin and Fu, 2013; Oberländer et al., 2013; Schmidt et al., 2013; Hardiman et al., 2014). Coincident with an acceleration of the residual circulation, models robustly simulate a decrease in the stratospheric AoA (e.g. Austin and Li, 2006; Garcia et al., 2007; Oman et al., 2009; Oberländer-Hayn et al., 2015; Li et al., 2018). The projected acceleration of tropical upwelling is found to take place throughout the depth of the stratosphere, albeit with a decreasing trend with increasing height, from the lower to the upper stratosphere (Figure 2; Hardiman et al., 2014). Decomposing the trends in the projected changes of residual circulation into the shallow and deep branches corroborates this finding (Lin and Fu, 2013) using an ensemble of CCMs, presented in Figure 1.5, where the acceleration occurs in both branches but is weaker in the deep branch (above $\sim$ 30 hPa). Overall, there is now a consensus (e.g. Butchart et al., 2006, 2010; Garcia and Randel, 2008; SPARC, 2010; Lin and Fu, 2013; Oberländer et al., 2013; Palmeiro et al., 2014; Hardiman et al., 2014) that the shallow branch (below $\sim$ 50 hPa) of the residual circulation has been accelerating and will continue to do so in the future. However, the changes in the deep branch of the circulation are characterised by larger uncertainty.

The projected increase in the residual circulation in the tropical lower stratosphere shows a distinct seasonality, with the largest increase occurring during boreal winter (Butchart et al., 2006; Li et al., 2008; McLandress and Shepherd, 2009; Butchart et al., 2010; Deushi and Shibata, 2011; Garny et al., 2011; Bunzel and Schmidt, 2013). This seasonality is also reflected in the hemispheric asymmetry of the annual mean extratropical downwelling trends in the lower stratosphere, where the NH downwelling cell is projected to accelerate more than the SH counterpart. Given the stronger tropical upwelling in the present day in boreal winter, it follows that the tropical upwelling seasonal cycle will also increase in amplitude, forcing an even stronger hemispheric asymmetry projected onto the extratropical downwelling fluxes. Other characteristics of the residual circulation response to climate change in modelling studies include, a narrowing of the tropical upwelling region in the lower stratosphere and a widening of the upwelling region higher up in the middle to upper stratosphere (e.g. Hardiman et al., 2014). The narrowing of the upwelling region in the lower stratosphere is in contrast with a robust

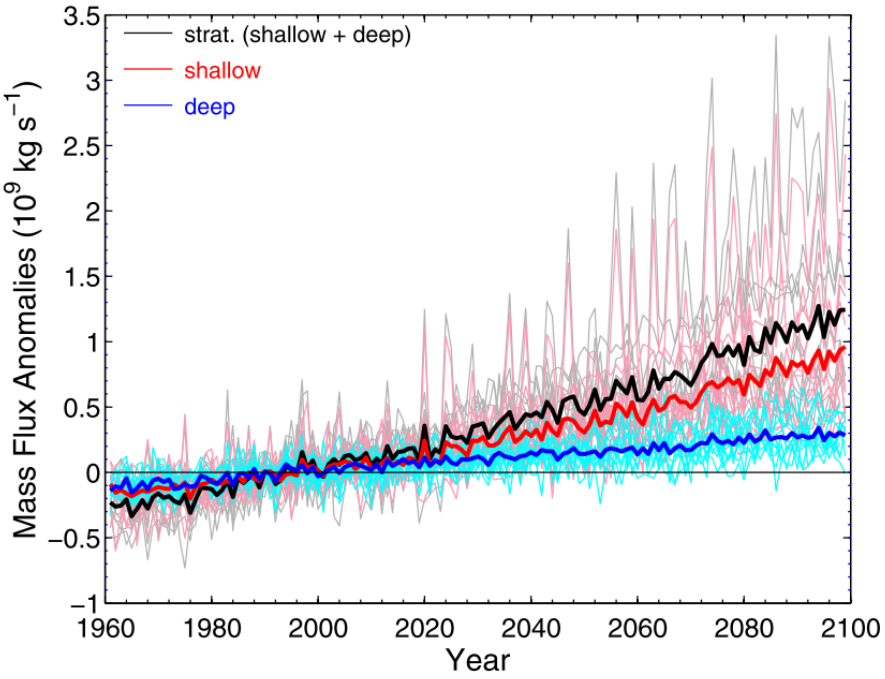

Figure 1.5: Annual mean tropical upwelling mass flux anomalies with respect to 1980-2009 climatology for the CCMVal-2 models. The shallow branch of the BDC is denoted with red lines, the deep branch with blue lines while their sum represents the total stratospheric branch of the BDC (black lines). Thick lines denote the multi-model mean (MMM). Taken from Lin and Fu (2013).

finding of projected tropospheric climate change in models (and in observations), which is associated with a widening of the tropical belt (e.g. Staten et al., 2018) and similar changes in the tropical tropopause layer (Seidel and Randel, 2007; Seidel et al., 2008).

In an effort to compare model simulations of the stratospheric circulation and related diagnostics with observations, the method of "specified-dynamics" simulations has become widely used in which meteorological fields are nudged or relaxed towards analysis or reanalysis fields (e.g. Jeuken et al., 1996; van Aalst et al., 2004; Solomon et al., 2015, 2016, Akiyoshi et al., 2016; Löffler et al., 2016; Schmidt et al., 2018; Hardiman et al., 2017a; Ball et al., 2018; Froidevaux et al., 2019). Recently, these simulations have been employed to compare stratospheric ozone trends and variability with observational

records (e.g. Solomon et al., 2016; Hardiman et al., 2017a; Ball et al., 2018). Nudged simulations typically constrain the surface pressure, horizontal winds and temperature fields of the model towards reanalyses in order to depict the atmospheric dynamics. They have been shown to be quite successful in simulating upper stratospheric ozone variability (Ball et al., 2016) and transport processes associated with the Asian Summer monsoon in the lower stratosphere (Solomon et al., 2016). However, as demonstrated by Ball et al. (2018), nudged simulations are not able to simulate other long-term behaviour such as the observed decline in extrapolar lower stratospheric ozone since 1998. Ball et al. (2018) suggested that one of the reasons for the discrepancy could be that the model-simulated tracer transport in the lower stratosphere is affected by the nudging methodology. However, a detailed investigation of the stratospheric residual circulation in nudged simulations from multiple models has not been undertaken so far.

1.4 Drivers and mechanisms for BDC changes

Regarding the influence of climate change on the residual circulation, the pioneering work of Rind et al. (1990) was the first modelling evidence for an increase in the residual circulation under increasing greenhouse gases ($2\times$ CO_2), consistent with findings decades later in multi-model studies (e.g. SPARC, 2010; Hardiman et al., 2014). Climate change manifests itself in the atmosphere via tropospheric warming (including warmer SSTs) and stratospheric cooling. Model studies have shown that the BDC response to climate change is primarily a response to the warming of the troposphere and not the radiative cooling of the stratosphere (Olsen et al., 2007; Oman et al., 2009). However, artificially decoupling (in model simulations) the direct atmospheric radiative response to increasing burdens of GHGs (rapid adjustment) and the ocean response (SST forcing) driven by the former, it was shown that the fast radiative impact can have a small, albeit insignificant increase on the STE (Olsen et al., 2007). Similarly, Oman et al. (2009) using a comparable sensitivity simulation set-up as the one noted above including ozone changes, found that the rapid adjustment due to the radiative impact of GHGs is projected to continue to cause an acceleration of the residual circulation along with a decrease in mean AoA during the ozone recovery phase. Additionally, the higher globally imposed SSTs associated with the tropospheric warming were demonstrated to accelerate the lower stratospheric residual circulation robustly in modelling

studies (e.g. Sigmond et al., 2004; Olsen et al., 2007; Oman et al., 2009; Lin et al., 2015). Nevertheless, the oceanic response to climate change in the Anthropocene exhibits spatial inhomogeneities (Latif and Keenlyside, 2009) mainly located in the vicinity of the tropical Pacific associated with the El Niño Southern Oscillation (ENSO) ultimately affecting the lower stratospheric residual circulation (e.g. Marsh and Garcia, 2007; Randel et al., 2009). Modelling studies have shown that during the warm phase of ENSO (El Niño), localised SST anomalies cause an increase in the boreal-winter lower stratospheric tropical upwelling (Calvo et al., 2010; Simpson et al., 2011). These were attributed contrastingly, owing to different types of waves, to changes in wave propagation and dissipation characteristics in the NH (Calvo et al., 2010) and modified wave sources in the troposphere in the SH (Simpson et al., 2011). Hence, the spatial SST patterns emerging in response to anthropogenic forcing under climate change have the potential to affect the residual circulation strength through a number of pathways that is hard to disentangle from the global-mean (uniform) ocean warming (Lin et al., 2015).

As the BDC is a wave-driven circulation, its simulated response to climate change can be attributed to wave-drag changes especially in the vicinity of the turnaround latitudes. Both resolved and parameterised waves drive a stronger residual circulation in climate projections, but the split among these types of waves is model dependent and differs from the wave forcing of the climatological circulation (Butchart et al., 2006, 2010, 2011; SPARC, 2010). The parameterised gravity waves (mostly the orographic) are obtained through simplified approximations of linear-wave dynamics theory and although their maximum momentum deposition is located in the lower stratosphere, their projected changes are located higher up in the stratosphere (e.g. Butchart et al., 2010). On the other hand, while resolved waves are explicitly represented in climate models, there are discrepancies between models related to the mechanism of the planetary and synoptic Rossby waves and their altered stratospheric wave drag in response to climate change (e.g. Butchart and Scaife, 2001; Garcia and Randel, 2008). The most promising mechanism of an altered resolved wave forcing driving the changes of the BDC has been suggested by Shepherd and McLandress (2011), building on previous work by McLandress and Shepherd (2009). Decomposing the resolved wave forcing into its stationary and transient components, Shepherd and McLandress (2011) suggest that the robust

climate change response of a strengthening and upward shift of the westerly subtropical jets causes a displacement of the Rossby wave breaking region, otherwise known as the critical layer, allowing enhanced wave drag around the vicinity of the turnaround latitudes in the subtropical lower stratosphere. This mechanism has also been corroborated in multi-model studies (Lin and Fu, 2013; Hardiman et al., 2014; Lin et al., 2015).

More recent work has addressed an impact of temporal changes in ozone on the residual circulation, pointing to a role of ODSs as forcing agents in driving past and future trends in the residual circulation (e.g. Li et al., 2008; Oman et al., 2009; McLandress et al., 2010; Oberländer et al., 2013; Oberländer-Hayn et al., 2015; Aquila et al., 2016; Garfinkel et al., 2017; Polvani et al., 2019, 2017, 2018; Abalos et al., 2019). Recent studies have provided evidence from models that ozone depletion in the SH has been the main driver of the strengthened residual circulation over the past several decades (e.g Garfinkel et al., 2017; Li et al., 2018; Morgenstern et al., 2018; Polvani et al., 2019, 2018). Model simulations show an increase in annual mean Antarctic polar cap downwelling until year 2000, associated with enhanced SH downwelling during austral summer and attributed to the role of ODSs (Polvani et al., 2018). This is also reflected in the annual mean tropical upwelling, with an estimated ODS contribution of $\sim 50\%$ of the past acceleration. Going into the 21st century, the projected ozone recovery due to the successful implementation of the Montreal Protocol in models drives an opposite trend with weaker SH polar cap downwelling. Nonetheless, this is projected to impact the global overturning circulation in the future as the decreasing ODSs are expected to counteract the GHG-induced acceleration of the BDC (e.g Figure 4; Polvani et al., 2018) through wave forcing changes associated with diabatic processes altering the zonal-mean state (Orr et al., 2013). Consistent with the reduction in observed cooling rate of the tropical lower stratosphere since 2000 (Randel et al., 2016), forcing from decreasing ODS amounts could also partly explain the observed slow-down of the lower stratospheric residual circulation at the beginning of the 21st century (Aschmann et al., 2014), though other drivers have been proposed, such as internal atmospheric variability (Garfinkel et al., 2017) or long-term decadal ocean variability (Aschmann et al., 2014).

1.5 Key scientific challenges

This section summarises the key scientific areas with current gaps of understanding tied to the specific objectives of this thesis that follow in Section 1.6.

1. A relatively new type of "specified-dynamics" simulation has recently emerged as very promising in terms of reproducing the observed meteorology via a process of Newtonian relaxation or "nudging" towards analysis or reanalysis fields (Jeuken et al., 1996). This type of simulation has been applied to the study of observed tracer variability in different parts of the stratosphere (e.g. Ball et al., 2016; Solomon et al., 2016), specific meteorological events (Akiyoshi et al., 2016) and the chemical and climatic effects surrounding volcanic eruptions (Löffler et al., 2016; Schmidt et al., 2018). However, Ball et al. (2018) found discrepancies pertaining the recent observed variability of lower stratospheric extrapolar ozone in nudged CCM simulations. Nudging is performed through the addition of extra tendencies to the model equations that append forcings which are inconsistent with the model state and may cause violations of global constraints such as conservation of mass and energy. It should be noted that the vertical winds emerging as residuals from horizontal divergence are not subject to nudging, and it has been shown that the model physics will not necessarily exhibit similar results to the dataset nudged towards (Telford et al., 2008; Hardiman et al., 2017a). Moreover, large discrepancies were found in the tropospheric tracer distributions between nudged CCM simulations in Orbe et al. (2018), reflecting convection scheme differences among models, partly attributed to the way the nudged models simulate the large-scale flow including their sub-grid parameterisations. Therefore, it is imperative that an expository evaluation of the stratospheric residual circulation in nudged CCM simulations materialises.

2. The acceleration of the BDC is strongly tied to surface, tropospheric and concomitant ocean warming, as attested by the approximately linear relationship between changes in the residual circulation and spatially averaged surface temperatures on interannual to decadal timescales found in models (Olsen et al., 2007; Sigmond et al., 2004; Lin et al., 2015). Nevertheless, the stratospheric response to increasing GHGs also includes a fast radiative response (or rapid adjustment) associated

with stratospheric cooling and the multi-year response exhibits localised SST patterns, which have been shown on interannual timescales to accelerate the lower stratospheric residual circulation (Calvo et al., 2010; Simpson et al., 2011). However, the quantitative importance of these distinct factors for projected changes in the BDC remains unclear. This is important to quantify because there may be different uncertainties attached to each of the three parts (rapid adjustment, global mean SST and SST patterns) in model simulations.

3. Quantifying the strength of the residual circulation from observations relies on the use of indirect measures that in some cases exhibit distinct inconsistencies in their behaviour. This includes measures based on stratospheric temperatures and tracers such as ozone. Comparing observed changes in the residual circulation is further complicated by the fact that different indirect measures based on different datasets with distinct uncertainties have been used in different studies. Hence, there is merit in providing a detailed comparison of different indirect measures of the residual circulation, and their degree of agreement on different timescales, within a modelling framework where they can be diagnosed in a self consistent manner to ascertain the extent to which they represent variations in the residual circulation.

1.6 Aim and objectives

The overarching aim of this thesis is to advance our understanding of the residual circulation and its representation in models through studies that cover both the historical period and projected changes under climate change. The specific objectives are based on the three research gaps detailed in Section 1.5:

1. Evaluate the representation of the stratospheric residual circulation in a suite of "specified dynamics or nudged" chemistry-climate simulations and assess their performance against free-running simulations and reanalysis datasets.

2. Design and perform climate model simulations to quantify the importance of radiative effects (rapid adjustment), global-average ocean warming and the local patterns of ocean warming for the BDC response to GHG-induced climate change,

and assess the extent to which they can be linearly combined to explain the overall response.

3. Investigate the robustness and interchangeability of different observational-based BDC measures within a modelling framework, to determine which measures most closely reproduce the simulated residual circulation and its variability on different timescales.

1.7 Thesis structure

Chapter 1 has served as the introduction of the thesis, providing a comprehensive, up-to-date literature review as well as defining the key scientific questions that will be addressed in the following results chapters $(2-4)$. A description of the methods and datasets used in this thesis is included separately in each chapter. In Chapter 2, I present a study published in Atmospheric Chemistry and Physics that evaluates the representation of the stratospheric residual circulation in a new set of chemistry-climate simulations. In Chapter 3, I present a study published in Weather and Climate Dynamics that analyses idealised climate model simulations that decompose the overall Brewer-Dobson circulation response to a quadrupling in CO_2. In Chapter 4, I present a manuscript that evaluates different metrics of the strength of the residual circulation and assesses their robustness based in an ensemble of chemistry-climate simulations. Finally, Chapter 5 provides a synthesis of the main findings of the results chapters, and places these into a wider context in order to address the overarching aim of my PhD project as well as suggested pathways for future work.

References

M. Abalos, B. Legras, F. Ploeger, and W. J. Randel. Evaluating the advective Brewer-Dobson circulation in three reanalyses for the period 1979–2012. *Journal of Geophysical Research: Atmospheres*, 120(15):7534–7554, 2015. ISSN 2169-897X. doi: 10.1002/2015JD023182. URL https://onlinelibrary.wiley.com/doi/abs/10.1002/2015JD023182. xi, 13, 14

M. Abalos, L. Polvani, N. Calvo, D. Kinnison, F. Ploeger, W. Randel, and S. Solomon. New Insights on the Impact of Ozone-Depleting Substances on the Brewer-Dobson

Circulation. *Journal of Geophysical Research: Atmospheres*, 124(5):2435–2451, 2019. ISSN 2169-897X. doi: 10.1029/2018JD029301. URL https://onlinelibrary.wiley.com/doi/abs/10.1029/2018JD029301. 16, 21

H. Akiyoshi, T. Nakamura, T. Miyasaka, M. Shiotani, and M. Suzuki. A nudged chemistry-climate model simulation of chemical constituent distribution at northern high-latitude stratosphere observed by SMILES and MLS during the 2009/2010 stratospheric sudden warming. *Journal of Geophysical Research: Atmospheres*, 121 (3):1361–1380, 2016. ISSN 2169897X. doi: 10.1002/2015JD023334. URL http://doi.wiley.com/10.1002/2015JD023334. 18, 22

D. G. Andrews and M. E. McIntyre. Planetary Waves in Horizontal and Vertical Shear: The Generalized Eliassen-Palm Relation and the Mean Zonal Acceleration. *Journal of the Atmospheric Sciences*, 33(11):2031–2048, 1976. ISSN 0022-4928. doi: 10.1175/1520-0469(1976)033<2031:PWIHAV>2.0.CO;2. URL http://journals.ametsoc.org/doi/abs/10.1175/1520-0469{%}281976{%}29033{%}3C2031{%}3APWIHAV{%}3E2.0.CO{%}3B2. 3, 4, 9, 10

D. G. Andrews and M. E. McIntyre. An exact theory of nonlinear waves on a Lagrangian-mean flow. *Journal of Fluid Mechanics*, 89(4):609–646, 1978a. ISSN 0022-1120. doi: 10.1017/S0022112078002773. URL https://www.cambridge.org/core/product/identifier/S0022112078002773/type/journal{_}article. 3

D. G. Andrews and M. E. McIntyre. Generalized Eliassen-Palm and Charney-Drazin Theorems for Waves on Axismmetric Mean Flows in Compressible Atmospheres. *Journal of the Atmospheric Sciences*, 35(2):175–185, 1978b. ISSN 0022-4928. doi: 10.1175/1520-0469(1978)035<0175:GEPACD>2.0.CO;2. URL https://journals.ametsoc.org/doi/abs/10.1175/1520-0469{%}281978{%}29035{%}3C0175{%}3AGEPACD{%}3E2.0.CO{%}3B2. 3, 4, 9, 10

D. G. Andrews, C. B. Leovy, J. R. Holton, and C. B. Leovy. *Middle Atmosphere Dynamics*. Academic press, 1987. 1, 2, 8

V. Aquila, W. H. Swartz, D. W. Waugh, P. R. Colarco, S. Pawson, L. M. Polvani, and R. S. Stolarski. Isolating the roles of different forcing agents in global stratospheric temperature changes using model integrations with incrementally added single forcings. *Journal of Geophysical Research*, 121(13):8067–8082, 2016. ISSN 21562202. doi: 10.1002/2015JD023841. URL http://doi.wiley.com/10.1002/2015JD023841. 21

J. Aschmann, J. P. Burrows, C. Gebhardt, A. Rozanov, R. Hommel, M. Weber, and A. M. Thompson. On the hiatus in the acceleration of tropical upwelling since the beginning of the 21st century. *Atmospheric Chemistry and Physics*, 14(23):12803–12814, 2014. ISSN 16807324. doi: 10.5194/acp-14-12803-2014. 21

J. Austin and F. Li. On the relationship between the strength of the Brewer-Dobson circulation and the age of stratospheric air. *Geophysical Research Letters*, 33(17): L17807, 2006. ISSN 00948276. doi: 10.1029/2006GL026867. URL http://doi.wiley.com/10.1029/2006GL026867. 17

W. T. Ball, A. Kuchai, E. V. Rozanov, J. Staehelin, F. Tummon, A. K. Smith, T. Sukhodolov, A. Stenke, L. Revell, A. Coulon, W. Schmutz, and T. Peter. An upper-branch Brewer-Dobson circulation index for attribution of stratospheric variability and improved ozone and temperature trend analysis. *Atmospheric Chemistry and Physics*, 16(24):15485–15500, 2016. ISSN 16807324. doi: 10.5194/acp-16-15485-2016. URL http://www.atmos-chem-phys-discuss.net/acp-2016-449/. 19, 22

W. T. Ball, J. Alsing, D. J. Mortlock, J. Staehelin, J. D. Haigh, T. Peter, F. Tummon, R. Stübi, A. Stenke, J. Anderson, A. Bourassa, S. M. Davis, D. Degenstein, S. Frith, L. Froidevaux, C. Roth, V. Sofieva, R. Wang, J. Wild, P. Yu, J. R. Ziemke, and E. V. Rozanov. Evidence for a continuous decline in lower stratospheric ozone offsetting ozone layer recovery. *Atmospheric Chemistry and Physics*, 18(2):1379–1394, 2018. ISSN 1680-7324. doi: 10.5194/acp-18-1379-2018. URL https://www.atmos-chem-phys.net/18/1379/2018/. 18, 19, 22

T. Birner and H. Bönisch. Residual circulation trajectories and transit times into the extratropical lowermost stratosphere. *Atmospheric Chemistry and Physics*, 11(2): 817–827, 2011. ISSN 1680-7324. doi: 10.5194/acp-11-817-2011. URL https://www.atmos-chem-phys.net/11/817/2011/. 4, 5, 6, 7

M. T. Boehm and S. Lee. The implications of tropical Rossby waves for tropical tropopause cirrus formation and for the equatorial upwelling of the brewer-dobson circulation. *Journal of the Atmospheric Sciences*, 60(2):247–261, 2003. ISSN 00224928. doi: 10.1175/1520-0469(2003)060<0247:TIOTRW>2.0.CO;2. 8

H. Bönisch, A. Engel, T. Birner, P. Hoor, D. W. Tarasick, and E. A. Ray. On the structural changes in the Brewer-Dobson circulation after 2000. *Atmospheric Chemistry and Physics*, 11(8):3937–3948, 2011. ISSN 16807316. doi: 10.5194/acp-11-3937-2011. 4

A. W. Brewer. Evidence for a world circulation provided by the measurements of helium and water vapour distribution in the stratosphere. *Quarterly Journal of the Royal Meteorological Society*, 75(326):351–363, 1949. ISSN 00359009. doi: 10.1002/qj.49707532603. URL http://doi.wiley.com/10.1002/qj.49707532603. 2

F. Bunzel and H. Schmidt. The Brewer–Dobson Circulation in a Changing Climate: Impact of the Model Configuration. *Journal of the Atmospheric Sciences*, 70(5): 1437–1455, 2013. ISSN 0022-4928. doi: 10.1175/JAS-D-12-0215.1. URL http://journals.ametsoc.org/doi/abs/10.1175/JAS-D-12-0215.1. 16, 17

N. Butchart. The Brewer-Dobson circulation. *Reviews of Geophysics*, 52(2):157–184, 2014. ISSN 87551209. doi: 10.1002/2013RG000448. URL http://doi.wiley.com/10.1002/2013RG000448. 9, 11

N. Butchart and A. A. Scaife. Removal of chlorofluorocarbons by increased mass exchange between the stratosphere and troposphere in a changing climate. *Nature*, 410(6830):799–802, 2001. ISSN 0028-0836. doi: 10.1038/35071047. URL http://www.nature.com/articles/35071047. 10, 16, 17, 20

N. Butchart, A. A. Scaife, M. Bourqui, J. de Grandpré, S. H. E. Hare, J. Kettleborough, U. Langematz, E. Manzini, F. Sassi, K. Shibata, D. Shindell, and M. Sigmond. Simulations of anthropogenic change in the strength of the Brewer–Dobson circulation. *Climate Dynamics*, 27(7-8):727–741, 2006. ISSN 0930-7575. doi: 10.1007/s00382-006-0162-4. URL http://link.springer.com/10.1007/s00382-006-0162-4. 11, 16, 17, 20

N. Butchart, I. Cionni, V. Eyring, T. G. Shepherd, D. W. Waugh, H. Akiyoshi, J. Austin, C. Brühl, M. P. Chipperfield, E. Cordero, M. Dameris, R. Deckert, S. Dhomse, S. M. Frith, R. R. Garcia, A. Gettelman, M. A. Giorgetta, D. E. Kinnison, F. Li, E. Mancini, C. McLandress, S. Pawson, G. Pitari, D. A. Plummer, E. Rozanov, F. Sassi, J. F. Scinocca, K. Shibata, B. Steil, and W. Tian. Chemistry–Climate Model Simulations of Twenty-First Century Stratospheric Climate and Circulation Changes. *Journal of Climate*, 23(20):5349–5374, 2010. ISSN 0894-8755. doi: 10.1175/2010JCLI3404.1. URL http://journals.ametsoc.org/doi/10.1175/2010JCLI3404.1. 11, 16, 17, 20

N. Butchart, A. J. Charlton-Perez, I. Cionni, S. C. Hardiman, P. H. Haynes, K. Krüger, P. J. Kushner, P. A. Newman, S. M. Osprey, J. Perlwitz, M. Sigmond, L. Wang, H. Akiyoshi, J. Austin, S. Bekki, A. Baumgaertner, P. Braesicke, C. Brühl, M. Chipperfield, M. Dameris, S. Dhomse, V. Eyring, R. Garcia, H. Garny, P. Jöckel, J.-F. Lamarque, M. Marchand, M. Michou, O. Morgenstern, T. Nakamura, S. Pawson, D. Plummer, J. Pyle, E. Rozanov, J. Scinocca, T. G. Shepherd, K. Shibata, D. Smale, H. Teyssèdre, W. Tian, D. Waugh, and Y. Yamashita. Multimodel climate and variability of the stratosphere. *Journal of Geophysical Research*, 116(D5):D05102, 2011. ISSN 0148-0227. doi: 10.1029/2010JD014995. URL http://doi.wiley.com/10.1029/2010JD014995. 11, 16, 20

N. Calvo and R. R. Garcia. Wave Forcing of the Tropical Upwelling in the Lower Stratosphere under Increasing Concentrations of Greenhouse Gases. *Journal of the Atmospheric Sciences*, 66(10):3184–3196, 2009. ISSN 0022-4928. doi: 10.1175/2009jas3085.1. URL http://journals.ametsoc.org/doi/abs/10.1175/2009JAS3085.1. 8, 16, 17

N. Calvo, R. R. Garcia, W. J. Randel, and D. R. Marsh. Dynamical Mechanism for the Increase in Tropical Upwelling in the Lowermost Tropical Stratosphere during Warm ENSO Events. *Journal of the Atmospheric Sciences*, 67(7):2331–2340, 2010. ISSN 0022-4928. doi: 10.1175/2010JAS3433.1. URL http://journals.ametsoc.org/doi/10.1175/2010JAS3433.1. 20, 23

J. G. Charney and P. G. Drazin. Propagation of planetary-scale disturbances from the lower into the upper atmosphere. *Journal of Geophysical Research*, 66(1):83–109,

1961. ISSN 2156-2202. doi: 10.1029/jz066i001p00083. URL http://dx.doi.org/10.1029/JZ066i001p00083. 7

N. Y. Cohen, E. P. Gerber, and O. Bühler. Compensation between Resolved and Unresolved Wave Driving in the Stratosphere: Implications for Downward Control. *Journal of the Atmospheric Sciences*, 70(12):3780–3798, 2013. ISSN 0022-4928. doi: 10.1175/JAS-D-12-0346.1. URL http://journals.ametsoc.org/doi/10.1175/JAS-D-12-0346.1. 16

M. Deushi and K. Shibata. Development of a Meteorological Research Institute Chemistry-Climate Model version 2 for the Study of Tropospheric and Stratospheric Chemistry. *Papers in Meteorology and Geophysics*, 62:1–46, 2011. ISSN 1880-6643. doi: 10.2467/mripapers.62.1. URL http://joi.jlc.jst.go.jp/JST.JSTAGE/mripapers/62.1?from=CrossRef. 17

M. Diallo, B. Legras, and A. Chédin. Age of stratospheric air in the ERA-Interim. *Atmospheric Chemistry and Physics*, 12(24):12133–12154, 2012. ISSN 16807316. doi: 10.5194/acp-12-12133-2012. URL http://www.atmos-chem-phys.net/12/12133/2012/. 12

G. M. B. Dobson. Origin and distribution of the polyatomic molecules in the atmosphere. *Proceedings of the Royal Society of London. Series A. Mathematical and Physical Sciences*, 236(1205):187–193, 1956. ISSN 0080-4630. doi: 10.1098/rspa.1956.0127. URL https://royalsocietypublishing.org/doi/10.1098/rspa.1956.0127. 2

G. M. B. Dobson, D. N. Harrison, and J. Lawrence. Measurements of the Amount of Ozone in the Earth's Atmosphere and Its Relation to Other Geophysical Conditions. Part III. *Proceedings of the Royal Society A: Mathematical, Physical and Engineering Sciences*, 122(790):456–486, 1929. ISSN 1364-5021. doi: 10.1098/rspa.1929.0034. URL http://rspa.royalsocietypublishing.org/cgi/doi/10.1098/rspa.1929.0034. 2

T. Dunkerton. On the Mean Meridional Mass Motions of the Stratosphere and Mesosphere. *Journal of the Atmospheric Sciences*, 35(12):2325–2333, 1978. ISSN 0022-4928. doi: 10.1175/1520-0469(1978)035<2325:OTMMMM>2.0.CO;2. URL https://doi.org/10.1175/1520-0469(1978)035{%}3C2325:OTMMMM{%}3E2.

0.COhttp://0.0.0.2http://journals.ametsoc.org/doi/abs/10.1175/1520-0469{%}281978{%}29035{%}3C2325{%}3AOTMMMM{%}3E2.0.CO{%}3B2. 3, 9

A. J. Dyer and B. B. Hicks. Global spread of volcanic dust from the Bali eruption of 1963. *Quarterly Journal of the Royal Meteorological Society*, 96(408):341–341, 1968. ISSN 1477870X. doi: 10.1002/qj.49709640820. 3

A. Engel, T. Möbius, H. Bönisch, U. Schmidt, R. Heinz, I. Levin, E. Atlas, S. Aoki, T. Nakazawa, S. Sugawara, F. Moore, D. Hurst, J. Elkins, S. Schauffler, A. Andrews, and K. Boering. Age of stratospheric air unchanged within uncertainties over the past 30 years. *Nature Geoscience*, 2(1):28–31, 2009. ISSN 1752-0894. doi: 10.1038/ngeo388. URL http://www.nature.com/articles/ngeo388. 11

A. Engel, H. Bönisch, M. Ullrich, R. Sitals, O. Membrive, F. Danis, and C. Crevoisier. Mean age of stratospheric air derived from AirCore observations. *Atmospheric Chemistry and Physics*, 17(11):6825–6838, 2017. ISSN 1680-7324. doi: 10.5194/acp-17-6825-2017. URL https://www.atmos-chem-phys.net/17/6825/2017/. 11

T. Flury, D. L. Wu, and W. G. Read. Variability in the speed of the Brewer-Dobson circulation as observed by Aura/MLS. *Atmospheric Chemistry and Physics*, 13(9):4563–4575, 2013. ISSN 16807316. doi: 10.5194/acp-13-4563-2013. 15

P. M. F. Forster and K. P. Shine. Radiative forcing and temperature trends from stratospheric ozone changes. *Journal of Geophysical Research: Atmospheres*, 102 (D9):10841–10855, 1997. ISSN 01480227. doi: 10.1029/96JD03510. URL http://doi.wiley.com/10.1029/96JD03510. 2

P. M. F. Forster and K. P. Shine. Stratospheric water vapour changes as a possible contributor to observed stratospheric cooling. *Geophysical Research Letters*, 26(21):3309–3312, 1999. ISSN 00948276. doi: 10.1029/1999GL010487. URL http://doi.wiley.com/10.1029/1999GL010487. 2

P. M. F. Forster and K. P. Shine. Assessing the climate impact of trends in stratospheric water vapor. *Geophysical Research Letters*, 29(6):10–1–10–4, 2002. ISSN 00948276. doi: 10.1029/2001GL013909. URL http://doi.wiley.com/10.1029/2001GL013909. 2

L. Froidevaux, D. E. Kinnison, R. Wang, J. Anderson, and R. A. Fuller. Evaluation of CESM1 (WACCM) free-running and specified dynamics atmospheric composition simulations using global multispecies satellite data records. *Atmospheric Chemistry and Physics*, 19(7):4783–4821, 2019. ISSN 1680-7324. doi: 10.5194/acp-19-4783-2019. URL https://www.atmos-chem-phys.net/19/4783/2019/. 18

Q. Fu, S. Solomon, and P. Lin. On the seasonal dependence of tropical lower-stratospheric temperature trends. *Atmospheric Chemistry and Physics*, 10(6): 2643–2653, 2010. ISSN 16807324. doi: 10.5194/acp-10-2643-2010. URL www.atmos-chem-phys.net/10/2643/2010/. 14, 15

Q. Fu, P. Lin, S. Solomon, and D. L. Hartmann. Observational evidence of strengthening of the brewer-dobson circulation since 1980. *Journal of Geophysical Research*, 120 (19):10214–10228, 2015. ISSN 21562202. doi: 10.1002/2015JD023657. URL http://doi.wiley.com/10.1002/2015JD023657. 14, 15

Q. Fu, S. Solomon, H. Pahlavan, and P. Lin. Observed changes in Brewer-Dobson circulation for 1980-2018. *Environmental Research Letters*, 2019. ISSN 1748-9326. doi: 10.1088/1748-9326/ab4de7. 14, 15

S. Fueglistaler, M. Abalos, T. J. Flannaghan, P. Lin, and W. J. Rande. Variability and trends in dynamical forcing of tropical lower stratospheric temperatures. *Atmospheric Chemistry and Physics*, 14(24):13439–13453, 2014. ISSN 16807324. doi: 10.5194/acp-14-13439-2014. 13

R. R. Garcia and W. J. Randel. Acceleration of the Brewer–Dobson Circulation due to Increases in Greenhouse Gases. *Journal of the Atmospheric Sciences*, 65(8):2731–2739, 2008. ISSN 0022-4928. doi: 10.1175/2008JAS2712.1. URL http://journals.ametsoc.org/doi/10.1175/2008JAS2712.1. 16, 17, 20

R. R. Garcia, D. R. Marsh, D. E. Kinnison, B. A. Boville, and F. Sassi. Simulation of secular trends in the middle atmosphere, 1950–2003. *Journal of Geophysical Research*, 112(D9):D09301, 2007. ISSN 0148-0227. doi: 10.1029/2006JD007485. URL http://doi.wiley.com/10.1029/2006JD007485. 16, 17

R. R. Garcia, W. J. Randel, and D. E. Kinnison. On the Determination of Age of Air Trends from Atmospheric Trace Species. *Journal of the Atmospheric Sciences*,

68(1):139–154, 2011. ISSN 0022-4928. doi: 10.1175/2010JAS3527.1. URL http://journals.ametsoc.org/doi/10.1175/2010JAS3527.1. 11

C. I. Garfinkel, V. Aquila, D. W. Waugh, and L. D. Oman. Time-varying changes in the simulated structure of the Brewer-Dobson Circulation. *Atmospheric Chemistry and Physics*, 17(2):1313–1327, 2017. ISSN 16807324. doi: 10.5194/acp-17-1313-2017. URL http://www.atmos-chem-phys.net/17/1313/2017/. 21

H. Garny, M. Dameris, W. Randel, G. E. Bodeker, and R. Deckert. Dynamically Forced Increase of Tropical Upwelling in the Lower Stratosphere. *Journal of the Atmospheric Sciences*, 68(6):1214–1233, 2011. ISSN 0022-4928. doi: 10.1175/2011JAS3701.1. URL http://journals.ametsoc.org/doi/10.1175/2011JAS3701.1. 8, 16, 17

H. Garny, T. Birner, H. Bönisch, and F. Bunzel. The effects of mixing on age of air. *Journal of Geophysical Research: Atmospheres*, 119(12):7015–7034, 2014. ISSN 2169897X. doi: 10.1002/2013JD021417. URL http://doi.wiley.com/10.1002/2013JD021417. xi, 6, 7, 12

A. E. Gill. Some simple solutions for heat-induced tropical circulation. *Quarterly Journal of the Royal Meteorological Society*, 106(449):447–462, 1980. ISSN 00359009. doi: 10.1002/qj.49710644905. URL http://doi.wiley.com/10.1002/qj.49710644905. 8

A. A. Glanville and T. Birner. Role of vertical and horizontal mixing in the tape recorder signal near the tropical tropopause. *Atmospheric Chemistry and Physics*, 17 (6):4337–4353, 2017. ISSN 16807324. doi: 10.5194/acp-17-4337-2017. 15

F. J. Haenel, G. P. Stiller, T. von Clarmann, B. Funke, E. Eckert, N. Glatthor, U. Grabowski, S. Kellmann, M. Kiefer, A. Linden, and T. Reddmann. Reassessment of MIPAS age of air trends and variability. *Atmospheric Chemistry and Physics*, 15 (22):13161–13176, 2015. ISSN 1680-7324. doi: 10.5194/acp-15-13161-2015. URL https://www.atmos-chem-phys.net/15/13161/2015/. 11

T. M. Hall and R. A. Plumb. Age as a diagnostic of stratospheric transport. *Journal of Geophysical Research: Atmospheres*, 99(D1):1059–1070, 1994. ISSN 0148-0227. doi: 10.1029/93JD03192. URL https://doi.org/10.1029/93JD03192. 6

S. C. Hardiman, N. Butchart, and N. Calvo. The morphology of the Brewer-Dobson circulation and its response to climate change in CMIP5 simulations. *Quarterly Journal of the Royal Meteorological Society*, 140(683):1958–1965, 2014. ISSN 00359009. doi: 10.1002/qj.2258. URL http://doi.wiley.com/10.1002/qj.2258. 11, 16, 17, 19, 21

S. C. Hardiman, N. Butchart, F. M. O'Connor, and S. T. Rumbold. The Met Office HadGEM3-ES chemistry-climate model: evaluation of stratospheric dynamics and its impact on ozone. *Geoscientific Model Development*, 10(3):1209–1232, 2017a. ISSN 1991-9603. doi: 10.5194/gmd-10-1209-2017. URL https://www.geosci-model-dev.net/10/1209/2017/. 18, 19, 22

S. C. Hardiman, P. Lin, A. A. Scaife, N. J. Dunstone, and H.-L. Ren. The influence of dynamical variability on the observed Brewer-Dobson circulation trend. *Geophysical Research Letters*, 44(6):2885–2892, 2017b. ISSN 00948276. doi: 10.1002/2017GL072706. URL http://doi.wiley.com/10.1002/2017GL072706. 11

P. Haynes. Stratospheric Dynamics. *Annual Review of Fluid Mechanics*, 37(1):263–293, 2005. ISSN 0066-4189. doi: 10.1146/annurev.fluid.37.061903.175710. URL http://www.annualreviews.org/doi/10.1146/annurev.fluid.37.061903.175710. 2, 9

P. H. Haynes and M. E. McIntyre. On the Evolution of Vorticity and Potential Vorticity in the Presence of Diabatic Heating and Frictional or Other Forces. *Journal of the Atmospheric Sciences*, 44(5):828–841, 1987. ISSN 0022-4928. doi: 10.1175/1520-0469(1987)044<0828:oteova>2.0.co;2. 4

P. H. Haynes, M. E. McIntyre, T. G. Shepherd, C. J. Marks, and K. P. Shine. On the "Downward Control" of Extratropical Diabatic Circulations by Eddy-Induced Mean Zonal Forces. *Journal of the Atmospheric Sciences*, 48 (4):651–678, 1991. ISSN 0022-4928. doi: 10.1175/1520-0469(1991)048<0651:OTCOED>2.0.CO;2. URL http://journals.ametsoc.org/doi/abs/10.1175/1520-0469{%}281991{%}29048{%}3C0651{%}3AOTCOED{%}3E2.0.CO{%}3B2. 4, 10, 13

M. I. Hegglin, D. A. Plummer, T. G. Shepherd, J. F. Scinocca, J. Anderson, L. Froidevaux, B. Funke, D. Hurst, A. Rozanov, J. Urban, T. Von Clarmann, K. A. Walker, H. J. Wang, S. Tegtmeier, and K. Weigel. Vertical structure of stratospheric water vapour trends derived from merged satellite data. *Nature Geoscience*, 7(10):768–776,

2014. ISSN 17520908. doi: 10.1038/NGEO2236. URL http://dx.doi.org/10.1038/ngeo2236. 11, 15

J. R. Holton. On the Global Exchange of Mass between the Stratosphere and Troposphere. *Journal of the Atmospheric Sciences*, 47(3): 392–395, 1990. ISSN 0022-4928. doi: 10.1175/1520-0469(1990)047<0392:OTGEOM>2.0.CO;2. URL http://journals.ametsoc.org/doi/abs/10.1175/1520-0469{%}281990{%}29047{%}3C0392{%}3AOTGEOM{%}3E2.0.CO{%}3B2. 12

J. R. Holton, P. H. Haynes, M. E. McIntyre, A. R. Douglass, R. B. Rood, and L. Pfister. Stratosphere-troposphere exchange. *Reviews of Geophysics*, 33(4):403, 1995. ISSN 8755-1209. doi: 10.1029/95RG02097. URL http://doi.wiley.com/10.1029/95RG02097. 2, 4, 7

Y. Hu and Q. Fu. Stratospheric warming in Southern Hemisphere high latitudes since 1979. *Atmospheric Chemistry and Physics*, 9(13):4329–4340, 2009. ISSN 16807324. doi: 10.5194/acp-9-4329-2009. 15

T. Iwasaki, H. Hamada, and K. Miyazaki. Comparisons of Brewer-Dobson circulations diagnosed from reanalyses. *Journal of the Meteorological Society of Japan*, 87(6): 997–1006, 2009. ISSN 00261165. doi: 10.2151/jmsj.87.997. 12

A. B. M. Jeuken, P. C. Siegmund, L. C. Heijboer, J. Feichter, and L. Bengtsson. On the potential of assimilating meteorological analyses in a global climate model for the purpose of model validation. *Journal of Geophysical Research: Atmospheres*, 101 (D12):16939–16950, 1996. ISSN 01480227. doi: 10.1029/96JD01218. URL http://doi.wiley.com/10.1029/96JD01218. 18, 22

J. H. Jiang, H. Su, C. Zhai, L. Wu, K. Minschwaner, A. M. Molod, and A. M. Tompkins. An assessment of upper troposphere and lower stratosphere water vapor in MERRA, MERRA2, and ECMWF reanalyses using Aura MLS observations. *Journal of Geophysical Research*, 120(22):11,468–11,485, 2015. ISSN 21562202. doi: 10.1002/2015JD023752. 15

C. M. Johanson and Q. Fu. Antarctic atmospheric temperature trend patterns from satellite observations. *Geophysical Research Letters*, 34(12):1–5, 2007. ISSN 00948276. doi: 10.1029/2006GL029108. 15

A. M. Kerr-Munslow and W. A. Norton. Tropical wave driving of the annual cycle in tropical tropopause temperatures. Part I: ECMWF analyses. *Journal of the Atmospheric Sciences*, 63(5):1410–1419, 2006. ISSN 00224928. doi: 10.1175/JAS3697.1. 8

H. Kida. General Circulation of Air Parcels and Transport Characteristics Derived from a hemispheric GCM- Part 1. A Determination of Advective Mass Flow in the Lower Stratosphere. *Journal of the Meteorological Society of Japan. Ser. II*, 61(2): 171–187, 1983. ISSN 0026-1165. doi: 10.2151/jmsj1965.61.2_171. URL https://www.jstage.jst.go.jp/article/jmsj1965/61/2/61{_}2{_}171/{_}article. 3, 6

J. T. Kiehl and S. Solomon. On the radiative balance of the stratosphere. *Journal of the Atmospheric Sciences*, 43(14):1525–1534, 1986. ISSN 00224928. doi: 10.1175/1520-0469(1986)043<1525:OTRBOT>2.0.CO;2. 2

D. E. Kinnison, H. S. Johnston, and D. J. Wuebbles. Model study of atmospheric transport using carbon 14 and strontium 90 as inert tracers. *Journal of Geophysical Research*, 99(D10), 1994. ISSN 01480227. doi: 10.1029/94jd01822. 3

C. Kobayashi and T. Iwasaki. Brewer-Dobson circulation diagnosed from JRA-55. *Journal of Geophysical Research: Atmospheres*, 121(4):1493–1510, 2016. ISSN 2169897X. doi: 10.1002/2015JD023476. URL http://doi.wiley.com/10.1002/2015JD023476. 13

M. Latif and N. S. Keenlyside. El Nino/Southern Oscillation response to global warming. *Proceedings of the National Academy of Sciences*, 106(49):20578–20583, 2009. ISSN 0027-8424. doi: 10.1073/pnas.0710860105. URL https://www.pnas.org/content/pnas/106/49/20578.full.pdf. 20

F. Li, J. Austin, and J. Wilson. The Strength of the Brewer–Dobson Circulation in a Changing Climate: Coupled Chemistry–Climate Model Simulations. *Journal of Climate*, 21(1):40–57, 2008. ISSN 0894-8755. doi: 10.1175/2007JCLI1663.1. URL http://journals.ametsoc.org/doi/10.1175/2007JCLI1663.1. 16, 17, 21

F. Li, P. Newman, S. Pawson, and J. Perlwitz. Effects of Greenhouse Gas Increase and Stratospheric Ozone Depletion on Stratospheric Mean Age of Air in 1960-2010. *Journal of Geophysical Research: Atmospheres*, 123(4):2098–2110, 2018. ISSN 2169897X. doi: 10.1002/2017JD027562. URL https://agupubs.onlinelibrary.wiley.com/doi/abs/10.1002/2017JD027562. 17, 21

P. Lin and Q. Fu. Changes in various branches of the Brewer-Dobson circulation from an ensemble of chemistry climate models. *Journal of Geophysical Research: Atmospheres*, 118(1):73–84, 2013. ISSN 2169897X. doi: 10.1029/2012JD018813. URL http://doi.wiley.com/10.1029/2012JD018813. xi, 16, 17, 18, 21

P. Lin, Q. Fu, S. Solomon, and J. M. Wallace. Temperature trend patterns in Southern Hemisphere high latitudes: Novel indicators of stratospheric change. *Journal of Climate*, 22(23):6325–6341, 2009. ISSN 08948755. doi: 10.1175/2009JCLI2971.1. 15

P. Lin, Y. Ming, and V. Ramaswamy. Tropical climate change control of the lower stratospheric circulation. *Geophysical Research Letters*, 42(3):941–948, 2015. ISSN 00948276. doi: 10.1002/2014GL062823. URL http://doi.wiley.com/10.1002/2014GL062823. 20, 21, 22

M. Linz, R. A. Plumb, E. P. Gerber, F. J. Haenel, G. Stiller, D. E. Kinnison, A. Ming, and J. L. Neu. The strength of the meridional overturning circulation of the stratosphere. *Nature Geoscience*, 10(9):663–667, 2017. ISSN 1752-0894. doi: 10.1038/ngeo3013. URL http://www.nature.com/articles/ngeo3013. 11

M. Linz, M. Abalos, A. S. Glanville, D. E. Kinnison, A. Ming, and J. L. Neu. The global diabatic circulation of the stratosphere as a metric for the Brewer–Dobson circulation. *Atmospheric Chemistry and Physics*, 19(7):5069–5090, 2019. ISSN 1680-7324. doi: 10.5194/acp-19-5069-2019. URL https://www.atmos-chem-phys.net/19/5069/2019/. 11, 15

M. Löffler, S. Brinkop, and P. Jöckel. Impact of major volcanic eruptions on stratospheric water vapour. *Atmospheric Chemistry and Physics*, 16(10):6547–6562, 2016. ISSN 1680-7324. doi: 10.5194/acp-16-6547-2016. URL https://www.atmos-chem-phys.net/16/6547/2016/. 18, 22

E. Mahieu, M. P. Chipperfield, J. Notholt, T. Reddmann, J. Anderson, P. F. Bernath, T. Blumenstock, M. T. Coffey, S. S. Dhomse, W. Feng, B. Franco, L. Froidevaux, D. W. T. Griffith, J. W. Hannigan, F. Hase, R. Hossaini, N. B. Jones, I. Morino, I. Murata, H. Nakajima, M. Palm, C. Paton-Walsh, J. M. R. III, M. Schneider, C. Servais, D. Smale, and K. A. Walker. Recent Northern Hemisphere stratospheric HCl increase due to atmospheric circulation changes. *Nature*, 515(7525):104–107, 2014. ISSN 0028-0836. doi: 10.1038/nature13857. URL http://www.nature.com/articles/nature13857. 11

D. R. Marsh and R. R. Garcia. Attribution of decadal variability in lower-stratospheric tropical ozone. *Geophysical Research Letters*, 34(21):L21807, 2007. ISSN 0094-8276. doi: 10.1029/2007GL030935. URL http://doi.wiley.com/10.1029/2007GL030935. 20

A. C. Maycock, W. J. Randel, A. K. Steiner, A. Y. Karpechko, J. Christy, R. Saunders, D. W. J. Thompson, C.-Z. Zou, A. Chrysanthou, N. Luke Abraham, H. Akiyoshi, A. T. Archibald, N. Butchart, M. Chipperfield, M. Dameris, M. Deushi, S. Dhomse, G. Di Genova, P. Jöckel, D. E. Kinnison, O. Kirner, F. Ladstädter, M. Michou, O. Morgenstern, F. O'Connor, L. Oman, G. Pitari, D. A. Plummer, L. E. Revell, E. Rozanov, A. Stenke, D. Visioni, Y. Yamashita, and G. Zeng. Revisiting the Mystery of Recent Stratospheric Temperature Trends. *Geophysical Research Letters*, 45(18):9919–9933, 2018. ISSN 00948276. doi: 10.1029/2018GL078035. URL http://doi.wiley.com/10.1029/2018GL078035. 14

M. McIntyre. Breaking Waves and Global-Scale Chemical Transport in the Earth's Atmosphere, with Spinoffs for the Sun's Interior. *Progress of Theoretical Physics Supplement*, 130(130):137–166, 1998. ISSN 0375-9687. doi: 10.1143/PTPS.130.137. URL https://academic.oup.com/ptps/article-lookup/doi/10.1143/PTPS.130.137. 7

M. E. McIntyre and T. N. Palmer. The 'surf zone'in the stratosphere. *Journal of atmospheric and terrestrial physics*, 46(9):825–849, 1984. ISSN 00219169. doi: 10.1016/0021-9169(84)90063-1. 4, 6

C. McLandress and T. G. Shepherd. Simulated Anthropogenic Changes in the Brewer–Dobson Circulation, Including Its Extension to High Latitudes. *Journal of*

Climate, 22(6):1516–1540, 2009. ISSN 0894-8755. doi: 10.1175/2008JCLI2679.1. URL http://journals.ametsoc.org/doi/10.1175/2008JCLI2679.1. 16, 17, 20

C. McLandress, A. I. Jonsson, D. A. Plummer, M. C. Reader, J. F. Scinocca, and T. G. Shepherd. Separating the dynamical effects of climate change and ozone depletion. Part I: Southern hemisphere stratosphere. *Journal of Climate*, 23(18):5002–5020, 2010. ISSN 08948755. doi: 10.1175/2010JCLI3586.1. 21

A. Ming, P. Hitchcock, and P. Haynes. The Double Peak in Upwelling and Heating in the Tropical Lower Stratosphere. *Journal of the Atmospheric Sciences*, 73(5): 1889–1901, 2016. ISSN 0022-4928. doi: 10.1175/JAS-D-15-0293.1. URL http://journals.ametsoc.org/doi/10.1175/JAS-D-15-0293.1. 9

K. Minschwaner, H. Su, and J. H. Jiang. The upward branch of the Brewer-Dobson circulation quantified by tropical stratospheric water vapor and carbon monoxide measurements from the Aura Microwave Limb Sounder. *Journal of Geophysical Research: Atmospheres*, 121(6):2790–2804, 2016. ISSN 2169897X. doi: 10.1002/2015JD023961. URL http://doi.wiley.com/10.1002/2015JD023961. 15, 16

K. Miyazaki, T. Iwasaki, Y. Kawatani, C. Kobayashi, S. Sugawara, and M. I. Hegglin. Inter-comparison of stratospheric mean-meridional circulation and eddy mixing among six reanalysis data sets. *Atmospheric Chemistry and Physics*, 16(10): 6131–6152, 2016. ISSN 1680-7324. doi: 10.5194/acp-16-6131-2016. URL https://www.atmos-chem-phys.net/16/6131/2016/. 13

O. Morgenstern, K. A. Stone, R. Schofield, H. Akiyoshi, Y. Yamashita, D. E. Kinnison, R. R. Garcia, K. Sudo, D. A. Plummer, J. Scinocca, L. D. Oman, M. E. Manyin, G. Zeng, E. Rozanov, A. Stenke, L. E. Revell, G. Pitari, E. Mancini, G. Di Genova, D. Visioni, S. S. Dhomse, and M. P. Chipperfield. Ozone sensitivity to varying greenhouse gases and ozone-depleting substances in CCMI-1 simulations. *Atmospheric Chemistry and Physics*, 18(2):1091–1114, 2018. ISSN 1680-7324. doi: 10.5194/acp-18-1091-2018. URL https://www.atmos-chem-phys.net/18/1091/2018/. 21

P. W. Mote, K. H. Rosenlof, E. Mcintyre, E. S. Carr, J. C. Gille, R. Holton, S. Kinnersley, H. C. Pumphrey, M. Russell, and J. W. Wal. An atmospheric tape recorder '

The imprint of tropical tropopause temperatures on stratospheric water vapor s observed phase lag agrees with the phase lag calculated assuming advection by the The phase agreement confirms the overall robustness of the calc. *Journal of Geophysical Research*, 101(95):3989–4006, 1996. ISSN 0148-0227. doi: 10.1029/95JD03422. 15

R. J. Murgatroyd and F. Singleton. Possible meridional circulations in the stratosphere and mesosphere. *Quarterly Journal of the Royal Meteorological Society*, 87(372):125–135, 1961. ISSN 00359009. doi: 10.1002/qj.49708737202. URL https://rmets.onlinelibrary.wiley.com/doi/abs/10.1002/qj.49708737202. 3, 12, 13

J. L. Neu and R. A. Plumb. Age of air in a "leaky pipe" model of stratospheric transport. *Journal of Geophysical Research: Atmospheres*, 104(D16):19243–19255, 1999. ISSN 01480227. doi: 10.1029/1999JD900251. URL https://agupubs.onlinelibrary.wiley.com/doi/abs/10.1029/1999JD900251. 6, 11

M. Niwano, K. Yamazaki, and M. Shiotani. Seasonal and QBO variations of ascent rate in the tropical lower stratosphere as inferred from UARS HALOE trace gas data. *Journal of Geophysical Research D: Atmospheres*, 108(24), 2003. ISSN 01480227. doi: 10.1029/2003jd003871. 15

S. Oberländer, U. Langematz, and S. Meul. Unraveling impact factors for future changes in the Brewer-Dobson circulation. *Journal of Geophysical Research Atmospheres*, 118(18):10296–10312, 2013. ISSN 21698996. doi: 10.1002/jgrd.50775. URL http://doi.wiley.com/10.1002/jgrd.50775. 16, 17, 21

S. Oberländer-Hayn, S. Meul, U. Langematz, J. Abalichin, and F. Haenel. A chemistry-climate model study of past changes in the Brewer-Dobson circulation. *Journal of Geophysical Research*, 120(14):6742–6757, 2015. ISSN 21562202. doi: 10.1002/2014JD022843. URL http://doi.wiley.com/10.1002/2014JD022843. 16, 17, 21

S. Oberländer-Hayn, E. P. Gerber, J. Abalichin, H. Akiyoshi, A. Kerschbaumer, A. Kubin, M. Kunze, U. Langematz, S. Meul, M. Michou, O. Morgenstern, and L. D. Oman. Is the Brewer-Dobson circulation increasing or moving upward? *Geophysical Research Letters*, 43(4):1772–1779, 2016. ISSN 19448007. doi: 10.1002/2015GL067545. URL http://doi.wiley.com/10.1002/2015GL067545. 16

M. A. Olsen, M. R. Schoeberl, and J. E. Nielsen. Response of stratospheric circulation and stratosphere-troposphere exchange to changing sea surface temperatures. *Journal of Geophysical Research*, 112(D16):D16104, 2007. ISSN 0148-0227. doi: 10.1029/2006JD008012. URL http://doi.wiley.com/10.1029/2006JD008012. 19, 20, 22

L. Oman, D. W. Waugh, S. Pawson, R. S. Stolarski, and P. A. Newman. On the influence of anthropogenic forcings on changes in the stratospheric mean age. *Journal of Geophysical Research*, 114(D3):D03105, 2009. ISSN 0148-0227. doi: 10.1029/2008JD010378. URL http://doi.wiley.com/10.1029/2008JD010378. 16, 17, 19, 20, 21

A. H. Oort and J. P. Peixóto. Global angular momentum and energy balance requirements from observations. In *Advances in Geophysics*, volume 25, pages 355–490. Elsevier, 1983. 12

C. Orbe, H. Yang, D. W. Waugh, G. Zeng, O. Morgenstern, D. E. Kinnison, J.-F. Lamarque, S. Tilmes, D. A. Plummer, J. F. Scinocca, B. Josse, V. Marecal, P. Jöckel, L. D. Oman, S. E. Strahan, M. Deushi, T. Y. Tanaka, K. Yoshida, H. Akiyoshi, Y. Yamashita, A. Stenke, L. Revell, T. Sukhodolov, E. Rozanov, G. Pitari, D. Visioni, K. A. Stone, R. Schofield, and A. Banerjee. Large-scale tropospheric transport in the Chemistry–Climate Model Initiative (CCMI) simulations. *Atmospheric Chemistry and Physics*, 18(10):7217–7235, 2018. ISSN 1680-7324. doi: 10.5194/acp-18-7217-2018. URL https://www.atmos-chem-phys.net/18/7217/2018/. 22

A. Orr, T. J. Bracegirdle, J. S. Hosking, W. Feng, H. K. Roscoe, and J. D. Haigh. Strong dynamical modulation of the cooling of the polar stratosphere associated with the antarctic ozone hole. *Journal of Climate*, 26(2):662–668, 2013. ISSN 08948755. doi: 10.1175/JCLI-D-12-00480.1. 21

A. Ossó, Y. Sola, K. Rosenlof, B. Hassler, J. Bech, and J. Lorente. How robust are trends in the Brewer-Dobson circulation derived from observed stratospheric temperatures? *Journal of Climate*, 28(8):3024–3040, 2015. ISSN 08948755. doi: 10.1175/JCLI-D-14-00295.1. 14, 15

F. M. Palmeiro, N. Calvo, and R. R. Garcia. Future Changes in the Brewer–Dobson Circulation under Different Greenhouse Gas Concentrations in WACCM4. *Journal of the Atmospheric Sciences*, 71(8):2962–2975, 2014. ISSN 0022-4928. doi: 10.1175/jas-d-13-0289.1. URL http://journals.ametsoc.org/doi/abs/10.1175/JAS-D-13-0289.1. 17

F. Ploeger and T. Birner. Seasonal and inter-annual variability of lower stratospheric age of air spectra. *Atmospheric Chemistry and Physics*, 16(15):10195–10213, 2016. ISSN 1680-7324. doi: 10.5194/acp-16-10195-2016. URL https://www.atmos-chem-phys.net/16/10195/2016/. 11

F. Ploeger, M. Abalos, T. Birner, P. Konopka, B. Legras, R. Müller, and M. Riese. Quantifying the effects of mixing and residual circulation on trends of stratospheric mean age of air. *Geophysical Research Letters*, 42(6):2047–2054, 2015a. ISSN 00948276. doi: 10.1002/2014GL062927. URL http://doi.wiley.com/10.1002/2014GL062927. 11, 12

F. Ploeger, M. Riese, F. Haenel, P. Konopka, R. Müller, and G. Stiller. Variability of stratospheric mean age of air and of the local effects of residual circulation and eddy mixing. *Journal of Geophysical Research: Atmospheres*, 120(2):716–733, 2015b. ISSN 2169897X. doi: 10.1002/2014JD022468. URL http://doi.wiley.com/10.1002/2014JD022468. 11

R. A. Plumb. Stratospheric Transport. *Journal of the Meteorological Society of Japan. Ser. II*, 80(4B):793–809, 2002. ISSN 0026-1165. doi: 10.2151/jmsj.80.793. URL https://www.jstage.jst.go.jp/article/jmsj/80/4B/80{_}4B{_}793/{_}article. xi, 3, 4, 7, 8

R. A. Plumb. Tracer interrelationships in the stratosphere. *Reviews of Geophysics*, 45 (4):1–33, 2007. ISSN 87551209. doi: 10.1029/2005RG000179. 6

R. A. Plumb and J. Eluszkiewicz. The Brewer–Dobson Circulation: Dynamics of the Tropical Upwelling. *Journal of the Atmospheric Sciences*, 56(6): 868–890, 1999. ISSN 0022-4928. doi: 10.1175/1520-0469(1999)056<0868:TBDCDO>2.0.CO;2. URL http://journals.ametsoc.org/doi/abs/10.1175/1520-0469{%}281999{%}29056{%}3C0868{%}3ATBDCDO{%}3E2.0.CO{%}3B2. 8, 9

L. Polvani, L. Wang, M. Abalos, N. Butchart, M. Chipperfield, M. Dameris, M. Deushi, S. Dhomse, P. Jöckel, D. Kinnison, M. Michou, O. Morgenstern, L. Oman, D. Plummer, and K. Stone. Large impacts, past and future, of ozone-depleting substances on Brewer-Dobson circulation trends: A multi-model assessment. *Journal of Geophysical Research: Atmospheres*, page 2018JD029516, 2019. ISSN 2169-897X. doi: 10.1029/2018JD029516. URL https://onlinelibrary.wiley.com/doi/abs/10.1029/2018JD029516. 16, 21

L. M. Polvani, L. Wang, V. Aquila, and D. W. Waugh. The impact of ozone-depleting substances on tropical upwelling, as revealed by the absence of lower-stratospheric cooling since the late 1990s. *Journal of Climate*, 30(7):2523–2534, 2017. ISSN 08948755. doi: 10.1175/JCLI-D-16-0532.1. URL http://journals.ametsoc.org/doi/10.1175/JCLI-D-16-0532.1. 16, 21

L. M. Polvani, M. Abalos, R. Garcia, D. Kinnison, and W. J. Randel. Significant Weakening of Brewer-Dobson Circulation Trends Over the 21st Century as a Consequence of the Montreal Protocol. *Geophysical Research Letters*, 45(1):401–409, 2018. ISSN 00948276. doi: 10.1002/2017GL075345. URL http://doi.wiley.com/10.1002/2017GL075345. 16, 21

V. Ramaswamy, M. D. Schwarzkopf, and K. P. Shine. Radiative forcing of climate from halocarbon-induced global stratospheric ozone loss. *Nature*, 355(6363):810–812, 1992. ISSN 0028-0836. doi: 10.1038/355810a0. URL http://www.nature.com/articles/355810a0. 2

W. J. Randel, F. Wu, H. Vömel, G. E. Nedoluha, and P. Forster. Decreases in stratospheric water vapor after 2001: Links to changes in the tropical tropopause and the Brewer-Dobson circulation. *Journal of Geophysical Research Atmospheres*, 111(12): 1–11, 2006. ISSN 01480227. doi: 10.1029/2005JD006744. 14

W. J. Randel, R. Garcia, and F. Wu. Dynamical Balances and Tropical Stratospheric Upwelling. *Journal of the Atmospheric Sciences*, 65(11):3584–3595, 2008. ISSN 0022-4928. doi: 10.1175/2008JAS2756.1. URL http://journals.ametsoc.org/doi/10.1175/2008JAS2756.1. 8

W. J. Randel, R. R. Garcia, N. Calvo, and D. Marsh. ENSO influence on zonal mean temperature and ozone in the tropical lower stratosphere. *Geophysical Research Letters*, 36(15):n/a–n/a, 2009. ISSN 00948276. doi: 10.1029/2009GL039343. URL http://doi.wiley.com/10.1029/2009GL039343. 20

W. J. Randel, A. K. Smith, F. Wu, C. Z. Zou, and H. Qian. Stratospheric temperature trends over 1979-2015 derived from combined SSU, MLS, and SABER satellite observations. *Journal of Climate*, 29(13):4843–4859, 2016. ISSN 08948755. doi: 10.1175/JCLI-D-15-0629.1. 21

E. A. Ray, F. L. Moore, K. H. Rosenlof, S. M. Davis, C. Sweeney, P. Tans, T. Wang, J. W. Elkins, H. Bönisch, A. Engel, S. Sugawara, T. Nakazawa, and S. Aoki. Improving stratospheric transport trend analysis based on SF6 and CO2 measurements. *Journal of Geophysical Research*, 119(24):14,110–14,128, 2014. ISSN 21562202. doi: 10.1002/2014JD021802. URL http://doi.wiley.com/10.1002/2014JD021802. 11

D. Rind, R. Suozzo, N. K. Balachandran, and M. J. Prather. Climate Change and the Middle Atmosphere. Part I: The Doubled CO2 Climate. *Journal of the Atmospheric Sciences*, 47(4):475–494, 1990. ISSN 0022-4928. doi: 10.1175/1520-0469(1990)047<0475:CCATMA>2.0.CO;2. URL http://journals.ametsoc.org/doi/abs/10.1175/1520-0469{%}281990{%}29047{%}3C0475{%}3ACCATMA{%}3E2.0.CO{%}3B2. 19

K. H. Rosenlof. Seasonal cycle of the residual mean meridional circulation in the stratosphere. *Journal of Geophysical Research*, 100(D3):5173, 1995. ISSN 0148-0227. doi: 10.1029/94JD03122. URL http://doi.wiley.com/10.1029/94JD03122. 8, 10, 11, 12

K. H. Rosenlof and J. R. Holton. Estimates of the stratospheric residual circulation using the downward control principle. *Journal of Geophysical Research*, 98(D6):10465, 1993. ISSN 0148-0227. doi: 10.1029/93jd00392. URL http://doi.wiley.com/10.1029/93JD00392. 10, 11, 12

K. H. Rosenlof and G. C. Reid. Trends in the temperature and water vapor content of the tropical lower stratosphere: Sea surface connection. *Journal of Geophysical Research Atmospheres*, 113(6):1–15, 2008. ISSN 01480227. doi: 10.1029/2007JD009109. 14

A. Schmidt, M. J. Mills, S. Ghan, J. M. Gregory, R. P. Allan, T. Andrews, C. G. Bardeen, A. Conley, P. M. Forster, A. Gettelman, R. W. Portmann, S. Solomon, and O. B. Toon. Volcanic Radiative Forcing From 1979 to 2015. *Journal of Geophysical Research: Atmospheres*, 123(22):12491–12508, 2018. ISSN 2169-897X. doi: 10.1029/2018JD028776. URL https://onlinelibrary.wiley.com/doi/abs/10.1029/2018JD028776. 18, 22

H. Schmidt, S. Rast, F. Bunzel, M. Esch, M. Giorgetta, S. Kinne, T. Krismer, G. Stenchikov, C. Timmreck, L. Tomassini, and M. Walz. Response of the middle atmosphere to anthropogenic and natural forcings in the CMIP5 simulations with the Max Planck Institute Earth system model. *Journal of Advances in Modeling Earth Systems*, 5(1):98–116, 2013. ISSN 19422466. doi: 10.1002/jame.20014. 16, 17

M. R. Schoeberl, A. R. Douglas, R. S. Stolarski, S. Pawson, S. E. Strahan, and W. Read. Comparison of lower stratospheric tropical mean vertical velocities. *Journal of Geophysical Research Atmospheres*, 113(24):1–11, 2008. ISSN 01480227. doi: 10.1029/2008JD010221. 15

M. J. Schwartz, A. Lambert, G. L. Manney, W. G. Read, N. J. Livesey, L. Froidevaux, C. O. Ao, P. F. Bernath, C. D. Boone, R. E. Cofield, W. H. Daffer, B. J. Drouin, E. J. Fetzer, R. A. Fuller, R. F. Jarnot, J. H. Jiang, Y. B. Jiang, B. W. Knosp, K. Krüger, J.-L. F. Li, M. G. Mlynczak, S. Pawson, J. M. Russell, M. L. Santee, W. V. Snyder, P. C. Stek, R. P. Thurstans, A. M. Tompkins, P. A. Wagner, K. A. Walker, J. W. Waters, and D. L. Wu. Validation of the Aura Microwave Limb Sounder temperature and geopotential height measurements. *Journal of Geophysical Research*, 113(D15): 1–23, 2008. ISSN 0148-0227. doi: 10.1029/2007jd008783. 15

D. J. Seidel and W. J. Randel. Recent widening of the tropical belt: Evidence from tropopause observations. *Journal of Geophysical Research*, 112(D20):D20113, 2007. ISSN 0148-0227. doi: 10.1029/2007JD008861. URL http://doi.wiley.com/10.1029/2007JD008861. 18

D. J. Seidel, Q. Fu, W. J. Randel, and T. J. Reiohler. Widening of the tropical belt in a changing climate. *Nature Methods*, 1(1):21–24, 2008. ISSN 15487105. doi: 10.1038/ngeo.2007.38. 18

K. Semeniuk and T. G. Shepherd. Mechanisms for Tropical Upwelling in the Stratosphere. *Journal of the Atmospheric Sciences*, 58(21):3097–3115, 2001. ISSN 0022-4928. doi: 10.1175/1520-0469(2001)058<3097:MFTUIT>2.0.CO;2. URL http://journals.ametsoc.org/doi/abs/10.1175/1520-0469{%}282001{%}29058{%}3C3097{%}3AMFTUIT{%}3E2.0.CO{%}3B2. 8

W. J. M. Seviour, N. Butchart, and S. C. Hardiman. The Brewer-Dobson circulation inferred from ERA-Interim. *Quarterly Journal of the Royal Meteorological Society*, 138(665):878–888, 2012. ISSN 00359009. doi: 10.1002/qj.966. URL http://doi.wiley.com/10.1002/qj.966. 13

T. G. Shepherd and C. McLandress. A Robust Mechanism for Strengthening of the Brewer–Dobson Circulation in Response to Climate Change: Critical-Layer Control of Subtropical Wave Breaking. *Journal of the Atmospheric Sciences*, 68 (4):784–797, 2011. ISSN 0022-4928. doi: 10.1175/2010JAS3608.1. URL http://journals.ametsoc.org/doi/10.1175/2010JAS3608.1. 16, 17, 20

M. Sigmond and T. G. Shepherd. Compensation between Resolved Wave Driving and Parameterized Orographic Gravity Wave Driving of the Brewer–Dobson Circulation and Its Response to Climate Change. *Journal of Climate*, 27(14):5601–5610, 2014. ISSN 0894-8755. doi: 10.1175/JCLI-D-13-00644.1. URL http://journals.ametsoc.org/doi/10.1175/JCLI-D-13-00644.1. 16

M. Sigmond, P. C. Siegmund, E. Manzini, and H. Kelder. A Simulation of the Separate Climate Effects of Middle-Atmospheric and Tropospheric CO 2 Doubling. *Journal of Climate*, 17(12):2352–2367, 2004. ISSN 0894-8755. doi: 10.1175/1520-0442(2004)017<2352:ASOTSC>2.0.CO;2. URL http://journals.ametsoc.org/doi/abs/10.1175/1520-0442{%}282004{%}29017{%}3C2352{%}3AASOTSC{%}3E2.0.CO{%}3B2. 20, 22

I. R. Simpson, T. G. Shepherd, and M. Sigmond. Dynamics of the Lower Stratospheric Circulation Response to ENSO. *Journal of the Atmospheric Sciences*, 68(11):2537–2556, 2011. ISSN 0022-4928. doi: 10.1175/JAS-D-11-05.1. URL http://journals.ametsoc.org/doi/10.1175/JAS-D-11-05.1. 20, 23

S. Solomon, D. Kinnison, J. Bandoro, and R. Garcia. Simulation of polar ozone depletion: An update. *Journal of Geophysical Research: Atmospheres*, 120(15): 7958–7974, 2015. ISSN 2169-897X. doi: 10.1002/2015JD023365. URL https://onlinelibrary.wiley.com/doi/abs/10.1002/2015JD023365. 18

S. Solomon, D. Kinnison, R. R. Garcia, J. Bandoro, M. Mills, C. Wilka, R. R. Neely, A. Schmidt, J. E. Barnes, J.-P. Vernier, and M. Höpfner. Monsoon circulations and tropical heterogeneous chlorine chemistry in the stratosphere. *Geophysical Research Letters*, 43(24):12,624–12,633, 2016. ISSN 00948276. doi: 10.1002/2016GL071778. URL http://doi.wiley.com/10.1002/2016GL071778. 18, 19, 22

SPARC. SPARC CCMVal Report on the Evaluation of Chemistry-Climate Models. V. Eyring, T. Shepherd and D. Waugh (Eds.). *SPARC Report No. 5, WCRP-30/2010,WMO/TD-No.40*, 2010. ISSN 1428-345X. URL http://www.sparc-climate.org/publications/sparc-reports/sparc-report-no5/. 10, 16, 17, 19, 20

P. W. Staten, J. Lu, K. M. Grise, S. M. Davis, and T. Birner. Re-examining tropical expansion. *Nature Climate Change*, 8(9):768–775, 2018. ISSN 17586798. doi: 10.1038/s41558-018-0246-2. URL http://dx.doi.org/10.1038/s41558-018-0246-2. 18

G. P. Stiller, T. von Clarmann, F. Haenel, B. Funke, N. Glatthor, U. Grabowski, S. Kellmann, M. Kiefer, A. Linden, S. Lossow, and M. López-Puertas. Observed temporal evolution of global mean age of stratospheric air for the 2002 to 2010 period. *Atmospheric Chemistry and Physics*, 12(7):3311–3331, 2012. ISSN 1680-7324. doi: 10.5194/acp-12-3311-2012. URL https://www.atmos-chem-phys.net/12/3311/2012/. 11

K. Telegadas. The Relationship Between Stratospheric Circulation Patterns and Radioactive Debris in Early 1963. *Journal of Applied Meteorology*, 6(1):134–141, 1967. ISSN 0021-8952. doi: 10.1175/1520-0450(1967)006<0134:trbscp>2.0.co;2. 3

K. Telegadas. The seasonal atmospheric distribution and inventories of excess carbon-14 from March 1955 to July 1969. *Report HASL*, 243:12–187, 1971. 3

K. Telegadas, J. Gray Jr, R. E. Sowl, and T. E. Ashenfelter. Carbon-14 Measurements in the Stratosphere from a Balloon-borne Molecular Sieve Sampler. *Rep*, 246:69–106, 1972. 3

P. J. Telford, P. Braesicke, O. Morgenstern, and J. A. Pyle. Technical Note: Description and assessment of a nudged version of the new dynamics Unified Model. *Atmospheric Chemistry and Physics*, 8(6):1701–1712, 2008. ISSN 1680-7324. doi: 10.5194/acp-8-1701-2008. URL https://www.atmos-chem-phys.net/8/1701/2008/. 22

D. W. Thompson and S. Solomon. Recent stratospheric climate trends as evidenced in radiosonde data: Global structure and tropospheric linkages. *Journal of Climate*, 18 (22):4785–4795, 2005. ISSN 08948755. doi: 10.1175/JCLI3585.1. 14

D. W. Thompson and S. Solomon. Understanding recent stratospheric climate change. *Journal of Climate*, 22(8):1934–1943, 2009. ISSN 08948755. doi: 10.1175/2008JCLI2482.1. 14

D. W. Thompson and J. M. Wallace. Annular modes in the extratropical circulation. Part I: Month-to-month variability. *Journal of Climate*, 13(5):1000–1016, 2000. ISSN 08948755. doi: 10.1175/1520-0442(2000)013<1000:AMITEC>2.0.CO;2. 2

D. W. Thompson, D. J. Seidel, W. J. Randel, C. Z. Zou, A. H. Butler, C. Mears, A. Osso, C. Long, and R. Lin. The mystery of recent stratospheric temperature trends. *Nature*, 491(7426):692–697, 2012. ISSN 00280836. doi: 10.1038/nature11579. URL http://www.ncbi.nlm.nih.gov/pubmed/23192146. 14

M. K. van Aalst, M. M. P. van den Broek, A. Bregman, C. Brühl, B. Steil, G. C. Toon, S. Garcelon, G. M. Hansford, R. L. Jones, T. D. Gardiner, G. J. Roelofs, J. Lelieveld, and P. Crutzen. Trace gas transport in the 1999/2000 Arctic winter: comparison of nudged GCM runs with observations. *Atmospheric Chemistry and Physics*, 4(1):81–93, 2004. ISSN 1680-7324. doi: 10.5194/acp-4-81-2004. URL http://www.atmos-chem-phys.net/4/81/2004/. 18

D. G. Vincent. Mean meridional circulations in the Northern Hemisphere lower stratosphere during 1964 and 1965. *Quarterly Journal of the Royal Meteorological Society*, 94(401):333–349, 1968. ISSN 0035-9009. doi: 10.1002/qj.49709440109. URL https://doi.org/10.1002/qj.49709440109. 3, 12

D. Waugh. The age of stratospheric air. *Nature Geoscience*, 2(1):14–16, 2009. ISSN 1752-0894. doi: 10.1038/ngeo397. URL http://www.nature.com/doifinder/10.1038/ngeo397. 11

D. Waugh and T. Hall. Age of stratospheric air : Theory, observations, and models. *Reviews of Geophysics*, 40(4):1–26, 2002. ISSN 8755-1209. doi: 10.1029/2000RG000101. URL http://doi.wiley.com/10.1029/2000RG000101. 6

WMO. (World Meteorological Organization), Scientific Assessment of Ozone Depletion: 2014, Global Ozone Research and Monitoring Project – Report No. 55. Technical report, Geneva, Switzerland, 2014. xi, 5

WMO. (World Meteorological Organization), Scientific Assessment of Ozone Depletion: 2018, Global Ozone Research and Monitoring Project – Report No. 58. Technical report, Geneva, Switzerland, 2018. 7, 12

P. J. Young, K. H. Rosenlof, S. Solomon, S. C. Sherwood, Q. FU, and J. F. Lamarque. Changes in stratospheric temperatures and their implications for changes: In the brewer-dobson circulation, 1979-2005. *Journal of Climate*, 25(5):1759–1772, 2012. ISSN 08948755. doi: 10.1175/2011JCLI4048.1. URL http://journals.ametsoc.org/doi/abs/10.1175/2011JCLI4048.1. 14, 15

E. Yulaeva, J. R. Holton, and J. M. Wallace. On the Cause of the Annual Cycle in Tropical Lower-Stratospheric Temperatures. *Journal of the Atmospheric Sciences*, 51(2):169–174, 1994. ISSN 0022-4928. doi: 10.1175/1520-0469(1994)051<0169:OTCOTA>2.0.CO;2. URL http://journals.ametsoc.org/doi/abs/10.1175/1520-0469{%}281994{%}29051{%}3C0169{%}3AOTCOTA{%}3E2.0.CO{%}3B2. 14, 15

Chapter 2

The effect of atmospheric nudging on the stratospheric residual circulation in chemistry-climate models

Authors: **Andreas Chrysanthou, Amanda C. Maycock, Martyn P. Chipperfield, Sandip Dhomse, Hella Garny, Douglas Kinnison, Hideharu Akiyoshi, Makoto Deushi, Rolando R. Garcia, Patrick Jöckel, Oliver Kirner, Giovanni Pitari, David A. Plummer, Laura Revell, Eugene Rozanov, Andrea Stenke, Taichu Y. Tanaka, Daniele Visioni, and Yousuke Yamashita**

Abstract

We perform the first multi-model intercomparison of the impact of nudged meteorology on the stratospheric residual circulation using hindcast simulations from the Chemistry-Climate Model Initiative (CCMI). We examine simulations over the period 1980-2009 from seven models in which the meteorological fields are nudged towards a reanalysis dataset and compare these with their equivalent free-running simulations and the reanalyses themselves. We show that for the current implementations, nudging mete-

orology does not constrain the mean strength of the stratospheric residual circulation and that the inter-model spread is similar, or even larger, than in the free-running simulations. The nudged models generally show slightly stronger upwelling in the tropical lower stratosphere compared to the free-running versions and exhibit marked differences compared to the directly estimated residual circulation from the reanalysis dataset they are nudged towards. Downward control calculations applied to the nudged simulations reveal substantial differences between the climatological lower stratospheric tropical upward mass flux (TUMF) computed from the modelled wave forcing and that calculated directly from the residual circulation. This explicitly shows that nudging decouples the wave forcing and the residual circulation so that the divergence of the angular momentum flux due to the mean motion is not balanced by eddy motions, as would typically be expected in the time mean. Overall, nudging meteorological fields leads to increased intermodel spread for most of the measures of the mean climatological stratospheric residual circulation assessed in this study. In contrast, the nudged simulations show a high degree of consistency in the inter-annual variability in the TUMF in the lower stratosphere, which is primarily related to the contribution to variability from the resolved wave forcing. The more consistent inter-annual variability in TUMF in the nudged models also compares more closely with the variability found in the reanalyses, particularly in boreal winter. We apply a multiple linear regression (MLR) model to separate the drivers of inter-annual and long-term variations in the simulated TUMF; this explains up to $\sim 75\%$ of the variance in TUMF in the nudged simulations. The MLR model reveals a statistically significant positive trend in TUMF for most models over the period 1980-2009. The TUMF trend magnitude is generally larger in the nudged models compared to their free-running counterparts, but the intermodel range of trends doubles from around a factor of 2 to a factor of 4 due to nudging. Furthermore, the nudged models generally do not match the TUMF trends in the reanalysis they are nudged towards for trends over different periods in the interval 1980-2009. Hence, we conclude that nudging does not strongly constrain long-term trends simulated by the chemistry-climate model (CCM) in the residual circulation. Our findings show that while nudged simulations may, by construction, produce accurate temperatures and realistic representations of fast horizontal transport, this is not typically the case for the slower zonal mean vertical transport in the stratosphere. Consequently, caution

is required when using nudged simulations to interpret the behaviour of stratospheric tracers that are affected by the residual circulation.

2.1 Introduction

The Brewer-Dobson circulation (BDC) is characterised by upwelling of air in the tropics, poleward flow in the stratosphere, and downwelling at mid-latitudes and high latitudes. The circulation can be separated into two branches: the shallow branch in the lower stratosphere and the deep branch in the middle stratosphere and upper stratosphere (Plumb 2002; Birner and Bönisch 2011). The BDC affects the distribution of trace species in the stratosphere, such as ozone, and its strength partly determines the lifetimes of long-lived gases such as chlorofluorocarbons (CFCs; Butchart and Scaife 2001). It also determines stratosphere-to-troposphere exchange of ozone (Hegglin and Shepherd, 2009), which is important for the tropospheric ozone budget (Wild, 2007). In the tropical lower stratosphere, where the photochemical lifetime of ozone is long, variations and trends in the strength of the BDC are the main drivers of ozone within the annual cycle (Weber et al., 2011) for inter-annual and longer-term variability (Randel and Thompson, 2011) and in response to climate change (e.g. Keeble et al. 2017). Here we focus on the advective part of the BDC, or the residual circulation, which is driven by wave breaking in the stratosphere from planetary-scale Rossby waves and gravity waves (Holton et al., 1995). It is important to note that the overall tracer transport in the stratosphere is also affected by turbulent eddy mixing, which has been evaluated separately in previous studies (Garny et al. 2014; Ploeger et al. 2015a,b; Dietmüller et al. 2018; Eichinger et al. 2019; Šácha et al. 2019). The residual circulation is commonly evaluated in model (Butchart et al., 2010, 2011) and reanalysis (Abalos et al., 2015; Kobayashi and Iwasaki, 2016) studies using the transformed Eulerian mean circulation (TEM; Andrews and McIntyre, 1976, 1978; Andrews et al., 1987).

Past studies have shown substantial spread across chemistry-climate models (CCMs) in the mean strength of the residual circulation (e.g. Butchart et al., 2010). Nevertheless, CCMs consistently simulate a long-term strengthening of the residual circulation with an increase of $\sim 2\%$ per decade (e.g. Butchart et al., 2010; Hardiman et al., 2014), though there are differences across models in the relative contribution to trends from

resolved and parameterised wave forcing. Reanalysis datasets also suggest a strengthening of the residual circulation over the past few decades of the order of 2% per decade to 5% per decade (Abalos et al., 2015; Miyazaki et al., 2016), apart from one dataset (ERA-Interim - ERA-I) which shows a weakening of both branches of the BDC (Seviour et al., 2012, Abalos et al., 2015). However, reanalyses are subject to multiple caveats, particularly in their suitability for trend studies, and there can be substantial differences in residual circulation trends calculated from the same reanalysis using different methods (Abalos et al., 2015).

Given the limitations of reanalyses, evaluating the fidelity of model estimates of residual circulation variability and trends is challenging, since there are no direct measurements of the residual circulation. The only direct estimates of the stratospheric mass circulation come from tracer measurements, which can be used to calculate the stratospheric age of air (AoA; Kida, 1983; Schmidt and Khedim, 1991; Waugh and Hall, 2002). The AoA represents the combined effects of advection and mixing processes and as such cannot be directly related to the residual circulation. While progress has been made in separating the relative effects of advection and mixing for the AoA calculated from models (Garny et al., 2014; Dietmüller et al., 2018; Eichinger et al., 2019; Šácha et al., 2019) from Lagrangian models driven by reanalysis data (Ploeger and Birner, 2016; Ploeger et al., 2015a,b, 2019), and comparing the effects in both CCMs and Lagrangian models (Dietmüller et al., 2017), this is more difficult to achieve in observations. Engel et al. (2009) used balloon-borne measurements of stratospheric trace gases and found a statistically non-significant increase in the AoA in the middle stratosphere at northern mid-latitudes; this has been corroborated in a more recent study using longer measurement records at two mid-latitude sites in the Northern Hemisphere (NH; Engel et al., 2017). It has been hypothesized based on analyses of recent satellite tracer datasets, which have greater spatial and temporal coverage, that sub-tropical AoA trends can be explained by a weakening of the mixing barriers at the edge of the tropical pipe (Neu and Plumb, 1999) that is masking the effects of an increase in tropical upwelling on the AoA (Stiller et al., 2012; Haenel et al., 2015). In contrast with AoA trends derived from observations, CCMs forced with observed sea-surface temperatures (SSTs), greenhouse gases, and ozone-depleting substances (ODSs) show a decrease in the AoA throughout the stratosphere (Karpechko and Maycock, 2018; Li et al., 2018; Morgenstern et al.,

2018; Abalos et al., 2019; Polvani et al., 2019). Theoretical approaches based on the tropical leaky pipe model (Neu and Plumb, 1999) have shown promise for bridging the information on the stratospheric circulation derived from observations with outputs from general circulation models (GCMs) and CCMs (Ray et al., 2016), but differences remain (Karpechko and Maycock, 2018).

More recent theoretical developments offer a means of calculating the diabatic circulation using stratospheric tracers (Linz et al., 2017), which is a promising avenue, as this is more closely related to the residual circulation than the AoA. Linz et al. (2017) showed consistent estimates of the diabatic circulation in the lower stratosphere based on two independent satellite tracer datasets but identified large uncertainties of up to a factor of 2 in the mean circulation strength in the upper stratosphere. Hence, the available tracer datasets are not yet suitable for characterizing trends in the diabatic circulation using these methods. Targeted measurement strategies to better characterize long-term changes in the stratospheric meridional circulation have been proposed (Moore et al., 2014; Ray et al., 2016).

In an attempt to obtain a closer comparison with observed stratospheric trace species, some studies have used model simulations with meteorological fields nudged or relaxed towards analysis or reanalysis datasets (Jeuken et al., 1996). These include studies of stratospheric ozone variability and trends (e.g. van Aalst et al., 2004; Solomon et al., 2016; Hardiman et al., 2017a; Ball et al., 2018) and comparisons between models and satellite-based multi-species observational records (Froidevaux et al., 2019), in particular focusing on specific meteorological events such as the sudden stratospheric warming in the 2009-2010 winter (Akiyoshi et al., 2016) as well as the chemical and climatic effects of volcanic eruptions (Löffler et al., 2016; Solomon et al., 2016; Schmidt et al., 2018). Nudged simulations have also been used to study mechanisms for dynamical coupling between the stratosphere and troposphere (Hitchcock and Simpson, 2014) and to examine the effects of different regions on atmospheric predictability (e.g. Douville, 2009; Jung et al., 2010). Nudging involves adding additional tendencies to the model equations to constrain the modelled variables. Nudged variables can include horizontal winds (or divergence and vorticity), temperature, surface pressure, and latent and sensible heat fluxes. However, vertical winds, which are a small residual from horizontal

divergence, are not nudged, and the underlying model physics can yield quite different results from the datasets they are nudged towards (Telford et al., 2008; Hardiman et al., 2017a).

The approach of nudging a CCM towards reanalysis data follows a similar philosophy to traditional offline chemical transport models (CTMs), though there are fundamental differences between these types of models in terms of their tracer advection. CTMs need to match the mass transport with the evolution of the pressure field. This can be done exactly in isobaric coordinates (often used in the stratosphere) but requires a correction in regions where grid box mass changes (e.g. as surface pressure changes). CCMs are less affected by this mass-wind inconsistency than CTMs (Jöckel et al., 2001), but nudging will add forcings that are inconsistent with the model state. CTMs use the full 3-D circulation from the analyses and reanalyses directly and have been widely developed and used over the past few decades (e.g. Rood et al., 1989; Chipperfield et al., 1994; Lefèvre et al., 1994). They have proven to be very successful at simulating stratospheric tracers on a range of timescales (Chipperfield, 1999), including decadal changes (Mahieu et al., 2014). However, this success has been built on extensive testing of the optimum way to use the reanalysis data to force the CTMs. For example, Chipperfield (2006) showed how different approaches to calculating the vertical velocity in the TOMCAT/SLIMCAT model could lead to very different distributions of stratospheric age of air, while (Monge-Sanz et al., 2013a) compared the performance of different European Centre for Medium-Range Weather Forecasts (ECMWF) analyses within the same CTM framework. Krol et al. (2018) recently provided a summary of how current CTMs intercompare for tracer calculations. Monge-Sanz et al. (2013b) compared the approaches of using ECMWF analyses directly in a CTM with the ECMWF CCM nudged using the same analyses. They found that the CTM and nudged CCM were consistent in showing a degraded performance when using older ERA-40 reanalysis compared to the later ERA-Interim. However, they also showed some differences between CTM and nudged-CCM tracers using the same analyses, with the nudged CCM showing stronger upward motion in the tropical stratosphere. Therefore, with regards to the slow residual circulation, one cannot assume that a nudged CCM will behave in a similar way to a CTM even when using the same meteorological analyses. Recently, Ball et al. (2018) showed two nudged CCMs which failed to capture the observed variations

in the lower-stratospheric ozone as measured by satellite observations, while Chipperfield et al. (2018), using the TOMCAT CTM, simulated a better agreement of modelled ozone variations with the observations. Overall, the success of some CTM simulations in simulating long-lived stratospheric tracers has been built on many years of model development and testing. In contrast, nudged CCMs are much newer tools and have not yet been evaluated to the same extent. A recent study by Orbe et al. (2018) analysed tropospheric tracers in nudged-CCM simulations and found large differences in the distributions of the tracers, which could be partly traced to differences in the model convection schemes. They urged users to adopt a cautious approach when interpreting tracers in nudged simulations given their dependence not only on large-scale flow but also on sub-grid parameterisations. However, a critical evaluation of the stratospheric residual circulation in nudged-CCM simulations has been lacking to date.

To examine the effect of nudging on the stratospheric residual circulation this study compares hindcast simulations from free-running and nudged versions of the same models that participated in the phase 1 of the Chemistry-Climate Model Initiative (CCMI; Morgenstern et al., 2017). Nudged experiments were not performed in previous chemistry-climate multi-model comparisons (Chemistry- Climate Model Validation Activity 2; CCMVal-2), so CCMI offers a timely opportunity to evaluate the effect of nudging on simulated mean biases, variability, and long-term trends in the residual circulation. For completeness, we also present a comparison between the nudged simulations and the reanalysis datasets the models are nudged towards. The paper is laid out as follows. Section 2.2 describes the CCMI and the reanalysis data used in the present study along with the diagnostics for the residual circulation; Sect. 2.3 presents results covering the mean circulation, annual cycle, inter-annual variability, and trends; and Sect. 2.4 summarizes the results and discusses the implications for using nudged simulations to study aspects of the observational record.

2.2 Data and methods

2.2.1 Models and experiments

CCMI is the successor activity to CCMVal-2 and the Atmospheric Chemistry and Climate Model Intercomparison Project (ACCMIP; Lamarque et al., 2013). We use the

hindcast free-running simulations, REF-C1, and the nudged specified dynamics simulations, REF-C1SD, which cover the periods 1960 – 2009 and 1980 – 2009, respectively. Here we analyse the common 30-year period 1980 – 2009 that was run by all models for both experiments with prescribed observed SSTs and sea ice concentrations. The CCMI data were downloaded from the British Atmospheric Data Centre (Hegglin and Lamarque, 2015). For an extensive overview of the CCMI models, see Morgenstern et al. (2017). We analyse those CCMI models (Table 2.1) that output the necessary TEM diagnostics.

Model name	Reference(s)	Resolution	Top level	REF-C1 ensemble members	Coord. sys.	NOGWD reference
CCSRNIES-MIROC3.2	Imai et al. (2013), Akiyoshi et al. (2016)	T42, L34	1.2 Pa	3	TP	Hines (1997b)
CESM1-WACCM	Marsh et al. (2013), Solomon et al. (2015), Garcia et al. (2017)	1.9° × 2.5°, L66	140 km	5	TP	Beres (2005), Richter et al. (2010)
CMAM (v2.1)	Jonsson et al. (2004) Scinocca et al. (2008)	T47, L71	0.08 Pa	3	TP	Scinocca (2003)
EMAC (v2.51; L47 & L90)	Jöckel et al. (2010, 2016)	T42, L47, L90	1Pa	2	TP	Hines (1997a,b)
GEOSCCM	Molod et al. (2012, 2015) Oman et al. (2011, 2013)	∼ 2° × 2°, L72	1.5 Pa	1	TP	Garcia and Boville (1994)
MRI-ESM1r1	Yukimoto et al. (2011, 2012) Deushi and Shibata (2011)	TL159, L80	1 Pa	1	TP	Hines (1997b)
NIWA-UKCA	Morgenstern et al. (2009, 2013) Stone et al. (2016)	∼ 3.75° × 2.5°, CP60	84 km	3	TA	Scaife et al. (2002)
SOCOL3	Stenke et al. (2013) Revell et al. (2015a)	T42, L39	1 Pa	4	TP	Hines (1997a,b)
ULAQ CCM	Pitari et al. (2014)	T21, CP126	4 Pa	3	NTP	NO NOGWD

Table 2.1: CCMI models that provided TEM diagnostic model output used in this study. CP is Charney-Phillips, T21 ≈ 5.6° × 5.6°, T42 ≈ 2.8° × 2.8°, T47 ≈ 2.5° × 2.5°, TL159 ≈ 1.125° × 1.125°, TA is hybrid terrain-following altitude, TP is hybrid terrain-following pressure, and NTP is non-terrain-following pressure.

At a minimum, this requires the residual vertical velocity ($\overline{w}^*$) and the residual meridional velocity ($\overline{v}^*$; Andrews et al., 1987); where available we also use the resolved and parameterised wave forcing fields from the models. This gives results from a total of 10 models, which differ from one another in various aspects, such as their horizontal resolution, ranging from 1.9° to 5.6°, their vertical resolution, and their sub-grid parameterisations (see Table 2.1). The main text concentrates on the 7 out of 10 models that performed both the REF-C1 and REF-C1SD experiments (Table 2.2).

Model name	Pressure and height range	Newtonian relaxation	Spectral nudging (yes - Y; no - N)	Nudged variables	Source of nudging data	Reference
CCSRNIES-MIROC3.2	1000-1 hPa	1 d	N	u, v, T	ERA-I	Akiyoshi et al. (2016)
	1-0.01 hPa	1 d	N	u and T zonal mean	CIRA	
CESM1-WACCM	Surface-50 km (transition 40-(50 km)	50 h	N	u, v, T, surface pressure, surface stress latent and sensible heat flux	MERRA	Lamarque et al. (2012)
CMAM	Surface-1 hPa	24 h	Y	Divergence, vorticity temperature	ERA-I	McLandress et al. (2013)
EMAC (L47 and L90)	920-780 hPa (transition)	48 h	Y	Divergence, vorticity	ERA-I	Jöckel et al. (2016)
	710-10 hPa (full)	6 h		T (with wave O),		
	10-6 hPa (transition)	24 h		(logarithm of) surface pressure		
MRI-ESM1r1	870-1 hPa	24 h	N	u, v, T	JRA-55	Deushi and Shibata (2011)
	(870-40 hPa)					
	24-∞ h					
	(40-1 hPa)					
SOCOL3	Surface-0.01 hPa	48 h	Y	Divergence, vorticity	ERA-I	
		6 h		T, (logarithm of) surface pressure		
		24 h				
		24 h				

Table 2.2: Details of nudging in the CCMI REF-C1SD simulations that provided TEM diagnostics model output used in this study. ERA-I is ERA-Interim, CIRA is Cooperative Institute for Research in the Atmosphere, MERRA is Modern-Era Retrospective reanalysis, and JRA-55 is Japanese 55-year Reanalysis. T (with wave 0) for EMAC refers to the additional nudging of the global mean temperature.

However, the broad conclusions drawn in the main text for the characteristics of the seven-member REF-C1 ensemble are consistent with the behaviour for all 10 models. Hence the three models that only performed the REF-C1 experiment (GEOSCCM, NIWA-UKCA, and ULAQ-CCM) are not discussed further, but for completeness a subset of diagnostics from those models is shown in the Supplement (Figs. S2.1 - S2.5).

For the REF-C1 simulations we analyse between one and five ensemble members (depending on what was available), and for REF-C1SD the one realization submitted from each model. The REF-C1SD simulations nudge temperature and other meteorological fields such as horizontal winds, vorticity and divergence, and some surface fields (Table 2.2), while the chemical fields are left to evolve freely. The nudging timescales range from 6 to 50 h, and the height range over which nudging is applied varies (Table 2.2). The TEM and related diagnostics that were available from each model are shown in Ta-

ble 2.3. The models use different reanalysis fields for nudging taken from ERA-Interim (Dee et al., 2011), JRA-55 (Ebita et al., 2011; Kobayashi et al., 2015), or MERRA (Rienecker et al., 2011). The differences in the residual circulation diagnosed from reanalyses have been identified and documented in previous studies (e.g. Abalos et al., 2015).

Model name	REF-C1	REF-C1SD
CCSRNIES-MIROC3.2	✓ ● ✚ ✱ ▲ ■	✓ ● ✚ ✱ ▲ ■
CESM1-WACCM	✓ ● ✚ ▲ ■	✓ ● ✚ ▲ ■
CMAM	✓ ● ✚ ▲ ■	✓ ● ✚ ▲ ■
EMAC (L47 and L90)	✓ ● ✚ ✱ ▲ ■	✓ ● ✚ ✱ ▲ ■
GEOSCCM	✓ ● ✚ ✱ ▲ ■	
MRI-ESM1r1	✓ ● ✚ ✱ ▲ ■	✓ ● ✚ ✱ ▲ ■
NIWA-UKCA	✓ ● ✚ ✱	
SOCOL3	✓ ●	✓ ●
ULAQ-CCM	✓ ●	

Table 2.3: Available TEM-related model output for each model from the CCMI-1 archive: $\overline{w}^*$ (✓), $\overline{v}^*$ (●), EPFD (✚), gravity wave drag (OGWD and NOGWD; ✱), OGWD (▲), and NOGWD (■).

2.2.2 Model diagnostics

2.2.2.1 TEM residual circulation

The TEM velocities ($\overline{v}^*$, $\overline{w}^*$) are defined as (Andrews et al., 1987)

$$\overline{v}^* = \frac{1}{\rho_0 \alpha \cos\phi} \frac{\partial \overline{\Psi}^*}{\partial z} \qquad \overline{w}^* = \frac{1}{\rho_0 \alpha \cos\phi} \frac{\partial \overline{\Psi}^*}{\partial \phi}, \tag{2.1}$$

where $\overline{\Psi}^*(\phi, z)$ is the residual meridional mass streamfunction, ρ_0 is log-pressure density, α is Earth's radius, and ϕ is latitude. As most of the models analysed here use a hybrid-pressure vertical coordinate, the prognostic variable is the pressure vertical velocity $\overline{\omega}^*$ (calculated in Pa s^{-1}), which must be converted to metres per second in order to get the residual vertical velocity, $\overline{w}^*$. The conversion of ω to w in isobaric coordinates is given by the following equation:

$$\omega = \frac{dp}{dt} = \frac{dz}{dt}\frac{dp}{dz} = w\frac{-pg}{RT} = w\frac{-p}{H} \tag{2.2}$$

where p is pressure, $R = 287\ J\ K^{-1}\ kg^{-1}$ is the gas constant for dry air, and H is a fixed scale height. Both TEM velocity components were submitted as monthly mean fields to the CCMI data archive. Upon close examination of the CCMI model output, some discrepancies were found in the way that the residual vertical velocity was calculated among the models. Although a fixed scale height of $H = 6960m$ was recommended in the CCMI data request (Eyring et al., 2013; Hegglin and Lamarque, 2015), the TEM output from some models (EMAC and SOCOL3) was calculated incorrectly using a temperature-dependent density, $\rho_0 = p/RT$, instead of the log-pressure definition of the density, $\rho_0 = \rho_s\ e^{-z/H}$, such that z has a unique 1:1 correspondence with p. This methodological error leads to artificial spread in the model $\overline{w}^*$ fields. We note that previous multi-model comparisons of the residual circulation that use $\overline{w}^*$ taken directly from models may have been subject to the same issue (e.g. Butchart et al., 2010; SPARC, 2010), though we cannot confirm this. To avoid this methodological inconsistency, Dietmüller et al. (2018) recalculated $\overline{w}^*$ from $\overline{v}^*$ using the continuity equation, which requires a vertical integration and a derivative along the meridional direction. The recalculation of $\overline{w}^*$ from $\overline{v}^*$ was also explored for this study, but it was found to introduce additional errors affecting the latitudinal structure of $\overline{w}^*$ (not shown) specifically because of the reduced number of CCMI-requested pressure levels compared to the native model levels. We were able to overcome the discrepancy in the submitted $\overline{w}^*$ fields for the EMAC simulations by reconverting high-frequency $\overline{\omega}^*$ output to $\overline{w}^*$ using the log-pressure density as in Eq. 2.2. However, for SOCOL3 the required output for this was not available, and hence we use the submitted $\overline{w}^*$ for which the absolute values should be treated with caution. For the other models, the results presented in this study are based on the original diagnostics submitted to the CCMI data archive, which we have verified were calculated in the correct way.

We compute the mass flux across a given pressure surface as (Rosenlof, 1995)

$$2\pi \int_{\phi}^{pole} \rho_0 \alpha^2 \cos\phi \overline{w}^* d\phi = 2\pi\alpha\Psi^*(\phi) \tag{2.3}$$

using the boundary condition in which $\Psi = 0$ is at the poles. By finding, at each pressure level, the latitude at which Ψ_{max} and Ψ_{min} occur, which corresponds to the height-dependent turnaround (TA) latitudes, we can calculate the net downward mass

flux in each hemisphere. The net tropical upward mass flux, equal to the sum of the downward mass fluxes in each hemisphere, can then be expressed as (Rosenlof, 1995)

$$tropical\ upward\ mass\ flux\ (TUMF) = 2\pi\alpha(\Psi^*_{max} - \Psi^*_{min}) \tag{2.4}$$

The tropical upward mass flux (TUMF) has been used widely as a measure of the strength of the BDC (e.g. Rosenlof, 1995; Butchart and Scaife, 2001; Butchart et al., 2006, 2010, 2011; Butchart, 2014 and references therein; Seviour et al., 2012), so its use here enables a direct comparison with earlier studies. Arguably, the strength of the TUMF is a first-order metric for evaluating changes in the stratospheric mass circulation as a consequence of nudging. As mentioned above, by calculating the annual means of TUMF accounting for the seasonal cycle of the TA latitudes, we capture the correct evolution of the intra-seasonal (not shown) and inter-annual variability in the TUMF.

2.2.2.2 Downward control principle calculations

Under steady-state conditions, $\overline{\Psi}^*(\phi, z)$ at a specified latitude ϕ and log-pressure height z is given by the vertically integrated eddy-induced total zonal force, $\overline{F}$, above that level (Haynes et al., 1991):

$$\Psi^*(\phi, z) = \int_z^\infty \left\{ \frac{\rho_0 \alpha^2 \overline{F} \cos^2\phi}{\overline{m}_\phi} \right\}_{\phi=\phi(z')} dz, \tag{2.5}$$

where in the quasi-geostrophic limit, $\overline{m}_\phi \approx -2\Omega\alpha^2 \sin\phi\cos\phi$. The above integration applies along lines of constant mean absolute angular momentum per unit mass, $\overline{m} = \alpha\cos\phi(\overline{u} + \alpha\Omega\cos\phi)$, where $\overline{u}$ is the zonal mean zonal wind and Ω is Earth's rotation rate, with boundary conditions of $\Psi \to 0$ and $\rho_0\overline{w}^* \to 0$ as $z \to \infty$. These lines of constant angular momentum are approximately vertical except near the Equator (up to $\sim \pm 20°$) such that we can calculate the solution of the above integral using the constant ϕ for the limits of the integral (Haynes et al., 1991). In climate models, $\overline{F}$ has contributions from resolved waves due to the Eliassen-Palm flux divergence (EPFD) and from parameterised gravity wave drag due to sub-grid-scale waves that originate from orography, convection and frontal instabilities. This enables us to estimate the contribution to the tropical upward mass flux of both resolved planetary wave driving (EPFD) and the orographic and non-orographic parameterised gravity wave drag (OGWD and NOGWD, respectively) from the CCMI model output (Table 2.3) and

compare with the direct estimates derived from $\overline{w}^*$.

Applying the downward control principle (Haynes et al., 1991) can provide useful insights into the driving mechanisms of the stratospheric residual circulation and therefore explain part of the inter-model spread found in both REF-C1 and REF-C1SD simulations. While the downward control principle enables the contributions of EPFD and OGWD and NOGWD to TUMF to be calculated under various assumptions (Haynes et al., 1991), one has to keep in mind that the different wave forcings can interact and thus are not independent of each other (Cohen et al., 2013).

It is important to note some possible limitations of the diagnostic approaches chosen for this study. Both the direct and downward control principle methods rely on the applicability of quasi-geostrophic theory to interpret the results. In addition to the two approaches used here, the residual circulation can also be estimated using the thermodynamic equation. Studies have shown that the estimates from the different methods for evaluating the residual circulation can differ (Seviour et al., 2012; Abalos et al., 2015; Linz et al., 2019), particularly in reanalyses where standard global conservation laws (e.g. conservation of mass) must generally not be met. Similar issues are likely to beset the nudged model simulations, owing to the additional tendencies included in the model equations. The differences between the calculation methods for the residual circulation can be as large as, or larger than, the differences between reanalysis datasets for the same diagnostic (Abalos et al., 2015; Linz et al., 2019) and may further depend on choices around averaging between fixed latitudes or the TA latitudes (Linz et al., 2019), so it is important to bear this in mind in interpretation of the results presented here. Unfortunately, heating rates were not available from all CCMI model simulations to perform the thermodynamic equation calculation. Nevertheless, we compute the direct and downward control principle diagnostics for the residual circulation in a self-consistent manner in the models and reanalyses to enable comparison with earlier multi-model studies (Butchart et al., 2006, 2010; SPARC, 2010).

2.2.3 Multiple linear regression model

To investigate the drivers of inter-annual variability in the residual circulation we apply a multiple linear regression (MLR) model (Eq. 2.6) to the annual mean time series

of TUMF. The model includes terms for known drivers of variations in tropical lower-stratospheric upwelling: major volcanic eruptions (Pitari and Rizi, 1993), the El Niño-Southern Oscillation (ENSO; García-Herrera et al., 2006; Marsh and Garcia, 2007; Randel et al., 2009), the quasi-biennial oscillation (QBO; Baldwin et al., 2001), and a linear trend (Calvo et al., 2010):

$$\begin{aligned} TUMF(t) = \beta_0 &+ \beta_{VOL} \cdot x_{VOLC}(t) + \beta_{ENSO} \cdot x_{ENSO}(t) \\ &+ \beta_{TREND} \cdot x_{TREND}(t) + \beta_{QBO1} \cdot x_{QBO1}(t) \\ &+ \beta_{QBO2} \cdot x_{QBO2}(t) + \epsilon(t) \end{aligned} \tag{2.6}$$

where β_0 is a constant, β_i is the regression coefficient for basis function x_i, and $\epsilon(t)$ is the residual. Following Maycock et al. (2018), the volcanic basis function is defined as the tropical lower-stratospheric average volcanic surface-area density (SAD), the ENSO basis function is the time series of eastern-central equatorial Pacific Ocean SST anomalies (Niño 3.4 index; 5°S to 5°N; 170 to 120°W); the two QBO terms are the first two principal-component time series from an empirical orthogonal function (EOF) analysis of the zonal mean zonal winds between 10°S and 10°N and 70 to 5 hPa and a linear trend. The first three regressors, the volcanic, ENSO, and the linear trend, are identical for both REF-C1 and REF-C1SD runs, while the QBO terms are calculated using the model winds for each model and experiment. For the REF-C1 runs, CMAM does not include a QBO; hence when we apply the MLR to the CMAM REF-C1 simulation the QBO terms are omitted. We opted not to include an equivalent effective stratospheric chlorine (EESC) MLR term to account for changes in ozone-depleting substances (Abalos et al., 2019; Morgenstern et al., 2018; Polvani et al., 2019, 2018), as the period considered in the study may not be sufficiently long for the linear trend to be separated properly from EESC. Since we are regressing annual mean TUMF we do not consider a seasonal cycle term or any lag in the terms. The results in Sect. 2.3.5 focus on the first ensemble member (in the rip-nomenclature, where r stands for realization, i for initialization, and p for physics - r1i1p1), but where applicable the results from the MLR model for the rest of the ensemble members of the REF-C1 runs are presented in the Supplement (Figs. S2.6 - S2.9).

2.2.4 Reanalysis Data

In order to compare the REF-C1 and REF-C1SD simulations against the reanalysis datasets used for the nudging, we use the SPARC Reanalysis Intercomparison Project (S-RIP) dataset (Martineau, 2017; Martineau et al., 2018). This provides a common gridded version of the reanalysis TEM fields on a 2.5° × 2.5° grid up to 1 hPa. The pressure vertical velocity, $\overline{\omega}^*$, is converted to the residual vertical velocity, $\overline{w}^*$, using Eq. 2.2. A detailed comparison of the stratospheric residual circulation in reanalysis datasets is given by Abalos et al. (2015).

2.3 Results

2.3.1 Climatological residual circulation: $\overline{w}^*$

Figure 2.1 shows latitude-pressure cross-sections of the climatological (1980-2009) multi-model mean (MMM) annual mean $\overline{w}^*$ for the REF-C1 (Fig. 2.1a) and REF-C1SD (Fig. 2.1b) simulations and their differences (Fig. 2.1c). In Fig. 2.1c absolute differences are computed, so positive values indicate where the magnitude of the circulation in REF-C1SD (whether upwelling or downwelling) is larger than in REF-C1. As expected, the climatologies show upwelling in the tropics between around 30°S to 30°N and downwelling at higher latitudes. In the lowermost stratosphere (100-80 hPa), within the region of tropical upwelling, the REF-C1SD MMM generally shows larger $\overline{w}^*$ values in the subtropics and smaller values at the Equator compared to REF-C1, indicating a tendency for a more double-peaked $\overline{w}^*$ structure in the tropics in the lowermost stratosphere (Ming et al., 2016a). Above this, between ∼ 70 and 4 hPa, the REF-C1SD MMM shows on average stronger upwelling at the Equator compared to REF-C1, indicating a less pronounced double-peaked $\overline{w}^*$ structure in the REF-C1SD experiments in the lower stratosphere to middle stratosphere. Between 1 and 2 hPa, the REF-C1SD MMM shows larger inter-hemispheric asymmetry than in REF-C1, with stronger upwelling in the northern tropics (Fig. 2.1b). At the southern mid-latitudes, between ∼ 30° and 60°S, the REF-C1SD MMM exhibits on average slightly weaker downwelling than in REF-C1, with the largest magnitude differences found in the upper stratosphere. In the Arctic, the REF-C1SD MMM shows significantly stronger downwelling over the poles than in REF-C1. In the Antarctic the picture is more complex, with the REF-C1SD MMM

showing weaker downwelling right at the pole in the upper stratosphere (2-10 hPa) but stronger downwelling between around 75° and 88°S. In the middle stratosphere, from 50 to 10 hPa, the REF-C1SD MMM shows stronger downwelling between 60° and 80°S.

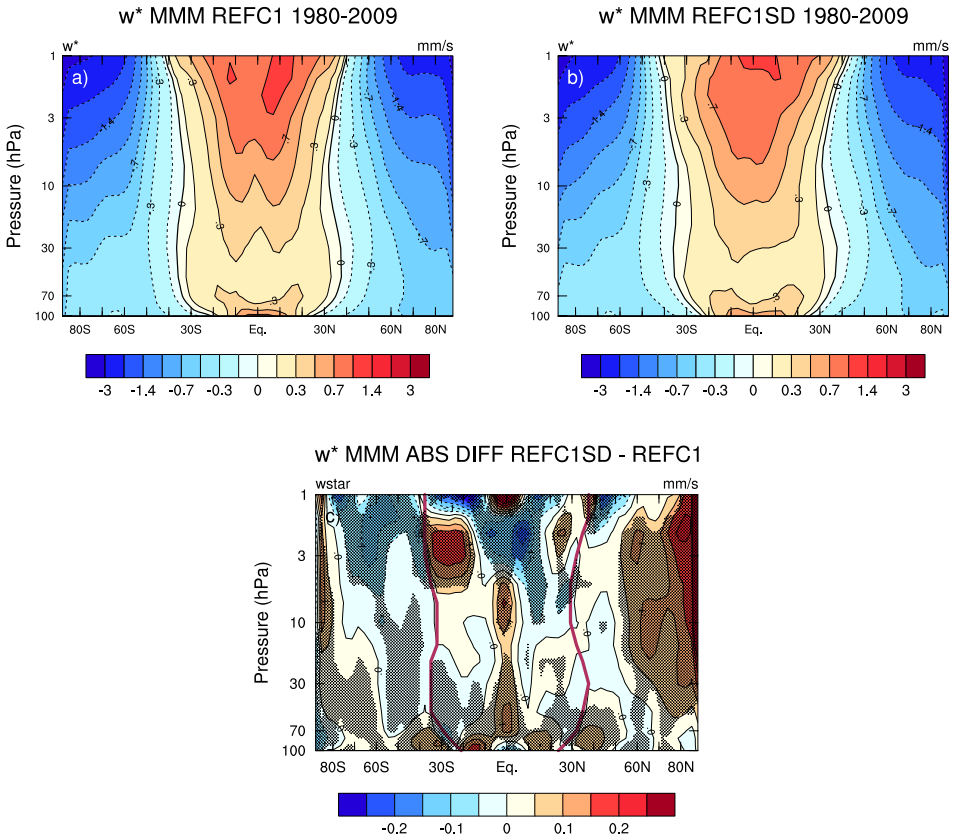

Figure 2.1: Latitude vs. pressure climatology (1980-2009) of MMM annual mean $\overline{w}^*$ for (a) REF-C1 simulations, (b) REF-C1SD simulations, and (c) the REF-C1SD-REF-C1 absolute differences. Shading denotes statistical significance at the 95% confidence level, and the red lines in (c) denote the climatological turnaround latitudes in REF-C1SD.

To show the differences in the transition between regions of upwelling and downwelling motion, Fig. 2.2 shows vertical profiles of the climatological annual mean turnaround (TA) latitudes in each hemisphere for the REF-C1 and REF-C1SD MMM and the three reanalysis datasets used for nudging. Note that since five of the REF-C1SD models were

nudged towards ERA-I, the REF-C1SD MMM may be more weighted towards ERA-I than the other reanalyses.

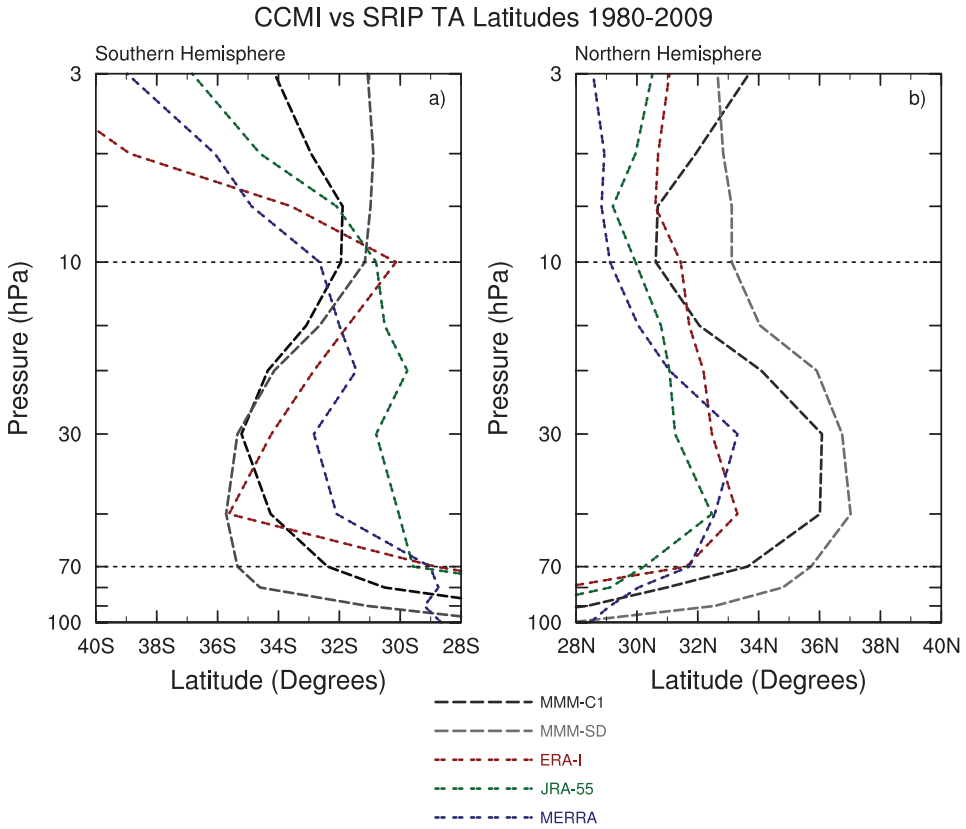

Figure 2.2: Vertical profiles of the climatological turnaround latitudes in the stratosphere for the MMM of the REF-C1 runs (black dashes), the MMM of the REF-C1SD runs (grey dashes), and the S-RIP reanalysis datasets (ERA-I, JRA-55, and MERRA) for the (a) Southern Hemisphere and (b) Northern Hemisphere.

In the NH, the REF-C1SD MMM shows a more poleward TA latitude compared to both REF-C1 and the reanalyses throughout almost the entire depth of the stratosphere (Fig. 2.2b). A more poleward TA latitude for REF-C1SD than in both REF-C1 and the reanalyses is also found in the Southern Hemisphere (SH) at pressures greater than 30 hPa (Fig. 2.2a). Hence the nudged simulations show, on average, a wider region of tropical upwelling in the lower stratosphere compared to their free-running counterparts by up to around 5° latitude. In the middle stratosphere and upper stratosphere

the REF-C1SD MMM shows a narrower upwelling region in the SH. Interestingly, above 10 hPa in the SH (Fig. 2.2a), the REF-C1SD does not show a progressive widening of the upwelling region with decreasing pressure as seen in the reanalyses. This is reflected in the structural differences in $\overline{w}^*$ in the SH upper stratosphere found in some models (Fig. S2.10). It should be noted though that the differences in TA latitudes between the REF-C1 and REF-C1SD MMMs are comparable to the differences found between the three reanalysis datasets.

Focusing on the lower stratosphere, Fig. 2.3 shows the climatological annual mean $\overline{w}^*$ at 70 hPa in the individual models for the (a) REF-C1 and (b) REF-C1SD simulations and (c) their differences. Also plotted in Fig. 2.3b is $\overline{w}^*$ from the reanalyses, and Fig. 2.3d shows the difference between each REF-C1SD simulation and the reanalysis they were nudged towards. Within the upwelling region, all the models show a clear double-peaked $\overline{w}^*$ structure in the tropics, with the exception of the CCSRNIES-MIROC3.2 and MRI-ESM1r1 models in the REF-C1SD experiment. In those two cases, CCSRNIES-MIROC3.2 simulates a tri-modal $\overline{w}^*$ structure, while MRI-ESMr1 shows a relatively constant $\overline{w}^*$ across the tropics. For the REF-C1 experiment, both EMAC simulations, CMAM and SOCOL3, show a narrower double-peaked structure, with EMAC-L47 exhibiting a rather pronounced NH subtropical maximum. Conversely, CESM1-WACCM simulates the broadest region of tropical upwelling in the lower stratosphere, with the SH subtropical maximum occurring at higher latitudes compared with the rest of the models. The other REF-C1 simulations also exhibit a double-peaked $\overline{w}^*$ structure, which is generally more hemispherically symmetric, but with varying amplitudes.

A double-peaked $\overline{w}^*$ structure in the lower stratosphere has previously been shown in reanalysis datasets (Abalos et al., 2015; Ming et al., 2016a) and some CCMs (Butchart et al., 2006, 2010). This can also be seen in Fig. 2.3b for the three reanalysis datasets (ERA-I, JRA-55, and MERRA), where ERA-I and JRA-55 show an asymmetric double-peaked structure with stronger upwelling in the NH subtropics compared to the SH. As documented by Abalos et al. (2015), based on the direct calculation of the residual circulation, MERRA exhibits downwelling at the Equator, an issue which was highlighted in Abalos et al. (2015) and manifested as a negative cell in the streamfunction.

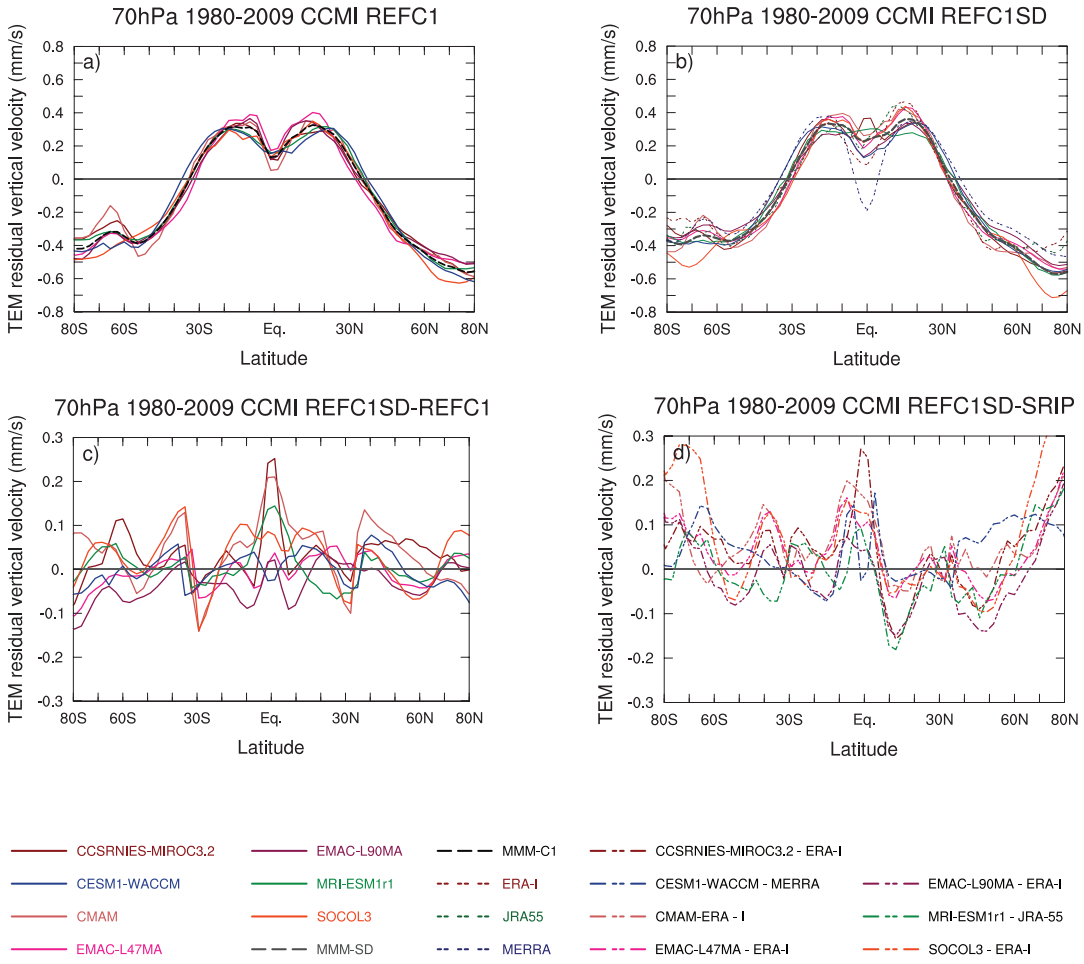

Figure 2.3: Mean strength of annual mean $\overline{w}^*$ ($mm\ s^{-1}$) at 70 hPa for (a) REF-C1 free-running models, (b) REF-C1SD nudged models, (c) absolute differences between the REF-C1SD and REF-C1 experiment for each model, and (d) absolute differences between each REF-C1SD simulation and the respective reanalysis used for nudging.

Figure 2.3c shows the absolute differences in $\overline{w}^*$ at 70 hPa between the REF-C1SD and REF-C1 experiments. Positive values show where the magnitude of the circulation in REF-C1SD is larger than in REF-C1. The largest differences are generally found within the inner tropics, where CCSRNIES-MIROC3.2, CMAM, and MRI-ESM1r1 exhibit significantly stronger upwelling (up to 3 times more for CMAM) near the local $\overline{w}^*$ minimum at the Equator. There are also larger differences in many models near edges of the upwelling region (30-40° S), which reflect differences in the width of the tropical pipe between the free-running and nudged simulations (Fig. 2.2 and Sect. 2.3.3). Around the subpolar and polar latitudes of the SH, the majority of the REF-C1 models simulate stronger downwelling than their nudged counterparts, while in the NH extratropics no consistent picture emerges across the models. EMAC-L47 and EMAC-L90 show markedly different behaviours despite the fact they are nudged towards the same reanalysis (ERA-I) and differ only in their vertical resolution. This indicates that the effect of nudging on the mean residual circulation is likely to be sensitive to a great number of factors that vary from model to model.

Another interesting result from Fig. 2.3 is that the inter-model spread in $\overline{w}^*$ for both experiments is larger in the NH downwelling region than in the equivalent region of the SH. Specifically, the inter-model spread is 0.14 $mm\ s^{-1}$ for the REF-C1 runs for all points between 30 and 80° S and 0.2 $mm\ s^{-1}$ for points between 30 and 80° N, while for REF-C1SD the values are 0.12 and 0.19 $mm\ s^{-1}$, respectively. This also demonstrates that the inter-model spread in $\overline{w}^*$ in the REF-C1SD simulations is comparable to that in REF-C1 at extratropical latitudes. In contrast, in the tropics between 30° S and 30° N the REF-C1SD simulations exhibit a slightly larger inter-model spread than the free-running simulations (0.09 $mm\ s^{-1}$ vs. 0.07 $mm\ s^{-1}$).

Figure 2.3d shows the absolute differences in $\overline{w}^*$ between the REF-C1SD simulations and the respective reanalysis dataset used for nudging. In the upwelling region, the REF-C1SD experiments generally show stronger upwelling near the Equator than in the reanalyses. Although CESM1-WACCM is nudged towards MERRA, it does not simulate downwelling at the Equator as seen in the MERRA direct estimate. The relatively larger $\overline{w}^*$ differences near 10-15° N in CCSRNIES-MIROC3.2, EMAC-L90, and MRI-ESMr1 reflect a lack of inter-hemispheric asymmetry in the double-peaked

$\overline{w}^*$ structure in the REF-C1SD experiment compared to the reanalyses. Outside of the tropics, the REF-C1SD experiments generally show weaker downwelling in the NH mid-latitudes, while at polar latitudes ($> 65°$) the REF-C1SD runs consistently show stronger downwelling than in the reanalyses. The difference in $\overline{w}^*$ at high latitudes between the REF-C1SD and reanalysis datasets extends throughout the depth of the stratosphere (see Fig. S2.10). More generally, 2.3b shows that the different models that all nudge towards ERA-I (CCSRNIES-MIROC3.2, CMAM, EMAC-L47 and EMAC-L90, and SOCOL3) produce very different mean residual circulations.

In summary, we conclude based on the results in Figs. 2.1 to 2.3 that nudging meteorology affects the strength and structure of the climatological residual circulation throughout the stratosphere. However, as implemented in these simulations (Table 2.2), nudging neither strongly constrains the mean amplitude and structure of the residual circulation nor produces circulations that closely resemble the direct estimates from the reanalyses.

2.3.2 Climatological residual circulation: tropical upward mass flux

Figure 2.4 shows vertical profiles of the climatological TUMF between 100 and 3 hPa calculated from annual means of $\overline{w}^*$ for the (a) REF-C1 and (b) REF-C1SD experiments and (c) their difference. Note the logarithmic x-axis scale and that the CCMI and S-RIP fields have been interpolated from their native model levels to a set of predefined common pressure levels, which are rather sparse in the upper stratosphere; hence the TUMF calculation could be different if it were performed on the native model grid of both CCMI models and the reanalyses.

In terms of the differences between the REF-C1SD and REF-C1 simulations (Fig. 2.4c), there is no consistent picture of the effect of nudging on the TUMF at different stratospheric levels. In the lowermost stratosphere between 70 and 100 hPa, most models (apart from EMAC-L90) simulate stronger TUMF in the REF-C1SD runs than in REF-C1. The largest TUMF differences in the lower stratosphere due to nudging occur in EMAC-L90 and SOCOL3, which show differences at 90 hPa of around -20 % and $+25$ %, respectively. In the middle stratosphere, between 10 and 70 hPa, some models show almost no difference in TUMF due to nudging (MRI-ESMr1), some show a

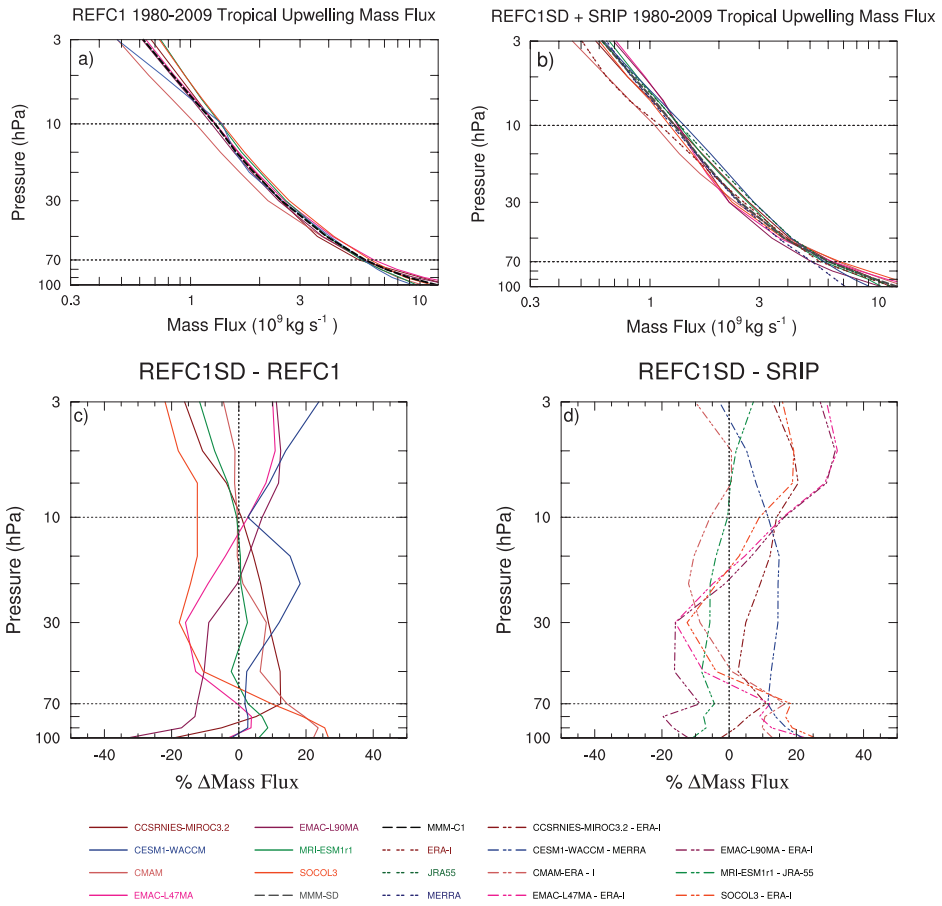

Figure 2.4: Vertical profiles of climatological (1980-2009) tropical upward mass flux (10^9 $kg\ s^{-1}$) averaged between the turnaround latitudes for (a) REF-C1 and (b) REF-C1SD, (c) differences % between REF-C1SD and REF-C1, and (d) % differences between REF-C1SD and the respective reanalysis used for nudging. Note the logarithmic x axis in panels (a) and (b).

stronger mass flux (CCSRNIES-MIROC3.2, CESM1-WACCM, and CMAM) and others show a weaker mass flux (EMAC-L47 and SOCOL3). In the upper stratosphere (above 10 hPa) the picture is also mixed, as half of the models show higher TUMF in the nudged experiments (CESM1-WACCM and EMAC-L47 and EMAC-L90) and the others show weaker TUMF (CCSRNIES-MIROC3.2, MRI-ESM1r1, and SOCOL3). CMAM shows the smallest change in TUMF in the upper stratosphere due to nudging. CESM1-WACCM is the only model to show a consistent sign of the TUMF differences between REF-C1SD and REF-C1 at all levels, with higher TUMF found throughout the stratosphere. There is no apparently simple relationship between the free-running model TUMF climatologies (Fig. 2.4a) and the effect of nudging (Fig. 2.4c).

We now compare the TUMF in each REF-C1SD experiment with the reanalysis it was nudged towards (Fig. 2.4d). Taking at first a broad view of the entire profiles, there is a resemblance between the profiles of TUMF differences in EMAC-L47 and SOCOL3 as compared to ERA-I, which may be related to the similarities in the implementation of nudging in these models; for example, vorticity and divergence were nudged with the same relaxation parameters (see Table 2.2). The CESM1-WACCM REF-C1SD simulation generally shows larger TUMF values than MERRA by up to $10-15$ % apart from in the upper stratosphere, where they start to converge. MRI-ESM1r1 exhibits relatively better agreement of TUMF with JRA-55 throughout the stratosphere. Looking across the models, most of the REF-C1SD simulations simulate stronger upwelling than their respective reanalysis in the upper stratosphere, with differences reaching up to $30-35$ % in the two EMAC models. In fact, EMAC-L47 and EMAC-L90 show a high degree of similarity in the vertical structure of the TUMF differences between REF-C1SD and ERA-I at pressures less than 30 hPa, despite showing substantial differences in the lower stratosphere. This could be because in EMAC nudging is only imposed strongly up to 10 hPa, while higher model layers have weakening nudging coefficients, as they serve as transition layers. In the middle stratosphere ($50-20$ hPa), most of the REF-C1SD models simulate a lower TUMF compared to the reanalysis. Again, a key message is that the nudged REF-C1SD simulations show a comparable, if not a slightly larger, spread in the climatological TUMF compared to the free-running REF-C1 simulations throughout almost the whole depth of the stratosphere.

To understand the dynamical factors that contribute to the modelled climatological residual circulation and its spread, Fig. 2.5 shows the annual mean TUMF at 70 hPa along with the downward control calculations (Sect. 2.2.2.2) to quantify the contribution of resolved and parameterised wave forcing to the TUMF. The black bars on the left show the TUMF diagnosed from $\overline{w}^*$, and the grey bars on the right show the estimated contribution to TUMF from the EPFD (dark grey) and the orographic (medium grey) and non-orographic (light grey) gravity wave drag. Note that SOCOL3 did not provide wave forcing fields (Table 2.3), so we cannot perform the downward control calculations for that model.

In the free-running REF-C1 simulations (Fig. 2.5a), the estimated TUMF from the total wave forcing for the majority of the models (apart from CESM1-WACCM and EMAC-L90) slightly exceeds the TUMF calculated directly from $\overline{w}^*$. Since these simulations are internally consistent, the imperfect match indicates that the downward control principle as applied here relies on the close but inexact applicability of certain assumptions, such as the system being in a steady state in response to a steady mechanical forcing (Haynes et al., 1991). The REF-C1 inter-model range in TUMF at 70 hPa is 5.74×10^9 to 6.62×10^9 $kg\ s^{-1}$ (inter-model standard deviation of 0.29×10^9 $kg\ s^{-1}$). Comparing the CCMI results in Fig. 2.5a with the results from CCMVal-2 models (see Fig. 4.10; SPARC, 2010), the MMM TUMF at 70 hPa for the seven REF-C1 model simulations analysed here (6.05×10^9 $kg\ s^{-1}$) is within the inter-model range of the 14 CCMVal-2 models, which show a MMM TUMF around 4 % weaker (5.8×10^9 $kg\ s^{-1}$; SPARC, 2010). In terms of the contribution of the resolved wave forcing to the TUMF in the free-running simulations, there appears to be a decreased inter-model range (3.26×10^9 to 5.33×10^9 $kg\ s^{-1}$) in the present study compared with the CCMVal-2 models, albeit that study included more models (1.5×10^9 to 5.5×10^9 $kg\ s^{-1}$; SPARC, 2010). Some CCMI models have increased their horizontal resolution by up to a factor of 2 (CMAM, MRI-ESM1r1, SOCOL3) and also their vertical resolution by up to 80 vertical levels (MRI-ESM1r1) compared with CCMVal-2 models (Dietmüller et al., 2018), which could improve their ability to simulate resolved wave forcing. There is a notable feature of CMAM which shows that the NOGWD contributes negatively to TUMF (indicated with two red horizontal lines on Figs. 2.5 and S2.11); this was also found for CMAM

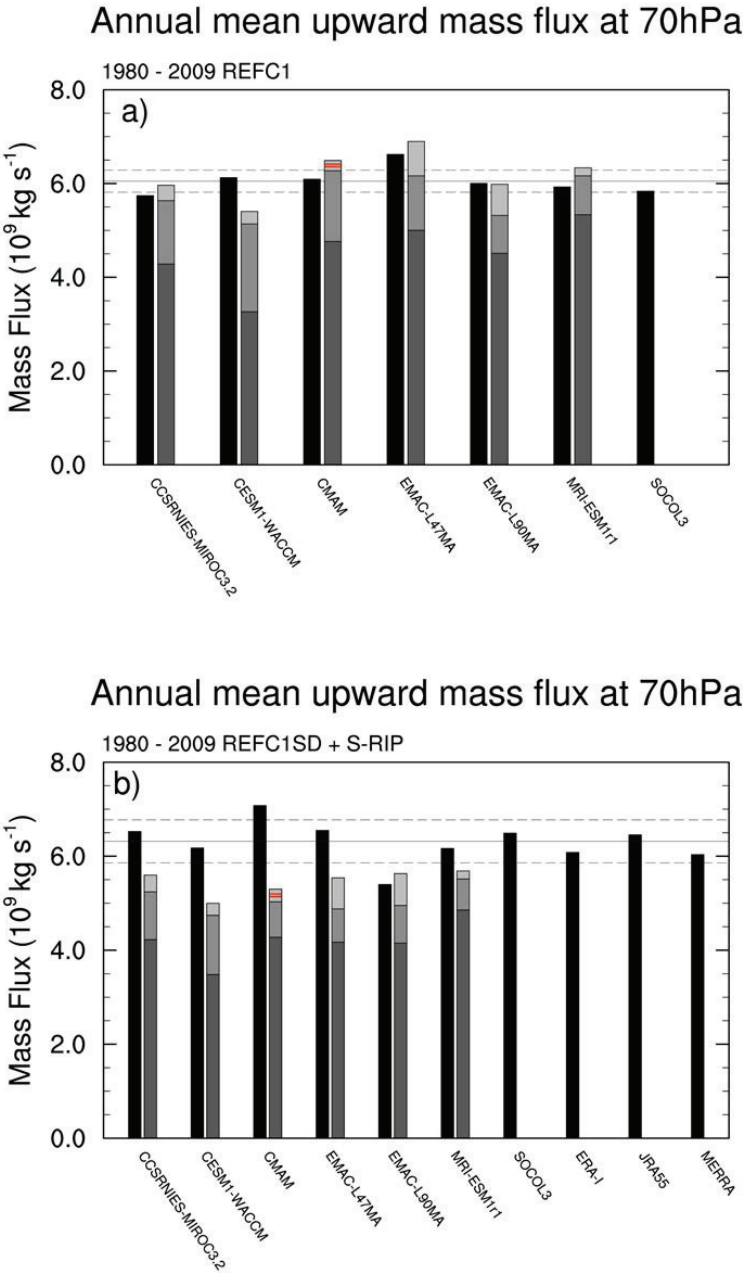

Figure 2.5: Tropical upward mass flux at 70 hPa (left bars) along with downward control calculations (right bars) showing contributions from EPFD (dark grey), OGWD(medium grey) and NOGWD (light grey) for (a) REF-C1 and (b) REF-C1SD and the reanalyses. For CMAM, the NOGWD contributes negatively to TUMF and is indicated with two red horizontal lines inside the lighter grey bar.

in CCMVal-2 (Fig. 4.10; SPARC, 2010).

The MMM TUMF at 70 hPa in the REF-C1SD simulations (Fig. 2.5b) is 6.32 × 10^9 $kg\ s^{-1}$, or around 5 % higher than in REF-C1. The REF-C1SD model range is larger than in REF-C1, being 5.39 × 10^9 to 7.08 × 10^9 $kg\ s^{-1}$ (inter-model standard deviation of 0.51 × 10^9 $kg\ s^{-1}$). A notable feature is that the contribution from the individual and total wave forcing contributions shows reduced inter-model spread in the REF-C1SD simulations (Fig. 2.5b; darker grey bars). For example, the inter-model standard deviation of the EPFD contribution to TUMF at 70 hPa is around 40 % smaller than in REF-C1 (0.44 × 10^9 and 0.72 × 10^9 $kg\ s^{-1}$, respectively). Nonetheless, the residuals (i.e. the difference between the directly calculated TUMF and the total downward control estimated contribution from the wave forcing) are substantially larger and more positive (except for EMAC-L90) in the REF-C1SD experiment than in REF-C1. This shows that nudging adds an additional non-physical tendency in the model equations which acts to decouple the wave forcing from the residual circulation; this means that the physical constraint that the divergence of the angular momentum flux due to the mean motion is balanced over some sufficient time average by that of all eddy motions does not apply in the nudged models (Haynes et al., 1991). The details of how this decoupling is manifested are likely to vary from one model to another, depending on multiple factors such as nudging timescales, nudging parameters, nudging height range, and model resolution. Comparison of the TUMF at 10 hPa for the REF-C1SD experiment (see Fig. S2.11b) also reveals substantial differences in some models between the direct and downward control TUMF estimates in the middle stratosphere. Variations in the residuals as a function of height may indicate differences in the effect of nudging on the connection between the climatological wave forcing and the shallow and deep branches of the circulation (Birner and Bönisch, 2011). However, the inter-model ranges in the directly calculated TUMF at 10 hPa are more comparable in the two experiments than those found at 70 hPa (1.45 × 10^9 to 1.7 × 10^9 and 1.51 × 10^9 to 1.72 × 10^9 $kg\ s^{-1}$ for REF-C1 and REF-C1SD, respectively; Fig. S2.11b).

Interestingly, for the single simulations that were nudged towards MERRA and JRA-55 (CESM1-WACCM and MRI-ESM1r1, respectively), the TUMF at 70 hPa in the REF-C1SD runs appears to be close to the estimates from the reanalyses they are nudged

towards (compare black bars in Fig. 2.5b). This may simply be a coincidence given that there are substantial differences in the structure of $\overline{w}^*$ between the REF-C1SD simulations for those models and the reanalyses (Fig. 2.3b and 2.3d), and this is not found for all five models that were nudged towards ERA-I. Indeed, given that there is substantial spread in TUMF amongst the five REF-C1SD models nudged to ERA-I, it is likely that the differences between the REF-C1SD and reanalysis datasets are related to how nudging was implemented in each model; a wide variety of relaxation timescales and vertical nudging ranges were used by the models (Table 2.2). Despite this, the lower TUMF calculated directly from $\overline{w}^*$ in EMAC-L90 compared to EMAC-L47, seen in both the REF-C1 and REF-C1SD experiments, is consistent with the results of Revell et al. (2015b), who also find that an increase in the model vertical resolution for SOCOL3 results in a slowdown of the BDC.

In summary, the results from Figs. 2.4 and 2.5 further demonstrate that nudging imparts an external and non-physical tendency in the model equations, which in turn might cause violations of the normal constraints on the global circulation, such as conservation of momentum and energy. This is found to alter the residual circulation but in a manner that cannot be understood from a closure of the circulation through the integrated wave forcing, as would ordinarily apply in the downward control principle (Haynes et al., 1991).

2.3.3 Annual cycle

We now evaluate the representation of the annual cycle in the residual circulation. Figure 2.6 shows the MMM climatological annual cycle of $\overline{w}^*$ at 70 hPa for the REF-C1 and REF-C1SD simulations and their difference. Both experiments show similar broad features in the annual cycle, with stronger tropical upwelling in boreal winter, a latitudinal asymmetry in the region of upwelling, with the TA latitude being further poleward in the summer hemisphere, and stronger downwelling over the winter pole. These features resemble the annual cycle found in other multi-model studies (e.g. Hardiman et al., 2014).

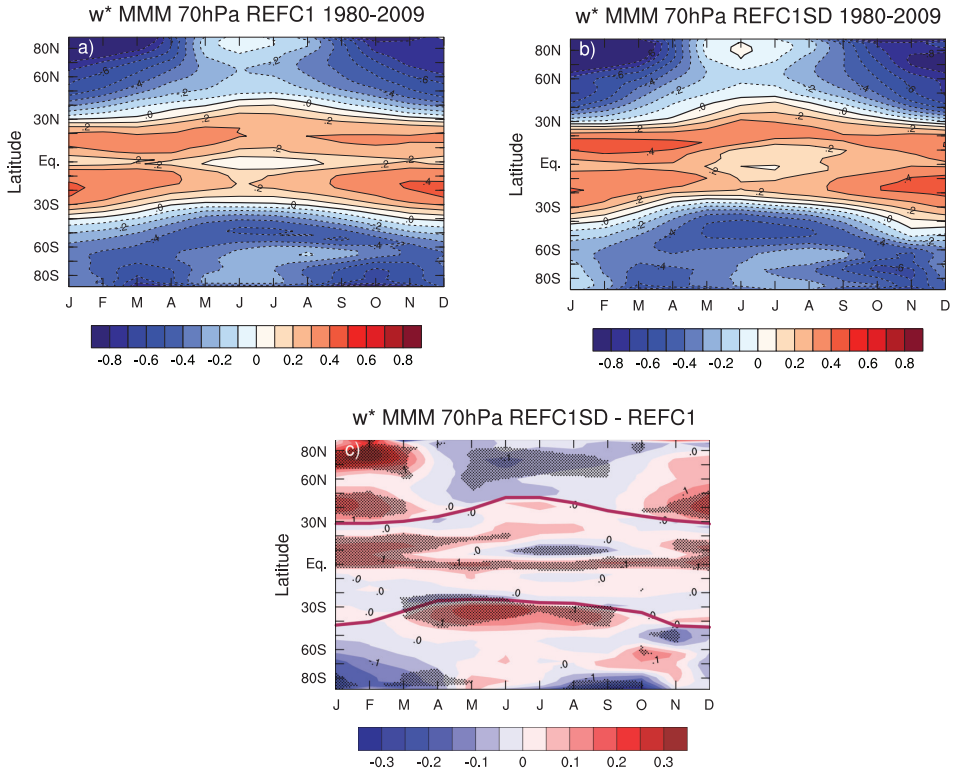

Figure 2.6: Climatological MMM annual cycle in $\overline{w}^*$ ($mm\ s^{-1}$) at 70 hPa for (a) REF-C1, (b) REF-C1SD, and (c) the REF-C1SD minus REF-C1 absolute differences. The shading in (c) denotes regions where the differences are statistically significant above 95% using a two-tailed Student's t test. The turnaround latitudes ($\overline{w}^* = 0$) are shown by the thick black lines in (a) and (b) and by the thick red lines for the REF-C1SD MMM in (c).

Figure 2.6c shows that on average the nudged models simulate stronger upwelling in the subtropics, particularly in the NH in boreal winter, with a few exceptions, the most prominent one being the narrow band between the Equator and 10° N, where the REF-C1 simulations exhibit stronger upwelling in austral winter. Consequently, the nudged models simulate substantially stronger downwelling in the mid-latitudes in winter. In the NH mid-latitudes in the summer months, nudged runs show weaker downwelling, which reverses for the SH mid-latitudes in the austral winter. At polar latitudes there is a distinct seasonality to the differences between the REF-C1SD and REF-C1 simulations, with the nudged models simulating stronger downwelling in boreal winter and weaker downwelling in the Arctic during the rest of the year, corresponding to an amplified annual cycle. Conversely in the Antarctic, the REF-C1SD simulations generally simulate weaker downwelling, particularly during austral summer and spring.

To compare the annual cycle in residual circulation in the individual models, Fig. 2.7a and 2.7b show the mean tropical (30° S - 30° N) $\overline{w}^*$ at 70 hPa for the REF-C1 and REF-C1SD simulations, respectively. Comparing the MMM annual cycle of the REF-C1 runs (Fig. 2.7a) with the MMM REF-C1SD (Fig. 2.7b) reveals that on average the nudged models show a slightly larger peak-to-peak annual cycle amplitude (0.16 $mm\ s^{-1}$ vs. 0.13 $mm\ s^{-1}$). In general, the amplitude of the annual cycle in tropical mean $\overline{w}^*$ is slightly more constrained across the REF-C1SD simulations with the spread in peak-to-peak amplitude, as measured by the inter-model standard deviation, being around 25% smaller than in REF-C1 ($\sigma = 0.015\ mm\ s^{-1}$ vs. $0.020\ mm\ s^{-1}$, respectively). In terms of seasonal mean behaviour, the nudging appears to constrain the tropical mean $\overline{w}^*$ in boreal summer (June-July-August - JJA), which exhibits $\sim 20\%$ less spread than in the REF-C1 experiments, but it does not constrain the tropical mean $\overline{w}^*$ in boreal winter (December-January-February - DJF), which shows a larger spread than the free-running models by a factor of 2. Furthermore, the differences in tropical mean $\overline{w}^*$ between the REF-C1SD runs and the respective reanalysis they are nudged towards are generally larger in boreal winter than in boreal summer for most models. In terms of spatially resolved differences in $\overline{w}^*$ between REF-C1SD and the reanalyses (Fig. S2.12), some consistent features include the REF-C1SD simulations showing stronger downwelling in the Arctic in boreal winter compared to the reanalyses and showing weaker upwelling in the northern subtropics in boreal summer and autumn. Overall, the REF-C1SD

minus reanalysis differences for the individual models highlight a wide variety in both the magnitude and the spatial patterns of their absolute differences, with no consistent picture emerging even for the models nudged towards the same reanalysis dataset.

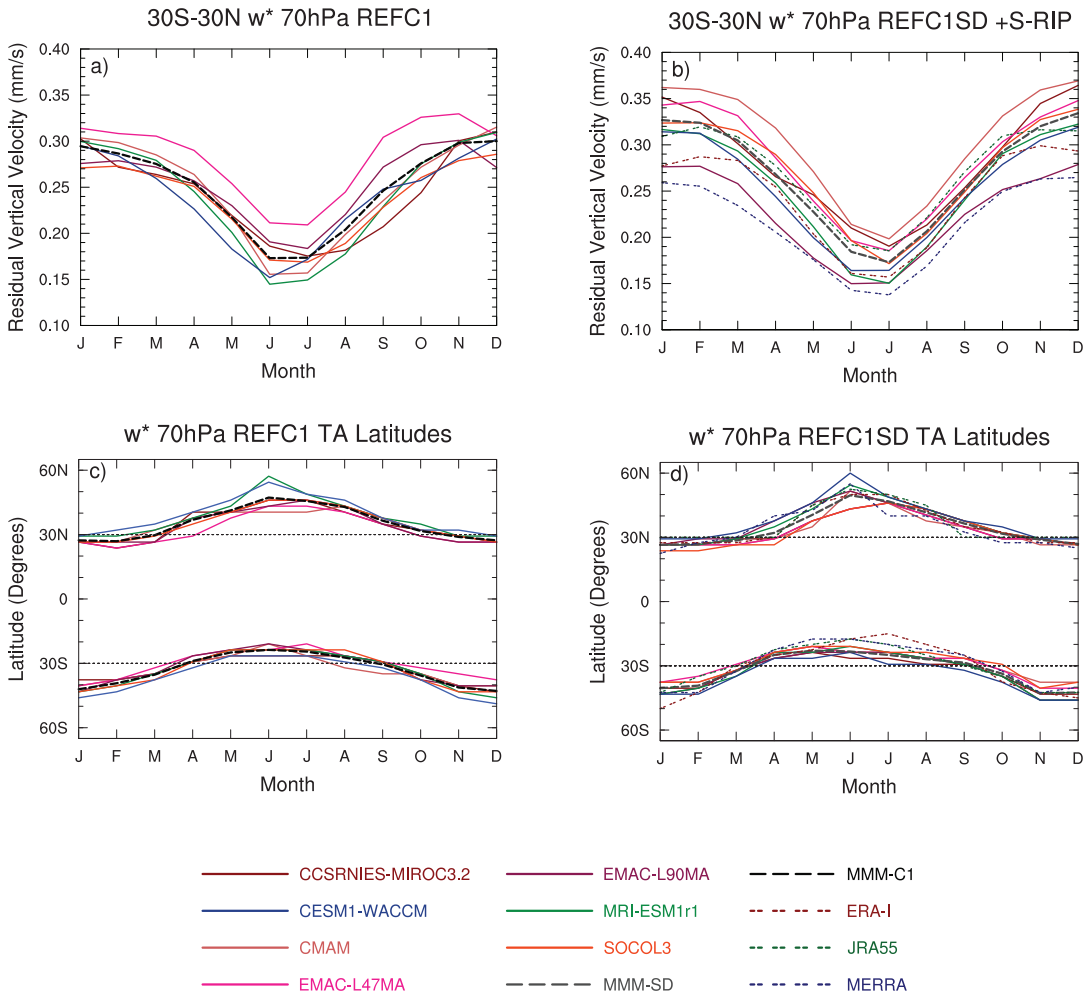

Figure 2.7: (a, b) Climatological annual cycle in $\overline{w}^*$ ($mm\ s^{-1}$) at 70 hPa between 30° S and 30° N in (a) REF-C1 and (b) REF-C1SD. (c, d) Climatological annual cycle in turnaround latitudes at 70 hPa for each model in (c) REF-C1 and (d) REF-C1SD.

Figure 2.7c and 2.7d show the climatological annual cycle in the TA latitudes at 70 hPa for the REF-C1 and REF-C1SD runs, respectively. This further breaks down the MMM annual mean perspective shown in Fig. 2.2 by model and by season. In the SH,

the spread in seasonal mean TA latitude across models, as measured by the intermodel standard deviation, is increased in the REF-C1SD experiment in all seasons by up to 30% compared to REF-C1. Conversely in the NH, the spread in seasonal mean TA latitude is decreased for REF-C1SD in all seasons except boreal spring (MAM), where it is increased. There are also substantial differences between the TA latitudes in the REF-C1SD experiment and the reanalyses in all months, which shows that nudging does not produce consistent structures of regions of upwelling and downwelling to those in the reanalysis. To summarize the results of Fig. 2.7, there is substantial inter-model spread in the TA latitudes and in the amplitude of the annual cycle in $\overline{w}^*$, highlighting significant inter-hemispheric differences in the upwelling region between both sets of simulations and between the nudged experiment and the reanalyses.

2.3.4 Interannual variability in the tropical upward mass flux

Figure 2.8 shows time series over $1980-2009$ for the annual, DJF, and JJA mean TUMF at 70 hPa for the REF-C1 (left column) and REF-C1SD (right column) simulations. As expected, the TUMF is larger in DJF compared to the annual and JJA means in both the REF-C1 and REF-C1SD runs because the average tropical upwelling is stronger in boreal winter. The individual REF-C1SD simulations show remarkably similar temporal variability in contrast to REF-C1, where the modelled inter-annual variability is very diverse despite the models all being forced with observed SSTs. Hence, although nudging does not constrain the mean TUMF in the lower stratosphere, it constrains the inter-annual variability; this is even more apparent for the DJF and JJA seasonal means (Fig. 2.8d, 2.8f). Additionally, the REF-C1SD simulations show a relatively high agreement in their temporal variability to the reanalysis datasets they were nudged towards, albeit with differences in magnitude and trend at the beginning of the 21st century, where ERA-I and MERRA show a decrease in TUMF.

To investigate the cause of the high temporal coherence of the REF-C1SD TUMF time series, Fig. 2.9 presents the annual mean TUMF anomalies at 70 hPa along with the relative contributions from EPFD, OGWD, NOGWD, and the total parameterised wave forcing (from top to bottom panels) for REF-C1 (left column) and REF-C1SD (right column), respectively.

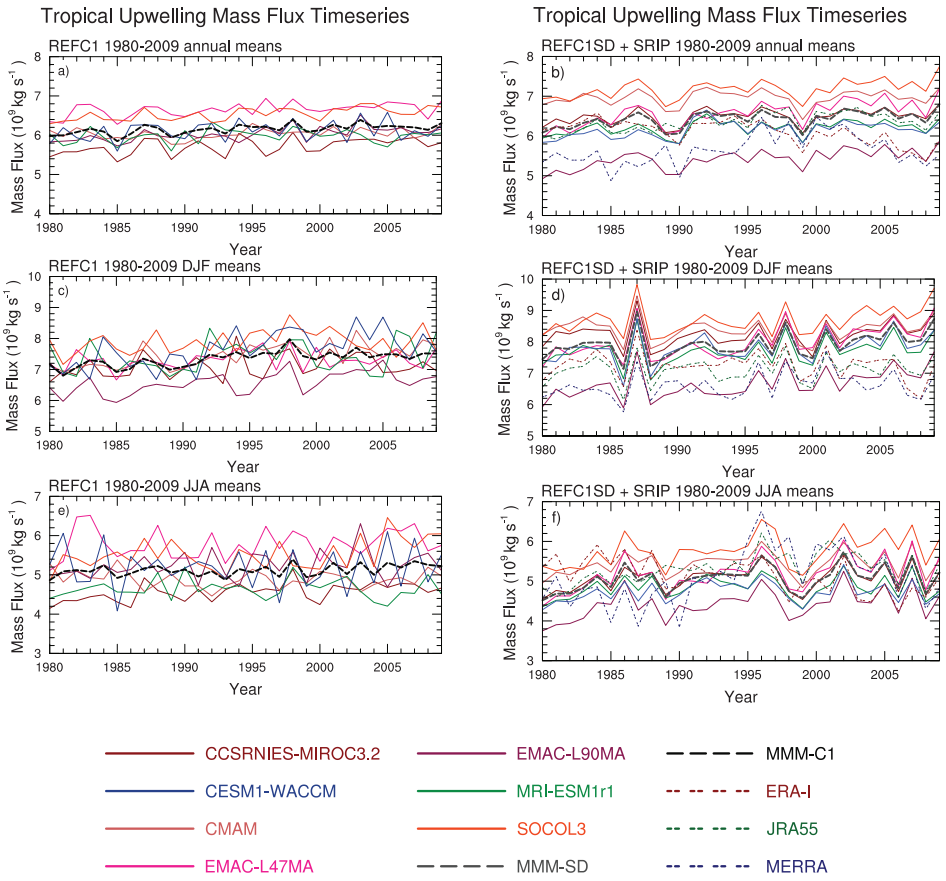

Figure 2.8: Top to bottom: time series of annual, DJF, and JJA means of tropical upward mass flux ($\times 10^9\ kg\ s^{-1}$) at 70 hPa for (a, c, e) REF-C1 and (b, d, f) REF-C1SD.

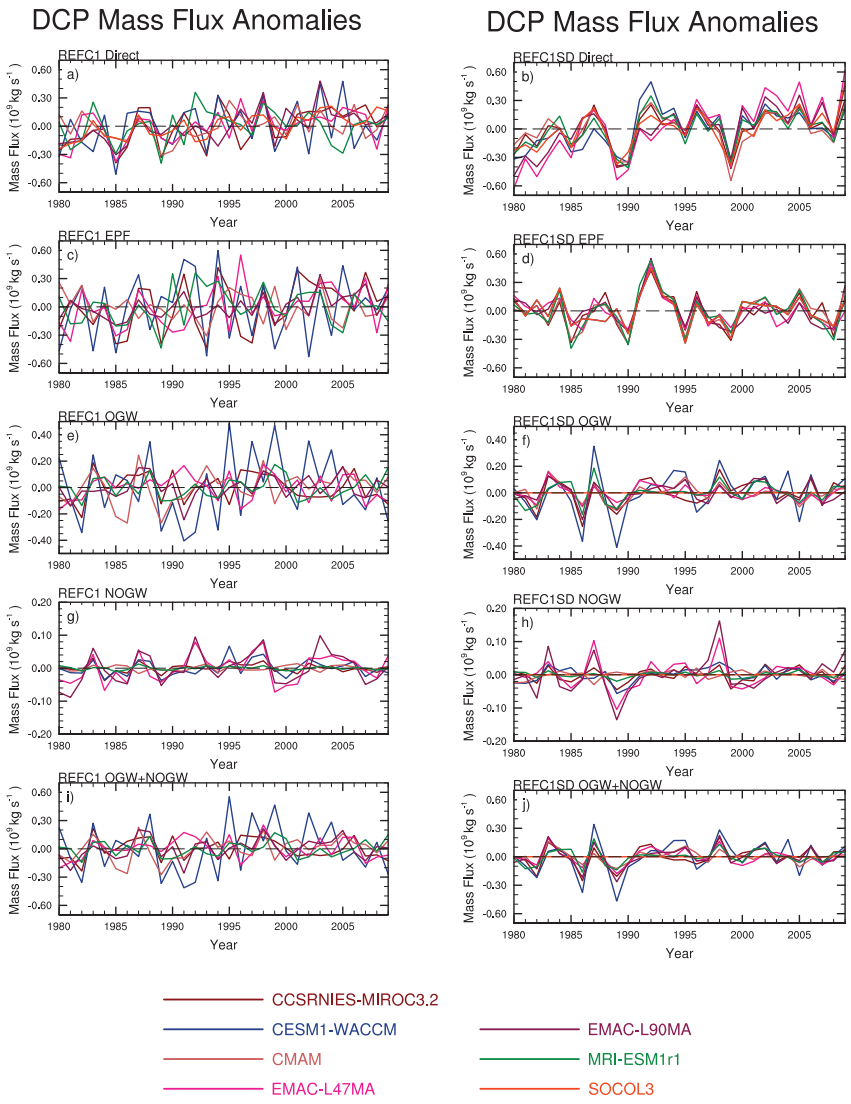

Figure 2.9: Time series of the annual tropical upward mass flux anomalies ($\times 10^9\ kg\ s^{-1}$) calculated from (top to bottom) $\overline{w}^*$ (a, b), and the downward control principle inferred contributions from resolved (EPFD) wave driving (c, d), orographic gravity wave drag (OGWD) (e, f), non-orographic gravity wave drag (NOGWD) (g, h), and from the total parameterised (OGWD and NOGWD) gravity wave drag (i, j) for REF-C1 (left panels) and REF-C1SD (right panels).

Figure 2.9b shows again the remarkably similar temporal variability in TUMF across the REF-C1SD runs, which can be contrasted against the weak inter-annual coherence in the REF-C1 runs (Fig. 2.9a).

Figure 2.9d and 2.9j show that both the EPFD and the total parameterised wave forcing contributions to the TUMF show a high degree of temporal coherence in the REF-C1SD simulations. The fact that the individual OGWD and NOGWD terms do not show such a strong inter-model agreement, while the total parameterised wave forcing does, could suggest that there is some compensation occurring between the different parameterised wave forcing components (e.g. Cohen et al., 2013). It should be noted that the reanalyses have been shown to exhibit strong similarities in their resolved EP fluxes as shown by the linear correlation in the time series of tropical upwelling at the 70 hPa level when considering the momentum balance estimates of $\overline{w}^*$ (Abalos et al., 2015). This result indicates that although nudging does not constrain the mean residual circulation, it constrains the inter-annual variability and produces similar contributions to variability across models from both resolved and parameterised wave forcing. In contrast, the REF-C1 simulations show a highly variable pattern of the estimated TUMF anomalies from EPFD and parameterised wave forcing (Fig. 2.9c and 2.9i), despite the fact that they use the same observed SSTs and that some nudge the phase of the QBO (CCSRNIES-MIRCO3.2, CESM1-WACCM, EMAC-L47 and EMAC-L90, and SOCOL3). In summary, the remarkably coherent inter-annual variability in the annual TUMF time series in the REF-C1SD simulations is due to both the resolved and parameterised wave forcing being constrained by nudging; this is in strong contrast to the climatological strength of the TUMF, where there were large differences between the directly calculated TUMF and that due to wave forces (Fig. 2.5b). The reasons for the difference in the effect of nudging on the behaviour of the residual circulation between the long-term mean and inter-annual variability are unclear.

2.3.5 Multiple linear regression analysis

Figures 2.10 and 2.11 show time series of annual TUMF anomalies at 70 hPa attributed to each of the basis functions in the MLR model described in Sect. 2.2.3 and the regression residuals for the REF-C1 and REF-C1SD runs, respectively. Also shown in Figs. S2.13 and S2.14 are the regression coefficients for each term and for each model

along with their uncertainties. Figure 2.10a shows a large spread in the diagnosed signal of volcanic eruptions in the TUMF time series. The majority of the REF-C1 simulations analysed here show a negative TUMF anomaly around the time of the El Chichón (1982) and Mount Pinatubo (1991) eruptions; however, the magnitude is within the estimated uncertainty range for all models except SOCOL3 (Fig. S2.13). In contrast to the REF-C1 results, most REF-C1SD simulations (except EMAC-L47 and EMAC-L90 - see above discussion) show a positive anomaly in TUMF attributed to volcanic eruptions (Fig. 2.11), consistent with earlier studies (Garcia et al., 2011; Diallo et al., 2017). However, there is still a considerable range of amplitudes, and only the CESM1-WACCM and MRI-ESM1r1 regression coefficients are highly significant (Fig. S2.14). The issue of establishing a robust response of the TUMF to volcanic forcing over a short period is demonstrated by the range in amplitudes of the volcanic regressors for different REF-C1 ensemble members from the same model (see Figs. S2.6 - S2.9). This highlights that in a free-running climate simulation, internal variability can overwhelm the response to forcing over short timescales. The "true" volcanic signal in TUMF will also depend on the representation of stratospheric heating due to aerosol in the various models. We note that the EMAC-L47 and EMAC-L90 models contained a unit conversion error where the extinction of stratospheric aerosols was set too low by a factor of ~ 500 (see Appendix B4 of Morgenstern et al., 2017); hence the stratospheric dynamical effects of the eruptions were not properly represented in the EMAC simulations (Jöckel et al., 2016).

The REF-C1 models all show a positive best-estimate regression coefficient for the TUMF response to ENSO (Fig. 2.10), which is quite consistent in amplitude, but it is only strongly statistically significant in CCSRNIES-MIROC3.2 and SOCOL3 (Fig. S2.5). This is in contrast to the REF-C1SD models, which all show a larger and more significant positive ENSO regression coefficient. The linear trend regression coefficient over $1980-2009$ is positive in all REF-C1 models and is statistically significantly different from zero at the 95% confidence level in five out of the seven models. The magnitude of the linear trend term varies by around a factor of 2 for REF-C1. In REF-C1SD, the amplitude of the linear trend regression coefficient increases in all models, but the intermodel spread increases to around a factor of 4. Hence, in these simulations nudging increases the disparity across models in the magnitude of the long-term TUMF trend.

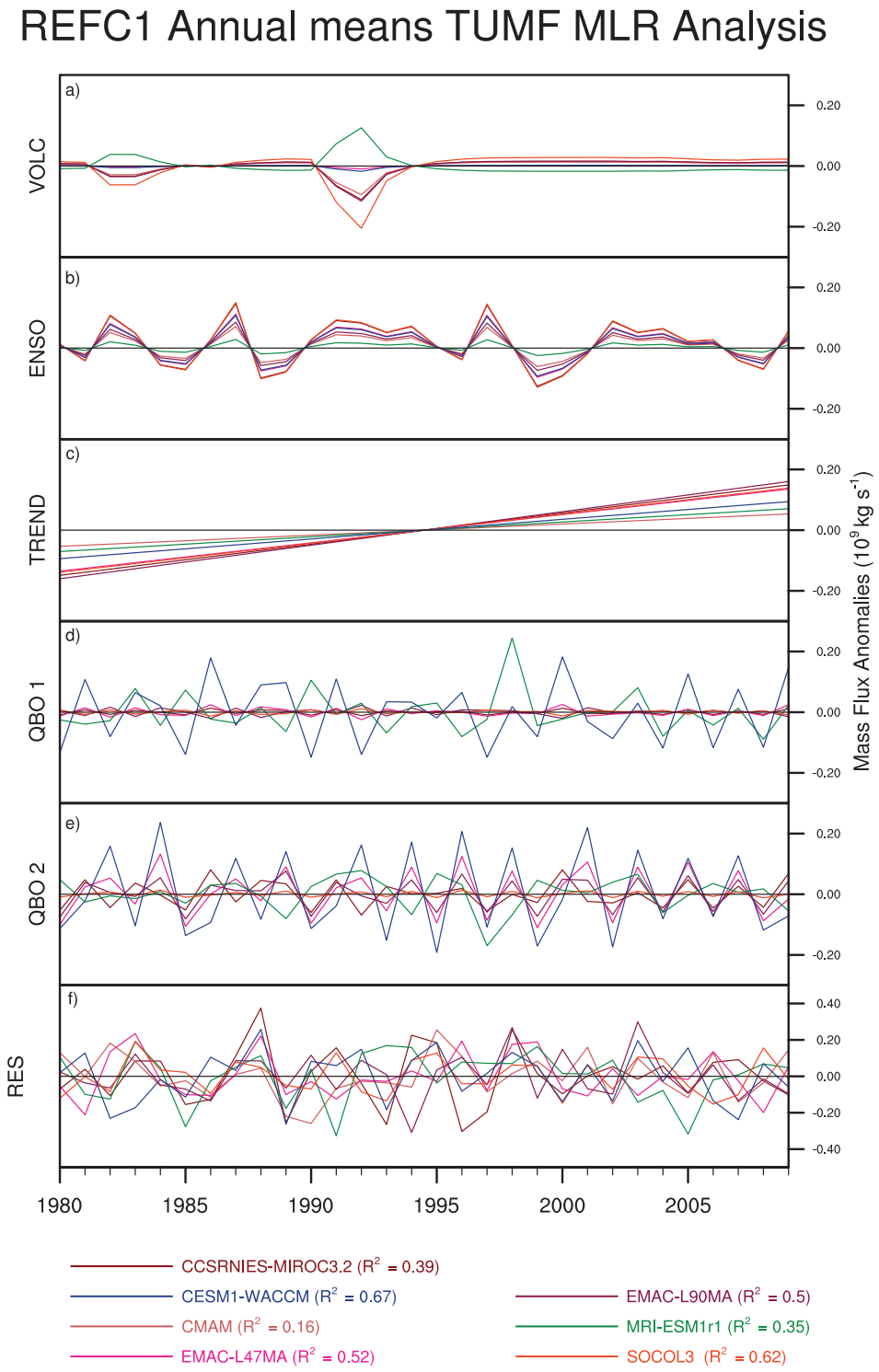

Figure 2.10: Time series for REF-C1 simulations of the components of the annual mean tropical upward mass flux ($\times 10^9\ kg\ s^{-1}$) attributed to (a) volcanic aerosol, (b) ENSO, (c) linear trend, (d, e) QBO, and (f) regression residuals.

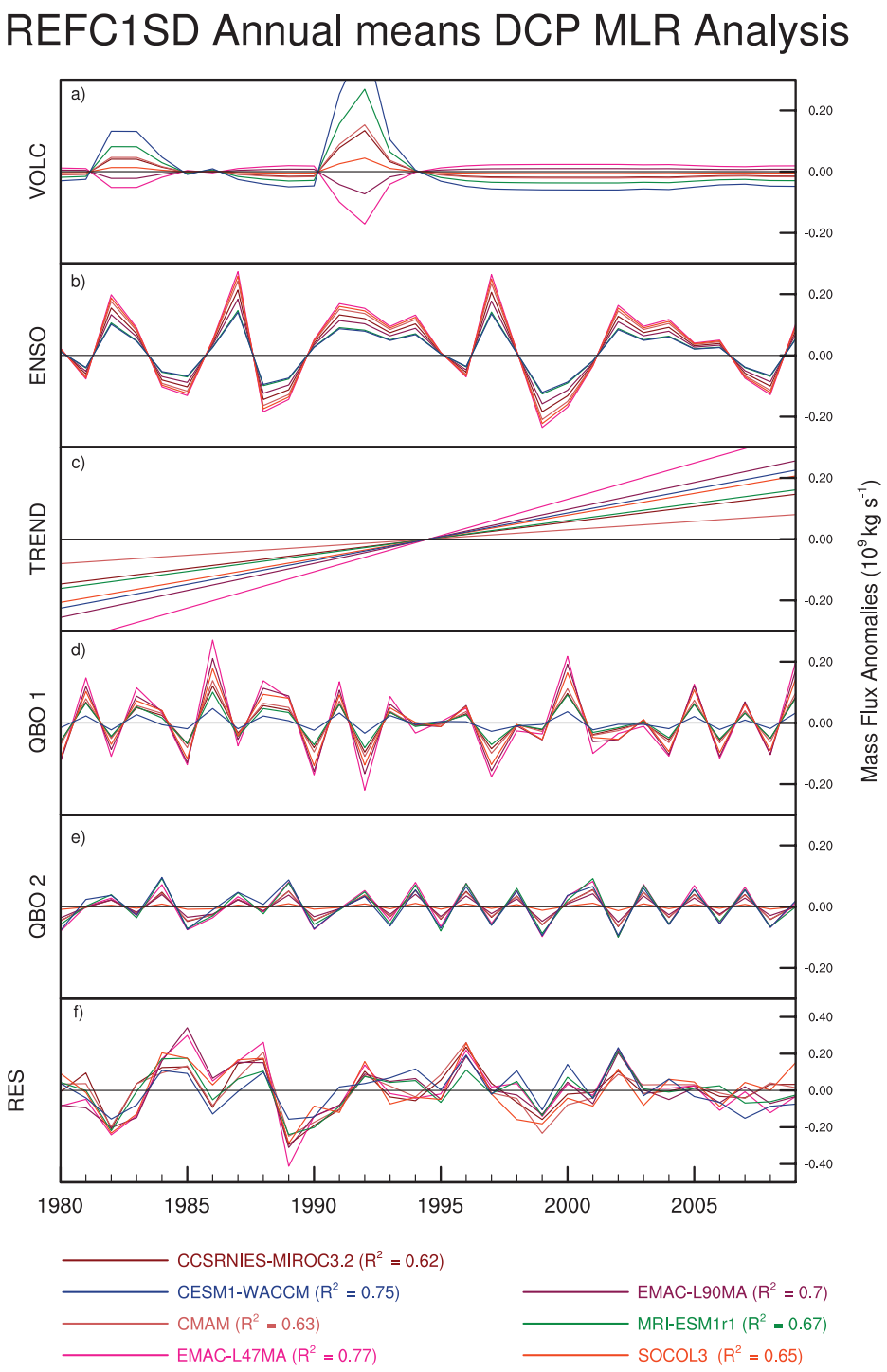

Figure 2.11: Time series for REF-C1SD simulations of the components of the annual mean tropical upward mass flux ($\times 10^9$ kg s^{-1}) attributed to (a) volcanic aerosol, (b) ENSO, (c) linear trend, (d, e) QBO, and (f) regression residuals.

As expected, the variations in TUMF attributed to the QBO is quite different in the REF-C1 and REF-C1SD runs for those models that do not nudge the QBO in REF-C1, as shown in Figs. 2.10 and 2.11. The nudging of zonal winds in REF-C1SD constrains the phase of the QBO, and hence there is strikingly similar variability in the TUMF anomalies attributed to the QBO in the REF-C1SD runs.

The overall R^2 values from the MLR model for the REF-C1 simulations vary between 0.16 (CMAM) and 0.67 (CESM1-WACCM). REF-C1SD runs generally give more consistent R^2 values across the models, ranging from 0.62 (CCSRNIES-MIROC3.2) to 0.77 (EMAC-L47). This means that there is still a substantial fraction ($> 23\%$) of unexplained variance in the annual TUMF time series in the REF-C1SD simulations after applying the MLR model, and the residuals exhibit a remarkable degree of temporal correlation. In contrast, the MLR residuals in the REF-C1 runs (Fig. 2.10f) show much less temporal coherence apart from a drop around 1989. The residuals in the REF-C1SD simulations (Fig. 2.11f) show a high degree of coherent inter-annual variability, another manifestation of the fact that the nudged runs do reproduce a much more consistent inter-annual variability. This makes a substantial contribution to the coherence of the TUMF time series in Fig. 2.9b, but it cannot be attributed to any of the terms included in the MLR model.

For completeness, the MLR model was also applied to the reanalysis TUMF at 70 hPa (Figs. S2.15 and S2.16). This highlights significant discrepancies in attributing the variance in TUMF in the different reanalysis datasets to the various basis functions in the MLR model. Both the volcanic activity and ENSO contributions to the variance in the TUMF are rather weak compared to the REF-C1SD runs. The negative linear trend in ERA-I is in strong contrast to the positive trends found in the other reanalyses and the REF-C1SD models. The negative trend in ERA-I found in the TUMF in the lower stratosphere over $1980 - 2009$ corroborates the findings of Abalos et al. (2015), who showed a negative trend in the direct $\overline{w}^*$ estimate in ERA-I over $1979 - 2012$. Despite this difference in the representation of the long-term TUMF trend, ERA-I shows the highest percentage of TUMF variance explained by the MLR model (66%), with MERRA showing a substantially lower R^2 (0.3) compared to the other reanalyses and the REF-C1SD models. The residuals are generally less correlated between the

reanalyses on inter-annual timescales than those found in the REF-C1SD simulations but are broadly similar on inter-decadal timescales. However, the regression residuals in the reanalyses show a different temporal behaviour from those in the REF-C1SD simulations (Fig. 2.11; note that the y-axis scale for the residuals in Fig. S2.15 is double that for the CCMI models in Figs. 2.10 and 2.11). In summary, although nudging constrains the inter-annual variability in the TUMF at 70 hPa, the attribution to some specific drivers differs across the models and, in comparison, to the reanalyses they were nudged towards.

2.3.6 Trend sensitivity analysis

Following the results of the MLR analysis described in Sect. 2.3.5, which showed a statistically significant positive linear trend in most REF-C1 and REF-C1SD models for the 30-year period $1980-2009$, we now explore the sensitivity of the linear trend to the time period considered. We apply the same MLR model as discussed in Sect. 2.3.5 to the annual mean 70 hPa TUMF time series of the first ensemble member for both REF-C1 and REF-C1SD runs as well as the reanalyses but systematically vary the start and end dates to cover all time periods in the window $1980-2009$ that are at least 10 years in length. We then extract the linear trend coefficient from the MLR model and its associated p value. Figures 2.12 and 2.13 present the linear trend calculations for the REF-C1 and REF-C1SD runs, respectively, as a function of trend start and end date. The same trend sensitivity analysis for the reanalyses is presented in the Supplement (Fig. S2.17). Statistically significant trends at the 95% confidence level are marked with black shading.

None of the periods considered in either the REF-C1 or REF-C1SD experiments show a significant negative TUMF trend. A statistically significant positive trend emerges in almost all of the REF-C1SD models for trends beginning in the mid-1980s to early 1990s extending to the mid-2000s. The trends are mainly significant for periods of 20 years or more and no less than around 12 years. This result broadly corroborates the findings of Hardiman et al. (2017b), who used a control run to estimate the period required to detect a BDC trend with an amplitude of 2% per decade against the background internal variability.

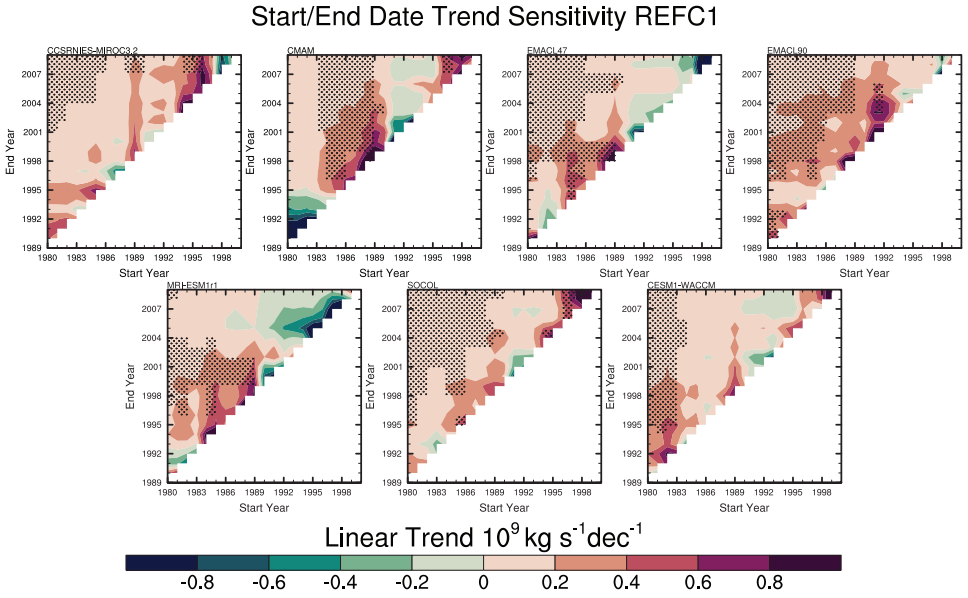

Figure 2.12: Tropical upward mass flux trends at 70 hPa ($\times$ 10^9 kg s^{-1} $decade^{-1}$) for different start (abscissa) and end (ordinate) dates over the period 1980 – 2009 for the REF-C1 (r1i1p1) simulations. Trends are not shown for periods of less than 10 years. Values with statistical significance greater than the 95% level are shaded.

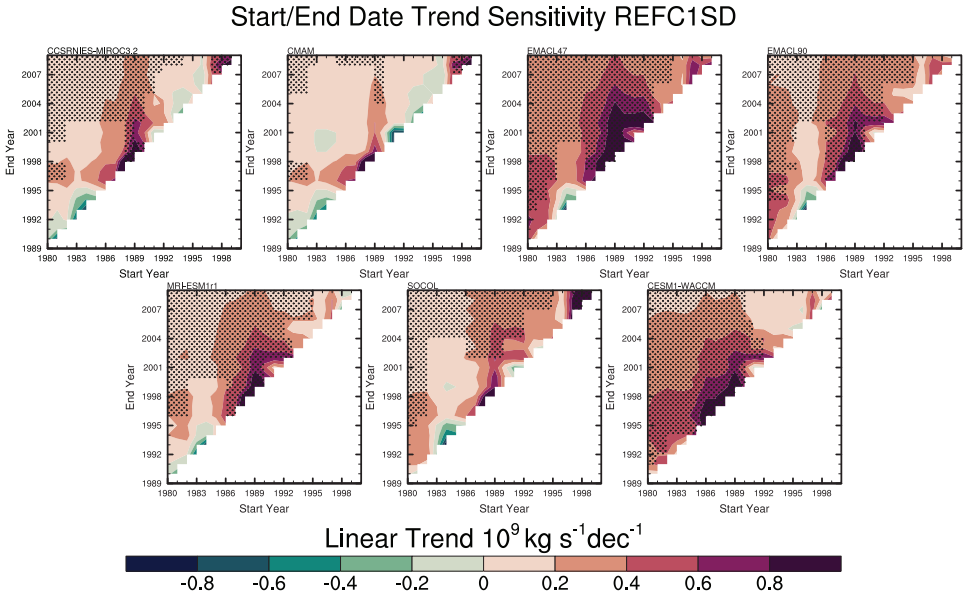

Figure 2.13: As in Fig. 2.12 but for the REF-C1SD simulations.

There is range of different structures in the diagnosed trends among models, particularly for the REF-C1 simulations, where a consistent pattern of positive trends only emerges across most models for the entire time period. This is because internal variability can mask BDC trends over short periods (Hardiman et al., 2017b). However, the REF-C1SD runs simulate more consistent variations in TUMF trends as a function of time period but generally show stronger positive trends than their free-running counterparts. Interestingly, the reanalysis trend sensitivity analysis highlights that nudging does not constrain the underlying trends of the REF-C1SD models in the TUMF at 70 hPa, as the reanalysis datasets exhibit a wide range of different trends from one another (Fig. S2.17) and differences compared to the trends in the REF-C1SD simulations (Fig. 2.13). For example, none of the REF-C1SD models simulate a statistically non-significant negative trend in TUMF, starting around mid-1990s up to 2009, as seen in all the reanalyses. However, it should also be noted that any trend combination starting around the end of 1990s in almost all cases of both REF-C1 and REF-C1SD runs exhibit no statistical significance possibly pointing towards the role of declining ODSs due to the implementation of the Montreal Protocol (Polvani et al., 2018).

2.4 Conclusions

This study has performed the first multi-model intercomparison of the impact of nudged meteorology on the representation of the stratospheric residual circulation. We use hindcast simulations over $1980 - 2009$ from CCMI, with identical prescribed external forcings in two configurations: REF-C1SD with meteorological fields nudged towards reanalysis data (specified dynamics - SD) and REF-C1 that is free-running. The nudged simulations use one of three different reanalysis datasets (ERA-Interim, JRA-55, and MERRA), nudge different variables (u, v, T, vorticity, divergence, and surface pressure), and use different time constants to impose the additional nudging tendencies in the model equations. The key findings of this study are as follows:

1. Nudging meteorology does not constrain the mean strength of the residual circulation compared to free-running simulations. In fact, for most of the metrics of the climatological residual circulation examined, including residual vertical velocities and mass fluxes, the inter-model spread is comparable or in some cases larger in the REF-C1SD simulations than in REF-C1.

2. Nudging leads to the models simulating on average stronger upwelling at the Equator in the lower stratosphere to middle stratosphere and a wider tropical pipe in the lower stratosphere. In most cases, the magnitude and structure of the climatological residual circulation in the REF-C1SD experiments differ markedly from those estimated for the reanalysis they are nudged towards.

3. In most of the nudged models there are large differences of up to 25% between the directly calculated tropical upward mass flux in the lower stratosphere and that calculated from the diagnosed total wave forcing using the downward control principle (Haynes et al., 1991). However, the spread in the contributions from the resolved and parameterised wave forcing to the tropical mass flux is slightly reduced in the REF-C1SD simulations compared to REF-C1.

4. Despite the lack of agreement in the mean circulation, nudging tightly constrains the inter-annual variability in the tropical upward mass flux (TUMF) in the lower stratosphere. This is associated with constraints to the contributions from both the resolved and parameterised wave forcing despite the fact that the models use different reanalysis datasets for nudging. The reanalysis datasets themselves exhibit broadly similar inter-annual variability in TUMF in the lower stratosphere, albeit with different long-term trends.

5. A multiple linear regression (MLR) analysis shows that up to 77% (67%) of the inter-annual variance of the lower-stratospheric TUMF in the REF-C1SD (REF-C1) experiments can be explained by volcanic eruptions, ENSO, the QBO, and a linear trend. The remaining unexplained TUMF variance in the nudged models shows a high degree of a temporal coherence, but this is not the case for the free-running simulations.

6. The results of the MLR analysis applied to the TUMF in the reanalyses show differences in the total variance explained and the attribution of variance to the different physical proxies. There are also marked differences between the individual regression coefficients derived for the REF-C1SD models and the reanalysis dataset used for nudging.

7. Most nudged simulations show a statistically significant positive trend in TUMF in the lower stratosphere over $1980 - 2009$, which is on average larger than the

trends simulated in the free-running models. This is despite the fact that five out of the seven models analysed were nudged towards ERA-Interim, which shows a negative long-term trend in TUMF (see also Abalos et al., 2015), while JRA-55 and MERRA show a positive trend. However, the magnitude of the TUMF trend varies by up to a factor of 4 across the nudged models, which is larger than the spread in the free-running simulations. This is an important limitation for using nudged-CCM simulations to interpret long-term changes in stratospheric tracers.

8. A sensitivity analysis of the time period for calculating lower-stratospheric TUMF trends shows that a statistically significant (at the 95% confidence level) positive trend in TUMF takes at least 12 years and in most cases around 20 years to emerge in the REF-C1SD runs. Despite the three reanalysis datasets showing different 30-year trends ($1980-2009$), they show a striking agreement in the statistically non-significant negative trends starting from the late 1990s up to 2009.

Our findings highlight that nudging strongly affects the representation of the stratospheric residual circulation in chemistry–climate model simulations, but it does not necessarily lead to improvements in the circulation. Similar disagreement in the characteristics of tropospheric transport in the CCMI nudged simulations has also been reported (Orbe et al., 2018). The differences found in the nudged runs compared with the free-running simulations suggest that although nudging horizontal fields can remove model biases in, for example, temperature and horizontal wind fields (Hardiman et al., 2017a), the simulated vertical wind field will not necessarily be similar to the reanalysis. A particularly interesting finding of our study is that while nudging does not constrain the mean strength of the residual circulation, it constrains the inter-annual variability. The reason for the distinct effects of nudging on the residual circulation across these different timescales is currently unknown.

Multiple factors are likely to determine the effect of nudging on the residual circulation in a given model, including model biases, nudging timescales, nudging parameters, nudging height range, and model resolution. The differences in the stratospheric residual circulation between the REF-C1SD and the REF-C1 runs may not arise solely from the dynamics but can also be partly influenced by the indirect effects of nudging the temperatures, which in turn affect the diabatic heating (Ming et al., 2016a,b). In addition to

nudging the horizontal winds (mechanical nudging), nudging the temperature (thermal nudging) might be systematically creating a spurious heat source in the model, which leads to a stronger BDC in the lower stratosphere, as suggested by Miyazaki et al. (2005) with the MRI GCM. Our results highlight that in the method by which the large-scale flow is specified and more specifically the choice of the reanalysis fields, the relaxation timescale and the vertical grid (pressure level versus model level) in which the nudging is applied need to be better understood and evaluated for their influence on the stratospheric circulation. Discrepancies between the vertical grid of the models and the reanalysis pressure levels they are interpolated onto or unbalanced dynamics are possible explanations for the differences found between the directly inferred circulation and that diagnosed from the wave forcing in the nudged simulations. Nudging would either violate continuity, or if continuity is maintained, it will come at the expense of the vertical fluxes, which are not nudged. The interesting aspect here seems to be that this results in substantial change to the net fluxes across a range of timescales; i.e. it does not only increase numerical noise in the $\overline{w}^*$ component. In order to reduce discrepancies between nudged and free-running simulations, various nudging techniques have been investigated. The role of gravity waves in the error growth that the nudging introduces over time has been highlighted for a single model (Smith et al., 2017). Constraining just the horizontal winds without the temperature was found to be a good strategy when investigating the aerosol indirect effects without affecting significantly the mean state (Zhang et al., 2014). The relaxation timescale when applying the nudging has been found to play an important role in single-model studies (Merryfield et al., 2013), but there is no general consensus for the value of the relaxation constant, which is specific to the model for the simulations considered here (Morgenstern et al., 2017). Given the varying implementations of nudging in the models analysed here, our study is ill-suited to investigate in detail the mechanisms for how nudging affects the residual circulation. A dedicated study of the sensitivities within one model to relaxation timescales, nudging parameters, nudging height range, and vertical resolution would help with offering a detailed explanation for these differences.

The large spread in climatological residual circulation in nudged-CCM simulations is an important limitation for those wishing to use them to examine tracer transport, for example in stratospheric ozone trends (Solomon et al., 2016), volcanic aerosols (Schmidt

et al., 2018), and diagnostics for the age of air (Dietmüller et al., 2018). Despite the limitations for transport within the stratosphere described here, some success has been reported in studies that used nudged simulations to investigate specific meteorological events such as sudden stratospheric warmings and, in particular, for exploring processes beyond the top of the nudging region in the mesosphere–lower thermosphere (e.g. Tweedy et al., 2013; Chandran and Collins, 2014; Pedatella et al., 2014). In conclusion, owing to the limitations of the current techniques for nudging models highlighted here, we urge caution in drawing quantitative comparisons of stratospheric tracers affected by the residual circulation in nudged simulations against stratospheric observational data.

2.5 Supplementary material

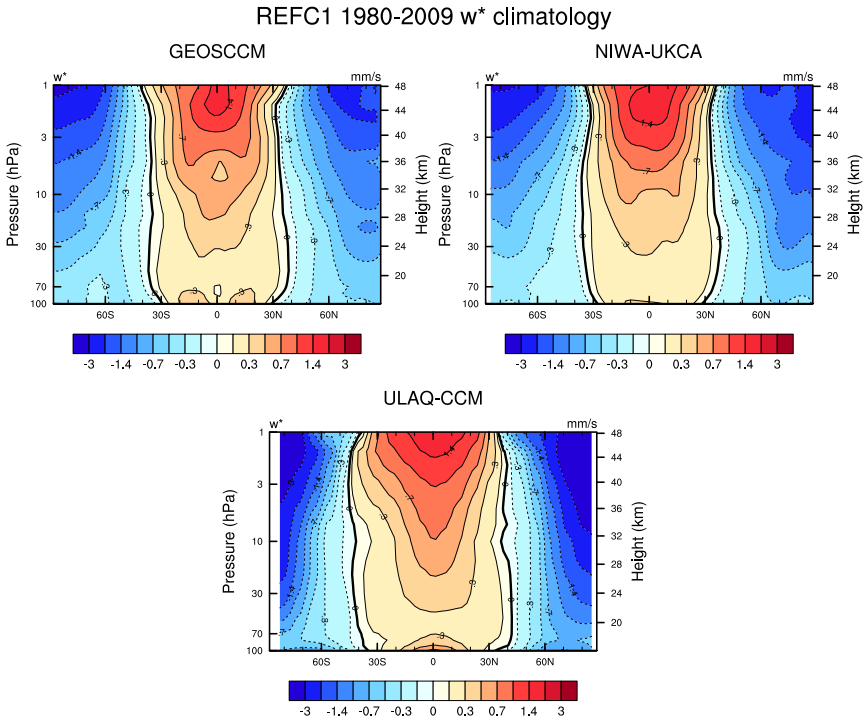

Figure S2.1: Latitude vs. pressure climatology (1980 – 2009) of the annual mean $\overline{w}^*$ for the extra REF-C1 simulations (GEOSCCM, NIWA-UKCA, ULAQ-CCM).

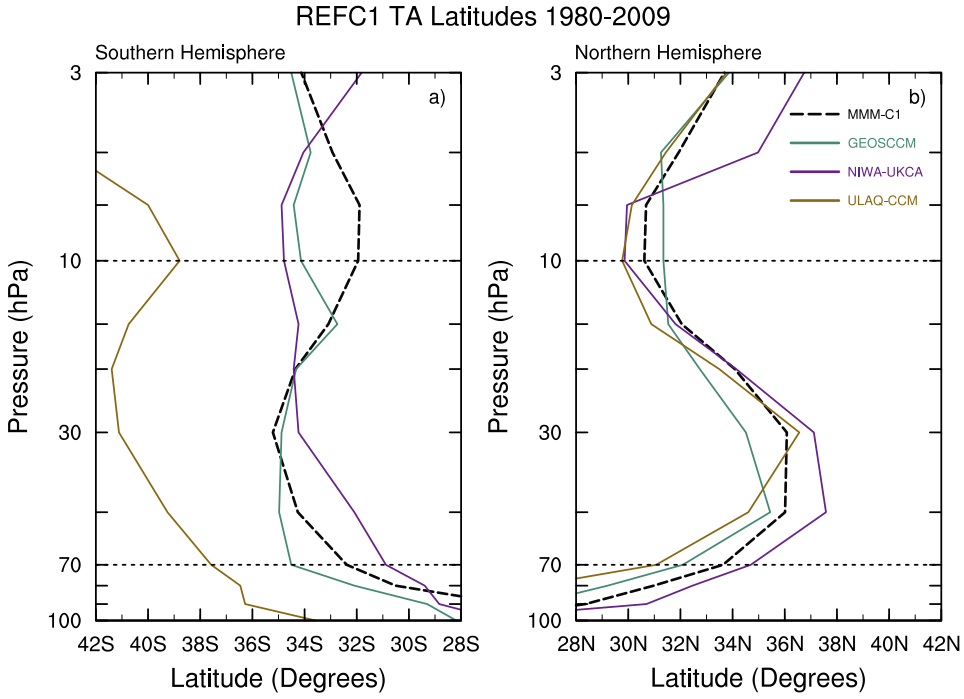

Figure S2.2: Vertical profiles of climatological turnaround latitudes in the stratosphere for the MMM of the REF-C1 runs (MMM-C1) analyzed in the manuscript along with the extra REF-C1 GEOSCCM, NIWA-UKCA, ULAQ-CCM model results for Southern Hemisphere (a) and Northern Hemisphere (b).

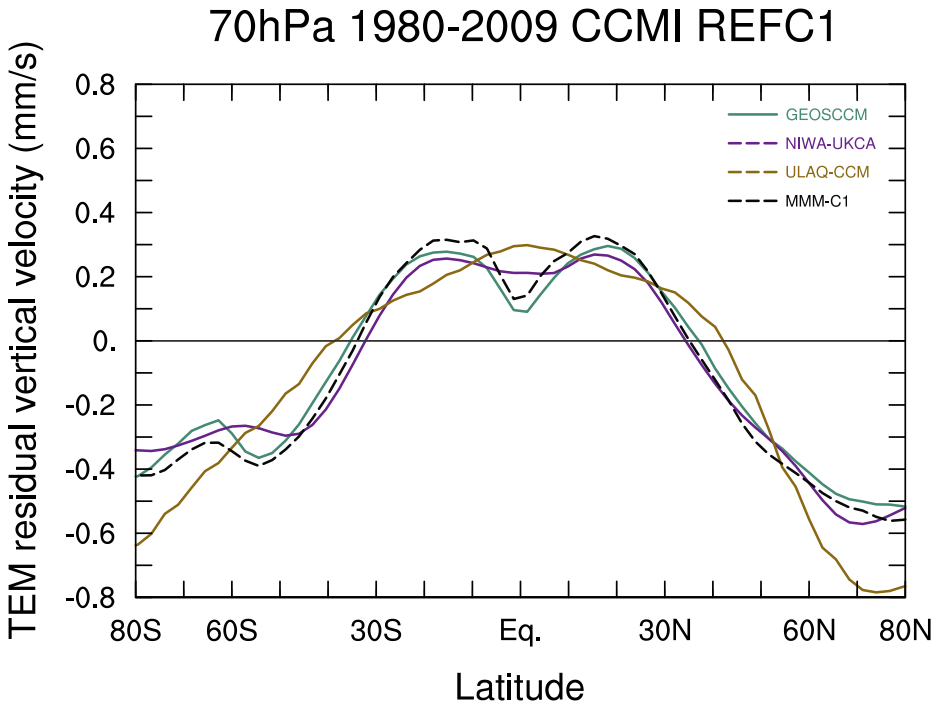

Figure S2.3: Mean strength of annual mean $\overline{w}^*$ mm s^{-1} at 70 hPa for the MMM of the REF-C1 runs (MMM-C1) analyzed in the manuscript along with the extra REF-C1 GEOSCCM, NIWA-UKCA, ULAQ-CCM model simulations

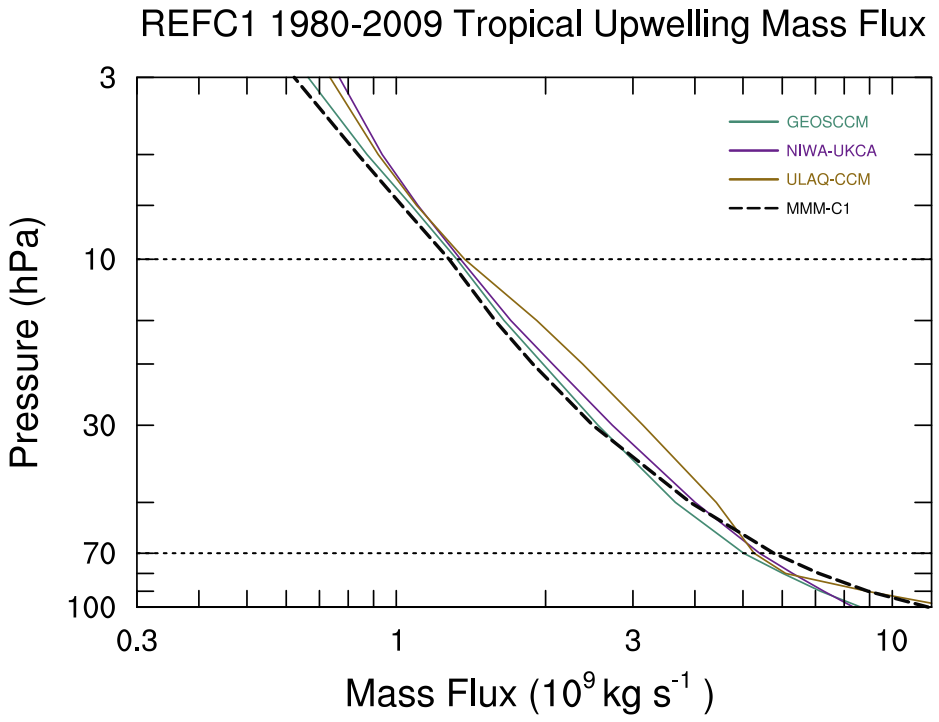

Figure S2.4: Vertical profiles of climatological (1980 – 2009) tropical upward mass flux ($\times 10^9$ kg s^{-1}) averaged between the turnaround latitudes for the MMM of the REF-C1 runs (MMM-C1) analyzed in the manuscript along with the extra REF-C1 GEOSCCM, NIWA-UKCA, ULAQ-CCM model results.

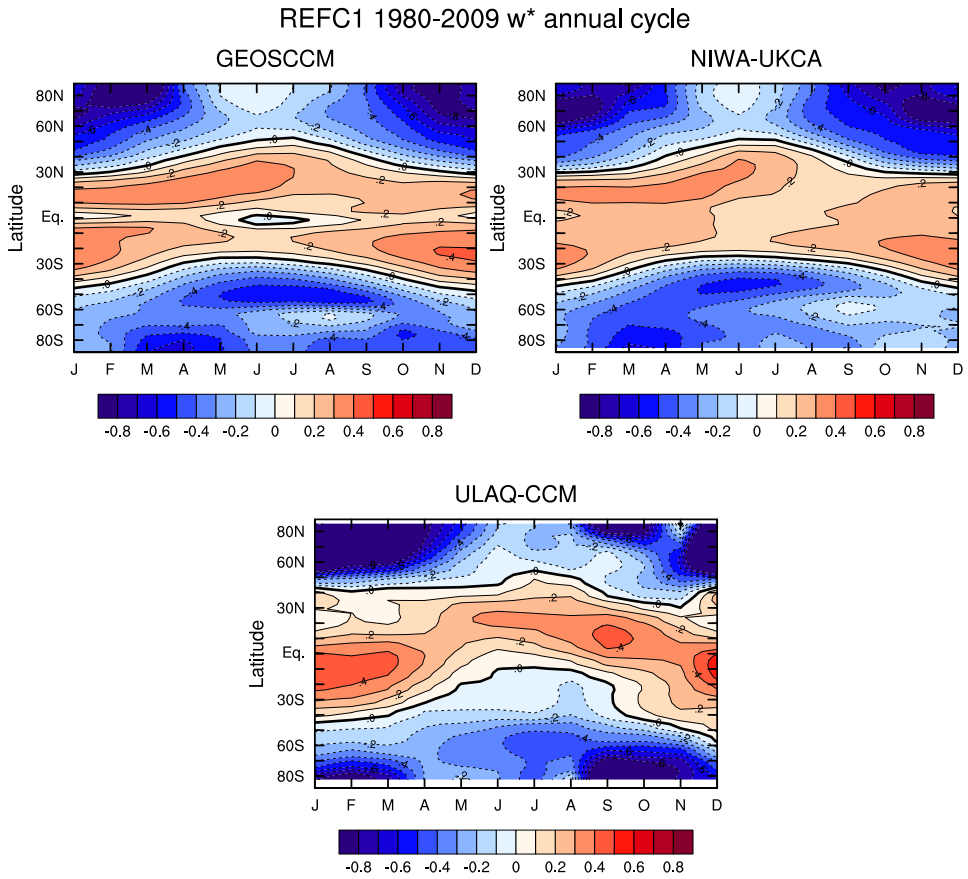

Figure S2.5: Climatological annual cycle in $\overline{w}^*$ ($mm\ s^{-1}$) at 70 hPa for the extra REF-C1 GEOSCCM, NIWA-UKCA, ULAQ-CCM model simulations.

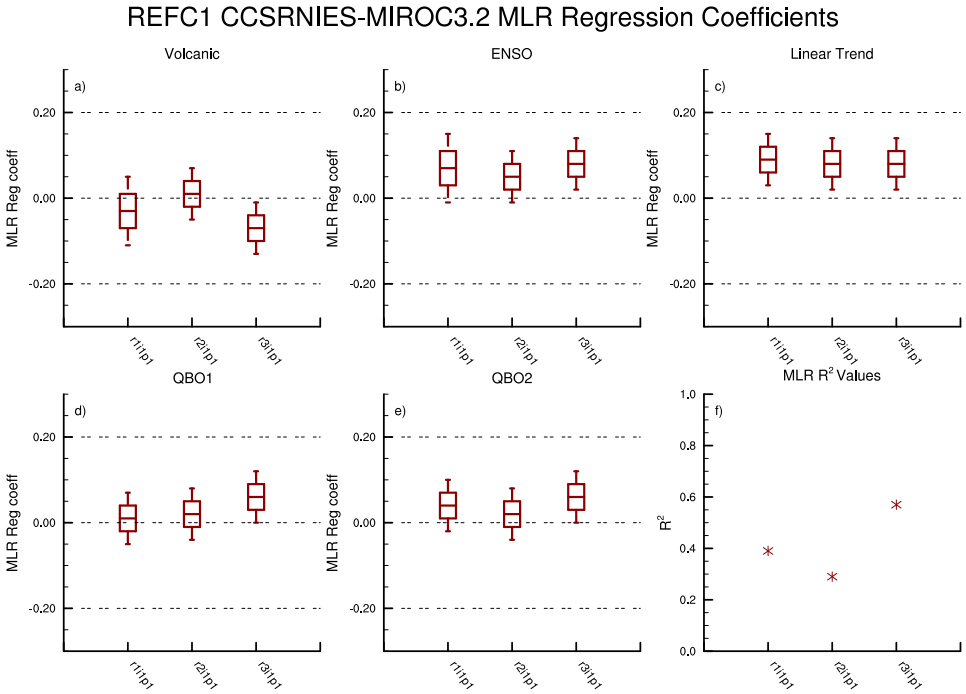

Figure S2.6: Regression coefficients of each regressor ±2 standard errors and R^2 values output from the MLR on the TUMF at 70 hPa for all available REF-C1 CCSRNIES-MIROC3.2 ensemble members.)

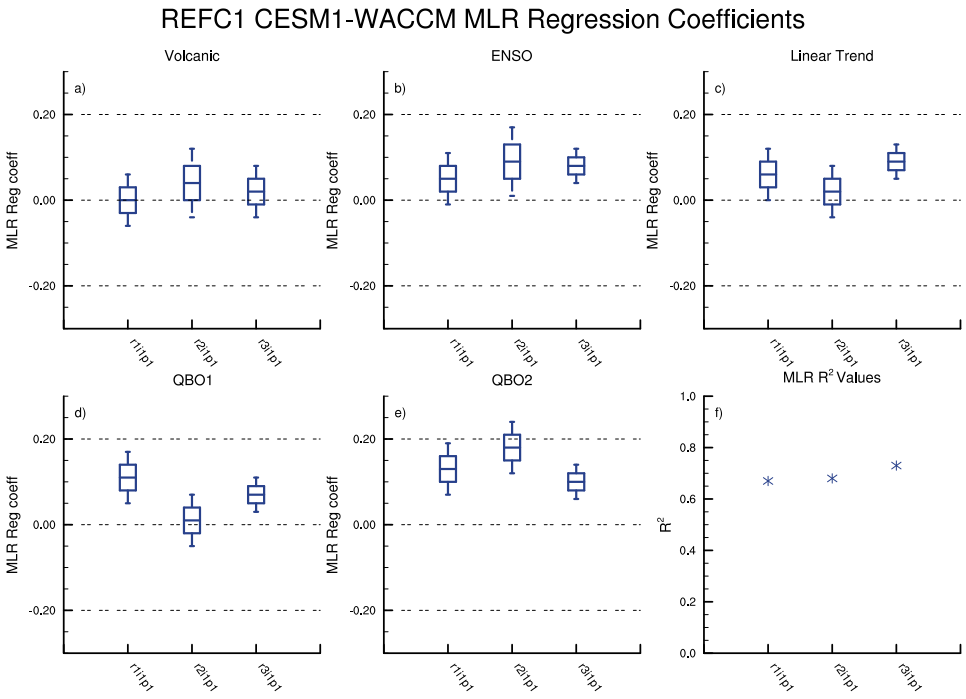

Figure S2.7: Regression coefficients of each regressor ±2 standard errors and R^2 values output from the MLR on the TUMF at 70 hPa for all available REF-C1 CESM1-WACCM ensemble members.

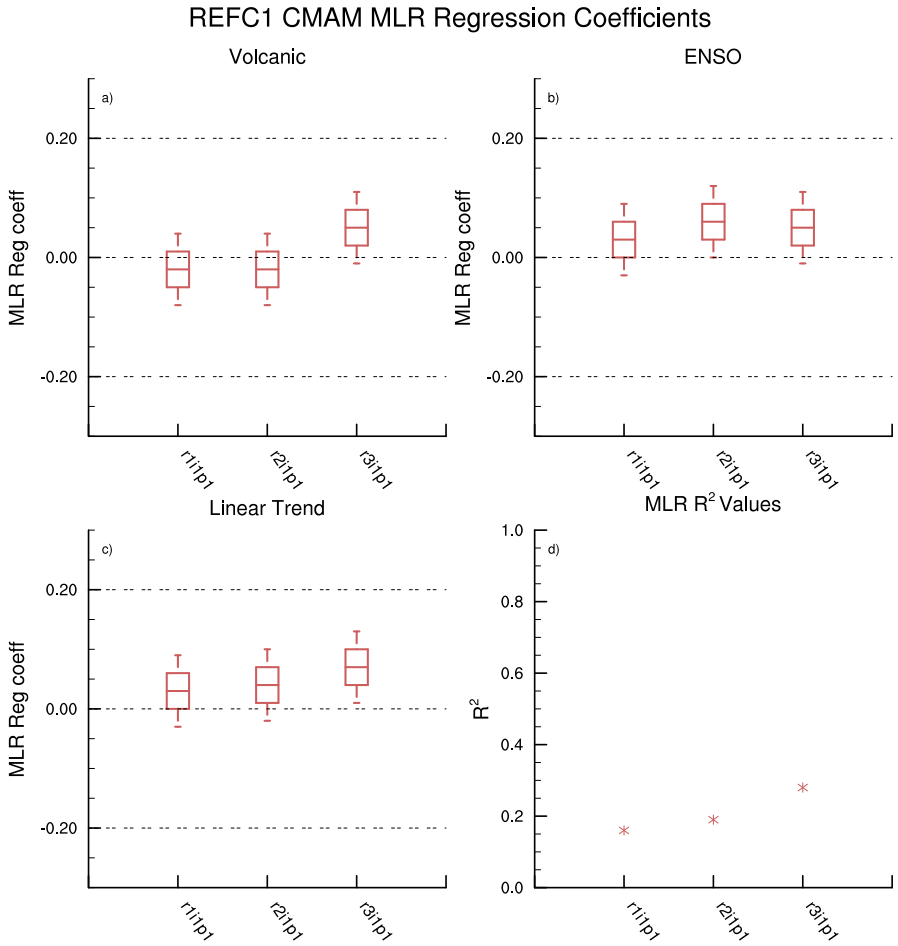

Figure S2.8: Regression coefficients of each regressor ±2 standard errors and R^2 values output from the MLR on the TUMF at 70 hPa for all available REF-C1 CMAM ensemble members. Note that CMAM does not simulate a QBO hence the QBO terms were omitted.

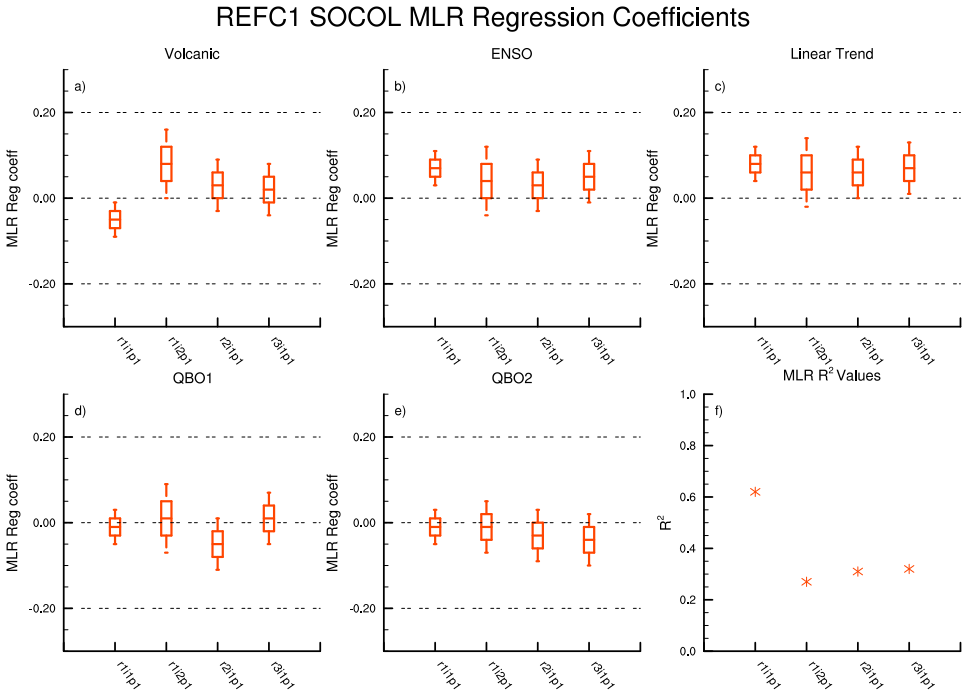

Figure S2.9: Regression coefficients of each regressor ±2 standard errors and R^2 values output from the MLR on the TUMF at 70 hPa for all available REF-C1 SOCOL ensemble members.

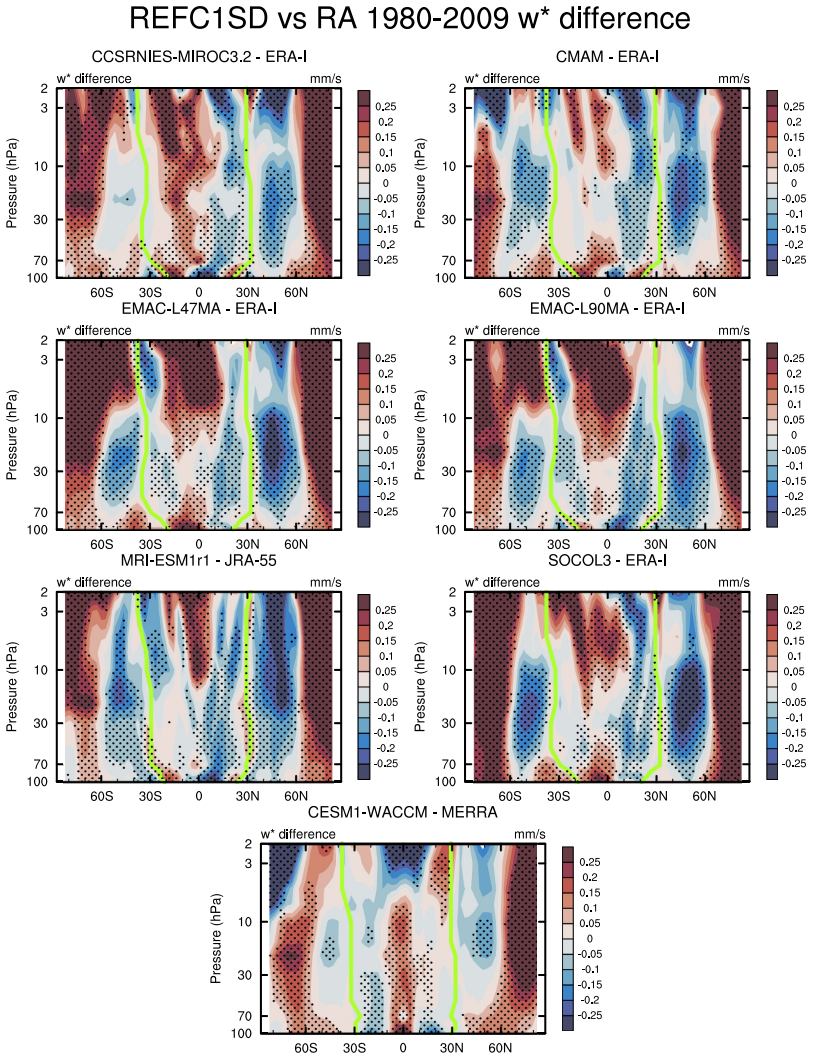

Figure S2.10: Latitude vs pressure cross sections of the stratosphere showing absolute $\overline{w}^*$ ($mm\ s^{-1}$) differences between the 7 REF-C1SD simulations and the respective reanalysis they were nudged towards to. Stippling denotes statistical significance at the 95 % confidence level. The turnaround latitudes of the respective reanalysis are overlaid with green-yellow lines.

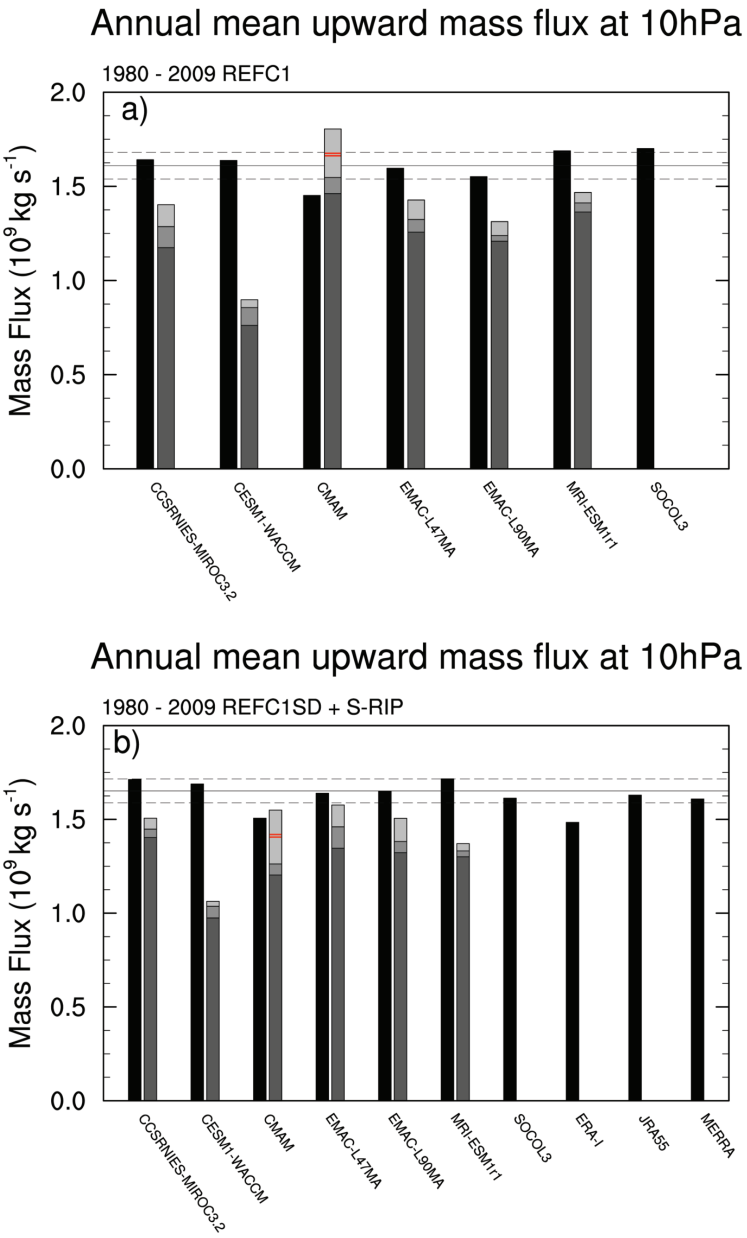

Figure S2.11: Tropical upward mass flux at 10 hPa (left bars) along with downward control calculations (right bars) showing contributions from EPFD (dark grey), OGW (mid-grey), and NOGW (light grey) for (a) REF-C1 and (b) REF-C1SD. For CMAM the NOGWD contributes negatively to TUMF and is indicated with two red horizontal lines inside the lighter grey bar.

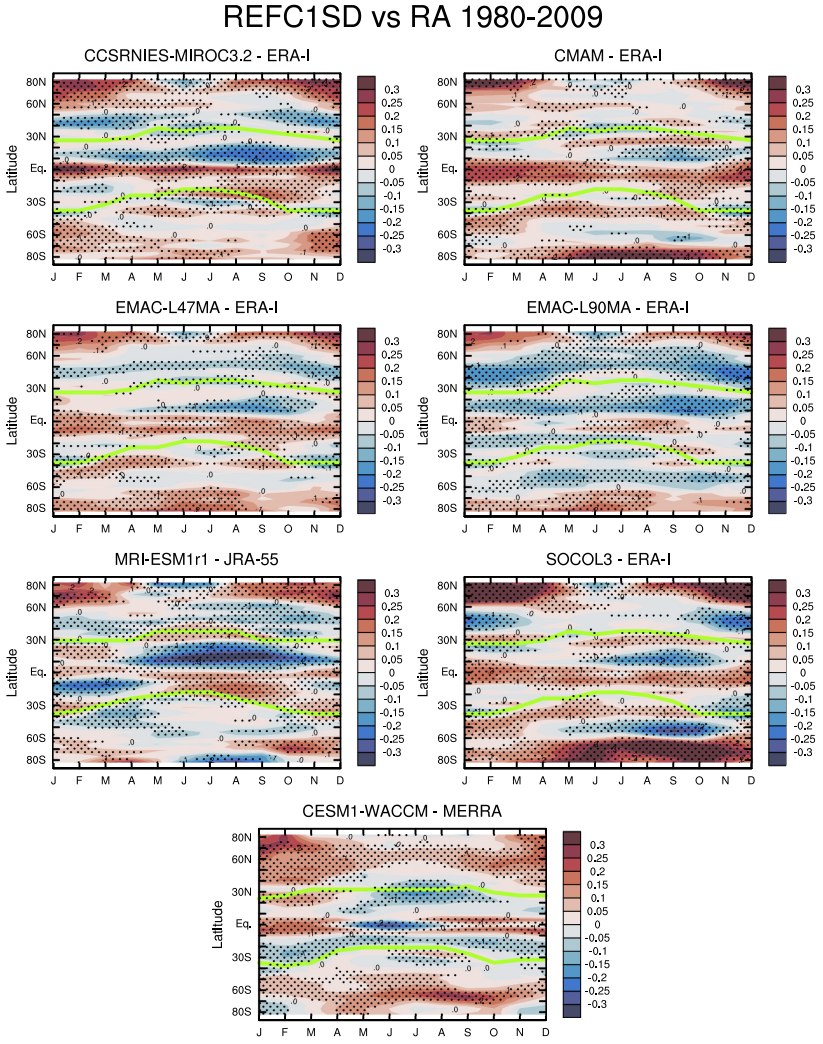

Figure S2.12: Climatological annual cycle $\overline{w}^*$ ($mm\ s^{-1}$) differences at 70 hPa between the 7 REF-C1SD simulations and the respective reanalysis they were nudged towards to. Stippling denotes statistical significance at the 95 % confidence level. The turnaround latitudes of the respective reanalysis are overlaid with green-yellow lines.

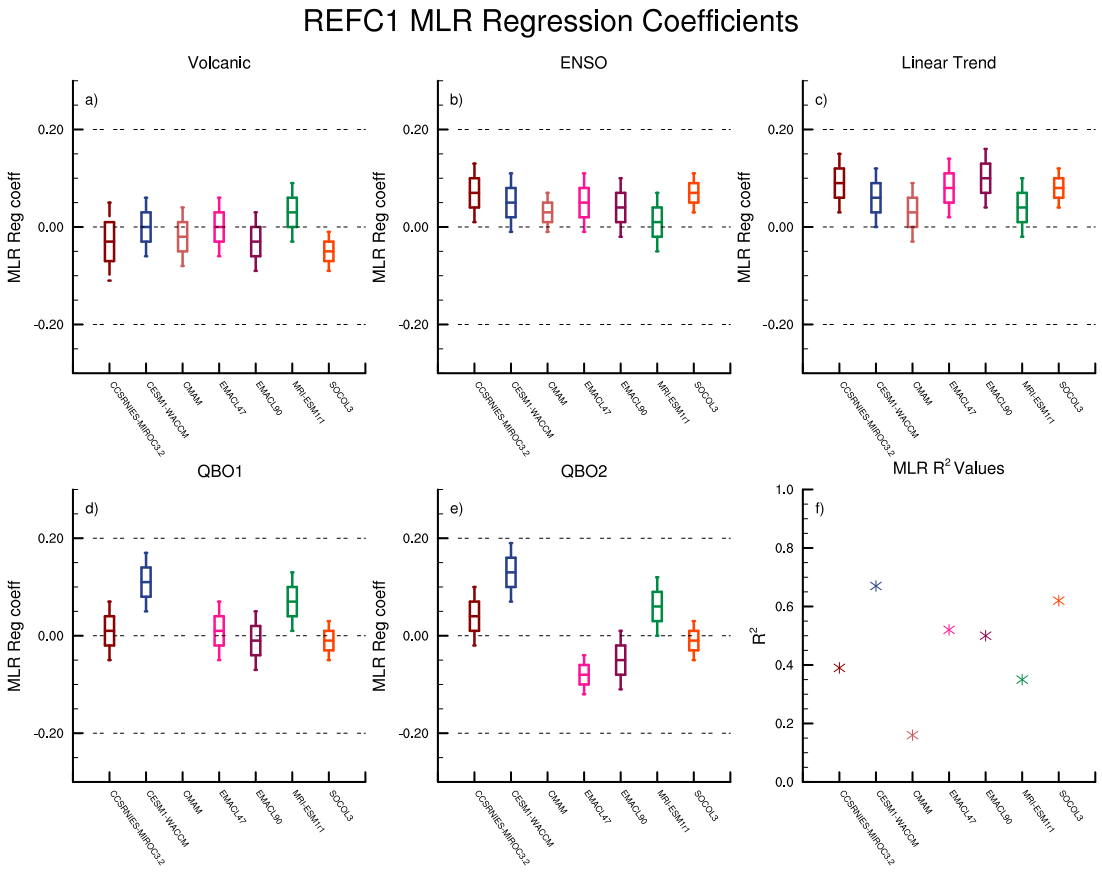

Figure S2.13: Partial regression coefficients of each regressor ±2 standard errors and R^2 values output from the MLR on the TUMF at 70 hPa for REF-C1 simulations.

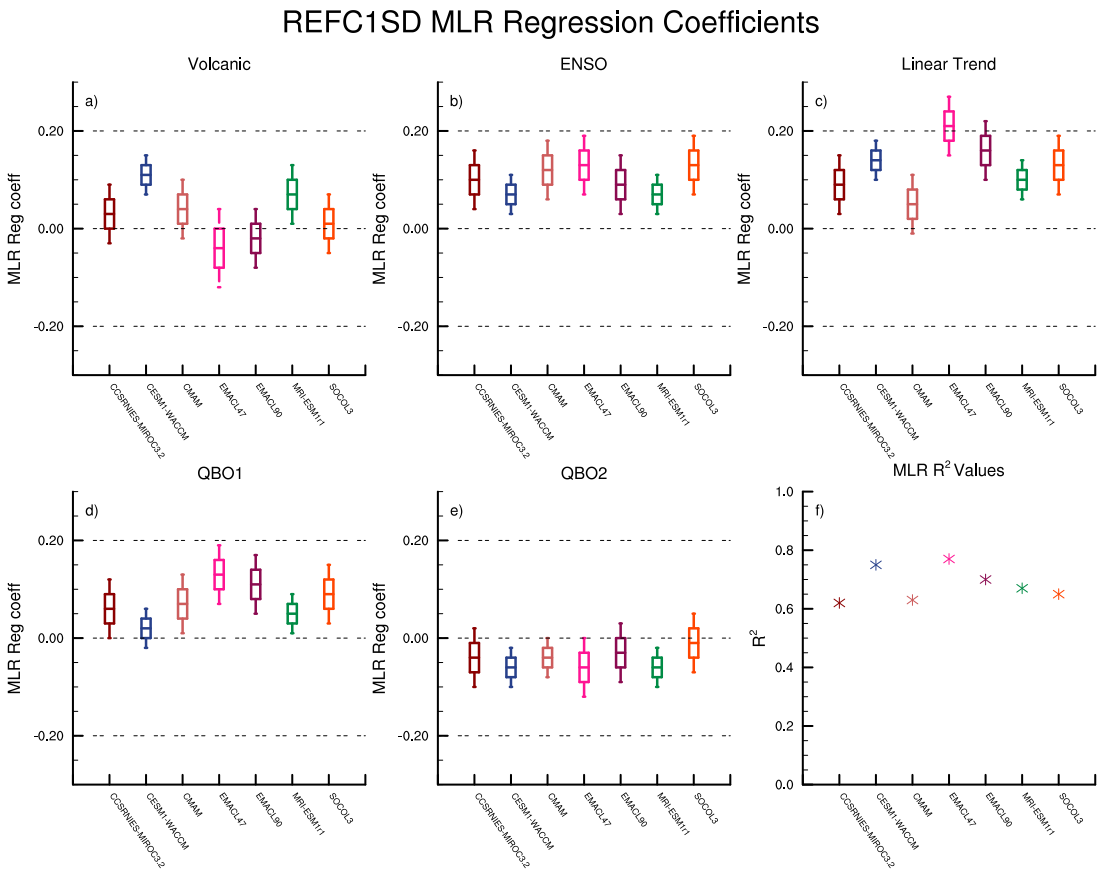

Figure S2.14: Partial regression coefficients of each regressor ±2 standard errors and R^2 values output from the MLR on the TUMF at 70 hPa for REF-C1SD simulations.

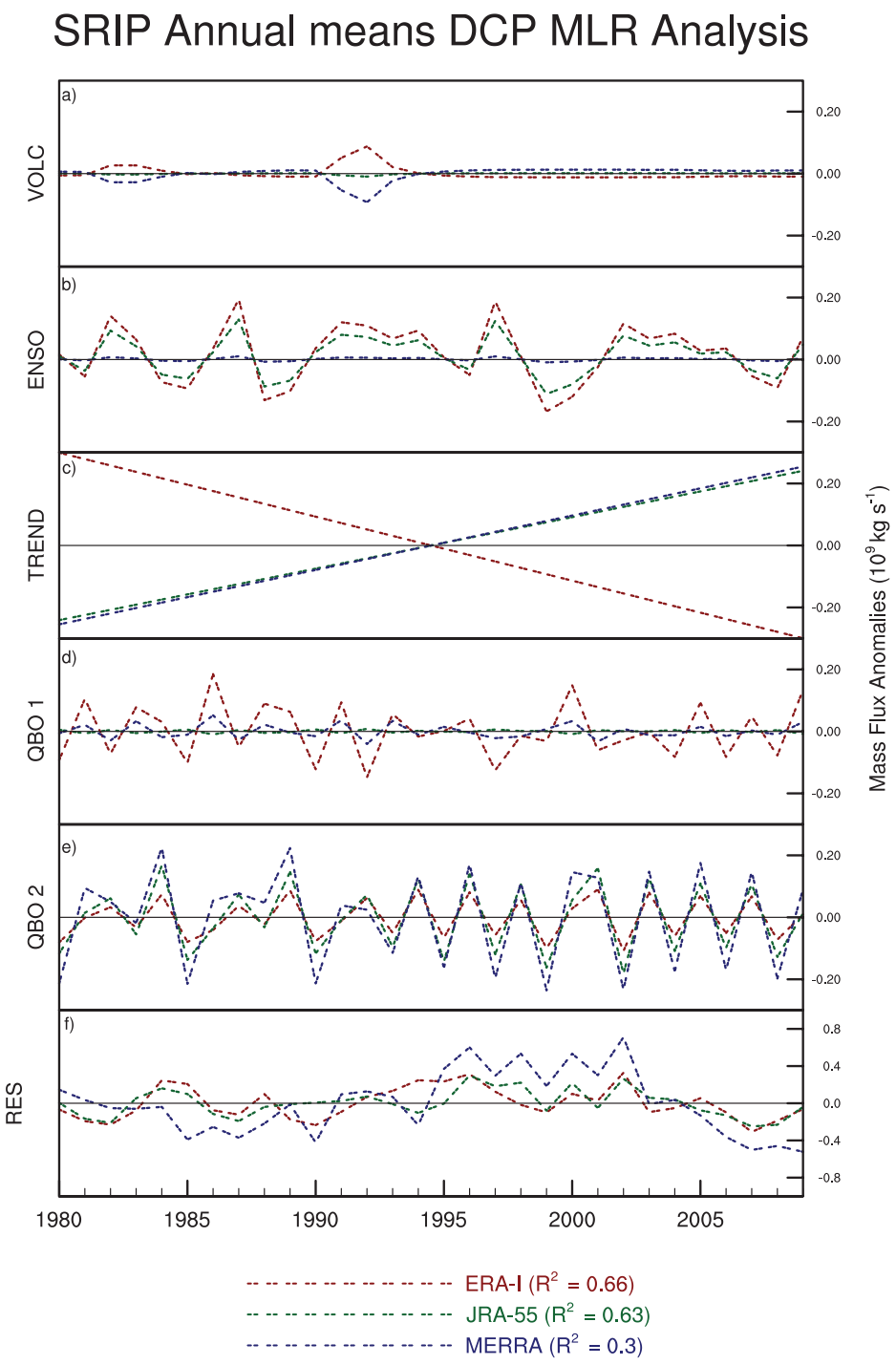

Figure S2.15: Timeseries for the reanalysis datasets of the components of the annual mean tropical upward mass flux attributed to (a) volcanic aerosol, (b) ENSO, (c) linear trend, (d, e) the QBO, and (f) the residuals from the mass flux timeseries and that reconstructed from the MLR.

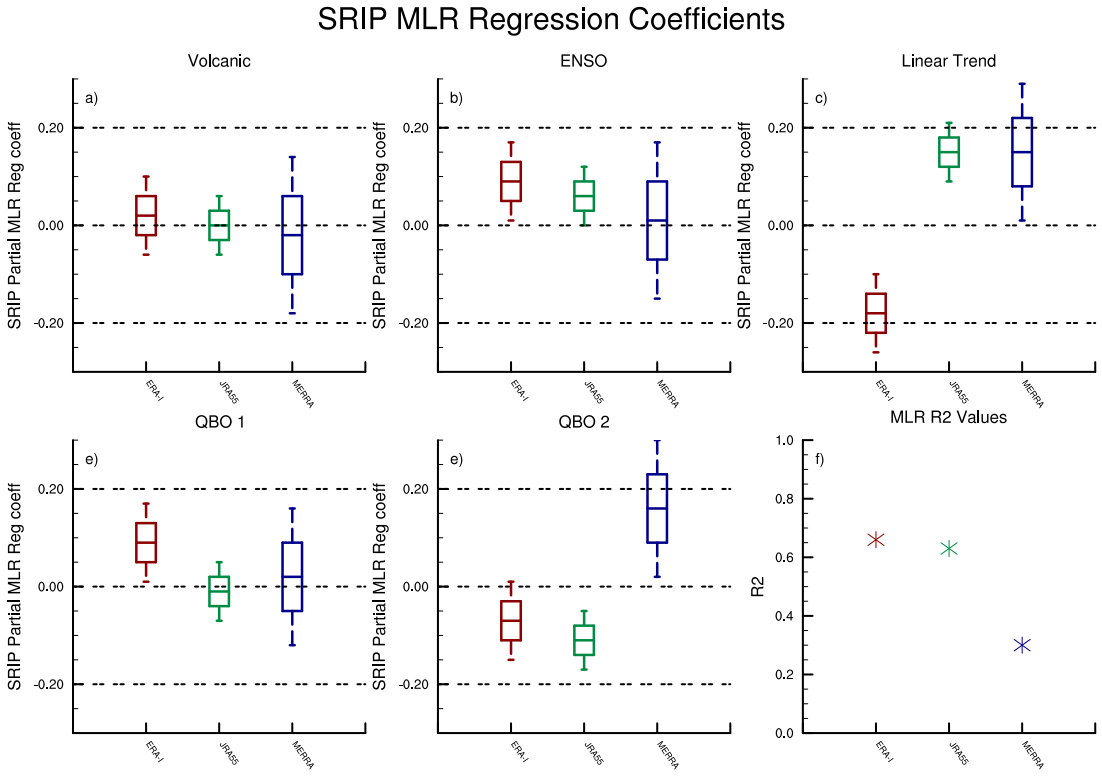

Figure S2.16: Partial regression coefficients of each regressor ±2 standard errors and R^2 values output from the MLR on the TUMF at 70 hPa for the reanalysis datasets.

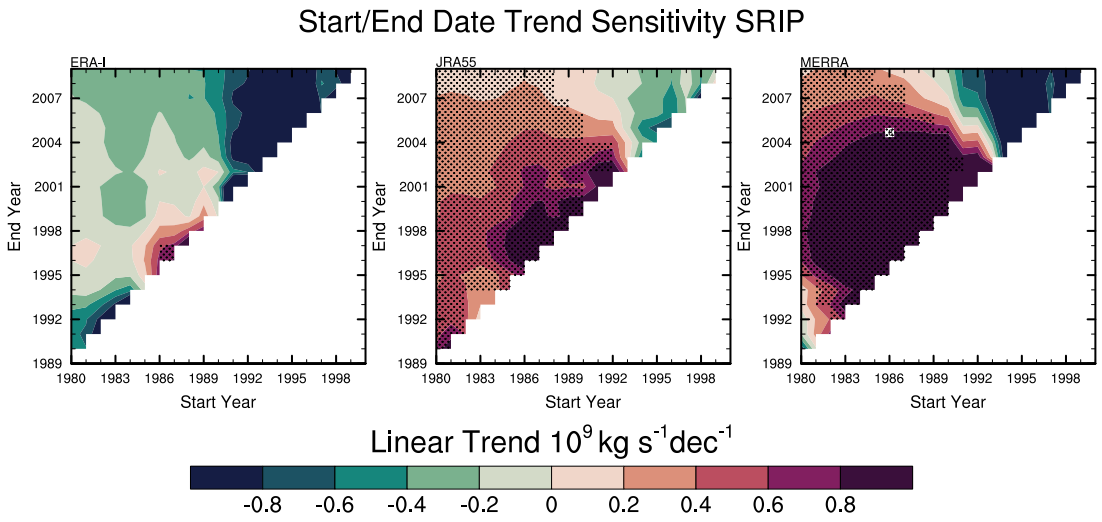

Figure S2.17: Trend sensitivity plots of the mass flux at 70 hPa linear trend per decade (values with statistical significance are stippled) over period $1980-2009$ for the reanalysis datasets.

References

M. Abalos, B. Legras, F. Ploeger, and W. J. Randel. Evaluating the advective Brewer-Dobson circulation in three reanalyses for the period 1979–2012. *Journal of Geophysical Research: Atmospheres*, 120(15):7534–7554, 2015. ISSN 2169-897X. doi: 10.1002/2015JD023182. URL https://onlinelibrary.wiley.com/doi/abs/10.1002/2015JD023182. 51, 52, 58, 61, 63, 66, 82, 86, 91

M. Abalos, L. Polvani, N. Calvo, D. Kinnison, F. Ploeger, W. Randel, and S. Solomon. New Insights on the Impact of Ozone-Depleting Substances on the Brewer-Dobson Circulation. *Journal of Geophysical Research: Atmospheres*, 124(5):2435–2451, 2019. ISSN 2169-897X. doi: 10.1029/2018JD029301. URL https://onlinelibrary.wiley.com/doi/abs/10.1029/2018JD029301. 53, 62

H. Akiyoshi, T. Nakamura, T. Miyasaka, M. Shiotani, and M. Suzuki. A nudged chemistry-climate model simulation of chemical constituent distribution at northern high-latitude stratosphere observed by SMILES and MLS during the 2009/2010 stratospheric sudden warming. *Journal of Geophysical Research: Atmospheres*, 121 (3):1361–1380, 2016. ISSN 2169897X. doi: 10.1002/2015JD023334. URL http://doi.wiley.com/10.1002/2015JD023334. 53, 56, 57

D. G. Andrews and M. E. McIntyre. Planetary Waves in Horizontal and Vertical Shear: The Generalized Eliassen-Palm Relation and the Mean Zonal Acceleration. *Journal of the Atmospheric Sciences*, 33(11):2031–2048, 1976. ISSN 0022-4928. doi: 10.1175/1520-0469(1976)033<2031:PWIHAV>2.0.CO;2. URL http://journals.ametsoc.org/doi/abs/10.1175/1520-0469{%}281976{%}29033{%}3C2031{%}3APWIHAV{%}3E2.0.CO{%}3B2. 51

D. G. Andrews and M. E. McIntyre. An exact theory of nonlinear waves on a Lagrangian-mean flow. *Journal of Fluid Mechanics*, 89(4):609–646, 1978. ISSN 0022-1120. doi: 10.1017/S0022112078002773. URL https://www.cambridge.org/core/product/identifier/S0022112078002773/type/journal{_}article. 51

D. G. Andrews, C. B. Leovy, J. R. Holton, and C. B. Leovy. *Middle Atmosphere Dynamics*. Academic press, 1987. 51, 56, 58

M. P. Baldwin, L. J. Gray, T. J. Dunkerton, K. Hamilton, P. H. Haynes, W. J. Randel, J. R. Holton, M. J. Alexander, I. Hirota, T. Horinouchi, D. B. A. Jones, J. S. Kinnersley, C. Marquardt, K. Sato, and M. Takahashi. The quasi-biennial oscillation. *Reviews of Geophysics*, 39(2):179–229, 2001. ISSN 87551209. doi: 10.1029/1999RG000073. URL http://doi.wiley.com/10.1029/1999RG000073. 62

W. T. Ball, J. Alsing, D. J. Mortlock, J. Staehelin, J. D. Haigh, T. Peter, F. Tummon, R. Stübi, A. Stenke, J. Anderson, A. Bourassa, S. M. Davis, D. Degenstein, S. Frith, L. Froidevaux, C. Roth, V. Sofieva, R. Wang, J. Wild, P. Yu, J. R. Ziemke, and E. V. Rozanov. Evidence for a continuous decline in lower stratospheric ozone offsetting ozone layer recovery. *Atmospheric Chemistry and Physics*, 18(2):1379–1394, 2018. ISSN 1680-7324. doi: 10.5194/acp-18-1379-2018. URL https://www.atmos-chem-phys.net/18/1379/2018/. 53, 54

J. H. Beres. Implementation of a gravity wave source spectrum parameterization dependent on the properties of convection in the Whole Atmosphere Community Climate Model (WACCM). *Journal of Geophysical Research*, 110(D10):D10108, 2005. ISSN 0148-0227. doi: 10.1029/2004JD005504. URL http://doi.wiley.com/10.1029/2004JD005504. 56

T. Birner and H. Bönisch. Residual circulation trajectories and transit times into the extratropical lowermost stratosphere. *Atmospheric Chemistry and Physics*, 11(2): 817–827, 2011. ISSN 1680-7324. doi: 10.5194/acp-11-817-2011. URL https://www.atmos-chem-phys.net/11/817/2011/. 51, 74

N. Butchart. The Brewer-Dobson circulation. *Reviews of Geophysics*, 52(2):157–184, 2014. ISSN 87551209. doi: 10.1002/2013RG000448. URL http://doi.wiley.com/10.1002/2013RG000448. 60

N. Butchart and A. A. Scaife. Removal of chlorofluorocarbons by increased mass exchange between the stratosphere and troposphere in a changing climate. *Nature*, 410(6830):799–802, 2001. ISSN 0028-0836. doi: 10.1038/35071047. URL http://www.nature.com/articles/35071047. 51, 60

N. Butchart, A. A. Scaife, M. Bourqui, J. de Grandpré, S. H. E. Hare, J. Kettleborough, U. Langematz, E. Manzini, F. Sassi, K. Shibata, D. Shindell, and

M. Sigmond. Simulations of anthropogenic change in the strength of the Brewer–Dobson circulation. *Climate Dynamics*, 27(7-8):727–741, 2006. ISSN 0930-7575. doi: 10.1007/s00382-006-0162-4. URL http://link.springer.com/10.1007/s00382-006-0162-4. 60, 61, 66

N. Butchart, I. Cionni, V. Eyring, T. G. Shepherd, D. W. Waugh, H. Akiyoshi, J. Austin, C. Brühl, M. P. Chipperfield, E. Cordero, M. Dameris, R. Deckert, S. Dhomse, S. M. Frith, R. R. Garcia, A. Gettelman, M. A. Giorgetta, D. E. Kinnison, F. Li, E. Mancini, C. McLandress, S. Pawson, G. Pitari, D. A. Plummer, E. Rozanov, F. Sassi, J. F. Scinocca, K. Shibata, B. Steil, and W. Tian. Chemistry–Climate Model Simulations of Twenty-First Century Stratospheric Climate and Circulation Changes. *Journal of Climate*, 23(20):5349–5374, 2010. ISSN 0894-8755. doi: 10.1175/2010JCLI3404.1. URL http://journals.ametsoc.org/doi/10.1175/2010JCLI3404.1. 51, 59, 60, 61, 66

N. Butchart, A. J. Charlton-Perez, I. Cionni, S. C. Hardiman, P. H. Haynes, K. Krüger, P. J. Kushner, P. A. Newman, S. M. Osprey, J. Perlwitz, M. Sigmond, L. Wang, H. Akiyoshi, J. Austin, S. Bekki, A. Baumgaertner, P. Braesicke, C. Brühl, M. Chipperfield, M. Dameris, S. Dhomse, V. Eyring, R. Garcia, H. Garny, P. Jöckel, J.-F. Lamarque, M. Marchand, M. Michou, O. Morgenstern, T. Nakamura, S. Pawson, D. Plummer, J. Pyle, E. Rozanov, J. Scinocca, T. G. Shepherd, K. Shibata, D. Smale, H. Teyssèdre, W. Tian, D. Waugh, and Y. Yamashita. Multimodel climate and variability of the stratosphere. *Journal of Geophysical Research*, 116(D5):D05102, 2011. ISSN 0148-0227. doi: 10.1029/2010JD014995. URL http://doi.wiley.com/10.1029/2010JD014995. 51, 60

N. Calvo, R. R. Garcia, W. J. Randel, and D. R. Marsh. Dynamical Mechanism for the Increase in Tropical Upwelling in the Lowermost Tropical Stratosphere during Warm ENSO Events. *Journal of the Atmospheric Sciences*, 67(7):2331–2340, 2010. ISSN 0022-4928. doi: 10.1175/2010JAS3433.1. URL http://journals.ametsoc.org/doi/10.1175/2010JAS3433.1. 62

A. Chandran and R. L. Collins. Stratospheric sudden warming effects on winds and temperature in the middle atmosphere at middle and low latitudes: a study using

WACCM. *Annales Geophysicae*, 32(7):859–874, 2014. ISSN 1432-0576. doi: 10.5194/angeo-32-859-2014. URL https://www.ann-geophys.net/32/859/2014/. 93

M. P. Chipperfield. Multiannual simulations with a three-dimensional chemical transport model. *Journal of Geophysical Research: Atmospheres*, 104(D1):1781–1805, 1999. ISSN 01480227. doi: 10.1029/98JD02597. URL http://doi.wiley.com/10.1029/98JD02597. 54

M. P. Chipperfield. New version of the TOMCAT/SLIMCAT off-line chemical transport model: Intercomparison of stratospheric tracer experiments. *Quarterly Journal of the Royal Meteorological Society*, 132(617):1179–1203, 2006. ISSN 00359009. doi: 10.1256/qj.05.51. URL http://doi.wiley.com/10.1256/qj.05.51. 54

M. P. Chipperfield, D. Cariolle, and P. Simon. A 3D transport model study of chlorine activation during EASOE. *Geophysical Research Letters*, 21(13):1467–1470, 1994. ISSN 00948276. doi: 10.1029/93GL01679. URL http://doi.wiley.com/10.1029/93GL01679. 54

M. P. Chipperfield, S. Dhomse, R. Hossaini, W. Feng, M. L. Santee, M. Weber, J. P. Burrows, J. D. Wild, D. Loyola, and M. Coldewey-Egbers. On the Cause of Recent Variations in Lower Stratospheric Ozone. *Geophysical Research Letters*, 45(11):5718–5726, 2018. ISSN 00948276. doi: 10.1029/2018GL078071. URL http://doi.wiley.com/10.1029/2018GL078071. 55

N. Y. Cohen, E. P. Gerber, and O. Bühler. Compensation between Resolved and Unresolved Wave Driving in the Stratosphere: Implications for Downward Control. *Journal of the Atmospheric Sciences*, 70(12):3780–3798, 2013. ISSN 0022-4928. doi: 10.1175/JAS-D-12-0346.1. URL http://journals.ametsoc.org/doi/10.1175/JAS-D-12-0346.1. 61, 82

D. P. Dee, S. M. Uppala, A. J. Simmons, P. Berrisford, P. Poli, S. Kobayashi, U. Andrae, M. A. Balmaseda, G. Balsamo, P. Bauer, P. Bechtold, A. C. M. Beljaars, L. van de Berg, J. Bidlot, N. Bormann, C. Delsol, R. Dragani, M. Fuentes, A. J. Geer, L. Haimberger, S. B. Healy, H. Hersbach, E. V. Hólm, L. Isaksen, P. Kållberg, M. Köhler, M. Matricardi, A. P. McNally, B. M. Monge-Sanz, J.-J. Morcrette, B.-K.

Park, C. Peubey, P. de Rosnay, C. Tavolato, J.-N. Thépaut, and F. Vitart. The ERA-Interim reanalysis: configuration and performance of the data assimilation system. *Quarterly Journal of the Royal Meteorological Society*, 137(656):553–597, 2011. ISSN 00359009. doi: 10.1002/qj.828. URL http://doi.wiley.com/10.1002/qj.828. 58

M. Deushi and K. Shibata. Development of a Meteorological Research Institute Chemistry-Climate Model version 2 for the Study of Tropospheric and Stratospheric Chemistry. *Papers in Meteorology and Geophysics*, 62:1–46, 2011. ISSN 1880-6643. doi: 10.2467/mripapers.62.1. URL http://joi.jlc.jst.go.jp/JST.JSTAGE/mripapers/62.1?from=CrossRef. 56, 57

M. Diallo, F. Ploeger, P. Konopka, T. Birner, R. Müller, M. Riese, H. Garny, B. Legras, E. Ray, G. Berthet, and F. Jegou. Significant Contributions of Volcanic Aerosols to Decadal Changes in the Stratospheric Circulation. *Geophysical Research Letters*, 44(20):10,780–10,791, 2017. ISSN 00948276. doi: 10.1002/2017GL074662. URL http://doi.wiley.com/10.1002/2017GL074662. 83

S. Dietmüller, H. Garny, F. Plöger, P. Jöckel, and D. Cai. Effects of mixing on resolved and unresolved scales on stratospheric age of air. *Atmospheric Chemistry and Physics*, 17(12):7703–7719, 2017. ISSN 1680-7324. doi: 10.5194/acp-17-7703-2017. URL https://www.atmos-chem-phys.net/17/7703/2017/. 52

S. Dietmüller, R. Eichinger, H. Garny, T. Birner, H. Boenisch, G. Pitari, E. Mancini, D. Visioni, A. Stenke, L. Revell, E. Rozanov, D. A. Plummer, J. Scinocca, P. Jöckel, L. Oman, M. Deushi, S. Kiyotaka, D. E. Kinnison, R. Garcia, O. Morgenstern, G. Zeng, K. A. Stone, and R. Schofield. Quantifying the effect of mixing on the mean age of air in CCMVal-2 and CCMI-1 models. *Atmospheric Chemistry and Physics*, 18(9):6699–6720, 2018. ISSN 1680-7324. doi: 10.5194/acp-18-6699-2018. URL https://www.atmos-chem-phys.net/18/6699/2018/. 51, 52, 59, 72, 93

H. Douville. Stratospheric polar vortex influence on Northern Hemisphere winter climate variability. *Geophysical Research Letters*, 36(18):L18703, 2009. ISSN 0094-8276. doi: 10.1029/2009GL039334. URL http://doi.wiley.com/10.1029/2009GL039334. 53

A. Ebita, S. Kobayashi, Y. Ota, M. Moriya, R. Kumabe, K. Onogi, Y. Harada, S. Yasui, K. Miyaoka, K. Takahashi, H. Kamahori, C. Kobayashi, H. Endo, M. Soma,

Y. Oikawa, and T. Ishimizu. The Japanese 55-year Reanalysis "JRA-55": An Interim Report. *SOLA*, 7:149–152, 2011. ISSN 1349-6476. doi: 10.2151/sola.2011-038. URL http://joi.jlc.jst.go.jp/JST.JSTAGE/sola/2011-038?from=CrossRef. 58

R. Eichinger, S. Dietmüller, H. Garny, P. Šácha, T. Birner, H. Bönisch, G. Pitari, D. Visioni, A. Stenke, E. Rozanov, L. Revell, D. A. Plummer, P. Jöckel, L. Oman, M. Deushi, D. E. Kinnison, R. Garcia, O. Morgenstern, G. Zeng, K. A. Stone, and R. Schofield. The influence of mixing on the stratospheric age of air changes in the 21st century. *Atmospheric Chemistry and Physics*, 19(2):921–940, 2019. ISSN 1680-7324. doi: 10.5194/acp-19-921-2019. URL https://www.atmos-chem-phys.net/19/921/2019/. 51, 52

A. Engel, T. Möbius, H. Bönisch, U. Schmidt, R. Heinz, I. Levin, E. Atlas, S. Aoki, T. Nakazawa, S. Sugawara, F. Moore, D. Hurst, J. Elkins, S. Schauffler, A. Andrews, and K. Boering. Age of stratospheric air unchanged within uncertainties over the past 30 years. *Nature Geoscience*, 2(1):28–31, 2009. ISSN 1752-0894. doi: 10.1038/ngeo388. URL http://www.nature.com/articles/ngeo388. 52

A. Engel, H. Bönisch, M. Ullrich, R. Sitals, O. Membrive, F. Danis, and C. Crevoisier. Mean age of stratospheric air derived from AirCore observations. *Atmospheric Chemistry and Physics*, 17(11):6825–6838, 2017. ISSN 1680-7324. doi: 10.5194/acp-17-6825-2017. URL https://www.atmos-chem-phys.net/17/6825/2017/. 52

V. Eyring, J.-F. Lamarque, I. Cionni, B. Duncan, A. Fiore, A. Gettel-Man, M. Hegglin, P. Hess, T. Nagashima, T. Ryerson, T. Shepherd, D. Shindell, D. Waugh, and P. Young. Report on the IGAC/SPARC Chemistry-Climate Model Initiative (CCMI) 2013 Science Workshop. Technical report, 2013. URL www.sparc-climate.org/publications/newsletter/. 59

L. Froidevaux, D. E. Kinnison, R. Wang, J. Anderson, and R. A. Fuller. Evaluation of CESM1 (WACCM) free-running and specified dynamics atmospheric composition simulations using global multispecies satellite data records. *Atmospheric Chemistry and Physics*, 19(7):4783–4821, 2019. ISSN 1680-7324. doi: 10.5194/acp-19-4783-2019. URL https://www.atmos-chem-phys.net/19/4783/2019/. 53

R. R. Garcia and B. A. Boville. "Downward Control" of the Mean Meridional Circulation and Temperature Distribution of the Polar Winter Stratosphere. *Journal of the Atmospheric Sciences*, 51(15):2238–2245, 1994. ISSN 0022-4928. doi: 10.1175/1520-0469(1994)051<2238:COTMMC>2.0.CO;2. URL http://journals.ametsoc.org/doi/abs/10.1175/1520-0469{%}281994{%}29051{%}3C2238{%}3ACOTMMC{%}3E2.0.CO{%}3B2. 56

R. R. Garcia, W. J. Randel, and D. E. Kinnison. On the Determination of Age of Air Trends from Atmospheric Trace Species. *Journal of the Atmospheric Sciences*, 68(1):139–154, 2011. ISSN 0022-4928. doi: 10.1175/2010JAS3527.1. URL http://journals.ametsoc.org/doi/10.1175/2010JAS3527.1. 83

R. R. Garcia, A. K. Smith, D. E. Kinnison, Á. de la Cámara, and D. J. Murphy. Modification of the Gravity Wave Parameterization in the Whole Atmosphere Community Climate Model: Motivation and Results. *Journal of the Atmospheric Sciences*, 74(1):275–291, 2017. ISSN 0022-4928. doi: 10.1175/JAS-D-16-0104.1. URL http://journals.ametsoc.org/doi/10.1175/JAS-D-16-0104.1. 56

R. García-Herrera, N. Calvo, R. R. Garcia, and M. A. Giorgetta. Propagation of ENSO temperature signals into the middle atmosphere: A comparison of two general circulation models and ERA-40 reanalysis data. *Journal of Geophysical Research*, 111(D6):D06101, 2006. ISSN 0148-0227. doi: 10.1029/2005JD006061. URL http://doi.wiley.com/10.1029/2005JD006061. 62

H. Garny, T. Birner, H. Bönisch, and F. Bunzel. The effects of mixing on age of air. *Journal of Geophysical Research: Atmospheres*, 119(12):7015–7034, 2014. ISSN 2169897X. doi: 10.1002/2013JD021417. URL http://doi.wiley.com/10.1002/2013JD021417. 51, 52

F. J. Haenel, G. P. Stiller, T. von Clarmann, B. Funke, E. Eckert, N. Glatthor, U. Grabowski, S. Kellmann, M. Kiefer, A. Linden, and T. Reddmann. Reassessment of MIPAS age of air trends and variability. *Atmospheric Chemistry and Physics*, 15 (22):13161–13176, 2015. ISSN 1680-7324. doi: 10.5194/acp-15-13161-2015. URL https://www.atmos-chem-phys.net/15/13161/2015/. 52

S. C. Hardiman, N. Butchart, and N. Calvo. The morphology of the Brewer-Dobson circulation and its response to climate change in CMIP5 simulations. *Quarterly Journal of the Royal Meteorological Society*, 140(683):1958–1965, 2014. ISSN 00359009. doi: 10.1002/qj.2258. URL http://doi.wiley.com/10.1002/qj.2258. 51, 75

S. C. Hardiman, N. Butchart, F. M. O'Connor, and S. T. Rumbold. The Met Office HadGEM3-ES chemistry-climate model: evaluation of stratospheric dynamics and its impact on ozone. *Geoscientific Model Development*, 10(3):1209–1232, 2017a. ISSN 1991-9603. doi: 10.5194/gmd-10-1209-2017. URL https://www.geosci-model-dev.net/10/1209/2017/. 53, 54, 91

S. C. Hardiman, P. Lin, A. A. Scaife, N. J. Dunstone, and H.-L. Ren. The influence of dynamical variability on the observed Brewer-Dobson circulation trend. *Geophysical Research Letters*, 44(6):2885–2892, 2017b. ISSN 00948276. doi: 10.1002/2017GL072706. URL http://doi.wiley.com/10.1002/2017GL072706. 87, 89

P. H. Haynes, M. E. McIntyre, T. G. Shepherd, C. J. Marks, and K. P. Shine. On the "Downward Control" of Extratropical Diabatic Circulations by Eddy-Induced Mean Zonal Forces. *Journal of the Atmospheric Sciences*, 48 (4):651–678, 1991. ISSN 0022-4928. doi: 10.1175/1520-0469(1991)048<0651:OTCOED>2.0.CO;2. URL http://journals.ametsoc.org/doi/abs/10.1175/1520-0469{%}281991{%}29048{%}3C0651{%}3AOTCOED{%}3E2.0.CO{%}3B2. 60, 61, 72, 74, 75, 90

M. I. Hegglin and J. F. Lamarque. The IGAC/SPARC Chemistry-Climate Model Initiative Phase-1 (CCMI-1) model data output. NCAS British Atmospheric Data Centre, 2015. URL http://catalogue.ceda.ac.uk/uuid/9cc6b94df0f4469d8066d69b5df879d5. 56, 59

M. I. Hegglin and T. G. Shepherd. Large climate-induced changes in ultraviolet index and stratosphere-to-troposphere ozone flux. *Nature Geoscience*, 2(10):687–691, 2009. ISSN 1752-0894. doi: 10.1038/ngeo604. URL http://www.nature.com/articles/ngeo604. 51

C. O. Hines. Doppler-spread parameterization of gravity-wave momentum deposition in the middle atmosphere. Part 1: Basic formulation. *Journal of Atmospheric and*

Solar-Terrestrial Physics, 59(4):371–386, 1997a. ISSN 13646826. doi: 10.1016/S1364-6826(96)00079-X. URL https://linkinghub.elsevier.com/retrieve/pii/S136468269600079X. 56

C. O. Hines. Doppler-spread parameterization of gravity-wave momentum deposition in the middle atmosphere. Part 2: Broad and quasi monochromatic spectra, and implementation. *Journal of Atmospheric and Solar-Terrestrial Physics*, 59(4):387–400, 1997b. ISSN 13646826. doi: 10.1016/S1364-6826(96)00080-6. URL https://linkinghub.elsevier.com/retrieve/pii/S1364682696000806. 56

P. Hitchcock and I. R. Simpson. The Downward Influence of Stratospheric Sudden Warmings. *Journal of the Atmospheric Sciences*, 71(10):3856–3876, 2014. ISSN 0022-4928. doi: 10.1175/JAS-D-14-0012.1. URL http://journals.ametsoc.org/doi/10.1175/JAS-D-14-0012.1. 53

J. R. Holton, P. H. Haynes, M. E. McIntyre, A. R. Douglass, R. B. Rood, and L. Pfister. Stratosphere-troposphere exchange. *Reviews of Geophysics*, 33(4):403, 1995. ISSN 8755-1209. doi: 10.1029/95RG02097. URL http://doi.wiley.com/10.1029/95RG02097. 51

K. Imai, N. Manago, C. Mitsuda, Y. Naito, E. Nishimoto, T. Sakazaki, M. Fujiwara, L. Froidevaux, T. von Clarmann, G. P. Stiller, D. P. Murtagh, P.-p. Rong, M. G. Mlynczak, K. A. Walker, D. E. Kinnison, H. Akiyoshi, T. Nakamura, T. Miyasaka, T. Nishibori, S. Mizobuchi, K.-i. Kikuchi, H. Ozeki, C. Takahashi, H. Hayashi, T. Sano, M. Suzuki, M. Takayanagi, and M. Shiotani. Validation of ozone data from the Superconducting Submillimeter-Wave Limb-Emission Sounder (SMILES). *Journal of Geophysical Research: Atmospheres*, 118(11):5750–5769, 2013. ISSN 2169897X. doi: 10.1002/jgrd.50434. URL http://doi.wiley.com/10.1002/jgrd.50434. 56

A. B. M. Jeuken, P. C. Siegmund, L. C. Heijboer, J. Feichter, and L. Bengtsson. On the potential of assimilating meteorological analyses in a global climate model for the purpose of model validation. *Journal of Geophysical Research: Atmospheres*, 101 (D12):16939–16950, 1996. ISSN 01480227. doi: 10.1029/96JD01218. URL http://doi.wiley.com/10.1029/96JD01218. 53

P. Jöckel, R. von Kuhlmann, M. G. Lawrence, B. Steil, C. A. M. Brenninkmeijer, P. J. Crutzen, P. J. Rasch, and B. Eaton. On a fundamental problem in implementing flux-form advection schemes for tracer transport in 3-dimensional general circulation and chemistry transport models. *Quarterly Journal of the Royal Meteorological Society*, 127(573):1035–1052, 2001. ISSN 00359009. doi: 10.1002/qj.49712757318. URL http://doi.wiley.com/10.1002/qj.49712757318. 54

P. Jöckel, A. Kerkweg, A. Pozzer, R. Sander, H. Tost, H. Riede, A. Baumgaertner, S. Gromov, and B. Kern. Development cycle 2 of the Modular Earth Submodel System (MESSy2). *Geoscientific Model Development*, 3(2):717–752, 2010. ISSN 1991-9603. doi: 10.5194/gmd-3-717-2010. URL https://www.geosci-model-dev.net/3/717/2010/. 56

P. Jöckel, H. Tost, A. Pozzer, M. Kunze, O. Kirner, C. A. M. Brenninkmeijer, S. Brinkop, D. S. Cai, C. Dyroff, J. Eckstein, F. Frank, H. Garny, K.-D. Gottschaldt, P. Graf, V. Grewe, A. Kerkweg, B. Kern, S. Matthes, M. Mertens, S. Meul, M. Neumaier, M. Nützel, S. Oberländer-Hayn, R. Ruhnke, T. Runde, R. Sander, D. Scharffe, and A. Zahn. Earth System Chemistry integrated Modelling (ESCiMo) with the Modular Earth Submodel System (MESSy) version 2.51. *Geoscientific Model Development*, 9(3):1153–1200, 2016. ISSN 1991-9603. doi: 10.5194/gmd-9-1153-2016. URL https://www.geosci-model-dev.net/9/1153/2016/. 56, 57, 83

A. I. Jonsson, J. de Grandpré, V. I. Fomichev, J. C. McConnell, and S. R. Beagley. Doubled CO2-induced cooling in the middle atmosphere: Photochemical analysis of the ozone radiative feedback. *Journal of Geophysical Research: Atmospheres*, 109 (D24):D24103, 2004. ISSN 0148-0227. doi: 10.1029/2004JD005093. URL https://agupubs.onlinelibrary.wiley.com/doi/abs/10.1029/2004JD005093. 56

T. Jung, M. J. Miller, and T. N. Palmer. Diagnosing the Origin of Extended-Range Forecast Errors. *Monthly Weather Review*, 138(6):2434–2446, 2010. ISSN 0027-0644. doi: 10.1175/2010MWR3255.1. URL http://journals.ametsoc.org/doi/10.1175/2010MWR3255.1. 53

A. Karpechko and A. C. Maycock. Karpechko, A.Yu and Maycock A.C. (Lead Authors), M. Abalos, H. Akiyoshi, J.M. Arblaster, C.I. Garfinkel, K.H. Rosenlof and M. Sig-

mond , Stratospheric Ozone Changes and Climate, Chapter 5 in Scientific Assessment of Ozone Depletion: 2018, Global Ozone Rese. Technical report, 2018. 52, 53

J. Keeble, E. M. Bednarz, A. Banerjee, N. L. Abraham, N. R. P. Harris, A. C. Maycock, and J. A. Pyle. Diagnosing the radiative and chemical contributions to future changes in tropical column ozone with the UM-UKCA chemistry–climate model. *Atmospheric Chemistry and Physics*, 17(22):13801–13818, 2017. ISSN 1680-7324. doi: 10.5194/acp-17-13801-2017. URL https://www.atmos-chem-phys.net/17/13801/2017/. 51

H. Kida. General Circulation of Air Parcels and Transport Characteristics Derived from a hemispheric GCM- Part 1. A Determination of Advective Mass Flow in the Lower Stratosphere. *Journal of the Meteorological Society of Japan. Ser. II*, 61(2): 171–187, 1983. ISSN 0026-1165. doi: 10.2151/jmsj1965.61.2_171. URL https://www.jstage.jst.go.jp/article/jmsj1965/61/2/61{_}2{_}171/{_}article. 52

C. Kobayashi and T. Iwasaki. Brewer-Dobson circulation diagnosed from JRA-55. *Journal of Geophysical Research: Atmospheres*, 121(4):1493–1510, 2016. ISSN 2169897X. doi: 10.1002/2015JD023476. URL http://doi.wiley.com/10.1002/2015JD023476. 51

S. Kobayashi, Y. Ota, Y. Harada, A. Ebita, M. Moriya, H. Onoda, K. Onogi, H. Kamahori, C. Kobayashi, H. Endo, K. Miyaoka, and K. Takahashi. The JRA-55 Reanalysis: General Specifications and Basic Characteristics. *Journal of the Meteorological Society of Japan. Ser. II*, 93(1):5–48, 2015. ISSN 0026-1165. doi: 10.2151/jmsj.2015-001. URL https://www.jstage.jst.go.jp/article/jmsj/93/1/93{_}2015-001/{_}article. 58

M. Krol, M. de Bruine, L. Killaars, H. Ouwersloot, A. Pozzer, Y. Yin, F. Chevallier, P. Bousquet, P. Patra, D. Belikov, S. Maksyutov, S. Dhomse, W. Feng, and M. P. Chipperfield. Age of air as a diagnostic for transport timescales in global models. *Geoscientific Model Development*, 11(8):3109–3130, 2018. ISSN 1991-9603. doi: 10.5194/gmd-11-3109-2018. URL https://www.geosci-model-dev.net/11/3109/2018/. 54

J.-F. Lamarque, L. K. Emmons, P. G. Hess, D. E. Kinnison, S. Tilmes, F. Vitt, C. L. Heald, E. A. Holland, P. H. Lauritzen, J. Neu, J. J. Orlando, P. J. Rasch, and G. K. Tyndall. CAM-chem: description and evaluation of interactive atmospheric

chemistry in the Community Earth System Model. *Geoscientific Model Development*, 5(2):369–411, 2012. ISSN 1991-9603. doi: 10.5194/gmd-5-369-2012. URL https://www.geosci-model-dev.net/5/369/2012/. 57

J.-F. Lamarque, D. T. Shindell, B. Josse, P. J. Young, I. Cionni, V. Eyring, D. Bergmann, P. Cameron-Smith, W. J. Collins, R. Doherty, S. Dalsoren, G. Faluvegi, G. Folberth, S. J. Ghan, L. W. Horowitz, Y. H. Lee, I. A. MacKenzie, T. Nagashima, V. Naik, D. Plummer, M. Righi, S. T. Rumbold, M. Schulz, R. B. Skeie, D. S. Stevenson, S. Strode, K. Sudo, S. Szopa, A. Voulgarakis, and G. Zeng. The Atmospheric Chemistry and Climate Model Intercomparison Project (ACCMIP): overview and description of models, simulations and climate diagnostics. *Geoscientific Model Development*, 6(1):179–206, 2013. ISSN 1991-9603. doi: 10.5194/gmd-6-179-2013. URL https://www.geosci-model-dev.net/6/179/2013/. 55

F. Lefèvre, G. P. Brasseur, I. Folkins, A. K. Smith, and P. Simon. Chemistry of the 1991–1992 stratospheric winter: Three-dimensional model simulations. *Journal of Geophysical Research*, 99(D4):8183, 1994. ISSN 0148-0227. doi: 10.1029/93JD03476. URL http://doi.wiley.com/10.1029/93JD03476. 54

F. Li, P. Newman, S. Pawson, and J. Perlwitz. Effects of Greenhouse Gas Increase and Stratospheric Ozone Depletion on Stratospheric Mean Age of Air in 1960-2010. *Journal of Geophysical Research: Atmospheres*, 123(4):2098–2110, 2018. ISSN 2169897X. doi: 10.1002/2017JD027562. URL https://agupubs.onlinelibrary.wiley.com/doi/abs/10.1002/2017JD027562. 52

M. Linz, R. A. Plumb, E. P. Gerber, F. J. Haenel, G. Stiller, D. E. Kinnison, A. Ming, and J. L. Neu. The strength of the meridional overturning circulation of the stratosphere. *Nature Geoscience*, 10(9):663–667, 2017. ISSN 1752-0894. doi: 10.1038/ngeo3013. URL http://www.nature.com/articles/ngeo3013. 53

M. Linz, M. Abalos, A. S. Glanville, D. E. Kinnison, A. Ming, and J. L. Neu. The global diabatic circulation of the stratosphere as a metric for the Brewer–Dobson circulation. *Atmospheric Chemistry and Physics*, 19(7):5069–5090, 2019. ISSN 1680-7324. doi: 10.5194/acp-19-5069-2019. URL https://www.atmos-chem-phys.net/19/5069/2019/. 61

M. Löffler, S. Brinkop, and P. Jöckel. Impact of major volcanic eruptions on stratospheric water vapour. *Atmospheric Chemistry and Physics*, 16(10):6547–6562, 2016. ISSN 1680-7324. doi: 10.5194/acp-16-6547-2016. URL https://www.atmos-chem-phys.net/16/6547/2016/. 53

E. Mahieu, M. P. Chipperfield, J. Notholt, T. Reddmann, J. Anderson, P. F. Bernath, T. Blumenstock, M. T. Coffey, S. S. Dhomse, W. Feng, B. Franco, L. Froidevaux, D. W. T. Griffith, J. W. Hannigan, F. Hase, R. Hossaini, N. B. Jones, I. Morino, I. Murata, H. Nakajima, M. Palm, C. Paton-Walsh, J. M. R. III, M. Schneider, C. Servais, D. Smale, and K. A. Walker. Recent Northern Hemisphere stratospheric HCl increase due to atmospheric circulation changes. *Nature*, 515(7525):104–107, 2014. ISSN 0028-0836. doi: 10.1038/nature13857. URL http://www.nature.com/articles/nature13857. 54

D. R. Marsh and R. R. Garcia. Attribution of decadal variability in lower-stratospheric tropical ozone. *Geophysical Research Letters*, 34(21):L21807, 2007. ISSN 0094-8276. doi: 10.1029/2007GL030935. URL http://doi.wiley.com/10.1029/2007GL030935. 62

D. R. Marsh, M. J. Mills, D. E. Kinnison, J.-F. Lamarque, N. Calvo, and L. M. Polvani. Climate Change from 1850 to 2005 Simulated in CESM1(WACCM). *Journal of Climate*, 26(19):7372–7391, 2013. ISSN 0894-8755. doi: 10.1175/JCLI-D-12-00558.1. URL http://journals.ametsoc.org/doi/10.1175/JCLI-D-12-00558.1. 56

P. Martineau. S-RIP: Zonal-mean dynamical variables of global atmospheric reanalyses on pressure levels. Centre for Environmental Data Analysis, 2017. URL https://catalogue.ceda.ac.uk/uuid/b241a7f536a244749662360bd7839312. 63

P. Martineau, J. S. Wright, N. Zhu, and M. Fujiwara. Zonal-mean data set of global atmospheric reanalyses on pressure levels. *Earth System Science Data*, 10(4):1925–1941, 2018. ISSN 1866-3516. doi: 10.5194/essd-10-1925-2018. URL https://www.earth-syst-sci-data.net/10/1925/2018/. 63

A. C. Maycock, W. J. Randel, A. K. Steiner, A. Y. Karpechko, J. Christy, R. Saunders, D. W. J. Thompson, C.-Z. Zou, A. Chrysanthou, N. Luke Abraham, H. Akiyoshi, A. T. Archibald, N. Butchart, M. Chipperfield, M. Dameris, M. Deushi, S. Dhomse,

G. Di Genova, P. Jöckel, D. E. Kinnison, O. Kirner, F. Ladstädter, M. Michou, O. Morgenstern, F. O'Connor, L. Oman, G. Pitari, D. A. Plummer, L. E. Revell, E. Rozanov, A. Stenke, D. Visioni, Y. Yamashita, and G. Zeng. Revisiting the Mystery of Recent Stratospheric Temperature Trends. *Geophysical Research Letters*, 45(18):9919–9933, 2018. ISSN 00948276. doi: 10.1029/2018GL078035. URL http://doi.wiley.com/10.1029/2018GL078035. 62

C. McLandress, J. F. Scinocca, T. G. Shepherd, M. C. Reader, and G. L. Manney. Dynamical Control of the Mesosphere by Orographic and Nonorographic Gravity Wave Drag during the Extended Northern Winters of 2006 and 2009. *Journal of the Atmospheric Sciences*, 70(7):2152–2169, 2013. ISSN 0022-4928. doi: 10.1175/JAS-D-12-0297.1. URL http://journals.ametsoc.org/doi/10.1175/JAS-D-12-0297.1. 57

W. J. Merryfield, W.-S. Lee, G. J. Boer, V. V. Kharin, J. F. Scinocca, G. M. Flato, R. S. Ajayamohan, J. C. Fyfe, Y. Tang, and S. Polavarapu. The Canadian Seasonal to Interannual Prediction System. Part I: Models and Initialization. *Monthly Weather Review*, 141(8):2910–2945, 2013. ISSN 0027-0644. doi: 10.1175/MWR-D-12-00216.1. URL http://journals.ametsoc.org/doi/10.1175/MWR-D-12-00216.1. 92

A. Ming, P. Hitchcock, and P. Haynes. The Double Peak in Upwelling and Heating in the Tropical Lower Stratosphere. *Journal of the Atmospheric Sciences*, 73(5):1889–1901, 2016a. ISSN 0022-4928. doi: 10.1175/JAS-D-15-0293.1. URL http://journals.ametsoc.org/doi/10.1175/JAS-D-15-0293.1. 63, 66, 91

A. Ming, P. Hitchcock, and P. Haynes. The Response of the Lower Stratosphere to Zonally Symmetric Thermal and Mechanical Forcing. *Journal of the Atmospheric Sciences*, 73(5):1903–1922, 2016b. ISSN 0022-4928. doi: 10.1175/JAS-D-15-0294.1. URL http://journals.ametsoc.org/doi/10.1175/JAS-D-15-0294.1. 91

K. Miyazaki, T. Iwasaki, K. Shibata, M. Deushi, and T. T. Sekiyama. The Impact of Changing Meteorological Variables to Be Assimilated into GCM on Ozone Simulation with MRI CTM. *Journal of the Meteorological Society of Japan*, 83(5):909–918, 2005. ISSN 0026-1165. doi: 10.2151/jmsj.83.909. URL http://joi.jlc.jst.go.jp/JST.JSTAGE/jmsj/83.909?from=CrossRef. 92

K. Miyazaki, T. Iwasaki, Y. Kawatani, C. Kobayashi, S. Sugawara, and M. I. Hegglin. Inter-comparison of stratospheric mean-meridional circulation and eddy mixing among six reanalysis data sets. *Atmospheric Chemistry and Physics*, 16(10): 6131–6152, 2016. ISSN 1680-7324. doi: 10.5194/acp-16-6131-2016. URL https://www.atmos-chem-phys.net/16/6131/2016/. 52

A. Molod, L. Takacs, M. Suarez, J. Bacmeister, I.-S. Song, and A. Eichmann. *The GEOS-5 Atmospheric General Circulation Model: Mean Climate and Development from MERRA to Fortuna*, volume 28. 2012. ISBN 2012104606. URL https://ntrs.nasa.gov/search.jsp?R=20120011790. 56

A. Molod, L. Takacs, M. Suarez, and J. Bacmeister. Development of the GEOS-5 atmospheric general circulation model: evolution from MERRA to MERRA2. *Geoscientific Model Development*, 8(5):1339–1356, 2015. ISSN 1991-9603. doi: 10.5194/gmd-8-1339-2015. URL https://www.geosci-model-dev.net/8/1339/2015/. 56

B. M. Monge-Sanz, M. P. Chipperfield, D. P. Dee, A. J. Simmons, and S. M. Uppala. Improvements in the stratospheric transport achieved by a chemistry transport model with ECMWF (re)analyses: identifying effects and remaining challenges. *Quarterly Journal of the Royal Meteorological Society*, 139(672):654–673, 2013a. ISSN 00359009. doi: 10.1002/qj.1996. URL http://doi.wiley.com/10.1002/qj.1996. 54

B. M. Monge-Sanz, M. P. Chipperfield, A. Untch, J.-J. Morcrette, A. Rap, and A. J. Simmons. On the uses of a new linear scheme for stratospheric methane in global models: water source, transport tracer and radiative forcing. *Atmospheric Chemistry and Physics*, 13(18):9641–9660, 2013b. ISSN 1680-7324. doi: 10.5194/acp-13-9641-2013. URL https://www.atmos-chem-phys.net/13/9641/2013/. 54

F. L. Moore, E. A. Ray, K. H. Rosenlof, J. W. Elkins, P. Tans, A. Karion, and C. Sweeney. A Cost-Effective Trace Gas Measurement Program for Long-Term Monitoring of the Stratospheric Circulation. *Bulletin of the American Meteorological Society*, 95(1):147–155, 2014. ISSN 0003-0007. doi: 10.1175/BAMS-D-12-00153.1. URL http://journals.ametsoc.org/doi/abs/10.1175/BAMS-D-12-00153.1. 53

O. Morgenstern, P. Braesicke, F. M. O'Connor, A. C. Bushell, C. E. Johnson, S. M. Osprey, and J. A. Pyle. Evaluation of the new UKCA climate-composition model –

Part 1: The stratosphere. *Geoscientific Model Development*, 2(1):43–57, 2009. ISSN 1991-9603. doi: 10.5194/gmd-2-43-2009. URL https://www.geosci-model-dev.net/2/43/2009/. 56

O. Morgenstern, G. Zeng, N. Luke Abraham, P. J. Telford, P. Braesicke, J. A. Pyle, S. C. Hardiman, F. M. O'Connor, and C. E. Johnson. Impacts of climate change, ozone recovery, and increasing methane on surface ozone and the tropospheric oxidizing capacity. *Journal of Geophysical Research: Atmospheres*, 118(2): 1028–1041, 2013. ISSN 2169897X. doi: 10.1029/2012JD018382. URL https://agupubs.onlinelibrary.wiley.com/doi/abs/10.1029/2012JD018382. 56

O. Morgenstern, M. I. Hegglin, E. Rozanov, F. M. O'Connor, N. L. Abraham, H. Akiyoshi, A. T. Archibald, S. Bekki, N. Butchart, M. P. Chipperfield, M. Deushi, S. S. Dhomse, R. R. Garcia, S. C. Hardiman, L. W. Horowitz, P. Jöckel, B. Josse, D. Kinnison, M. Lin, E. Mancini, M. E. Manyin, M. Marchand, V. Marécal, M. Michou, L. D. Oman, G. Pitari, D. A. Plummer, L. E. Revell, D. Saint-Martin, R. Schofield, A. Stenke, K. Stone, K. Sudo, T. Y. Tanaka, S. Tilmes, Y. Yamashita, K. Yoshida, and G. Zeng. Review of the global models used within phase 1 of the Chemistry–Climate Model Initiative (CCMI). *Geoscientific Model Development*, 10(2):639–671, 2017. ISSN 1991-9603. doi: 10.5194/gmd-10-639-2017. URL https://www.geosci-model-dev.net/10/639/2017/. 55, 56, 83, 92

O. Morgenstern, K. A. Stone, R. Schofield, H. Akiyoshi, Y. Yamashita, D. E. Kinnison, R. R. Garcia, K. Sudo, D. A. Plummer, J. Scinocca, L. D. Oman, M. E. Manyin, G. Zeng, E. Rozanov, A. Stenke, L. E. Revell, G. Pitari, E. Mancini, G. Di Genova, D. Visioni, S. S. Dhomse, and M. P. Chipperfield. Ozone sensitivity to varying greenhouse gases and ozone-depleting substances in CCMI-1 simulations. *Atmospheric Chemistry and Physics*, 18(2):1091–1114, 2018. ISSN 1680-7324. doi: 10.5194/acp-18-1091-2018. URL https://www.atmos-chem-phys.net/18/1091/2018/. 52, 62

J. L. Neu and R. A. Plumb. Age of air in a "leaky pipe" model of stratospheric transport. *Journal of Geophysical Research: Atmospheres*, 104(D16):19243–19255, 1999. ISSN 01480227. doi: 10.1029/1999JD900251. URL https://agupubs.onlinelibrary.wiley.com/doi/abs/10.1029/1999JD900251. 52, 53

L. D. Oman, J. R. Ziemke, A. R. Douglass, D. W. Waugh, C. Lang, J. M. Rodriguez, and J. E. Nielsen. The response of tropical tropospheric ozone to ENSO. *Geophysical Research Letters*, 38(13):n/a–n/a, 2011. ISSN 00948276. doi: 10.1029/2011GL047865. URL http://doi.wiley.com/10.1029/2011GL047865. 56

L. D. Oman, A. R. Douglass, J. R. Ziemke, J. M. Rodriguez, D. W. Waugh, and J. E. Nielsen. The ozone response to ENSO in Aura satellite measurements and a chemistry-climate simulation. *Journal of Geophysical Research: Atmospheres*, 118 (2):965–976, 2013. ISSN 2169897X. doi: 10.1029/2012JD018546. URL http://doi.wiley.com/10.1029/2012JD018546. 56

C. Orbe, H. Yang, D. W. Waugh, G. Zeng, O. Morgenstern, D. E. Kinnison, J.-F. Lamarque, S. Tilmes, D. A. Plummer, J. F. Scinocca, B. Josse, V. Marecal, P. Jöckel, L. D. Oman, S. E. Strahan, M. Deushi, T. Y. Tanaka, K. Yoshida, H. Akiyoshi, Y. Yamashita, A. Stenke, L. Revell, T. Sukhodolov, E. Rozanov, G. Pitari, D. Visioni, K. A. Stone, R. Schofield, and A. Banerjee. Large-scale tropospheric transport in the Chemistry–Climate Model Initiative (CCMI) simulations. *Atmospheric Chemistry and Physics*, 18(10):7217–7235, 2018. ISSN 1680-7324. doi: 10.5194/acp-18-7217-2018. URL https://www.atmos-chem-phys.net/18/7217/2018/. 55, 91

N. M. Pedatella, T. Fuller-Rowell, H. Wang, H. Jin, Y. Miyoshi, H. Fujiwara, H. Shinagawa, H.-L. Liu, F. Sassi, H. Schmidt, V. Matthias, and L. Goncharenko. The neutral dynamics during the 2009 sudden stratosphere warming simulated by different whole atmosphere models. *Journal of Geophysical Research: Space Physics*, 119(2):1306–1324, 2014. ISSN 21699380. doi: 10.1002/2013JA019421. URL http://doi.wiley.com/10.1002/2013JA019421. 93

G. Pitari and V. Rizi. An Estimate of the Chemical and Radiative Perturbation of Stratospheric Ozone Following the Eruption of Mt. Pinatubo. *Journal of the Atmospheric Sciences*, 50(19):3260–3276, 1993. ISSN 0022-4928. doi: 10.1175/1520-0469(1993)050<3260:AEOTCA>2.0.CO;2. URL http://journals.ametsoc.org/doi/abs/10.1175/1520-0469{%}281993{%}29050{%}3C3260{%}3AAEOTCA{%}3E2.0.CO{%}3B2. 62

G. Pitari, V. Aquila, B. Kravitz, A. Robock, S. Watanabe, I. Cionni, N. D. Luca, G. D. Genova, E. Mancini, and S. Tilmes. Stratospheric ozone response to sulfate geoengineering: Results from the Geoengineering Model Intercomparison Project (GeoMIP). *Journal of Geophysical Research: Atmospheres*, 119(5):2629–2653, 2014. ISSN 2169897X. doi: 10.1002/2013JD020566. URL http://doi.wiley.com/10.1002/2013JD020566. 56

F. Ploeger and T. Birner. Seasonal and inter-annual variability of lower stratospheric age of air spectra. *Atmospheric Chemistry and Physics*, 16(15):10195–10213, 2016. ISSN 1680-7324. doi: 10.5194/acp-16-10195-2016. URL https://www.atmos-chem-phys.net/16/10195/2016/. 52

F. Ploeger, M. Abalos, T. Birner, P. Konopka, B. Legras, R. Müller, and M. Riese. Quantifying the effects of mixing and residual circulation on trends of stratospheric mean age of air. *Geophysical Research Letters*, 42(6):2047–2054, 2015a. ISSN 00948276. doi: 10.1002/2014GL062927. URL http://doi.wiley.com/10.1002/2014GL062927. 51, 52

F. Ploeger, M. Riese, F. Haenel, P. Konopka, R. Müller, and G. Stiller. Variability of stratospheric mean age of air and of the local effects of residual circulation and eddy mixing. *Journal of Geophysical Research: Atmospheres*, 120(2):716–733, 2015b. ISSN 2169897X. doi: 10.1002/2014JD022468. URL http://doi.wiley.com/10.1002/2014JD022468. 51, 52

F. Ploeger, B. Legras, E. Charlesworth, X. Yan, M. Diallo, P. Konopka, T. Birner, M. Tao, A. Engel, and M. Riese. How robust are stratospheric age of air trends from different reanalyses? *Atmospheric Chemistry and Physics*, 19(9):6085–6105, 2019. ISSN 1680-7324. doi: 10.5194/acp-19-6085-2019. URL https://www.atmos-chem-phys.net/19/6085/2019/. 52

R. A. Plumb. Stratospheric Transport. *Journal of the Meteorological Society of Japan. Ser. II*, 80(4B):793–809, 2002. ISSN 0026-1165. doi: 10.2151/jmsj.80.793. URL https://www.jstage.jst.go.jp/article/jmsj/80/4B/80{_}4B{_}793/{_}article. 51

L. Polvani, L. Wang, M. Abalos, N. Butchart, M. Chipperfield, M. Dameris, M. Deushi, S. Dhomse, P. Jöckel, D. Kinnison, M. Michou, O. Morgenstern, L. Oman, D. Plummer, and K. Stone. Large impacts, past and future, of ozone-depleting substances on Brewer-Dobson circulation trends: A multi-model assessment. *Journal of Geophysical Research: Atmospheres*, page 2018JD029516, 2019. ISSN 2169-897X. doi: 10.1029/2018JD029516. URL https://onlinelibrary.wiley.com/doi/abs/10.1029/2018JD029516. 53, 62

L. M. Polvani, M. Abalos, R. Garcia, D. Kinnison, and W. J. Randel. Significant Weakening of Brewer-Dobson Circulation Trends Over the 21st Century as a Consequence of the Montreal Protocol. *Geophysical Research Letters*, 45(1):401–409, 2018. ISSN 00948276. doi: 10.1002/2017GL075345. URL http://doi.wiley.com/10.1002/2017GL075345. 62, 89

W. J. Randel and A. M. Thompson. Interannual variability and trends in tropical ozone derived from SAGE II satellite data and SHADOZ ozonesondes. *Journal of Geophysical Research*, 116(D7):D07303, 2011. ISSN 0148-0227. doi: 10.1029/2010JD015195. URL http://doi.wiley.com/10.1029/2010JD015195. 51

W. J. Randel, R. R. Garcia, N. Calvo, and D. Marsh. ENSO influence on zonal mean temperature and ozone in the tropical lower stratosphere. *Geophysical Research Letters*, 36(15):n/a–n/a, 2009. ISSN 00948276. doi: 10.1029/2009GL039343. URL http://doi.wiley.com/10.1029/2009GL039343. 62

E. A. Ray, F. L. Moore, K. H. Rosenlof, D. A. Plummer, F. Kolonjari, and K. A. Walker. An idealized stratospheric model useful for understanding differences between long-lived trace gas measurements and global chemistry-climate model output. *Journal of Geophysical Research: Atmospheres*, 121(10):5356–5367, 2016. ISSN 2169897X. doi: 10.1002/2015JD024447. URL http://doi.wiley.com/10.1002/2015JD024447. 53

L. E. Revell, F. Tummon, R. J. Salawitch, A. Stenke, and T. Peter. The changing ozone depletion potential of N 2 O in a future climate. *Geophysical Research Letters*, 42(22):10,047–10,055, 2015a. ISSN 00948276. doi: 10.1002/2015GL065702. URL http://doi.wiley.com/10.1002/2015GL065702. 56

L. E. Revell, F. Tummon, A. Stenke, T. Sukhodolov, A. Coulon, E. Rozanov, H. Garny, V. Grewe, and T. Peter. Drivers of the tropospheric ozone budget throughout the 21st century under the medium-high climate scenario RCP 6.0. *Atmospheric Chemistry and Physics*, 15(10):5887–5902, 2015b. ISSN 1680-7324. doi: 10.5194/acp-15-5887-2015. URL https://www.atmos-chem-phys.net/15/5887/2015/. 75

J. H. Richter, F. Sassi, and R. R. Garcia. Toward a Physically Based Gravity Wave Source Parameterization in a General Circulation Model. *Journal of the Atmospheric Sciences*, 67(1):136–156, 2010. ISSN 0022-4928. doi: 10.1175/2009JAS3112.1. URL http://journals.ametsoc.org/doi/10.1175/2009JAS3112.1. 56

M. M. Rienecker, M. J. Suarez, R. Gelaro, R. Todling, J. Bacmeister, E. Liu, M. G. Bosilovich, S. D. Schubert, L. Takacs, G.-K. Kim, S. Bloom, J. Chen, D. Collins, A. Conaty, A. da Silva, W. Gu, J. Joiner, R. D. Koster, R. Lucchesi, A. Molod, T. Owens, S. Pawson, P. Pegion, C. R. Redder, R. Reichle, F. R. Robertson, A. G. Ruddick, M. Sienkiewicz, and J. Woollen. MERRA: NASA's Modern-Era Retrospective Analysis for Research and Applications. *Journal of Climate*, 24 (14):3624–3648, 2011. ISSN 0894-8755. doi: 10.1175/JCLI-D-11-00015.1. URL http://journals.ametsoc.org/doi/10.1175/JCLI-D-11-00015.1. 58

R. B. Rood, D. J. Allen, W. E. Baker, D. J. Lamich, and J. A. Kaye. The Use of Assimilated Stratospheric Data in Constituent Transport Calculations. *Journal of the Atmospheric Sciences*, 46(5):687–702, 1989. ISSN 0022-4928. doi: 10.1175/1520-0469(1989)046<0687:TUOASD>2.0.CO;2. URL http://journals.ametsoc.org/doi/abs/10.1175/1520-0469{%}281989{%}29046{%}3C0687{%}3ATUOASD{%}3E2.0.CO{%}3B2. 54

K. H. Rosenlof. Seasonal cycle of the residual mean meridional circulation in the stratosphere. *Journal of Geophysical Research*, 100(D3):5173, 1995. ISSN 0148-0227. doi: 10.1029/94JD03122. URL http://doi.wiley.com/10.1029/94JD03122. 59, 60

P. Šácha, R. Eichinger, H. Garny, P. Pišoft, S. Dietmüller, L. de la Torre, D. A. Plummer, P. Jöckel, O. Morgenstern, G. Zeng, N. Butchart, and J. A. Añel. Extratropical age of air trends and causative factors in climate projection simulations. *Atmospheric Chemistry and Physics*, 19(11):7627–7647, 2019. ISSN 1680-7324. doi: 10.5194/

acp-19-7627-2019. URL https://www.atmos-chem-phys.net/19/7627/2019/. 51, 52

A. A. Scaife, N. Butchart, C. D. Warner, and R. Swinbank. Impact of a Spectral Gravity Wave Parameterization on the Stratosphere in the Met Office Unified Model. *Journal of the Atmospheric Sciences*, 59(9): 1473–1489, 2002. ISSN 0022-4928. doi: 10.1175/1520-0469(2002)059<1473:IOASGW>2.0.CO;2. URL http://journals.ametsoc.org/doi/abs/10.1175/1520-0469{%}282002{%}29059{%}3C1473{%}3AIOASGW{%}3E2.0.CO{%}3B2. 56

A. Schmidt, M. J. Mills, S. Ghan, J. M. Gregory, R. P. Allan, T. Andrews, C. G. Bardeen, A. Conley, P. M. Forster, A. Gettelman, R. W. Portmann, S. Solomon, and O. B. Toon. Volcanic Radiative Forcing From 1979 to 2015. *Journal of Geophysical Research: Atmospheres*, 123(22):12491–12508, 2018. ISSN 2169-897X. doi: 10.1029/2018JD028776. URL https://onlinelibrary.wiley.com/doi/abs/10.1029/2018JD028776. 53, 92

U. Schmidt and A. Khedim. In situ measurements of carbon dioxide in the winter Arctic vortex and at midlatitudes: An indicator of the 'age' of stratopheric air. *Geophysical Research Letters*, 18(4):763–766, 1991. ISSN 00948276. doi: 10.1029/91GL00022. URL http://doi.wiley.com/10.1029/91GL00022. 52

J. F. Scinocca. An Accurate Spectral Nonorographic Gravity Wave Drag Parameterization for General Circulation Models. *Journal of the Atmospheric Sciences*, 60(4):667–682, 2003. ISSN 0022-4928. doi: 10.1175/1520-0469(2003)060<0667:AASNGW>2.0.CO;2. URL http://journals.ametsoc.org/doi/abs/10.1175/1520-0469{%}282003{%}29060{%}3C0667{%}3AAASNGW{%}3E2.0.CO{%}3B2. 56

J. F. Scinocca, N. A. McFarlane, M. Lazare, J. Li, and D. Plummer. Technical Note: The CCCma third generation AGCM and its extension into the middle atmosphere. *Atmospheric Chemistry and Physics*, 8(23):7055–7074, 2008. ISSN 1680-7324. doi: 10.5194/acp-8-7055-2008. URL https://www.atmos-chem-phys.net/8/7055/2008/. 56

W. J. M. Seviour, N. Butchart, and S. C. Hardiman. The Brewer-Dobson circulation inferred from ERA-Interim. *Quarterly Journal of the Royal Meteorological Society*,

138(665):878–888, 2012. ISSN 00359009. doi: 10.1002/qj.966. URL http://doi.wiley.com/10.1002/qj.966. 52, 60, 61

A. K. Smith, N. M. Pedatella, D. R. Marsh, and T. Matsuo. On the Dynamical Control of the Mesosphere–Lower Thermosphere by the Lower and Middle Atmosphere. *Journal of the Atmospheric Sciences*, 74(3):933–947, 2017. ISSN 0022-4928. doi: 10.1175/JAS-D-16-0226.1. URL http://journals.ametsoc.org/doi/10.1175/JAS-D-16-0226.1. 92

S. Solomon, D. Kinnison, J. Bandoro, and R. Garcia. Simulation of polar ozone depletion: An update. *Journal of Geophysical Research: Atmospheres*, 120(15):7958–7974, 2015. ISSN 2169-897X. doi: 10.1002/2015JD023365. URL https://onlinelibrary.wiley.com/doi/abs/10.1002/2015JD023365. 56

S. Solomon, D. Kinnison, R. R. Garcia, J. Bandoro, M. Mills, C. Wilka, R. R. Neely, A. Schmidt, J. E. Barnes, J.-P. Vernier, and M. Höpfner. Monsoon circulations and tropical heterogeneous chlorine chemistry in the stratosphere. *Geophysical Research Letters*, 43(24):12,624–12,633, 2016. ISSN 00948276. doi: 10.1002/2016GL071778. URL http://doi.wiley.com/10.1002/2016GL071778. 53, 92

SPARC. SPARC CCMVal Report on the Evaluation of Chemistry-Climate Models. V. Eyring, T. Shepherd and D. Waugh (Eds.). *SPARC Report No. 5, WCRP-30/2010,WMO/TD-No.40*, 2010. ISSN 1428-345X. URL http://www.sparc-climate.org/publications/sparc-reports/sparc-report-no5/. 59, 61, 72, 74

A. Stenke, M. Schraner, E. Rozanov, T. Egorova, B. Luo, and T. Peter. The SOCOL version 3.0 chemistry–climate model: description, evaluation, and implications from an advanced transport algorithm. *Geoscientific Model Development*, 6(5):1407–1427, 2013. ISSN 1991-9603. doi: 10.5194/gmd-6-1407-2013. URL https://www.geosci-model-dev.net/6/1407/2013/. 56

G. P. Stiller, T. von Clarmann, F. Haenel, B. Funke, N. Glatthor, U. Grabowski, S. Kellmann, M. Kiefer, A. Linden, S. Lossow, and M. López-Puertas. Observed temporal evolution of global mean age of stratospheric air for the 2002 to 2010 period. *Atmospheric Chemistry and Physics*, 12(7):3311–3331, 2012. ISSN 1680-7324. doi: 10.

5194/acp-12-3311-2012. URL https://www.atmos-chem-phys.net/12/3311/2012/. 52

K. A. Stone, O. Morgenstern, D. J. Karoly, A. R. Klekociuk, W. J. French, N. L. Abraham, and R. Schofield. Evaluation of the ACCESS – chemistry–climate model for the Southern Hemisphere. *Atmospheric Chemistry and Physics*, 16(4):2401–2415, 2016. ISSN 1680-7324. doi: 10.5194/acp-16-2401-2016. URL https://www.atmos-chem-phys.net/16/2401/2016/. 56

P. J. Telford, P. Braesicke, O. Morgenstern, and J. A. Pyle. Technical Note: Description and assessment of a nudged version of the new dynamics Unified Model. *Atmospheric Chemistry and Physics*, 8(6):1701–1712, 2008. ISSN 1680-7324. doi: 10.5194/acp-8-1701-2008. URL https://www.atmos-chem-phys.net/8/1701/2008/. 54

O. V. Tweedy, V. Limpasuvan, Y. J. Orsolini, A. K. Smith, R. R. Garcia, D. Kinnison, C. E. Randall, O.-K. Kvissel, F. Stordal, V. L. Harvey, and A. Chandran. Nighttime secondary ozone layer during major stratospheric sudden warmings in specified-dynamics WACCM. *Journal of Geophysical Research: Atmospheres*, 118 (15):8346–8358, 2013. ISSN 2169897X. doi: 10.1002/jgrd.50651. URL http://doi.wiley.com/10.1002/jgrd.50651. 93

M. K. van Aalst, M. M. P. van den Broek, A. Bregman, C. Brühl, B. Steil, G. C. Toon, S. Garcelon, G. M. Hansford, R. L. Jones, T. D. Gardiner, G. J. Roelofs, J. Lelieveld, and P. Crutzen. Trace gas transport in the 1999/2000 Arctic winter: comparison of nudged GCM runs with observations. *Atmospheric Chemistry and Physics*, 4(1):81–93, 2004. ISSN 1680-7324. doi: 10.5194/acp-4-81-2004. URL http://www.atmos-chem-phys.net/4/81/2004/. 53

D. Waugh and T. Hall. Age of stratospheric air : Theory, observations, and models. *Reviews of Geophysics*, 40(4):1–26, 2002. ISSN 8755-1209. doi: 10.1029/2000RG000101. URL http://doi.wiley.com/10.1029/2000RG000101. 52

M. Weber, S. Dikty, J. P. Burrows, H. Garny, M. Dameris, A. Kubin, J. Abalichin, and U. Langematz. The Brewer-Dobson circulation and total ozone from seasonal to decadal time scales. *Atmospheric Chemistry and Physics*, 11(21):11221–

11235, 2011. ISSN 1680-7324. doi: 10.5194/acp-11-11221-2011. URL https://www.atmos-chem-phys.net/11/11221/2011/. 51

O. Wild. Modelling the global tropospheric ozone budget: exploring the variability in current models. *Atmospheric Chemistry and Physics*, 7(10):2643–2660, 2007. ISSN 1680-7324. doi: 10.5194/acp-7-2643-2007. URL http://www.atmos-chem-phys.net/7/2643/2007/. 51

S. Yukimoto, H. Yoshimura, M. Hosaka, T. Sakami, H. Tsujino, M. Hirabara, T. Y. Tanaka, M. Deushi, A. Obata, H. Nakano, Y. Adachi, E. Shindo, S. Yabu, T. Ose, and A. Kitoh. *Meteorological Research Institute-Earth System Model Version 1 (MRI-ESM1) - Model Description*, volume 64. 2011. 56

S. Yukimoto, Y. Adachi, M. Hosaka, T. Sakami, H. Yoshimura, M. Hirabara, T. Y. Tanaka, E. Shindo, H. Tsujino, M. Deushi, R. Mizuta, S. Yabu, A. Obata, H. Nakano, T. Koshiro, T. Ose, and A. Kitoh. A New Global Climate Model of the Meteorological Research Institute: MRI-CGCM3-Model Description and Basic Performance-. *Journal of the Meteorological Society of Japan*, 90A(0):23–64, 2012. ISSN 0026-1165. doi: 10.2151/jmsj.2012-A02. URL http://japanlinkcenter.org/DN/JST.JSTAGE/jmsj/2012-A02?lang=en{&}from=CrossRef{&}type=abstract. 56

K. Zhang, H. Wan, X. Liu, S. J. Ghan, G. J. Kooperman, P.-L. Ma, P. J. Rasch, D. Neubauer, and U. Lohmann. Technical Note: On the use of nudging for aerosol–climate model intercomparison studies. *Atmospheric Chemistry and Physics*, 14(16):8631–8645, 2014. ISSN 1680-7324. doi: 10.5194/acp-14-8631-2014. URL https://www.atmos-chem-phys.net/14/8631/2014/. 92

Chapter 3

Decomposing the response of the stratospheric Brewer-Dobson circulation to an abrupt quadrupling in CO_2

Authors: **Andreas Chrysanthou, Amanda C. Maycock and Martyn P. Chipperfield**

Abstract

We perform time-slice experiments using HadGEM3-A to decompose the long-term (years $101-150$) response of the Brewer-Dobson circulation (BDC) to an abrupt quadrupling in CO_2 ($4\times CO_2$) into: 1) a rapid atmospheric adjustment; 2) a contribution from the global-average sea surface temperature (SST) change (+3.4 K); and 3) an SST pattern effect. The SST fields are derived from the CMIP5 multi-model ensemble. Two further experiments explore the impact on the BDC of the spread in global-average SST response to $4\times CO_2$ across the CMIP5 models (range $2.1-4.9$ K). At 70 hPa (10 hPa) the annual-mean tropical upward mass flux increases by 45% (35%) to the $4\times CO_2$ perturbation. At 70 hPa, around 70% of the increase is from the global-uniform SST

warming, with the remainder coming in similar contributions from the rapid adjustment and SST pattern effect. In contrast, at 10 hPa the increase in mass flux comes mainly from the rapid adjustment ($\sim$ 40%) and the uniform SST warming ($\sim$ 45%), with a small contribution from the SST pattern. At 10 hPa, the effect of the multi-model spread in global-mean SST is comparable in magnitude to the rapid adjustment. Conversely, at 70 hPa the effect of spread in global-mean SST is substantially larger than both the rapid adjustment and the SST pattern effect. We derive an approximately linear sensitivity of the tropical upward mass flux to global surface air temperature change of 0.62×10^9 $kg\ s^{-1}\ K^{-1}$ (9% K^{-1}) at 70 hPa and 0.10×10^9 $kg\ s^{-1}\ K^{-1}$ (6% K^{-1}) at 10 hPa. The results confirm the most important factor for the acceleration of the BDC in the lower stratosphere under increased CO_2 is global SST changes. We also quantify for the first time that the rapid adjustment to CO_2 is of similar importance to SSTs for the increased BDC in the upper stratosphere. This demonstrates a potential for a fast and slow timescale of the response of the BDC to greenhouse gas forcing, with the relative prominence of those timescales being height dependent.

3.1 Introduction

The residual circulation in the stratosphere, or the Brewer-Dobson circulation (BDC), is characterised by slow ascent in the tropics, poleward flow and downwelling in the subtropics and extratropics (Andrews et al., 1987; Holton et al., 1995; Plumb, 2002). There is a strong seasonality in the strength and width of the BDC (Rosenlof, 1995). In the winter hemisphere, the poleward mass transport that occurs in the middle and upper stratosphere is termed the deep branch, while the shallow branch in the lower stratosphere is present year-round in both hemispheres (Birner and Bönisch, 2011). The BDC controls the transport and distribution of radiatively active trace gases such as stratospheric ozone and water vapour (Brewer, 1949; Dobson, 1956), as well as the lifetimes of chemically important trace gases such as chlorofluorocarbons (CFCs; Butchart and Scaife, 2001). The BDC is a wave-driven circulation forced by breaking of planetary-scale Rossby waves and small-scale gravity waves (Holton et al., 1995). The torque imposed by the wave breaking allows flow across lines of constant angular momentum.

General circulation models (GCMs) and chemistry-climate models (CCMs) consistently

simulate an acceleration of the BDC in scenarios that include increasing greenhouse gas concentrations (Rind, 2002; Rind et al., 1990; Sigmond et al., 2004; Butchart et al., 2006, 2010; Fomichev et al., 2007; Olsen et al., 2007; Deckert and Dameris, 2008; Garcia and Randel, 2008; Li et al., 2008; Calvo and Garcia, 2009; McLandress and Shepherd, 2009; Oman et al., 2009; SPARC, 2010; Garny et al., 2011; Shepherd and McLandress, 2011; Lin and Fu, 2013; Hardiman et al., 2014) . A strengthened BDC increases stratosphere-troposphere exchange (STE) of ozone (Rind, 2002; Hegglin and Shepherd, 2009; Banerjee et al., 2016) and affects projected ozone trends in the tropical lower stratosphere (e.g. Keeble et al., 2017), subtropics (e.g. Li et al., 2009), and polar regions (e.g. Oman et al., 2009).

The wave forcing that drives the BDC arises from various types of waves generated in the troposphere with different temporal and spatial scales (e.g. Randel et al., 2008), which propagate upwards, break and dissipate their momentum and energy (Holton et al., 1995; Plumb and Eluszkiewicz, 1999; Semeniuk and Shepherd, 2001). Changes in the BDC must, therefore, be accompanied by changes in stratospheric wave forcing. Three main mechanisms for the altered wave forcing of the BDC under climate change have been considered in the literature: 1) changes in the strength of tropospheric wave generation; 2) changes in the latitudinal distribution of wave forcing within the stratosphere in the vicinity of the turnaround latitudes, which separate the areas of tropical upwelling from extratropical downwelling; and 3) changes in the vertical penetration of tropospheric wave forcing into the stratosphere. Anomalous wave activity emanating from the extratropical troposphere has been shown to have a minimal impact on the overall strength of the BDC because it generally does not induce a torque in the vicinity of the turnaround latitudes (Butchart and Scaife, 2001; Sigmond et al., 2004; Garcia and Randel, 2008; Garny et al., 2011).

Many studies have pointed to an important role for the projected strengthening and upward shift of the subtropical jets with tropospheric warming to explain modelled increases in the BDC under climate change. Rossby wave breaking regions such as the upper flanks of the subtropical jets generally follow critical layers as demonstrated by the observational study of Randel and Held (1991). The robust change in the pattern of zonal winds under climate change (Collins et al., 2013) moves the Rossby wave critical

layers in the lower stratosphere upward, enabling enhanced penetration of Rossby wave activity in the subtropical lower stratosphere and an altered distribution of momentum deposition (Rind et al., 1990; Garcia and Randel, 2008; McLandress and Shepherd, 2009; Calvo and Garcia, 2009; Garny et al., 2011). Consistent with this theoretical basis, the multi-model spread in the end of 21st century lower stratospheric zonal wind trends near the turnaround latitudes was found to explain $\sim 70\%$ of the spread in tropical upward mass flux trends in the lower stratosphere across a set of CCMs (Lin and Fu, 2013). Some studies have also found a role for enhanced excitation of tropical waves under climate change for a strengthened BDC (Deckert and Dameris, 2008; Calvo and Garcia, 2009), but the potential for this to drive an increase in the total mass circulation rather than simply a redistribution within the tropics has been questioned (Garny et al., 2011; Shepherd and McLandress, 2011).

Although the signal of an increased BDC in a warmer climate is a highly robust feature of GCMs and CCMs, there are differences amongst models in the relative contributions to the increase from resolved and parameterised wave forcing (Butchart et al., 2006, 2010; Garcia and Randel, 2008; Calvo and Garcia, 2009; McLandress and Shepherd, 2009; Garny et al., 2011). This may be related to models having different climatological resolved and parameterised wave forcing (e.g. Chrysanthou et al., 2019) and/or the potential for a compensation effect between the different types of wave forcing in driving a change in the BDC (e.g. Cohen et al., 2013; Sigmond and Shepherd, 2014).

To understand the relative importance of different drivers, some modelling studies have performed idealised experiments to decompose the BDC response to climate change into different components. Sigmond et al. (2004) performed experiments with the Canadian Middle Atmosphere Model (CMAM) in which CO_2 was doubled separately in the troposphere and stratosphere. In each case, sea surface temperature (SST) changes were imposed as a fraction of the total SST response according to their respective radiative forcings. Sigmond et al. (2004) showed that the increase in residual circulation in DJF caused a small warming in the Arctic lower stratosphere, of which about two thirds could be attributed to the tropospheric CO_2 doubling and about one third to the middle-atmospheric CO_2 doubling. Their results were qualitatively consistent with the seminal results of Rind et al. (1990) who performed comparable experiments with the

NASA Goddard Institute for Space Studies (GISS) model but over a shorter period.

Olsen et al. (2007) performed experiments for the period 1949 to 1998 with the NASA Goddard Earth Observing System version 4 (GEOS-4) GCM using prescribed observed SSTs. They attributed the increase in residual circulation between the first and last decades of their simulations to a stronger SST gradient between the tropics and middle latitudes, resulting in a greater meridional temperature gradient in the subtropical troposphere and more poleward refraction of planetary-scale Rossby waves in the lower stratosphere. Further simulations by Olsen et al. (2007) added the radiative effects of atmospheric GHG changes and showed a small but insignificant increase in STE trend compared to the SST-only experiments. Oman et al. (2009) performed sensitivity experiments with the GEOS-CCM (based on GEOS-4) to decompose the relative effects of SSTs, GHGs and halogens on the stratospheric age of air distribution between 1960 and 2100. To isolate the effects of SST changes, they compared simulations using SSTs from two different climate models that differed in their climatological SST. They describe the SST experiment as "tropical SSTs" though the SST changes appear to be imposed globally. This comparison further combines the effects of differences in both global mean SST and SST patterns between the two climate model datasets, though this was not explicitly discussed. As with all other similar studies, they concluded that increased SSTs contribute to an increase in tropical lower stratospheric upwelling and a decrease in age of air.

While studies have demonstrated that higher SSTs increase the strength of the BDC (Olsen et al., 2007; Oman et al., 2009; Lin et al., 2015), one confounding factor is that the SST response to anthropogenic forcing shows an inhomogeneous pattern (e.g. Latif and Keenlyside, 2009), which may affect the overall BDC response. For example, regional SST anomalies associated with the El Niño Southern Oscillation (ENSO) have been shown to affect the BDC both through modulation of the Northern Hemisphere (NH) winter stratospheric circulation (Manzini et al., 2006) and tropical lower stratospheric upwelling (Marsh and Garcia, 2007; Randel et al., 2009). Using CMAM, Simpson et al. (2011) attribute the increase in boreal winter tropical lower stratospheric upwelling under El Niño to increased resolved wave forcing in the Southern Hemisphere (SH) subtropical lower stratosphere, which was caused by altered wave sources in the

troposphere under El Niño. In contrast, Calvo et al. (2010) using the Whole Atmosphere Community Climate Model (WACCM), attribute the increased tropical upwelling during El Niño to changes in the propagation and dissipation of parameterised gravity waves caused by the anomalous location and intensity of the subtropical jets. Garfinkel et al. (2013) showed that decadal trends comprising of warming in the Indian Ocean and the warm pool region can drive changes in tropical lower stratospheric upwelling. Therefore, while a uniform SST increase can generate much of the canonical pattern of long-term tropical upper tropospheric warming, through impacts on tropical convection and the water vapour and lapse rate feedbacks (e.g. Chen et al., 2013), the spatial pattern of SST trends may also affect the BDC. Lin et al. (2015) showed an approximately linear relationship between tropical annual mean surface temperature and anomalous lower stratospheric mass flux in the GFDL-CM3 model that held on interannual, decadal and centennial timescales. However, on multi-decadal timescales this calculation aliases the direct atmospheric radiative effects of GHGs, the SST pattern effect and the SST magnitude into one term (Olsen et al., 2007; Sigmond et al., 2004).

While previous literature suggests that the distinct radiative effects of GHGs, the SST magnitude and the SST pattern may contribute to projected changes in the BDC, no previous study has explicitly quantified their importance; this is the goal of our study. Here, we perform climate model experiments to decompose the response of the BDC to an abrupt quadrupling of CO_2 into three components: 1) the rapid adjustment, or direct component, associated with CO_2 radiative effects in the absence of SST change; 2) a contribution from the global-average sea surface temperature (SST) change termed throughout the rest of the study as a global uniform SST warming; and 3) the SST pattern effect. The goal is to understand the distinct contributions of the three components and assess the extent to which they can be combined to explain the overall BDC response. We further compare the magnitudes of the rapid adjustment and SST pattern effects on the BDC with the effect of spread in global mean SST change due to CO_2 across climate models. The remainder of the paper is laid out as follows: Section 3.2 describes the atmospheric model and experimental set-up; Section 3.3 presents the results and Section 3.4 summarises our main findings and conclusions.

3.2 Data and methods

3.2.1 Atmospheric model description

We use the Hadley Centre Global Environment Model version 3 (HadGEM3) variant of the Met Office Unified Model (MetUM) version 8.4, which has been used for both numerical weather prediction and climate simulation. It is configured with the Global Atmosphere (GA4.0) and comprises a non-hydrostatic fully compressible dynamical core that uses a semi-implicit semi-Lagrangian advection scheme in terrain-following hybrid height coordinates (Walters et al., 2014). We run the atmosphere-only configuration (HadGEM3-A) at N96 horizontal resolution ($1.875° \times 1.25°$, $\sim$ 135 km in mid-latitudes) with 85 levels (L85) from the surface to an altitude of $\sim$ 85 km. Interactions of the flow blocking drag associated with the orographic gravity wave drag (OGWD) are parameterised, as detailed in Webster et al. (2003). Similarly, a spectral sub-grid parameterisation is used for the representation of the gravity wave drag induced in the upper stratosphere and mesosphere, forced by non-orographic sources (NOGWD) such as convective processes and fronts, which enables HadGEM3 to simulate a realistic quasi-biennial oscillation (QBO) as detailed in Scaife et al. (2002).

3.2.2 Experiment design

Seven 50-year-long time-slice simulations were performed with HadGEM3-A with fixed boundary conditions including prescribed SSTs and sea ice. The experiment names and IDs are shown in Table 3.1. The reference simulation (run A) uses boundary conditions, including greenhouse gas (GHG) concentrations, natural and anthropogenic primary aerosol or reactive gas emissions, set to pre-industrial (year 1850) values following the Coupled Model Intercomparison Project 5 protocol (CMIP5; Lamarque et al., 2010; Taylor et al., 2012). The reference SSTs and sea ice concentrations (SIC) are annually repeating fields taken as the monthly-mean multi-model mean (MMM) from the CMIP5 piControl simulations (Taylor et al., 2012). The MMM reference SST and SIC fields are constructed from the average of the last 150 years of the piControl experiments from the 26 CMIP5 models listed in the Supplementary Information (Table S3.1).

Six perturbation experiments are performed to isolate different components of the long-term response in the CMIP5 abrupt-4×CO_2 experiment, which instantaneously

quadruples CO_2 from its preindustrial concentration. We first calculate the CMIP5 monthly-mean MMM SST in the abrupt-4×CO_2 experiment using the final 50 years (years $101 - 150$) of each model run (Table S3.1). The annual-mean SST anomalies compared to the reference preindustrial state are shown in Figure 3.1a. Note that in all the perturbation experiments, SIC is held fixed at the reference values. This is artificial, but it enables the effects of SSTs on the BDC and associated mechanisms to be isolated from the possible effects of changing sea ice on the stratosphere (e.g. Kim et al., 2014; McKenna et al., 2018). We performed a separate experiment in which SIC was also changed to the CMIP5 MMM 4×CO_2 response along with global SSTs and atmospheric CO_2, but this showed no significant effect of changing SIC on the BDC (not shown) and therefore will not be discussed further.

The first perturbation experiment (run B) accounts for the full (atmosphere + SST) abrupt-4×CO_2 response and is designed to simulate the long-term centennial response to CO_2 forcing. The second perturbation experiment (C) only accounts for the CO_2 rapid adjustment by quadrupling atmospheric CO_2 concentrations while holding SSTs and SIC at their preindustrial values. The third experiment (D) imposes a monthly-varying globally uniform SST anomaly derived from the global mean multi-model mean 4×CO_2 SST anomaly relative to the control. In the annual and multi-model mean this is equal to 3.4 K (Figure 3.1b). Note the CMIP5 MMM global SST anomaly is smaller than the global mean surface air temperature (GSAT) change in the abrupt-4×CO_2 experiment because land areas warm more than the ocean (e.g., Joshi and Gregory, 2008). In the fourth perturbation experiment (E), we subtract the monthly-varying uniform warming value from the 4×CO_2 anomalies to impose the local deviations in SST from the global uniform value (i.e. the SST pattern). The SST pattern is shown in Figure 3.1c; it is comprised of relatively stronger warming across the tropics in the Pacific, Atlantic and Indian Ocean basins and in the North Pacific, and relatively weaker warming across the Southern Ocean, in the North Pacific warming hole region and in the vicinity of the South Pacific stratocumulus decks.

By construction, the sum of the SST anomalies in runs D and E equals the full SST anomalies of run B. Note that the change in annual-mean GSAT simulated in runs B and D (4.3 K and 4.0 K, respectively) is larger than the imposed global mean SST

anomaly, partly because of the enhanced warming response over land. While SSTs are held fixed in run C, there are changes to land temperatures that cause a small GSAT response (0.43 K). Finally, although the global mean SST change in run E is zero by construction, there are changes to land temperatures that lead to a small GSAT response (0.45 K).

RUN	ID	**CO_2**	**SSTs (prescribed)**
A	piControl	Pre-industrial	Pre-industrial
B	Full 4×CO_2	4×CO_2	4×CO_2 (CMIP5)
C	Atmos	4×CO_2	Pre-industrial
D	SST UW	Pre-industrial	4×CO_2 (UW) - 3.4 K
E	SST patterns	Pre-industrial	4×CO_2 (patterns)
F	SST UW low	Pre-industrial	Low 4×CO_2 - 2.1 K
G	SST UW high	Pre-industrial	High 4×CO_2 - 4.9 K

Table 3.1: The sensitivity experiments used in this study with the atmospheric CO_2 and the SSTs used as boundary conditions. All other boundary conditions are as in piControl.

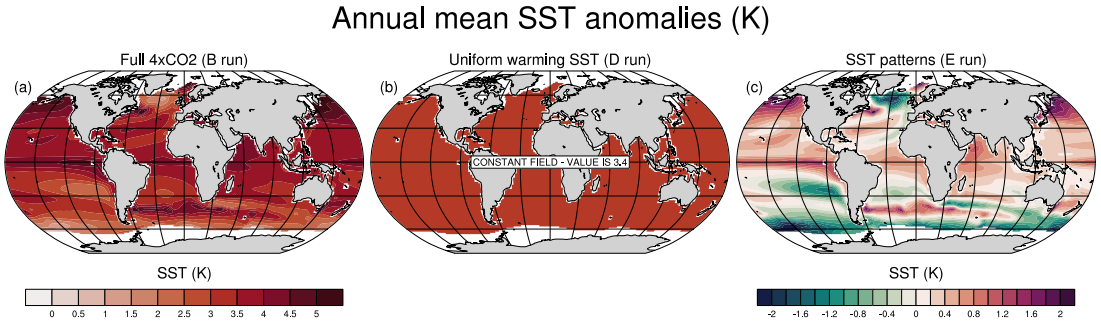

Figure 3.1: Prescribed annual-mean SST anomalies [K] with respect to the piControl climatology in the (a) full 4×CO_2, (b) Uniform SST warming and (c) SST pattern perturbation experiments.

There is substantial inter-model spread in the modelled global mean SST change in the abrupt-4×CO_2 experiments (Flato et al., 2013). To investigate the effect of this spread on the BDC, and to place the rapid adjustment and SST pattern effects into the context of model uncertainty in the global surface warming due to CO_2, we perform two further uniform SST warming sensitivity runs. These are chosen to be the lowest (annual-mean $\sim$ 2.1 K; run F) and highest (annual-mean $\sim$ 4.9 K; run G) global mean SST changes from the 26 CMIP5 models used in this study. These values come from the INMCM4 (Volodin, 2013) and IPSL-CM5A-LR (Dufresne et al., 2013) models, respectively. The annual-mean GSAT change in runs F and G is 3.0 and 6.1 K, respectively.

Since HadGEM3-A does not include interactive chemistry, we prescribe zonal-mean preindustrial ozone concentrations in all the experiments following the Coupled Model Intercomparison Project 6 (CMIP6; Eyring et al., 2016) protocol, based on the CMIP6 experiments run with HadGEM3-GC3.1 (Kuhlbrodt et al., 2018; Williams et al., 2018). It should be noted that keeping ozone concentrations fixed in all our experiments will implicitly neglect the effects of any ozone feedbacks from both the chemical effects of increased CO_2 and the transport effects from an altered BDC; this includes effects on the thermal structure of the upper troposphere especially around the tropical upper troposphere and lower stratosphere (Nowack et al., 2015; Chiodo and Polvani, 2017) and on upper stratospheric temperatures (Maycock, 2016).

3.2.3 Residual circulation diagnostics

To diagnose the BDC and its changes we make use of the Transformed Eulerian Mean circulation diagnostics (TEM; Andrews et al., 1987; Andrews and McIntyre, 1976, 1978) as calculated internally by the model. The TEM residual circulation velocities ($\overline{v}^*$, $\overline{w}^*$) are defined as Andrews et al. (1987):

$$\overline{v}^* = \overline{v} - \frac{1}{\rho_0}\frac{\partial}{\partial z}\left[\frac{\rho_0\,\overline{v'\theta'}}{\partial\overline{\theta}/\partial z}\right], \quad \overline{w}^* = \overline{w} + \frac{1}{\alpha\cos\phi}\frac{\partial}{\partial\phi}\left[\frac{\overline{v'\theta'}\cos\phi}{\partial\overline{\theta}/\partial z}\right] \tag{3.1}$$

where overbars denote a zonal-mean quantity and primes the departure from the zonal-mean. v and w are the meridional and vertical components of wind velocity respectively, ρ_0 is the log-pressure density, $z = -H\ln(p/p_s)$ is the log-pressure vertical coordinate

(height), H is the scale height, p is the pressure at a specified level with p_s the pressure at the surface, $\overline{v'\theta'}$ is the eddy heat flux, θ is the potential temperature, α is the Earth radius and ϕ is the latitude. Using $\overline{v}^*$ from equation 3.1 we further calculate the residual mass streamfunction $\overline{\Psi}^*(\phi, z)$ as:

$$\overline{\Psi}^*(\phi, z) = \frac{2\pi\alpha\cos\phi}{g} \int_{bottom}^{top} \overline{v}^* dp, \tag{3.2}$$

where g is the acceleration due to gravity. Equation 3.2 is integrated from the top of atmosphere to the surface using the boundary condition that $\overline{\Psi}^* = 0$ at the top of the atmosphere ($p = 0$). Subsequently, we calculate the net downward mass flux in each hemisphere, by finding $\overline{\Psi}^*_{max}$ and $\overline{\Psi}^*_{min}$ in the NH and SH, respectively, at each pressure level. The net tropical upward mass flux, which is equal to the sum of the downward mass fluxes in each hemisphere, can then be expressed as (Rosenlof, 1995):

$$Tropical\ upward\ mass\ flux = 2\pi\alpha(\overline{\Psi}^*_{max} - \overline{\Psi}^*_{min}) \tag{3.3}$$

We apply the "downward control" principle (DCP; Haynes et al., 1991) to further separate the contributions to the tropical upward mass flux from resolved waves due to the divergence of Eliassen-Palm flux (EPF) and contributions from OGWD and NOGWD. Resolved waves and parameterised gravity wave drag (OGWD/NOGWD) constitute the eddy-induced total zonal forces $\overline{F}$. Under steady-state conditions, the $\overline{\Psi}^*(\phi, z)$ at a specified log(pressure)-height, z, is related to the vertically integrated $\overline{F}$ above that level along a surface of constant zonal-mean absolute angular momentum $\overline{m} = \alpha\cos\phi(\overline{u} + \alpha\Omega\cos\phi)$, where $\overline{v}$ is the zonal-mean zonal wind and Ω is Earth's rotation rate (Haynes et al., 1991). Outside of the tropics, $\overline{m}$ is approximately constant at a fixed latitude, ϕ , resulting in the following equation (Haynes et al., 1991):

$$\overline{\Psi}^*(\phi, z) = \int_z^\infty \left\{ \frac{\rho_0\alpha^2\overline{F}\cos^2\phi}{\overline{m}_\phi} \right\}_{\phi=\phi(z')} dz, \tag{3.4}$$

where $\overline{m}_\phi \approx -2\Omega\alpha^2\sin\phi\cos\phi$ is the quasi-geostrophic limit. The boundary conditions are $\overline{\Psi}^* \to 0$ and $\rho_0\overline{w}^* \to 0$ as $z \to \infty$.

3.3 Results

3.3.1 Zonal-mean temperature response

Figure 3.2 shows latitude-pressure cross-sections of the annual-mean and zonal-mean temperature anomalies from the reference preindustrial simulation for perturbation runs B, C, D and E. The full response (Fig. 3.2a) exhibits the canonical pattern of temperature change due to increased CO_2, with tropospheric warming that maximizes in the tropical upper troposphere (by $\sim$ 8 K) and stratospheric cooling that increases with height (Collins et al., 2013). Note that Arctic amplification in the lower troposphere is small here compared to coupled atmosphere-ocean models (Collins et al., 2013), because we do not impose sea ice changes in the runs (not shown).

The rapid adjustment due to changes in atmospheric CO_2 (Fig. 3.2b) accounts for most of the stratospheric cooling seen in the full response, with cooling of $\sim$ 15 K in the upper stratosphere. However, the stratospheric cooling in run C (Fig. 3.2b) is more uniform in latitude than in the full experiment, and more closely resembles the purely radiative response to CO_2 (Fels et al., 1980). In the troposphere, the rapid adjustment induces a weak ($<$ 1 K) warming that is fairly homogeneous and comes partly from the small changes in GSAT, since land temperatures are not held fixed. Most of the tropospheric zonal-mean warming is reproduced by imposing the uniform SST warming (Fig. 3.2c), including the tropical upper tropospheric amplification of up to 9 K and the extension of warming into the subtropical lower stratosphere in both hemispheres. In the stratosphere, the uniform SST warming induces an anomalous meridional temperature gradient, with cooling of $2-3$ K in the tropical middle and upper stratosphere and warming in the extratropics and polar regions. This pattern accounts for most of the latitudinal variation in stratospheric cooling seen in the full response (Fig. 3.2a).

The SST pattern experiment (Fig. 3.2d) exhibits a similar morphology in the temperature response to the uniform SST warming run, albeit much weaker in amplitude. In the troposphere, the SST pattern induces a weak warming that is comparable in magnitude to the rapid adjustment (Fig. 3.2b), but with a weak upper tropospheric amplification that enhances the effect of the uniform warming (Fig. 3.2c). This upper tropospheric amplification suggests enhanced tropical deep convection, which may be consistent with

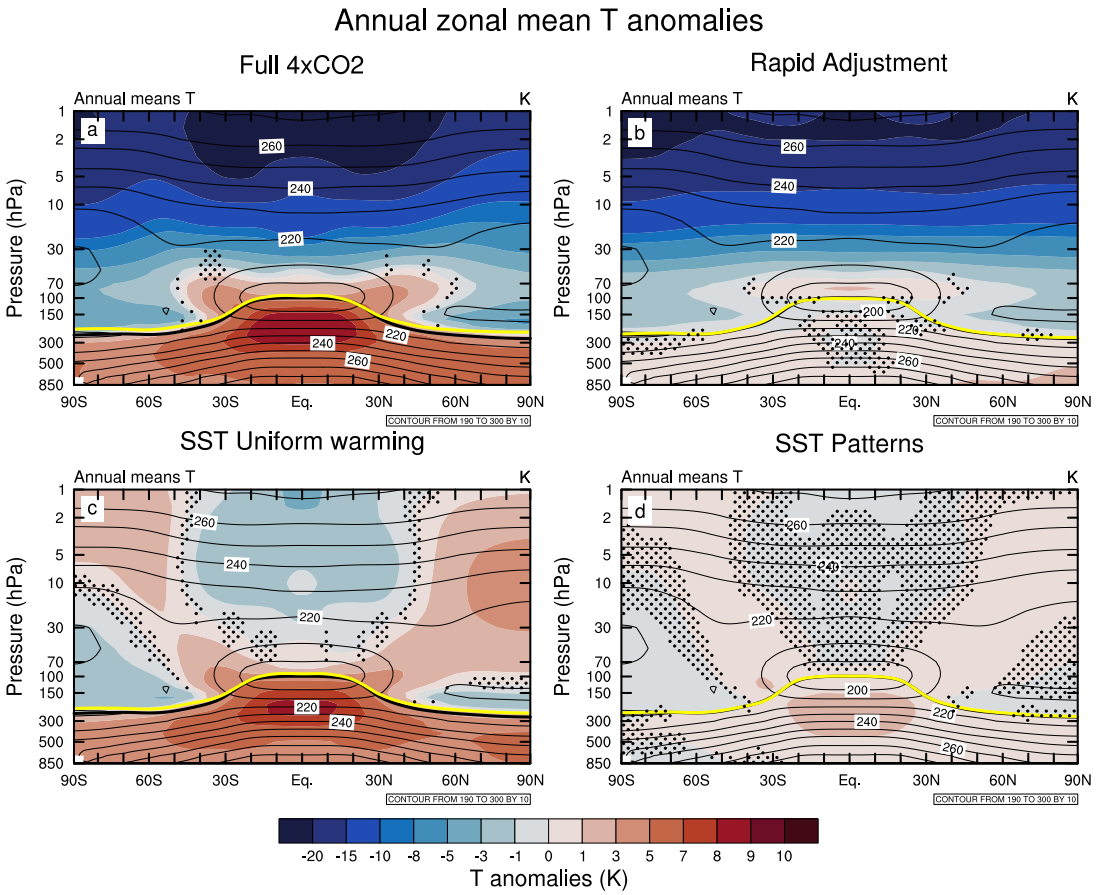

Figure 3.2: Latitude vs. pressure cross-sections of annual-mean and zonal-mean temperature anomalies [K] between $850 - 1$ hPa with respect to the piControl simulation for the (a) $4\times CO_2$ (run B), (b) rapid adjustment (run C), (c) Uniform SST warming (run D) and (d) SST pattern (run E) experiments. Contours show the piControl climatology. Stippling denotes where the differences are not statistically significant at the 95% confidence level using a two-tailed Student's t test. Thick yellow and black lines indicate the tropopause pressure levels in each perturbation run and in the reference simulation, respectively.

the imposed anomalous tropical SST warming (Fig. 3.2c).

The thick yellow lines in Figure 3.2 denote the tropopause pressure for each perturbation experiment. These can be compared to the climatological tropopause in the reference simulation (thick black lines). The lifting of the tropopause by ~ 1 km within the deep tropics in the full experiment comes mainly from the uniform SST warming ($\sim 80\%$) with the remaining 20% coming from the SST pattern. However, the maximum tropopause lifting (> 1.2 km) occurs in the extratropics of both hemispheres, especially over the Arctic polar cap (not shown).

3.3.2 Zonal-mean zonal wind response

The annual-mean zonal-mean zonal wind anomalies in the four perturbation experiments are shown in Figure 3.3. The full $4\times CO_2$ response (Fig. 3.3a) shows the familiar pattern of a strengthening and upward shift of the subtropical jets, a strengthening and poleward shift of the midlatitude westerlies in the SH, and increased westerlies in the SH stratosphere (Collins et al., 2013). The strengthened subtropical jets arise mainly from the uniform SST warming (Fig. 3.3c) with a small contribution from the SST pattern (Fig. 3.3d). In contrast, the rapid adjustment (Fig. 3.3b) does not induce a strengthening of the subtropical jets, but it does explain a significant part of the increased westerlies in the SH extratropics, particularly in the upper stratosphere. The SST pattern effect also contributes to the increased SH stratospheric westerlies, but the uniform SST warming shows the largest increase. In the NH, the full experiment shows stronger westerlies in the lower stratosphere and weakened westerlies near the subtropical stratopause. The anomalous lower stratospheric westerlies are contributed by the uniform warming in the subtropics and midlatitudes and the rapid adjustment in the extratropics and polar region. The uniform warming also causes weakened westerlies in the subtropical upper stratosphere, with a smaller effect from the rapid adjustment.

The full $4\times CO_2$ response shows significant zonal wind anomalies in the tropical stratosphere between $50 - 1$ hPa, which is also seen in the uniform SST warming experiment. This is likely related to changes to the QBO properties under climate change, which have been noted in other idealised GCM experiments (e.g. Kawatani et al., 2011), though a detailed investigation of the QBO is beyond the scope of this study.

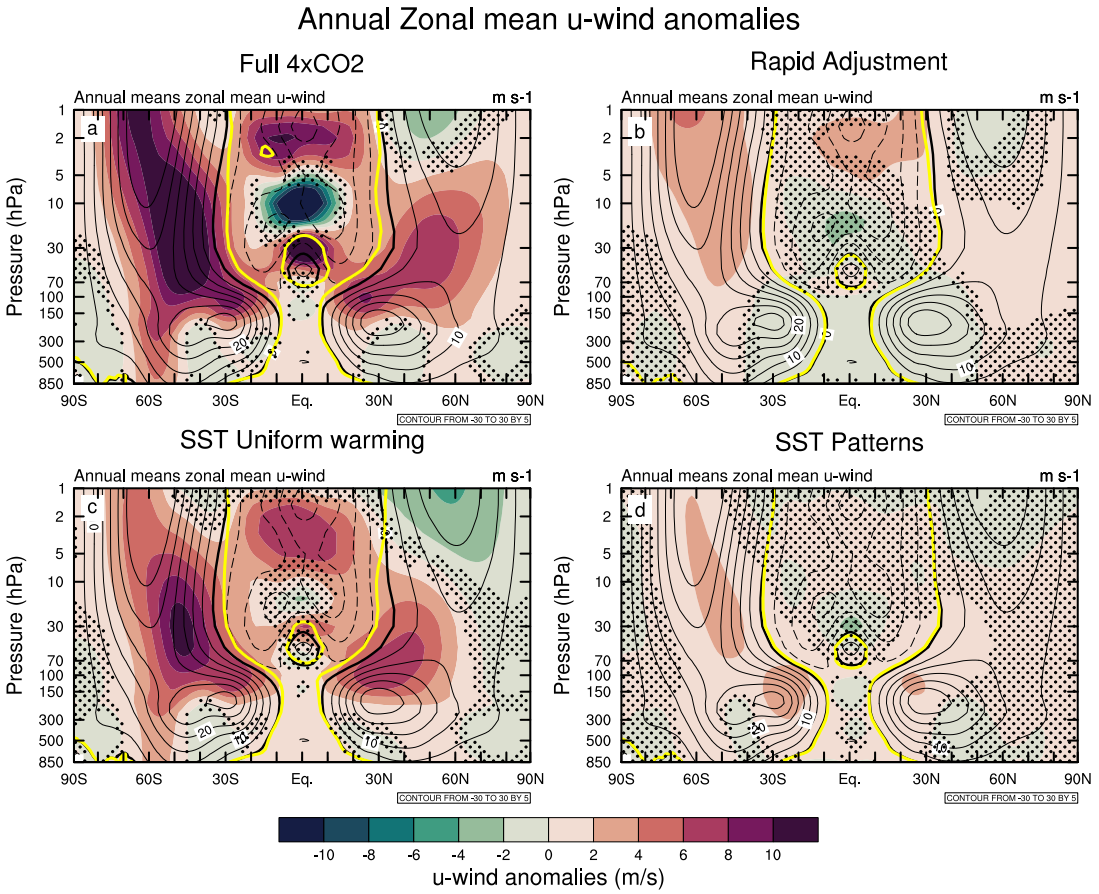

Figure 3.3: As in Figure 3.2, but for the annual and zonal-mean zonal wind anomalies [m s^{-1}] between 850 − 1 hPa. Contours show the piControl climatology. The thick black lines denote the critical lines for stationary waves ($\overline{u} = 0$) in piControl and the thick yellow lines for each perturbation experiment, respectively.

The zero wind lines ($\overline{u} = 0$), which demarcate the "critical lines" for linear stationary Rossby waves (Dickinson, 1968), are shown by the thick lines in Figure 3.3. In the stratosphere, there is a clear equatorward contraction of the zero wind lines in both hemispheres in the full $4\times CO_2$ experiment. Previous studies have connected this to increased penetration of Rossby wave activity into the subtropical lower stratosphere (Shepherd and McLandress, 2011). The contraction of the zero wind lines is primarily due to the uniform SST warming, with a modest contraction also seen in the rapid adjustment and SST pattern experiments.

3.3.3 Residual circulation response

Figure 3.4 shows latitude-pressure cross-sections of the annual-mean residual vertical velocity ($\overline{w}^*$) anomalies with respect to the reference simulation for experiments B, C, D and E. The uniform SST warming accounts for most of the increased tropical lower stratospheric upwelling ($\sim 70\%$ between 30°S and 30°N over the layer $100 - 50$ hPa) seen in the full $4\times CO_2$ response. However, there are also significant, but small, increases in tropical lower stratospheric upwelling induced by the rapid adjustment ($\sim 17\%$) and the SST pattern perturbations ($\sim 13\%$) (Fig. 3.4b, 3.4d). While comparatively small compared to the effect of the uniform SST warming, the increases in $\overline{w}^*$ in the tropical lower stratosphere from the SST pattern are broadly comparable in magnitude to the effects of ENSO on tropical upwelling found in other modelling studies (Calvo et al., 2010; Simpson et al., 2011).

The turnaround latitudes are overlaid as thick lines in Figure 3.4. A quadrupling of CO_2 leads to a narrowing of the upwelling region in the lower and middle stratosphere that maximises around ~ 30 hPa (Hardiman et al., 2014). This arises predominantly from the uniform SST warming (Fig. 3.4c), with additional weaker contributions from the rapid adjustment and SST patterns (Fig. 3.4b and 3.4d). In contrast, in the upper stratosphere (10 hPa) the upwelling region widens particularly in the NH (cf. Hardiman et al., 2014). The widening of the upwelling region in the NH upper stratosphere arises almost entirely from the rapid adjustment, while the smaller tropical widening in the SH upper stratosphere is contributed by all three components.

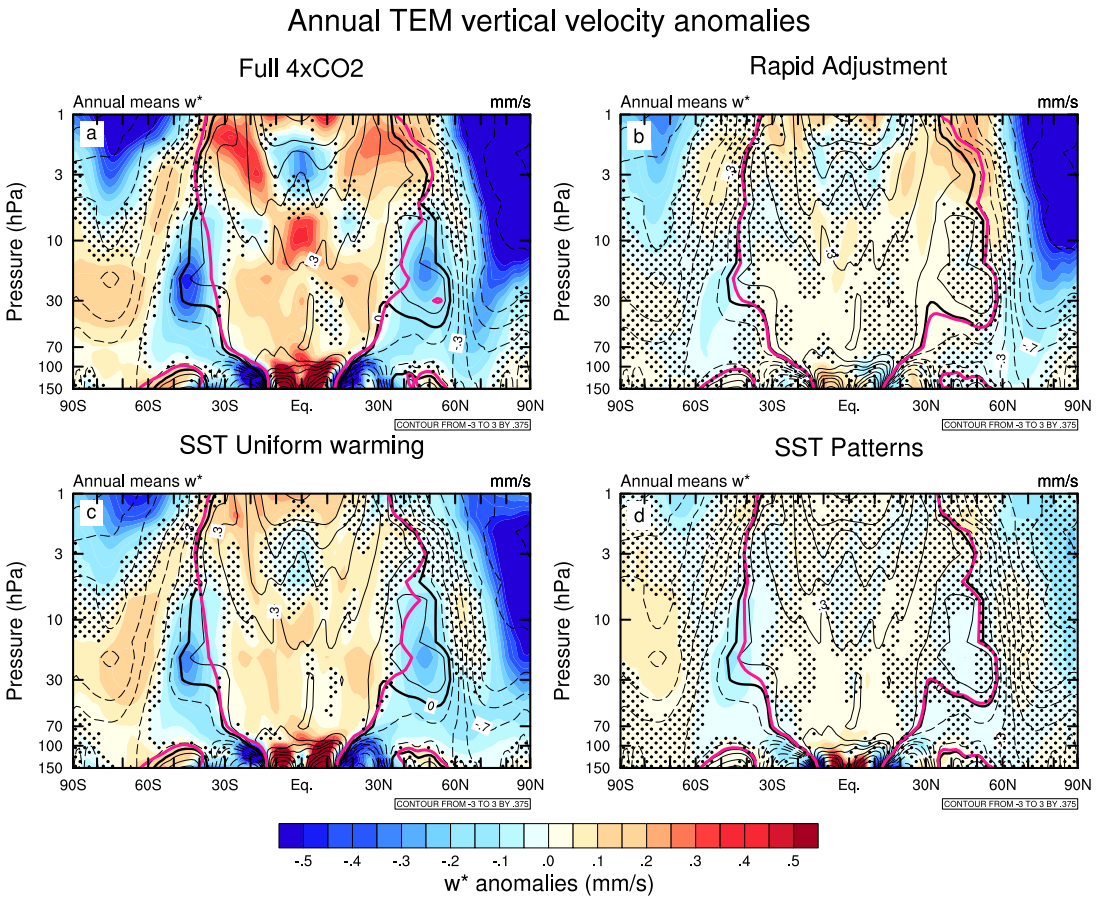

Figure 3.4: As in Figure 3.2, but for the annual-mean TEM residual vertical velocity anomalies [mm s^{-1}] between 150 − 1 hPa. Contours show the piControl climatology and range from −3 to 3 mm s^{-1} in increments of 0.375 mm s^{-1}. The thick black lines denote the turnaround latitudes ($\overline{w}^* = 0$) in piControl and pink thick lines for each perturbation experiment, respectively.

We move now to evaluating the changes in downwelling in the extratropics. The full $4\times CO_2$ experiment shows enhanced downwelling over the Arctic throughout the stratosphere. Both the rapid adjustment and uniform SST warming induce comparable increases in downwelling in the Arctic, while the SST patterns do not produce significant $\overline{w}^*$ changes in this region. In the SH, the full perturbation generates stronger downwelling in the upper stratosphere and weaker downwelling in the middle and lower stratosphere below 10 hPa. All three components produce increased downwelling in the Antarctic upper stratosphere, with the largest change from the uniform SST warming and the rapid adjustment. In the lower stratosphere, the uniform SST and SST patterns both generate reduced downwelling as seen in the full $4\times CO_2$ experiment.

The relationship of the changes in residual circulation to the overall mass transport in the stratosphere can be seen in Figures 3.5 and 3.6, which show the residual mass streamfunction ($\overline{\Psi}^*$) anomalies in the solstice seasons December-February (DJF) and June-August (JJA) in the four experiments. For comparison, Supplementary Information (Figure S3.1) shows the annual-mean $\overline{\Psi}^*$ responses. As the winter hemisphere cell is the dominant one, the climatological circulation in DJF and JJA is significantly stronger in the NH and SH, respectively. The largest response in both hemispheres occurs in DJF (Figure 3.5), while the NH exhibits a stronger response compared to the SH. In DJF, the response to the SST patterns in the NH is confined to the subtropical lower stratosphere (Fig 3.5d), while the rapid adjustment (Fig. 3.5b) and uniform SST warming (Fig. 3.5c) induce increased poleward transport across most of the stratosphere, with the latter showing around three times larger anomalies near the maximum in the subtropical lower stratosphere. The peak NH anomaly due to the rapid adjustment is around double that for the SST patterns in DJF. Specifically, in the lower stratosphere ($100-50$ hPa) between $0^\circ-60^\circ$N, the uniform SST warming accounts for $\sim 65\%$ of the full response, the rapid adjustment contributes $\sim 26\%$ and the SST patterns contribute the remainder. Conversely, in the middle and upper stratosphere between $30-1$ hPa, over the same latitude bands, the rapid adjustment effect becomes more important, surpassing the contribution of the uniform SST warming accounting for the 48% and 46% of the full response, respectively.

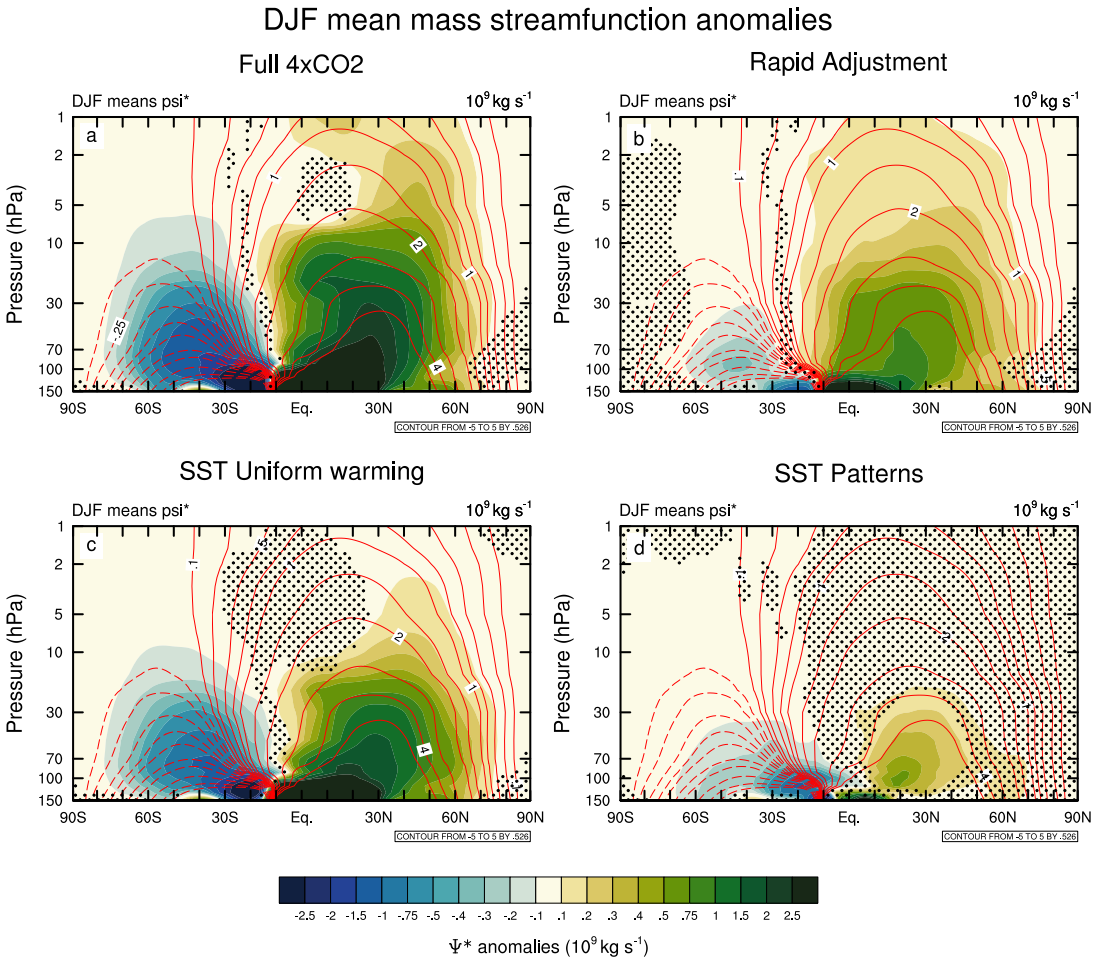

Figure 3.5: DJF mean residual mass streamfunction anomalies [10^9 kg s^{-1}] between 150 − 1 hPa with respect to the piControl simulation for the (a) 4×CO_2 (run B), (b) rapid adjustment (run C), (c) Uniform SST warming (run D) and (d) SST pattern (run E) experiments. Stippling denotes where the differences are not statistically significant at the 95% confidence level using a two-tailed Student's t test. Red contours plotted at −5, −4, −3, −2, −1.5, −1, −0.75, −0.5, −0.25, −0.1, 0.1, 0.25, 0.5, 0.75, 1, 1.5, 2, 3, 4 and 5 × 10^9 kg s^{-1} show the piControl climatology with negative values showed in dashed contours.

In JJA (Figure 3.6), the increase in the SH mass transport is largely present in the subtropics while the opposing changes in the mid-latitude lower stratosphere seen as a reduction in the streamfunction, arise from both the uniform SST warming (Fig. 3.6c) and the SST patterns (Fig. 3.6d). In the SH subtropical ($0° - 30°$S) lower stratosphere ($100 - 50$ hPa), the uniform SST warming accounts for $\sim$ 70% of the full response with the rapid adjustment contributing roughly $\sim$ 20% and the remaining 10% due to the SST pattern. The strengthened SH poleward transport due to the uniform SST warming is confined to the SH subtropical lower stratosphere, while the rapid adjustment (Fig. 3.6b) induces poleward flow that also extends into the NH and is associated with the deep branch of the BDC. However, it should be noted that the SH response is generally weaker than in the NH, especially in the middle and upper stratosphere over both solstice seasons. The deep branch of the circulation exhibits distinct hemispheric asymmetries explaining the differences in the magnitude of downwelling over the SH and NH polar caps seen in Figure 3.4. This asymmetry is associated with a significantly stronger poleward NH branch of the circulation compared to its SH counterpart with important contributions by an equally stronger NH mesospheric cell overall (not shown).

We lastly consider the extent to which the combined residual circulation anomalies from the rapid adjustment, global uniform SST, and SST pattern experiments match the full $4\times CO_2$ response. This comparison is shown in the Supplementary Information (Figure S3.2). The main differences are that the combined responses overpredict the enhanced poleward flow in the NH extratropical lower stratosphere, while there are dipole anomalies straddling the equator in the tropical mid-stratosphere associated with the differences seen in the QBO features across the experiments. Nevertheless, the differences between the linear sum of responses and the full experiment are generally small compared to the overall changes, which supports the use of the experiments to decompose the total response into separate parts.

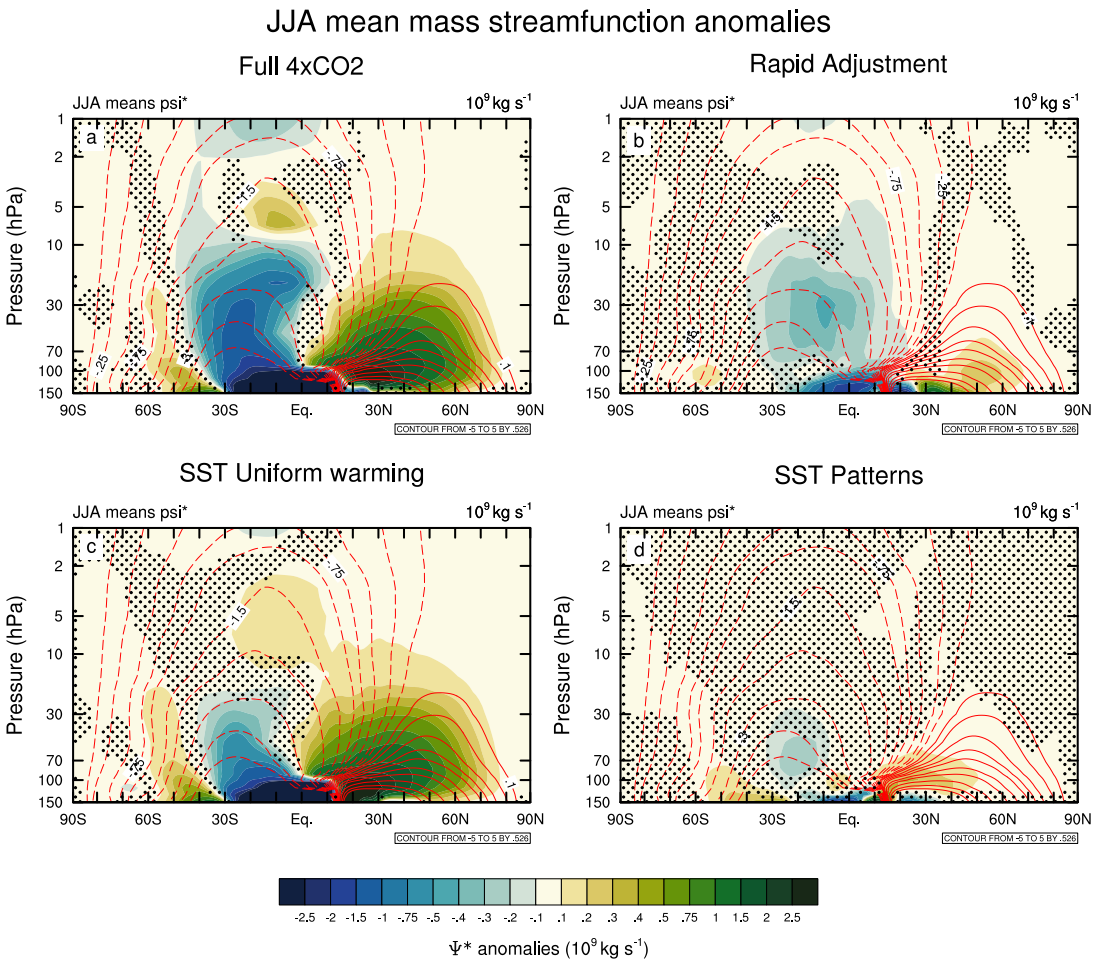

Figure 3.6: As in Figure 3.5, but for the JJA season.

3.3.4 Wave forcing and downward control

To understand the changes in residual circulation shown in Figures 3.4 - 3.6, we now focus on the wave forcing in each experiment. As the distribution of wave forcing shows a strong annual cycle, we separate the changes into the winter and summer seasons in each hemisphere (DJF and JJA) as in Figures 3.5 and 3.6. Figure 3.7 shows the DJF average Eliassen-Palm flux divergence (EPFD) anomalies from preindustrial for runs B, C, D and E along with the anomalous EPF vectors. We multiply the EPFD anomalies with $\cos\phi$ to represent the torque exerted on the zonal flow. The full experiment (Fig. 3.7a) shows increased EPF divergence in the NH extratropical upper stratosphere and in the midlatitude middle stratosphere. In the SH, there is a broad region of enhanced EPF convergence peaking around $50° - 60°$S over a layer spanning 3 to 70 hPa. There is a reduction in EPF convergence near the SH subtropical stratopause. Between $\sim 50-70$ hPa, there is enhanced EPF convergence in the tropics and subtropics in both hemispheres. This modulation in the location of the maximum in the resolved wave forcing is associated with the equatorward movement of the critical layers (Fig. 3.3), allowing more Rossby wave activity to penetrate into the subtropical latitudes, accelerating the shallow branch of the BDC, consistent with the findings of Shepherd and McLandress (2011).

The rapid adjustment and uniform SST warming contribute similar increases in EPF convergence in the NH upper stratosphere in DJF (Figs. 3.7b and 3.7c). In the NH middle stratosphere, the uniform SST warming explains most of the increase in EPF convergence seen in the full experiment, but the rapid adjustment does contribute in the region $20° - 40°$N. The uniform SST warming also contributes to most of the increase in EPF convergence in the lower to middle SH extratropical stratosphere in austral summer, but the rapid adjustment and SST pattern (Fig. 3.7d) do make smaller but significant contributions to the increased wave forcing in that region. The uniform SST warming produces most of the enhanced EPF convergence in the tropical and subtropical upper troposphere-lower stratosphere (UTLS).

Figure 3.8 shows the EPFD anomalies in JJA in each experiment. The picture in the summer NH in the full experiment is similar to that in the SH in DJF (Fig. 3.7a).

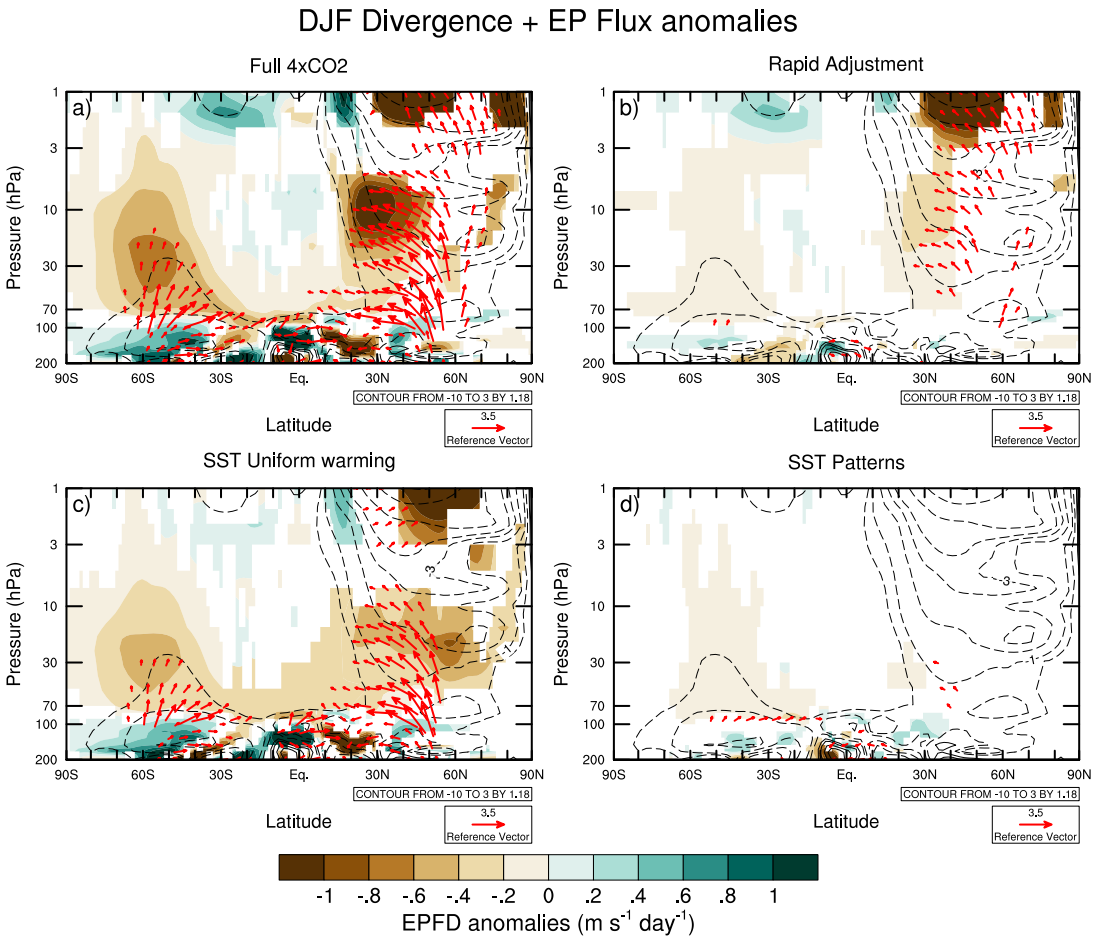

Figure 3.7: DJF average EP flux vector anomalies (red arrows) [m^2 s^{-2}] and EP flux divergence anomalies [m s^{-1} day^{-1}] (shading) between 200 – 1 hPa with respect to the piControl simulation for the (a) 4×CO_2 (run B), (b) rapid adjustment (run C), (c) Uniform SST warming (run D) and (d) SST pattern (run E) experiments. The EPF divergence here is multiplied by the cosine of latitude to represent the torque exerted on the zonal flow. Contours show the piControl climatology with contours plotted at −10, −8, −6, −4, −3, −2, −1, −0.5, 0.5, 1, 2, 3 m s^{-1} day^{-1}. The EP flux vector and divergence anomalies are only plotted where they are significant at the 95% confidence level using a two-tailed Student's t test. The EP flux vectors have been scaled following Edmon et al. (1980) and were scaled by a magnification factor of 5 in the stratosphere in order to enhance their visibility.

Specifically, there is anomalous EPF divergence in the extratropical lower stratosphere and anomalous EPF convergence in the middle to upper stratosphere, representing an upward shift and extension of the region of climatological EPF convergence in this region (contours). Near the subtropical stratopause there is anomalous EPF divergence that comes mainly from the rapid adjustment (Fig. 3.8b). The anomalous EPF convergence in the middle stratosphere comes mainly from the uniform SST warming (Fig. 3.8c) with smaller but significant contributions from the rapid adjustment and SST patterns (Fig. 3.8d). In the winter SH, the picture is rather different from the NH in DJF. The full experiment shows anomalous EPF divergence in the SH upper stratosphere, which represents a weakening of the climatological EPF convergence in this region (contours). This is attributed mainly to the uniform SST warming, but there are also significant EPF convergence anomalies near the SH subtropical stratopause from both the rapid adjustment as well as the SST patterns. The changes in EPFD in the SH middle and lower stratosphere in austral winter have a more complex structure. The full experiment shows a tripolar pattern between 30 to 70 hPa, with anomalous EPF convergence poleward of 60°S and between $20° - 40°$S and anomalous divergence between $40° - 60°$S. This pattern is mainly reproduced in the uniform SST warming experiment but with a smaller contribution to the two regions of anomalous EPF convergence from the rapid adjustment.

Previous studies have demonstrated mechanisms for tropospheric warming to influence the stratospheric EPFD and residual circulation (e.g., Shepherd and McLandress, 2011), but the mechanism through which the rapid adjustment acts on EPFD in the upper stratosphere is less well understood. The radiative cooling in the stratosphere due to increased CO_2 is relatively uniform in latitude (Fels et al., 1980), so we do not expect large direct changes in zonal wind through thermal wind balance. However, the temperature response to CO_2 represents a weakening of the vertical temperature gradient, particularly in the upper stratosphere where the cooling is larger. The characteristics for wave propagation and refraction can be quantified using a measure of refractive index (e.g., Matsuno, 1970) that is dependent on the Brunt-Väisälä frequency ($N^2 = g/\theta \ (d\theta/dz)$). Hence, we hypothesise that the changes in background temperature structure due to the CO_2 radiative effects alter the propagation of Rossby waves, particularly in the upper

stratosphere, and this leads to the changes in EPFD shown in Figures 3.7 and 3.8.

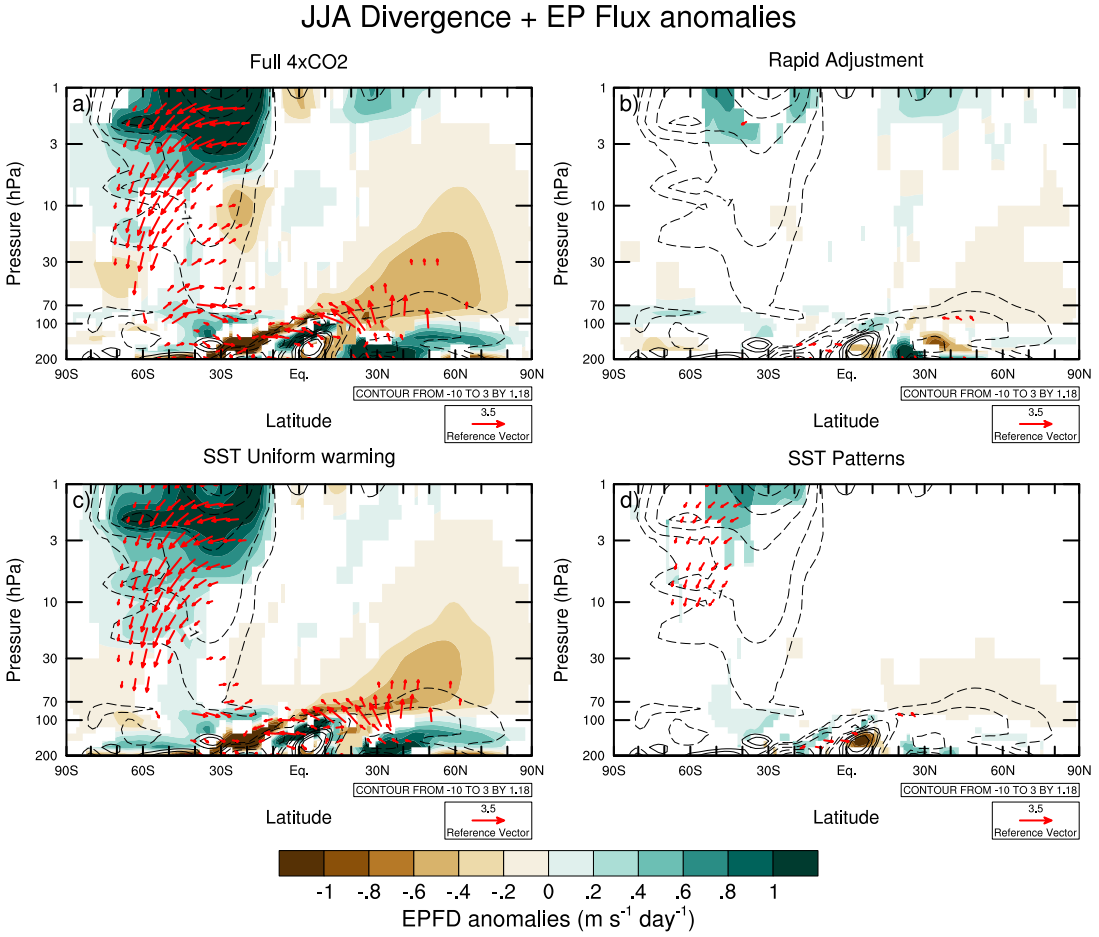

Figure 3.8: As in Figure 7, but for the JJA season.

The anomalous residual circulation is driven by both resolved and parameterised wave forcing. The seasonal parameterised wave forcing (NOGWD and OGWD) anomalies are shown in the Supplementary Information (Figures S3.3 - S3.4 for DJF and Figures S3.5 - S3.6 for JJA). The peak changes in parameterised wave forcing are smaller than the anomalous resolved wave forcing by around a factor of two. The anomalous NOGWD

is mainly in the upper stratosphere and comes from the uniform SST warming. There is anomalous OGWD (Figs. S3.4 and S3.6) in the winter hemispheres near the edge of the polar vortex, which has comparable contributions from the rapid adjustment and the uniform SST warming.

We now quantify the contributions of the different wave types to the anomalous mass circulation in the lower and upper stratosphere. Figures 3.9 and 3.10 show latitudinal profiles of the annual-mean mass streamfunction anomalies in each experiment at 70 hPa and 10 hPa, respectively, along with the DCP inferred contributions from the resolved and parameterised components of the wave forcing. The DCP calculation for the total wave forcing underestimates the directly calculated maximum streamfunction anomaly in the model by around 20%. In the lower stratosphere at 70 hPa, the estimated streamfunction anomalies from the total wave forcing in the full $4\times CO_2$ experiment come mainly ($> 80\%$) from the resolved wave forcing (Fig. 3.9a), with a smaller and more homogeneous contribution from the parameterised wave drag. The resolved wave forcing explains almost all of the DCP estimated response in the rapid adjustment experiment (Fig. 3.9b) and most of it in the uniform SST warming (Fig. 3.9c) case. The component that contributes the smallest increase in streamfunction at 70 hPa, the SST pattern experiment (Fig. 3.9d), shows roughly equal contributions from parameterised and resolved wave forcing. The overall dominance of the resolved wave forcing for the strengthened BDC in the lower stratosphere is consistent with the larger changes in resolved wave drag in this region (Figures 3.7 and 3.8) compared to the parameterised wave forcing changes in this region (Figures S3.3 - S3.6).

In the upper stratosphere (10 hPa), the full $4\times CO_2$ experiment shows contributions to the enhanced streamfunction from both resolved and parameterised wave forcing (Fig. 3.10a). In the NH, the EPFD contribution explains around two thirds of the total DCP estimated streamfunction anomalies and GWD around one third. The positive NH streamfunction anomaly from EPFD poleward of 30°N comes from both the rapid adjustment (Fig. 3.10b) and the uniform SST warming (Fig. 3.10c). In contrast, the positive streamfunction anomaly in the upper stratosphere from parameterised wave drag comes mainly from the uniform SST warming (Fig. 3.10c).

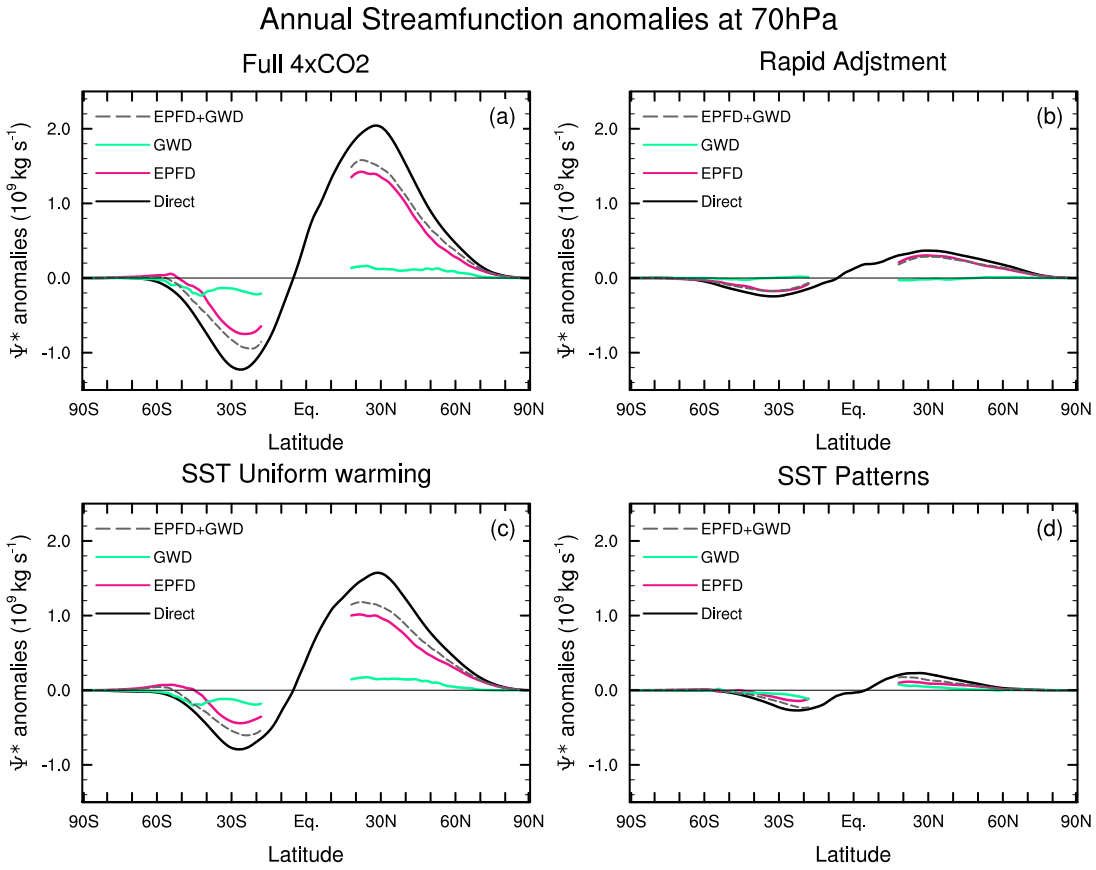

Figure 3.9: Annual-mean residual streamfunction anomalies [10^9 kg s^{-1}] at 70 hPa with respect to the piControl simulation for the (a) 4×CO_2 (run B), (b) rapid adjustment (run C), (c) Uniform SST warming (run D) and (d) SST pattern (run E) experiments. Black line shows the direct calculation, the downward control calculations for EPFD, OGWD + NOGWD and their sum (EPFD + OGWD + NOGWD) are shown in magenta, green and grey dashed, respectively.

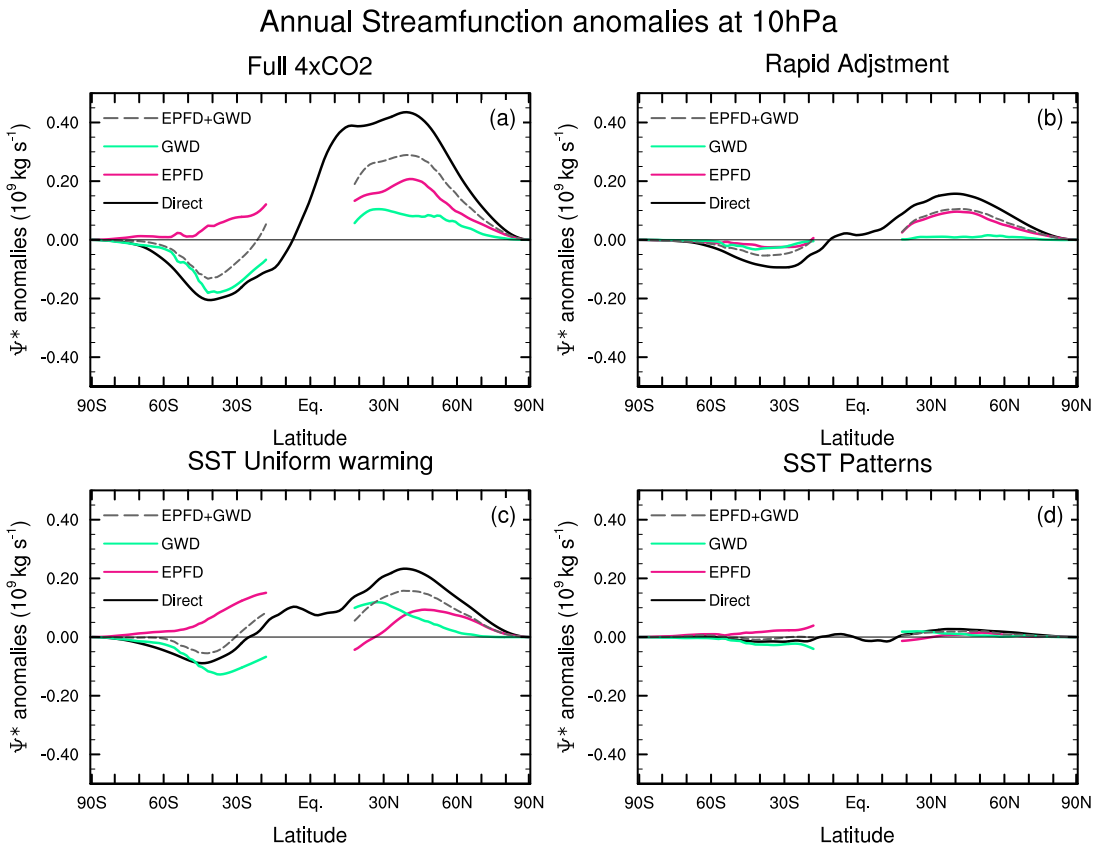

Figure 3.10: As in Figure 3.9, but at 10 hPa.

In the SH, the picture in the Full experiment is somewhat more complex, with the major contribution to the enhanced poleward mass transport coming from GWD, which is partly offset by an opposite contribution from the EPFD. This positive SH streamfunction anomaly associated with EPFD comes mainly from the uniform SST warming (Fig. 3.10c), which also generates enhanced SH poleward transport via enhanced GWD. This increased poleward flow in the SH upper stratosphere is further increased by the rapid adjustment (Fig. 3.10b) with contributions from both resolved and parameterised wave drag. In both hemispheres, the SST pattern has little effect on the wave forcing in the upper stratosphere (Fig. 3.10d).

3.3.5 Uncertainty in global mean SST response

Figure 3.11 summarises the results by showing the annual-mean tropical upward mass flux anomalies in the different experiments at 70 hPa (Fig. 3.11a) and 10 hPa (Fig. 3.11b), respectively. Also shown are the mass flux anomalies from the high and low uniform warming experiments (runs F and G), which span the spread in 4× CO_2 global mean SST response across the CMIP5 models. In the lower branch of the BDC, the annual-mean tropical upward mass flux increases by 45% in the full experiment compared to piControl (3.1×10^9 kg s^{-1}). The uniform SST warming accounts for $\sim$ 70% of this increase, with the rapid adjustment ($\sim$ 20%) and SST patterns ($\sim$ 10%) contributing the remainder in comparable amounts. The central estimates of the mass flux anomalies at 70 hPa in the three uniform SST warming (2.1, 3.4, 4.9 K) experiments are 1.4, 2.3 and 3.4×10^9 kg s^{-1}, which gives an approximate linear scaling of 0.7×10^9 kg s^{-1} K^{-1} ($\sim$ 10% K^{-1}). In the lower stratosphere, the uncertainty from the CMIP5 model spread in global mean SST response to 4× CO_2 is larger than the contribution from the rapid adjustment and the SST pattern effect.

In the upper stratosphere at 10 hPa, the total mass flux increases by around 35% in the full experiment (0.6×10^9 kg s^{-1}). This increase comes almost equally from the rapid adjustment ($\sim$ 40%) and the uniform SST warming ($\sim$ 45%), with the remaining $\sim$ 10% contribution coming from the SST pattern effect, though the latter is not statistically distinguishable from internal variability. The central estimates of mass flux anomalies at 10 hPa in the three uniform SST warming experiments are 0.17, 0.29 and 0.50×10^9 kg s^{-1}, which gives an approximate linear scaling with global mean SST

of 0.11×10^9 kg s^{-1} K^{-1} ($\sim 7\%$ K^{-1}). In the upper stratosphere, the magnitude of the anomalous mass flux due to the rapid adjustment is therefore comparable to the uncertainty from the model spread in global mean SST response to $4\times CO_2$.

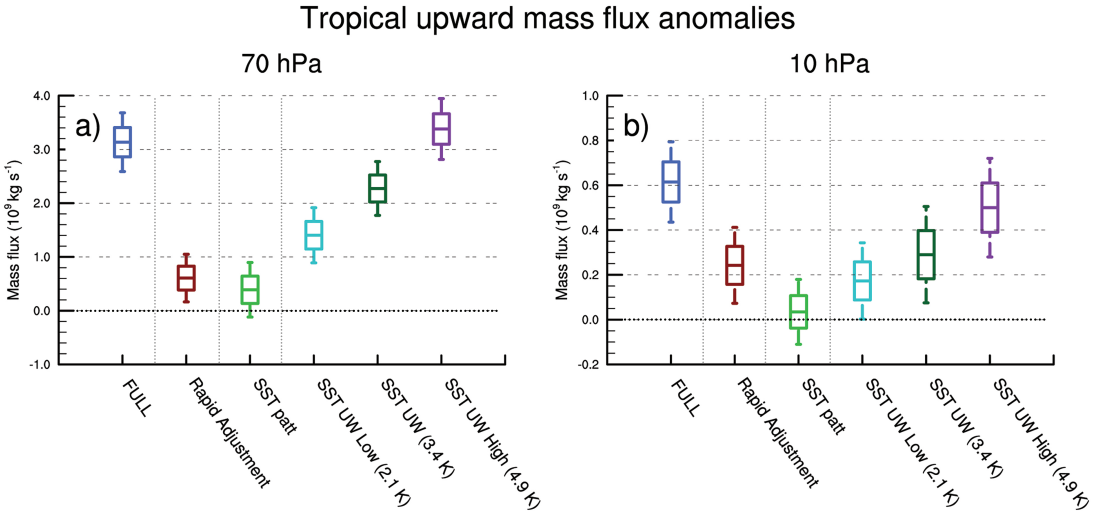

Figure 3.11: Annual-mean tropical upward mass flux anomalies [10^9 kg s^{-1}] at (a) 70 hPa and (b) 10 hPa in the different perturbation experiments as labelled. The edges of the boxplots indicate ± 1 standard deviation of the interannual variability and the whiskers indicate ± 2 standard deviations.

3.4 Discussion and conclusions

We have performed idealised experiments with the HadGEM3-A model to decompose the long-term Brewer-Dobson circulation response to an abrupt quadrupling in CO_2 into three components: 1) a rapid atmospheric adjustment where CO_2 is added to the atmosphere but sea surface temperatures (SST) are held fixed; 2) a contribution from the global-average SST change; and 3) an SST pattern effect. The SST anomalies in response to the abrupt $4\times CO_2$ perturbation were derived from the CMIP5 multi-model ensemble. The multi-model annual-mean global-mean SST anomaly over the final 50 years of the CMIP5 abrupt-$4\times CO_2$ runs is 3.4 K. The SST pattern (i.e. the local de-

viation from the global mean value) shows relatively higher SST across the tropical oceans and most of the Northern hemisphere and relatively cooler SST across much of the Southern Ocean and in the northern North Atlantic. The HadGEM3-A simulations are perturbed from a reference preindustrial state, and sea ice concentrations are held fixed to enable a clean separation of the effects of SST without combining this with the potential effect of sea ice changes on the stratosphere (e.g. Kim et al., 2014).

In the tropical lower stratosphere, the 45% increase in the annual-mean mass transport by the BDC under the full $4\times CO_2$ perturbation comes mainly ($\sim$ 70%) from the uniform SST warming consistent with the findings of Lin et al. (2015). The remainder comes from the rapid adjustment ($\sim$ 20%) and the SST pattern effect ($\sim$ 10%). The amplitude of the SST pattern effect on the mass transport in the lower stratosphere is broadly comparable to that found on interannual timescales associated with ENSO (Calvo et al., 2010; Simpson et al., 2011), though note that while the SST pattern imposed here shows enhanced warming in the equatorial Pacific, by construction it contains global structure; including relative warming across the tropical oceans and North Pacific and relative cooling in the Southern Ocean (Fig. 3.1c). In the upper stratosphere, where the deep branch of the BDC occurs, the increase in the BDC mass transport under abrupt-$4\times CO_2$ comes from the rapid adjustment and the uniform SST warming in roughly equal measure. The results are consistent with studies that show an important role for the strengthening of the subtropical jets under climate change (e.g. Garcia and Randel, 2008; Lin and Fu, 2013; McLandress and Shepherd, 2009; Shepherd and McLandress, 2011), which in the decomposition performed here comes mainly from the uniform SST warming. However, our results also demonstrate that an increase of the BDC in the upper stratosphere comes mainly from the radiative cooling of the stratosphere by CO_2, as seen in the rapid adjustment component of the response. This means that in transient atmosphere-ocean abrupt-$4\times CO_2$ experiments, there are expected to be different characteristic timescales for the BDC response. In the lower stratosphere, the timescale of the BDC response will be mainly determined by the rate of tropospheric warming and associated changes to upper tropospheric heating and subtropical jet strength, while in the upper stratosphere there will be a fast timescale associated with the CO_2 radiative cooling and a slow timescale also tied to the tropospheric warming. The results therefore demonstrate the existence of two timescales

in the response of the BDC to increasing CO_2, with the relative importance of each timescale for the long-term response being height dependent.

We further examined the effect of the uncertainty in global mean SST response to increased CO_2, as a proxy for model spread in equilibrium climate sensitivity. The range in the global mean SST response across the CMIP5 models is 2.1 to 4.9 K. Further experiments imposing these global uniform SST values show an increase in the lower stratosphere (70 hPa) upward mass flux of 1.4×10^9 and 3.4×10^9 kg s^{-1}, respectively, which can be compared to the increase of 2.3×10^9 kg s^{-1} in the multi-model mean global SST experiment. In the upper stratosphere (10 hPa), the upward mass flux change for uniform SST warming of 2.1 and 4.9 K is 0.17×10^9 and 0.5×10^9 kg s^{-1}, respectively, which can be compared to 0.29×10^9 kg s^{-1} in the multi-model mean global SST experiment. Therefore, in the lower stratosphere the contribution from the uniform SST warming and its uncertainty is larger than the rapid adjustment and SST pattern effects on the BDC in the lower stratosphere. However, in the upper stratosphere (10 hPa) the uncertainty in the magnitude of global mean SST increase across models is comparable to the magnitude of the rapid adjustment effect on the BDC.

Using the tropical mass flux anomalies described above and the GSAT changes in the experiments given in Section 3.2.2, we calculate a linear dependence of the tropical upward mass flux on GSAT of 0.62×10^9 kg s^{-1} K^{-1} ($\sim 9\%$ K^{-1}) at 70 hPa and 0.10×10^9 kg s^{-1} K^{-1} ($\sim 6\%$ K^{-1}) at 10 hPa. Hardiman et al. (2014) examined CMIP5 models and calculated a multi-model mean trend in 70 hPa upward mass flux of 3.2% decade^{-1} over $2006-2099$ in the Representative Concentration Pathway 8.5 (RCP8.5) emissions scenario. The multi-model mean change in GSAT between $2081-2100$ relative to $1986-2005$ is 3.7 K in the RCP8.5 scenario (Collins et al., 2013). This gives an approximate multi-model mean GSAT trend for the 21^{st} century of 0.35 K decade$^{-}1$. Dividing these two numbers gives an estimate for the relationship between 70 hPa mass flux and GSAT of $\sim 9\%$ K^{-1}. This is in almost exact agreement with our results, despite the different modelling approaches, though our estimate would be slightly larger if the contributions from the rapid adjustment and SST pattern effects, which are implicitly included in the simulations used by Hardiman et al. (2014), were accounted for. The comparison is further complicated by the projected reduction in the BDC due to ozone

recovery (e.g. Oman et al., 2009), which offsets part of the GHG-driven increase over the 21^{st} century; this effect is also included in the 21^{st} century scenario simulations used by Hardiman et al. (2014) and, if removed, this would presumably make the inferred relationship to GSAT larger than the $\sim 9\%$ K^{-1} estimated above based on the CMIP5 RCP8.5 scenario.

The CO_2 perturbation applied here is large compared to projected CO_2 concentrations during the 21^{st} century based on current mitigation commitments under the United Nations Framework Convention on Climate Change (UNFCCC) 2015 Paris Agreement. For a smaller increase in CO_2, the rapid adjustment and uniform SST warming contributions are expected to be smaller; in this case the SST pattern effect would become proportionately more important. Our experiments have neglected any feedbacks that induce stratospheric ozone changes; it has been shown that the ozone response to $4\times CO_2$ affects the zonal-mean extratropical circulation (Chiodo and Polvani, 2017); it would be interesting to also examine the effects of ozone on the BDC in the future. The experiments are designed to study the long-term centennial response to an abrupt quadrupling of CO_2, and they have only been performed with one model. The model contains mean state biases that could affect some of the details of the responses described here. Studies with other coupled atmosphere-ocean models and those that examine the transient response of the BDC to CO_2 would therefore be insightful.

3.5 Supplementary material

CMIP5 Models				
1. ACCESS1-0	2. ACCESS1-3	3. CCSM4	4. CNRM-CM5	5. CSIRO-Mk3-6-0
6. CanESM2	7. EC-EARTH	8. GFDL-CM3	9. GFDL-ESM2G	10. GFDL-ESM2M
11. GISS-E2-H	12. GISS-E2-R	13. HadGEM2-ES	14. IPSL-CM5A-LR	15. IPSL-CM5A-MR
16. IPSL-CM5B-LR	17. MIROC-ESM	18. MIROC5	19. MPI-ESM-LR	20. MPI-ESM-MR
21. MPI-ESM-P	22. MRI-CGCM3	23. NorESM1-M	24. BCC-CSM1-1-M	25. BCC-CSM1-1
26. INMCM4				

Table S3.1: The CMIP5 global coupled ocean-atmosphere general circulation models used to construct the SST and SIC boundary conditions in this study.

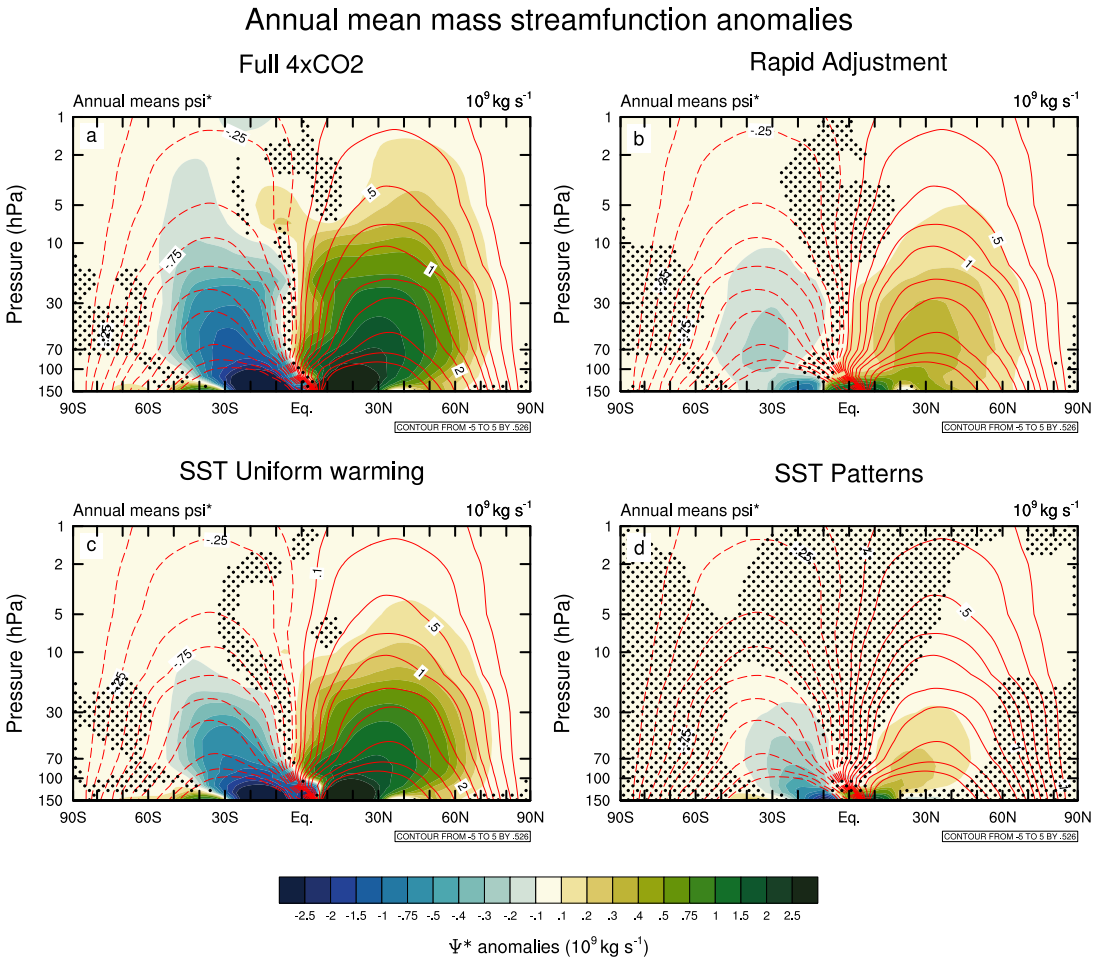

Figure S3.1: Annual mean residual mass streamfunction anomalies [10^9 kg s^{-1}] between 150 − 1 hPa with respect to the piControl simulation for the (a) 4×CO_2 (run B), (b) rapid adjustment (run C), (c) Uniform SST warming (run D) and (d) SST pattern (run E) experiments. Stippling denotes where the differences are not statistically significant at the 95% confidence level using a two-tailed Student's t test. Red contours plotted at −5, −4, −3, −2, −1.5, −1, −0.75, −0.5, −0.25, −0.1, 0.1, 0.25, 0.5, 0.75, 1, 1.5, 2, 3, 4 and 5 × 10^9 kg s^{-1} show the piControl climatology with negative values showed in dashed contours.

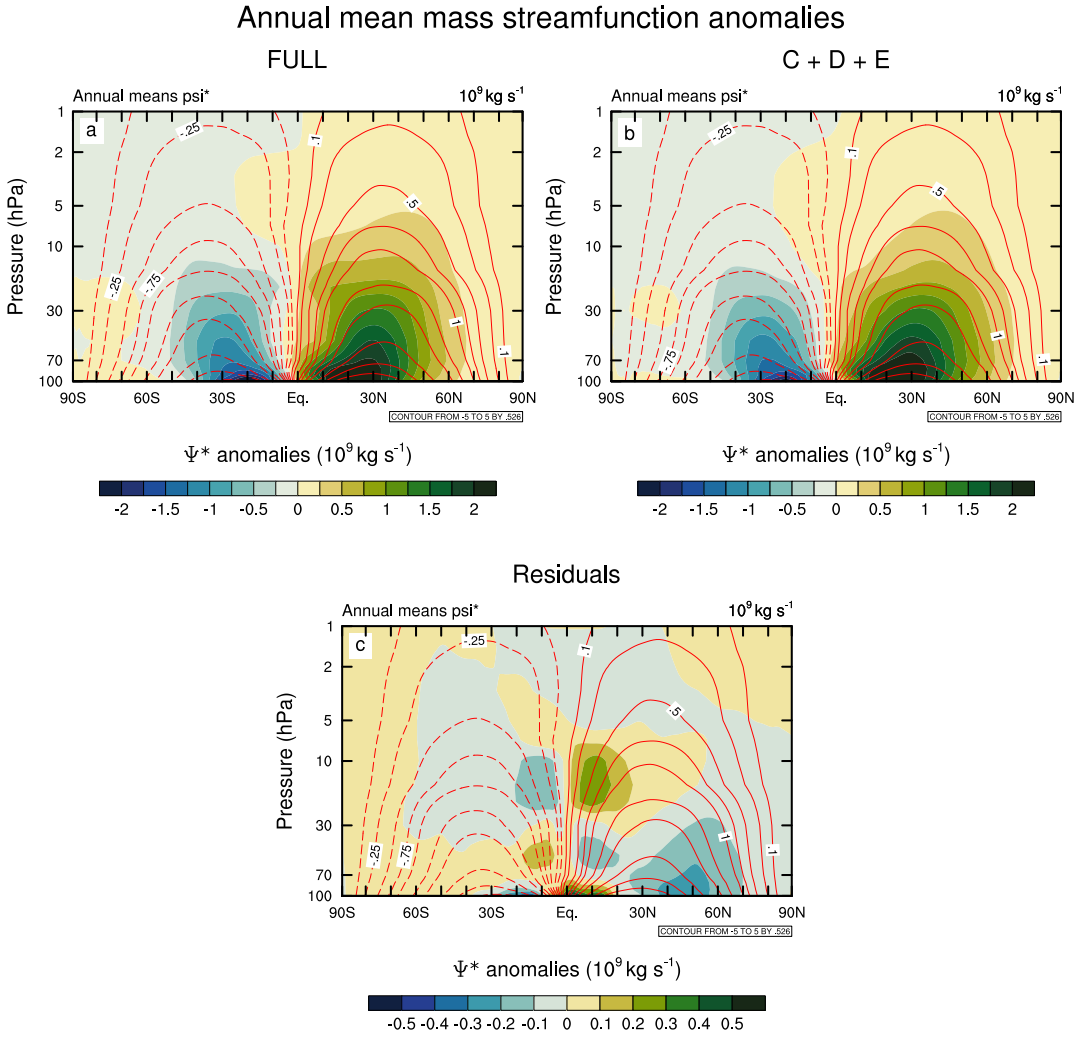

Figure S3.2: The residual mass streamfunction anomalies [10^9 kg s^{-1}] in (a) the full $4\times CO_2$ experiment (as in Fig. 3.5a), (b) the sum of experiments C+D+E and (c) a - b differences. Note panel (c) has a different colour scale. This shows the decomposition of the streamfunction response in the full experiment into the three components analysed in the main text works to leading order.

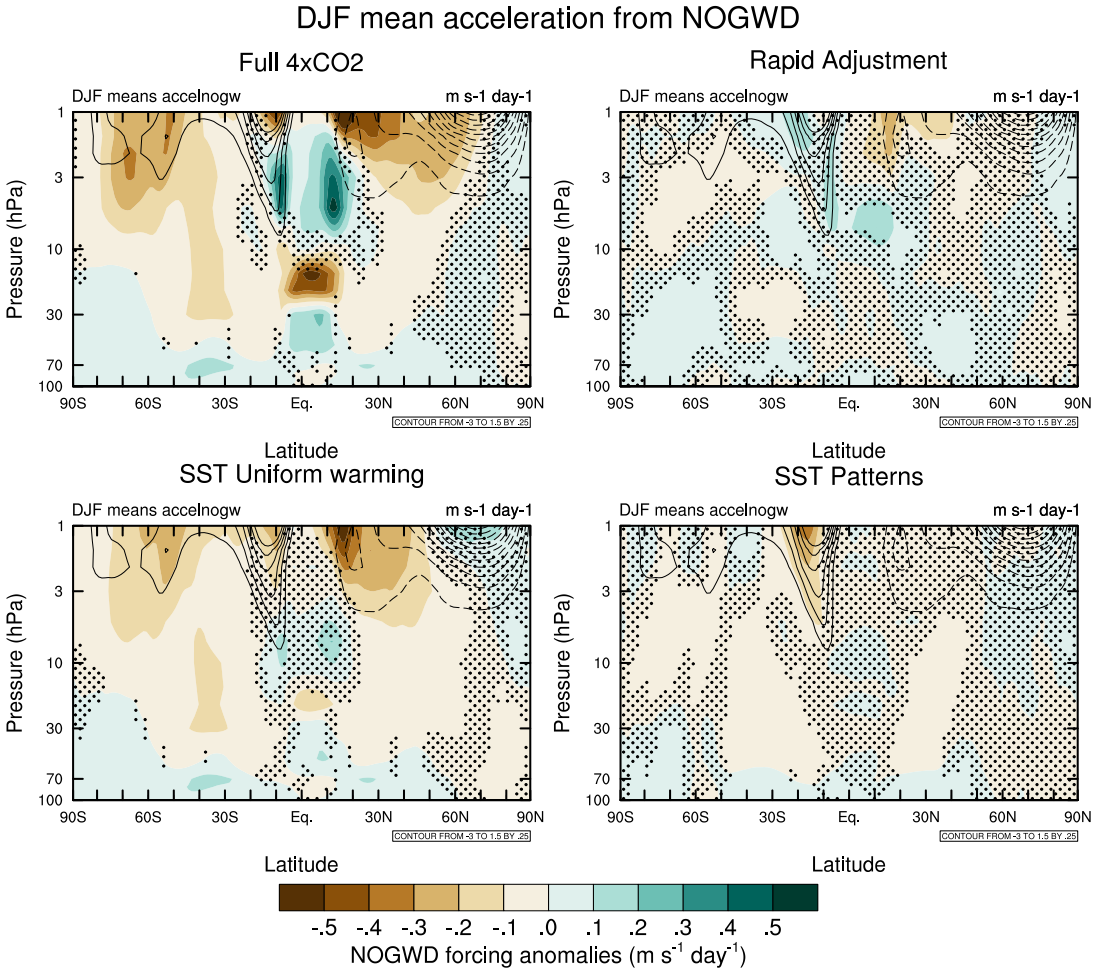

Figure S3.3: DJF average non-orographic GWD anomalies [m s^{-1} day^{-1}] (shading) in the four perturbation experiments. The NOGWD here is multiplied by the cosine of latitude to represent the torque exerted on the zonal flow. Contours show the piControl climatology with contours plotted from -3 to 1.5 in increments of 0.25 m s^{-1} day^{-1}. Hatching denotes where differences are not statistically significant at the 95% confidence level.

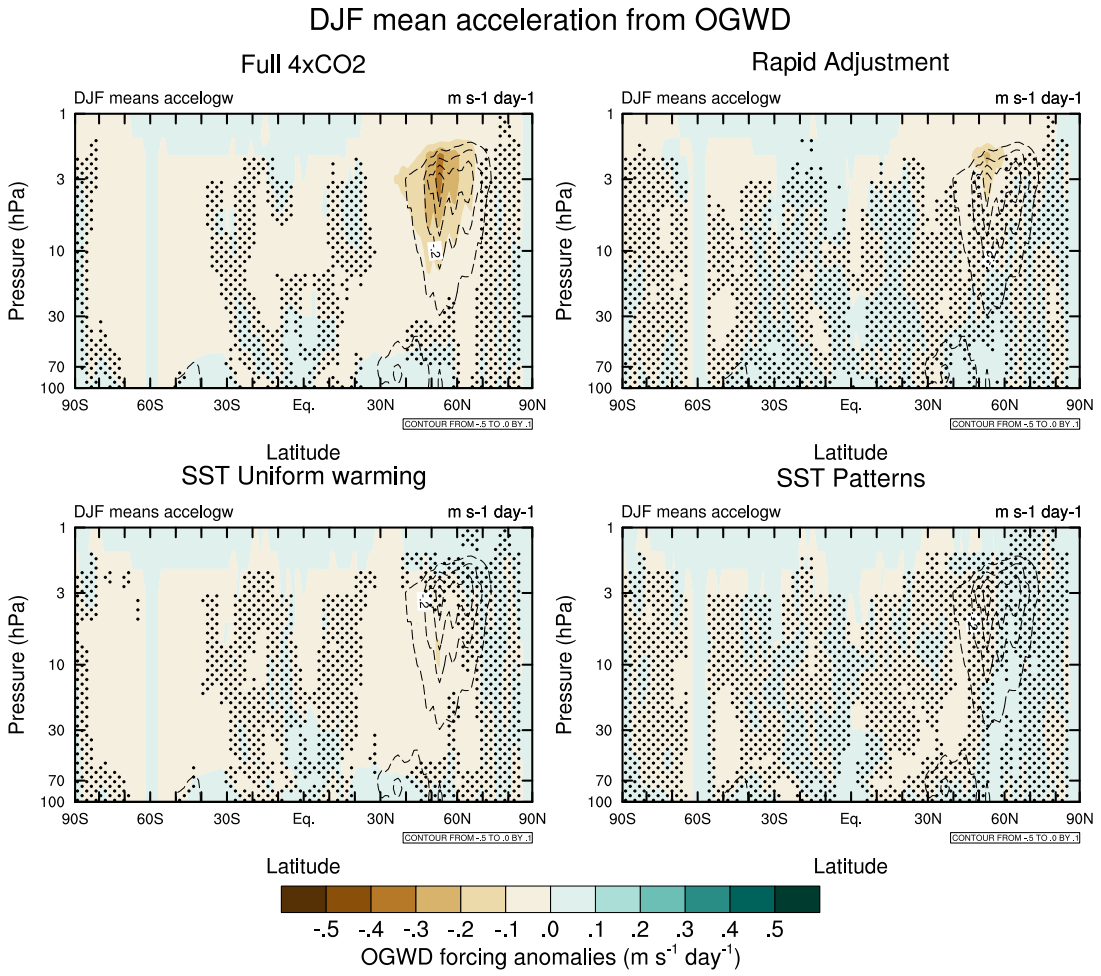

Figure S3.4: As in Figure S3.3, but for the DJF mean orographic GWD. Note the different piControl climatology contour range at the bottom right side.

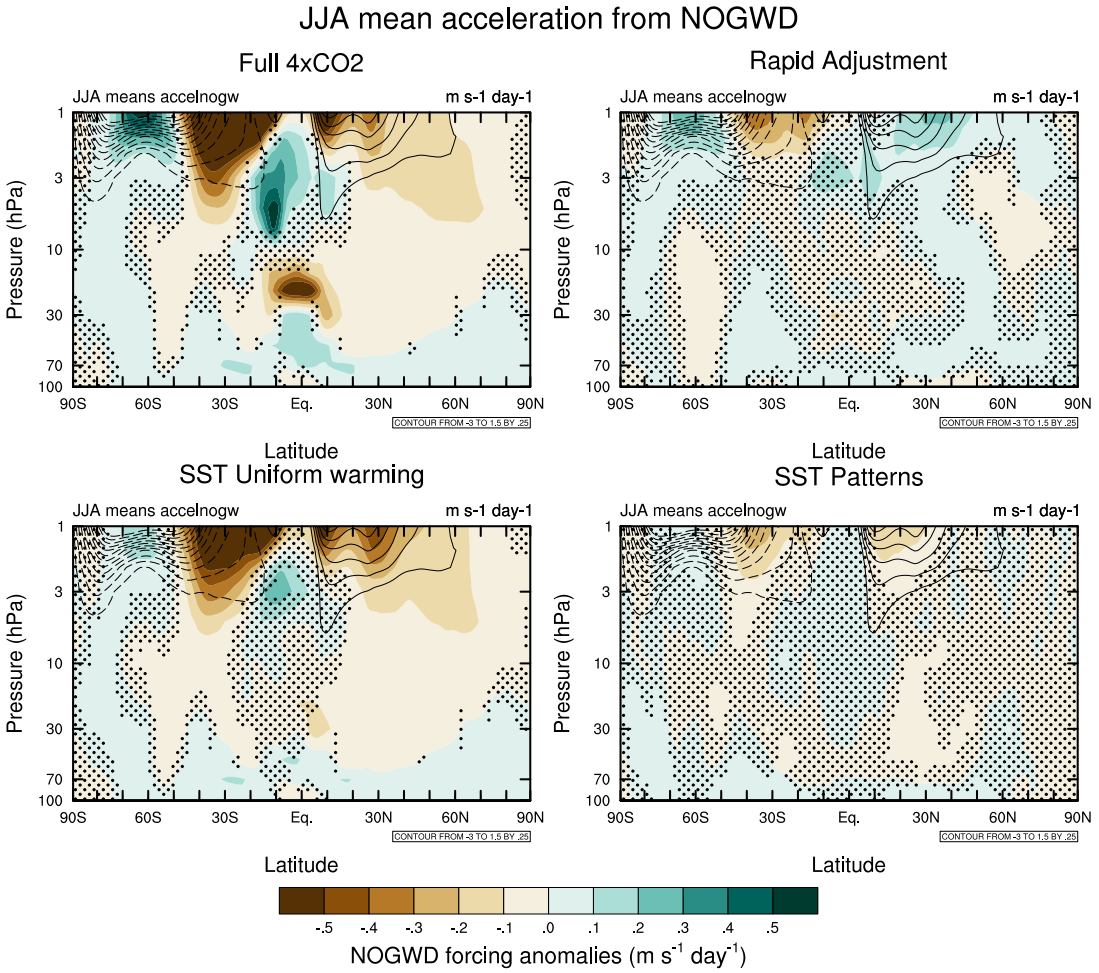

Figure S3.5: As in Figure S3.3, but for JJA.

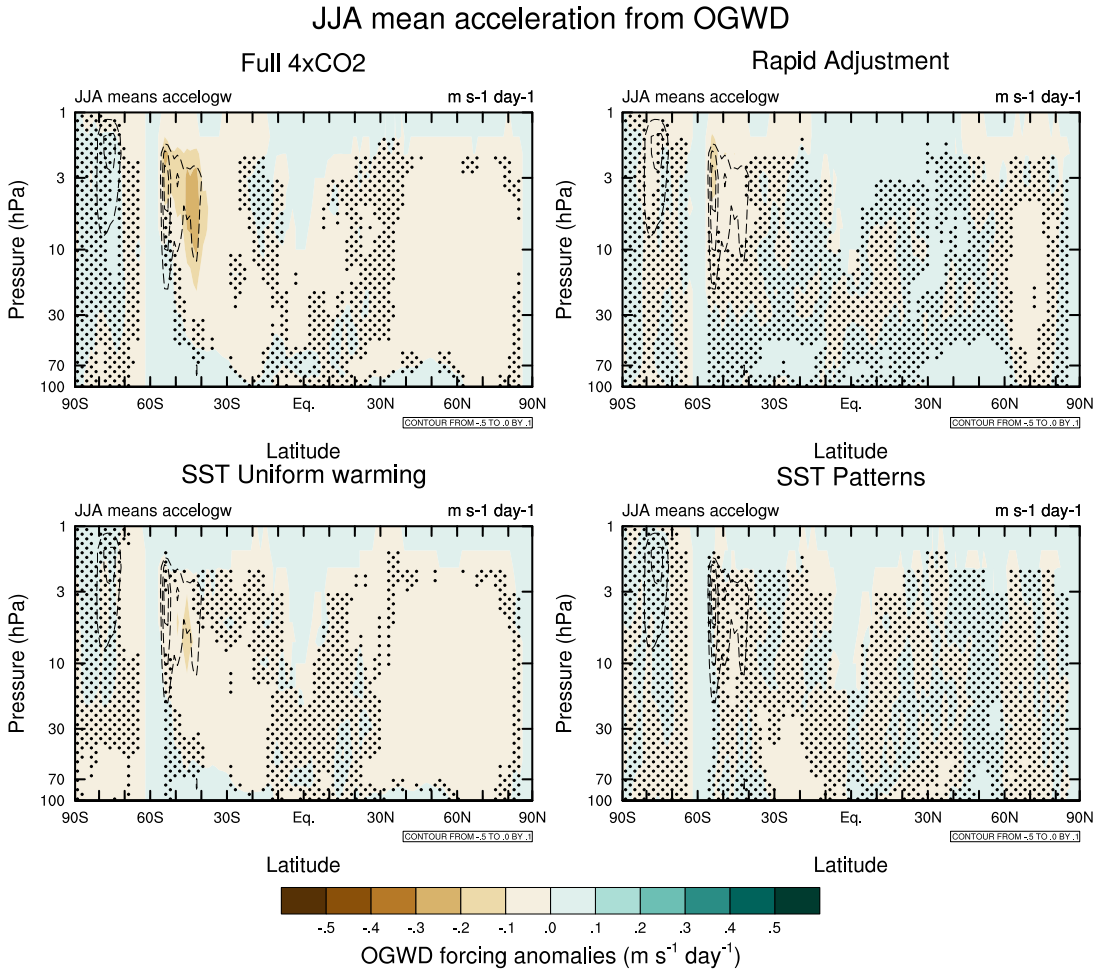

Figure S3.6: As in Figure S3.4, but for JJA.

References

D. G. Andrews and M. E. McIntyre. Planetary Waves in Horizontal and Vertical Shear: The Generalized Eliassen-Palm Relation and the Mean Zonal Acceleration. *Journal of the Atmospheric Sciences*, 33(11):2031–2048, 1976. ISSN 0022-4928. doi: 10.1175/1520-0469(1976)033<2031:PWIHAV>2.0.CO;2. URL http://journals.ametsoc.org/doi/abs/10.1175/1520-0469{%}281976{%}29033{%}3C2031{%}3APWIHAV{%}3E2.0.CO{%}3B2. 143

D. G. Andrews and M. E. McIntyre. An exact theory of nonlinear waves on a Lagrangian-mean flow. *Journal of Fluid Mechanics*, 89(4):609–646, 1978. ISSN 0022-1120. doi: 10.1017/S0022112078002773. URL https://www.cambridge.org/core/product/identifier/S0022112078002773/type/journal{_}article. 143

D. G. Andrews, C. B. Leovy, J. R. Holton, and C. B. Leovy. *Middle Atmosphere Dynamics*. Academic press, 1987. 135, 143

A. Banerjee, A. C. Maycock, A. T. Archibald, N. L. Abraham, P. Telford, P. Braesicke, and J. A. Pyle. Drivers of changes in stratospheric and tropospheric ozone between year 2000 and 2100. *Atmospheric Chemistry and Physics*, 16(5):2727–2746, 2016. ISSN 1680-7324. doi: 10.5194/acp-16-2727-2016. URL https://www.atmos-chem-phys.net/16/2727/2016/. 136

T. Birner and H. Bönisch. Residual circulation trajectories and transit times into the extratropical lowermost stratosphere. *Atmospheric Chemistry and Physics*, 11(2):817–827, 2011. ISSN 1680-7324. doi: 10.5194/acp-11-817-2011. URL https://www.atmos-chem-phys.net/11/817/2011/. 135

A. W. Brewer. Evidence for a world circulation provided by the measurements of helium and water vapour distribution in the stratosphere. *Quarterly Journal of the Royal Meteorological Society*, 75(326):351–363, 1949. ISSN 00359009. doi: 10.1002/qj.49707532603. URL http://doi.wiley.com/10.1002/qj.49707532603. 135

N. Butchart and A. A. Scaife. Removal of chlorofluorocarbons by increased mass exchange between the stratosphere and troposphere in a changing climate. *Nature*, 410(6830):799–802, 2001. ISSN 0028-0836. doi: 10.1038/35071047. URL http://www.nature.com/articles/35071047. 135, 136

N. Butchart, A. A. Scaife, M. Bourqui, J. de Grandpré, S. H. E. Hare, J. Kettleborough, U. Langematz, E. Manzini, F. Sassi, K. Shibata, D. Shindell, and M. Sigmond. Simulations of anthropogenic change in the strength of the Brewer–Dobson circulation. *Climate Dynamics*, 27(7-8):727–741, 2006. ISSN 0930-7575. doi: 10.1007/s00382-006-0162-4. URL http://link.springer.com/10.1007/s00382-006-0162-4. 136, 137

N. Butchart, I. Cionni, V. Eyring, T. G. Shepherd, D. W. Waugh, H. Akiyoshi, J. Austin, C. Brühl, M. P. Chipperfield, E. Cordero, M. Dameris, R. Deckert, S. Dhomse, S. M. Frith, R. R. Garcia, A. Gettelman, M. A. Giorgetta, D. E. Kinnison, F. Li, E. Mancini, C. McLandress, S. Pawson, G. Pitari, D. A. Plummer, E. Rozanov, F. Sassi, J. F. Scinocca, K. Shibata, B. Steil, and W. Tian. Chemistry–Climate Model Simulations of Twenty-First Century Stratospheric Climate and Circulation Changes. *Journal of Climate*, 23(20):5349–5374, 2010. ISSN 0894-8755. doi: 10.1175/2010JCLI3404.1. URL http://journals.ametsoc.org/doi/10.1175/2010JCLI3404.1. 136, 137

N. Calvo and R. R. Garcia. Wave Forcing of the Tropical Upwelling in the Lower Stratosphere under Increasing Concentrations of Greenhouse Gases. *Journal of the Atmospheric Sciences*, 66(10):3184–3196, 2009. ISSN 0022-4928. doi: 10.1175/2009jas3085.1. URL http://journals.ametsoc.org/doi/abs/10.1175/2009JAS3085.1. 136, 137

N. Calvo, R. R. Garcia, W. J. Randel, and D. R. Marsh. Dynamical Mechanism for the Increase in Tropical Upwelling in the Lowermost Tropical Stratosphere during Warm ENSO Events. *Journal of the Atmospheric Sciences*, 67(7):2331–2340, 2010. ISSN 0022-4928. doi: 10.1175/2010JAS3433.1. URL http://journals.ametsoc.org/doi/10.1175/2010JAS3433.1. 139, 149, 164

G. Chen, J. Lu, and L. Sun. Delineating the Eddy–Zonal Flow Interaction in the Atmospheric Circulation Response to Climate Forcing: Uniform SST Warming in an Idealized Aquaplanet Model. *Journal of the Atmospheric Sciences*, 70(7):2214–2233, 2013. ISSN 0022-4928. doi: 10.1175/JAS-D-12-0248.1. URL http://journals.ametsoc.org/doi/10.1175/JAS-D-12-0248.1. 139

G. Chiodo and L. M. Polvani. Reduced Southern Hemispheric circulation response to quadrupled CO 2 due to stratospheric ozone feedback. *Geophysical Research Letters*,

44(1):465–474, 2017. ISSN 00948276. doi: 10.1002/2016GL071011. URL http://doi.wiley.com/10.1002/2016GL071011. 143, 166

A. Chrysanthou, A. C. Maycock, M. P. Chipperfield, S. Dhomse, H. Garny, D. Kinnison, H. Akiyoshi, M. Deushi, R. R. Garcia, P. Jöckel, O. Kirner, G. Pitari, D. A. Plummer, L. Revell, E. Rozanov, A. Stenke, T. Y. Tanaka, D. Visioni, and Y. Yamashita. The effect of atmospheric nudging on the stratospheric residual circulation in chemistry–climate models. *Atmospheric Chemistry and Physics*, 19 (17):11559–11586, 2019. ISSN 1680-7324. doi: 10.5194/acp-19-11559-2019. URL https://www.atmos-chem-phys.net/19/11559/2019/. 137

N. Y. Cohen, E. P. Gerber, and O. Bühler. Compensation between Resolved and Unresolved Wave Driving in the Stratosphere: Implications for Downward Control. *Journal of the Atmospheric Sciences*, 70(12):3780–3798, 2013. ISSN 0022-4928. doi: 10.1175/JAS-D-12-0346.1. URL http://journals.ametsoc.org/doi/10.1175/JAS-D-12-0346.1. 137

M. Collins, R. Knutti, J. Arblaster, J.-L. Dufresne, T. Fichefet, P. Friedlingstein, X. Gao, W. J. Gutowski, T. Johns, G. Krinner, M. Shongwe, C. Tebaldi, A. J. Weaver, and M. Wehner. Chapter 12 - Long-term Climate Change: Projections, Commitments and Irreversibility. In Intergovernmental Panel on Climate Change, editor, *Climate Change 2013 - The Physical Science Basis*, volume 9781107057, pages 1029–1136. Cambridge University Press, Cambridge, 2013. ISBN 9781107415324. doi: 10.1017/CBO9781107415324.024. URL https://www.cambridge.org/core/product/identifier/CBO9781107415324A032/type/book{_}part. 136, 145, 147, 165

R. Deckert and M. Dameris. Higher tropical SSTs strengthen the tropical upwelling via deep convection. *Geophysical Research Letters*, 35(10):2–5, 2008. ISSN 00948276. doi: 10.1029/2008GL033719. URL http://doi.wiley.com/10.1029/2008GL033719. 136, 137

R. E. Dickinson. Planetary Rossby Waves Propagating Vertically Through Weak Westerly Wind Wave Guides. *Journal of the Atmospheric Sciences*, 25(6): 984–1002, 1968. ISSN 0022-4928. doi: 10.1175/1520-0469(1968)025<0984:

PRWPVT>2.0.CO;2. URL http://journals.ametsoc.org/doi/abs/10.1175/1520-0469{%}281968{%}29025{%}3C0984{%}3APRWPVT{%}3E2.0.CO{%}3B2. 149

G. M. B. Dobson. Origin and distribution of the polyatomic molecules in the atmosphere. *Proceedings of the Royal Society of London. Series A. Mathematical and Physical Sciences*, 236(1205):187–193, 1956. ISSN 0080-4630. doi: 10.1098/rspa.1956.0127. URL https://royalsocietypublishing.org/doi/10.1098/rspa.1956.0127. 135

J.-L. Dufresne, M.-A. Foujols, S. Denvil, A. Caubel, O. Marti, O. Aumont, Y. Balkanski, S. Bekki, H. Bellenger, R. Benshila, S. Bony, L. Bopp, P. Braconnot, P. Brockmann, P. Cadule, F. Cheruy, F. Codron, A. Cozic, D. Cugnet, N. de Noblet, J.-P. Duvel, C. Ethé, L. Fairhead, T. Fichefet, S. Flavoni, P. Friedlingstein, J.-Y. Grandpeix, L. Guez, E. Guilyardi, D. Hauglustaine, F. Hourdin, A. Idelkadi, J. Ghattas, S. Joussaume, M. Kageyama, G. Krinner, S. Labetoulle, A. Lahellec, M.-P. Lefebvre, F. Lefevre, C. Levy, Z. X. Li, J. Lloyd, F. Lott, G. Madec, M. Mancip, M. Marchand, S. Masson, Y. Meurdesoif, J. Mignot, I. Musat, S. Parouty, J. Polcher, C. Rio, M. Schulz, D. Swingedouw, S. Szopa, C. Talandier, P. Terray, N. Viovy, and N. Vuichard. Climate change projections using the IPSL-CM5 Earth System Model: from CMIP3 to CMIP5. *Climate Dynamics*, 40(9-10):2123–2165, 2013. ISSN 0930-7575. doi: 10.1007/s00382-012-1636-1. URL http://link.springer.com/10.1007/s00382-012-1636-1. 143

H. J. Edmon, B. J. Hoskins, and M. E. McIntyre. Eliassen-Palm Cross Sections for the Troposphere. *Journal of the Atmospheric Sciences*, 37(12): 2600–2616, 1980. ISSN 0022-4928. doi: 10.1175/1520-0469(1980)037<2600:EPCSFT>2.0.CO;2. URL http://journals.ametsoc.org/doi/abs/10.1175/1520-0469{%}281980{%}29037{%}3C2600{%}3AEPCSFT{%}3E2.0.CO{%}3B2. xvi, 156

V. Eyring, S. Bony, G. A. Meehl, C. A. Senior, B. Stevens, R. J. Stouffer, and K. E. Taylor. Overview of the Coupled Model Intercomparison Project Phase 6 (CMIP6) experimental design and organization. *Geoscientific Model Development*, 9(5):1937–1958, 2016. ISSN 1991-9603. doi: 10.5194/gmd-9-1937-2016. URL https://www.geosci-model-dev.net/9/1937/2016/. 143

S. B. Fels, J. D. Mahlman, M. D. Schwarzkopf, and R. W. Sinclair. Stratospheric Sensitivity to Perturbations in Ozone and Carbon Dioxide: Radiative and Dynamical Response. *Journal of the Atmospheric Sciences*, 37(10): 2265–2297, 1980. ISSN 0022-4928. doi: 10.1175/1520-0469(1980)037<2265:SSTPIO>2.0.CO;2. URL http://journals.ametsoc.org/doi/abs/10.1175/1520-0469{%}281980{%}29037{%}3C2265{%}3ASSTPIO{%}3E2.0.CO{%}3B2. 145, 157

G. Flato, J. Marotzke, B. Abiodun, P. Braconnot, S. C. Chou, W. Collins, P. Cox, F. Driouech, S. Emori, V. Eyring, C. Forest, P. Gleckler, E. Guilyardi, C. Jakob, V. Kattsov, C. Reason, and M. Rummukainen. Chapter 9 - Evaluation of Climate Models. In Intergovernmental Panel on Climate Change, editor, *Climate Change 2013 - The Physical Science Basis*, volume 9781107057, pages 741–866. Cambridge University Press, Cambridge, 2013. ISBN 9781107415324. doi: 10.1017/CBO9781107415324.020. URL https://ar5-syr.ipcc.ch/resources/htmlpdf/WG1AR5{_}Chapter09{_}FINAL/. 143

V. I. Fomichev, A. I. Jonsson, J. de Grandpré, S. R. Beagley, C. McLandress, K. Semeniuk, and T. G. Shepherd. Response of the Middle Atmosphere to CO2 Doubling: Results from the Canadian Middle Atmosphere Model. *Journal of Climate*, 20(7):1121–1144, 2007. ISSN 0894-8755. doi: 10.1175/JCLI4030.1. URL http://journals.ametsoc.org/doi/10.1175/JCLI4030.1. 136

R. R. Garcia and W. J. Randel. Acceleration of the Brewer–Dobson Circulation due to Increases in Greenhouse Gases. *Journal of the Atmospheric Sciences*, 65(8):2731–2739, 2008. ISSN 0022-4928. doi: 10.1175/2008JAS2712.1. URL http://journals.ametsoc.org/doi/10.1175/2008JAS2712.1. 136, 137, 164

C. I. Garfinkel, D. W. Waugh, L. D. Oman, L. Wang, and M. M. Hurwitz. Temperature trends in the tropical upper troposphere and lower stratosphere: Connections with sea surface temperatures and implications for water vapor and ozone. *Journal of Geophysical Research: Atmospheres*, 118(17):9658–9672, 2013. ISSN 2169897X. doi: 10.1002/jgrd.50772. URL http://doi.wiley.com/10.1002/jgrd.50772. 139

H. Garny, M. Dameris, W. Randel, G. E. Bodeker, and R. Deckert. Dynamically Forced Increase of Tropical Upwelling in the Lower Stratosphere. *Journal of the Atmospheric*

Sciences, 68(6):1214–1233, 2011. ISSN 0022-4928. doi: 10.1175/2011JAS3701.1. URL http://journals.ametsoc.org/doi/10.1175/2011JAS3701.1. 136, 137

S. C. Hardiman, N. Butchart, and N. Calvo. The morphology of the Brewer-Dobson circulation and its response to climate change in CMIP5 simulations. *Quarterly Journal of the Royal Meteorological Society*, 140(683):1958–1965, 2014. ISSN 00359009. doi: 10.1002/qj.2258. URL http://doi.wiley.com/10.1002/qj.2258. 136, 149, 165, 166

P. H. Haynes, M. E. McIntyre, T. G. Shepherd, C. J. Marks, and K. P. Shine. On the "Downward Control" of Extratropical Diabatic Circulations by Eddy-Induced Mean Zonal Forces. *Journal of the Atmospheric Sciences*, 48 (4):651–678, 1991. ISSN 0022-4928. doi: 10.1175/1520-0469(1991)048<0651: OTCOED>2.0.CO;2. URL http://journals.ametsoc.org/doi/abs/10.1175/1520-0469{%}281991{%}29048{%}3C0651{%}3AOTCOED{%}3E2.0.CO{%}3B2. 144

M. I. Hegglin and T. G. Shepherd. Large climate-induced changes in ultraviolet index and stratosphere-to-troposphere ozone flux. *Nature Geoscience*, 2(10):687–691, 2009. ISSN 1752-0894. doi: 10.1038/ngeo604. URL http://www.nature.com/articles/ngeo604. 136

J. R. Holton, P. H. Haynes, M. E. McIntyre, A. R. Douglass, R. B. Rood, and L. Pfister. Stratosphere-troposphere exchange. *Reviews of Geophysics*, 33(4):403, 1995. ISSN 8755-1209. doi: 10.1029/95RG02097. URL http://doi.wiley.com/10.1029/95RG02097. 135, 136

M. Joshi and J. Gregory. Dependence of the land-sea contrast in surface climate response on the nature of the forcing. *Geophysical Research Letters*, 35(24):L24802, 2008. ISSN 0094-8276. doi: 10.1029/2008GL036234. URL http://doi.wiley.com/10.1029/2008GL036234. 141

Y. Kawatani, K. Hamilton, and S. Watanabe. The Quasi-Biennial Oscillation in a Double CO 2 Climate. *Journal of the Atmospheric Sciences*, 68(2):265–283, 2011. ISSN 0022-4928. doi: 10.1175/2010JAS3623.1. URL http://journals.ametsoc.org/doi/10.1175/2010JAS3623.1. 147

J. Keeble, E. M. Bednarz, A. Banerjee, N. L. Abraham, N. R. P. Harris, A. C. Maycock, and J. A. Pyle. Diagnosing the radiative and chemical contributions to future

changes in tropical column ozone with the UM-UKCA chemistry–climate model. *Atmospheric Chemistry and Physics*, 17(22):13801–13818, 2017. ISSN 1680-7324. doi: 10.5194/acp-17-13801-2017. URL https://www.atmos-chem-phys.net/17/13801/2017/. 136

B.-M. Kim, S.-W. Son, S.-K. Min, J.-H. Jeong, S.-J. Kim, X. Zhang, T. Shim, and J.-H. Yoon. Weakening of the stratospheric polar vortex by Arctic sea-ice loss. *Nature Communications*, 5(1):4646, 2014. ISSN 2041-1723. doi: 10.1038/ncomms5646. URL http://www.nature.com/articles/ncomms5646. 141, 164

T. Kuhlbrodt, C. G. Jones, A. Sellar, D. Storkey, E. Blockley, M. Stringer, R. Hill, T. Graham, J. Ridley, A. Blaker, D. Calvert, D. Copsey, R. Ellis, H. Hewitt, P. Hyder, S. Ineson, J. Mulcahy, A. Siahaan, and J. Walton. The Low-Resolution Version of HadGEM3 GC3.1: Development and Evaluation for Global Climate. *Journal of Advances in Modeling Earth Systems*, 10(11):2865–2888, 2018. ISSN 1942-2466. doi: 10.1029/2018MS001370. URL https://onlinelibrary.wiley.com/doi/abs/10.1029/2018MS001370. 143

J.-F. Lamarque, T. C. Bond, V. Eyring, C. Granier, A. Heil, Z. Klimont, D. Lee, C. Liousse, A. Mieville, B. Owen, M. G. Schultz, D. Shindell, S. J. Smith, E. Stehfest, J. Van Aardenne, O. R. Cooper, M. Kainuma, N. Mahowald, J. R. McConnell, V. Naik, K. Riahi, and D. P. van Vuuren. Historical (1850–2000) gridded anthropogenic and biomass burning emissions of reactive gases and aerosols: methodology and application. *Atmospheric Chemistry and Physics*, 10(15):7017–7039, 2010. ISSN 1680-7324. doi: 10.5194/acp-10-7017-2010. URL https://www.atmos-chem-phys.net/10/7017/2010/. 140

M. Latif and N. S. Keenlyside. El Nino/Southern Oscillation response to global warming. *Proceedings of the National Academy of Sciences*, 106(49):20578–20583, 2009. ISSN 0027-8424. doi: 10.1073/pnas.0710860105. URL https://www.pnas.org/content/pnas/106/49/20578.full.pdf. 138

F. Li, J. Austin, and J. Wilson. The Strength of the Brewer–Dobson Circulation in a Changing Climate: Coupled Chemistry–Climate Model Simulations. *Journal of Climate*, 21(1):40–57, 2008. ISSN 0894-8755. doi: 10.1175/2007JCLI1663.1. URL http://journals.ametsoc.org/doi/10.1175/2007JCLI1663.1. 136

F. Li, R. S. Stolarski, and P. A. Newman. Stratospheric ozone in the post-CFC era. *Atmospheric Chemistry and Physics*, 9(6):2207–2213, 2009. ISSN 1680-7324. doi: 10.5194/acp-9-2207-2009. URL https://www.atmos-chem-phys.net/9/2207/2009/. 136

P. Lin and Q. Fu. Changes in various branches of the Brewer-Dobson circulation from an ensemble of chemistry climate models. *Journal of Geophysical Research: Atmospheres*, 118(1):73–84, 2013. ISSN 2169897X. doi: 10.1029/2012JD018813. URL http://doi.wiley.com/10.1029/2012JD018813. 136, 137, 164

P. Lin, Y. Ming, and V. Ramaswamy. Tropical climate change control of the lower stratospheric circulation. *Geophysical Research Letters*, 42(3):941–948, 2015. ISSN 00948276. doi: 10.1002/2014GL062823. URL http://doi.wiley.com/10.1002/2014GL062823. 138, 139, 164

E. Manzini, M. A. Giorgetta, M. Esch, L. Kornblueh, and E. Roeckner. The Influence of Sea Surface Temperatures on the Northern Winter Stratosphere: Ensemble Simulations with the MAECHAM5 Model. *Journal of Climate*, 19(16):3863–3881, 2006. ISSN 0894-8755. doi: 10.1175/JCLI3826.1. URL http://journals.ametsoc.org/doi/10.1175/JCLI3826.1. 138

D. R. Marsh and R. R. Garcia. Attribution of decadal variability in lower-stratospheric tropical ozone. *Geophysical Research Letters*, 34(21):L21807, 2007. ISSN 0094-8276. doi: 10.1029/2007GL030935. URL http://doi.wiley.com/10.1029/2007GL030935. 138

T. Matsuno. Vertical Propagation of Stationary Planetary Waves in the Winter Northern Hemisphere. *Journal of the Atmospheric Sciences*, 27(6):871–883, 1970. ISSN 0022-4928. doi: 10.1175/1520-0469(1970)027<0871:VPOSPW>2.0.CO;2. URL http://journals.ametsoc.org/doi/abs/10.1175/1520-0469{%}281970{%}29027{%}3C0871{%}3AVPOSPW{%}3E2.0.CO{%}3B2. 157

A. C. Maycock. The contribution of ozone to future stratospheric temperature trends. *Geophysical Research Letters*, 43(9):4609–4616, 2016. ISSN 00948276. doi: 10.1002/2016GL068511. URL http://doi.wiley.com/10.1002/2016GL068511. 143

C. M. McKenna, T. J. Bracegirdle, E. F. Shuckburgh, P. H. Haynes, and M. M. Joshi. Arctic Sea Ice Loss in Different Regions Leads to Contrasting Northern Hemisphere Impacts. *Geophysical Research Letters*, 45(2):945–954, 2018. ISSN 0094-8276. doi: 10.1002/2017GL076433. URL https://onlinelibrary.wiley.com/doi/abs/10.1002/2017GL076433. 141

C. McLandress and T. G. Shepherd. Simulated Anthropogenic Changes in the Brewer–Dobson Circulation, Including Its Extension to High Latitudes. *Journal of Climate*, 22(6):1516–1540, 2009. ISSN 0894-8755. doi: 10.1175/2008JCLI2679.1. URL http://journals.ametsoc.org/doi/10.1175/2008JCLI2679.1. 136, 137, 164

P. J. Nowack, N. Luke Abraham, A. C. Maycock, P. Braesicke, J. M. Gregory, M. M. Joshi, A. Osprey, and J. A. Pyle. A large ozone-circulation feedback and its implications for global warming assessments. *Nature Climate Change*, 5(1):41–45, 2015. ISSN 1758-678X. doi: 10.1038/nclimate2451. URL http://www.nature.com/articles/nclimate2451. 143

M. A. Olsen, M. R. Schoeberl, and J. E. Nielsen. Response of stratospheric circulation and stratosphere-troposphere exchange to changing sea surface temperatures. *Journal of Geophysical Research*, 112(D16):D16104, 2007. ISSN 0148-0227. doi: 10.1029/2006JD008012. URL http://doi.wiley.com/10.1029/2006JD008012. 136, 138, 139

L. Oman, D. W. Waugh, S. Pawson, R. S. Stolarski, and P. A. Newman. On the influence of anthropogenic forcings on changes in the stratospheric mean age. *Journal of Geophysical Research*, 114(D3):D03105, 2009. ISSN 0148-0227. doi: 10.1029/2008JD010378. URL http://doi.wiley.com/10.1029/2008JD010378. 136, 138, 166

R. A. Plumb. Stratospheric Transport. *Journal of the Meteorological Society of Japan. Ser. II*, 80(4B):793–809, 2002. ISSN 0026-1165. doi: 10.2151/jmsj.80.793. URL https://www.jstage.jst.go.jp/article/jmsj/80/4B/80{_}4B{_}793/{_}article. 135

R. A. Plumb and J. Eluszkiewicz. The Brewer–Dobson Circulation: Dynamics of the Tropical Upwelling. *Journal of the Atmospheric Sciences*, 56(6):868–890, 1999. ISSN 0022-4928. doi: 10.1175/1520-0469(1999)056<0868:

TBDCDO>2.0.CO;2. URL http://journals.ametsoc.org/doi/abs/10.1175/1520-0469{%}281999{%}29056{%}3C0868{%}3ATBDCDO{%}3E2.0.CO{%}3B2. 136

W. J. Randel and I. M. Held. Phase Speed Spectra of Transient Eddy Fluxes and Critical Layer Absorption. *Journal of the Atmospheric Sciences*, 48(5): 688–697, 1991. ISSN 0022-4928. doi: 10.1175/1520-0469(1991)048<0688:PSSOTE>2.0.CO;2. URL http://journals.ametsoc.org/doi/abs/10.1175/1520-0469{%}281991{%}29048{%}3C0688{%}3APSSOTE{%}3E2.0.CO{%}3B2. 136

W. J. Randel, R. Garcia, and F. Wu. Dynamical Balances and Tropical Stratospheric Upwelling. *Journal of the Atmospheric Sciences*, 65(11):3584–3595, 2008. ISSN 0022-4928. doi: 10.1175/2008JAS2756.1. URL http://journals.ametsoc.org/doi/10.1175/2008JAS2756.1. 136

W. J. Randel, R. R. Garcia, N. Calvo, and D. Marsh. ENSO influence on zonal mean temperature and ozone in the tropical lower stratosphere. *Geophysical Research Letters*, 36(15):n/a–n/a, 2009. ISSN 00948276. doi: 10.1029/2009GL039343. URL http://doi.wiley.com/10.1029/2009GL039343. 138

D. Rind. Sensitivity of tracer transports and stratospheric ozone to sea surface temperature patterns in the doubled CO 2 climate. *Journal of Geophysical Research*, 107 (D24):4800, 2002. ISSN 0148-0227. 136

D. Rind, R. Suozzo, N. K. Balachandran, and M. J. Prather. Climate Change and the Middle Atmosphere. Part I: The Doubled CO2 Climate. *Journal of the Atmospheric Sciences*, 47(4):475–494, 1990. ISSN 0022-4928. doi: 10.1175/1520-0469(1990)047<0475:CCATMA>2.0.CO;2. URL http://journals.ametsoc.org/doi/abs/10.1175/1520-0469{%}281990{%}29047{%}3C0475{%}3ACCATMA{%}3E2.0.CO{%}3B2. 136, 137

K. H. Rosenlof. Seasonal cycle of the residual mean meridional circulation in the stratosphere. *Journal of Geophysical Research*, 100(D3):5173, 1995. ISSN 0148-0227. doi: 10.1029/94JD03122. URL http://doi.wiley.com/10.1029/94JD03122. 135, 144

A. A. Scaife, N. Butchart, C. D. Warner, and R. Swinbank. Impact of a Spectral Gravity Wave Parameterization on the Stratosphere in the Met Office Unified Model. *Journal of the Atmospheric Sciences*, 59(9):

1473–1489, 2002. ISSN 0022-4928. doi: 10.1175/1520-0469(2002)059<1473:IOASGW>2.0.CO;2. URL http://journals.ametsoc.org/doi/abs/10.1175/1520-0469{%}282002{%}29059{%}3C1473{%}3AIOASGW{%}3E2.0.CO{%}3B2. 140

K. Semeniuk and T. G. Shepherd. Mechanisms for Tropical Upwelling in the Stratosphere. *Journal of the Atmospheric Sciences*, 58(21):3097–3115, 2001. ISSN 0022-4928. doi: 10.1175/1520-0469(2001)058<3097:MFTUIT>2.0.CO;2. URL http://journals.ametsoc.org/doi/abs/10.1175/1520-0469{%}282001{%}29058{%}3C3097{%}3AMFTUIT{%}3E2.0.CO{%}3B2. 136

T. G. Shepherd and C. McLandress. A Robust Mechanism for Strengthening of the Brewer–Dobson Circulation in Response to Climate Change: Critical-Layer Control of Subtropical Wave Breaking. *Journal of the Atmospheric Sciences*, 68 (4):784–797, 2011. ISSN 0022-4928. doi: 10.1175/2010JAS3608.1. URL http://journals.ametsoc.org/doi/10.1175/2010JAS3608.1. 136, 137, 149, 155, 157, 164

M. Sigmond and T. G. Shepherd. Compensation between Resolved Wave Driving and Parameterized Orographic Gravity Wave Driving of the Brewer–Dobson Circulation and Its Response to Climate Change. *Journal of Climate*, 27(14):5601–5610, 2014. ISSN 0894-8755. doi: 10.1175/JCLI-D-13-00644.1. URL http://journals.ametsoc.org/doi/10.1175/JCLI-D-13-00644.1. 137

M. Sigmond, P. C. Siegmund, E. Manzini, and H. Kelder. A Simulation of the Separate Climate Effects of Middle-Atmospheric and Tropospheric CO 2 Doubling. *Journal of Climate*, 17(12):2352–2367, 2004. ISSN 0894-8755. doi: 10.1175/1520-0442(2004)017<2352:ASOTSC>2.0.CO;2. URL http://journals.ametsoc.org/doi/abs/10.1175/1520-0442{%}282004{%}29017{%}3C2352{%}3AASOTSC{%}3E2.0.CO{%}3B2. 136, 137, 139

I. R. Simpson, T. G. Shepherd, and M. Sigmond. Dynamics of the Lower Stratospheric Circulation Response to ENSO. *Journal of the Atmospheric Sciences*, 68(11):2537–2556, 2011. ISSN 0022-4928. doi: 10.1175/JAS-D-11-05.1. URL http://journals.ametsoc.org/doi/10.1175/JAS-D-11-05.1. 138, 149, 164

SPARC. SPARC CCMVal Report on the Evaluation of Chemistry-Climate Models. V. Eyring, T. Shepherd and D. Waugh (Eds.). *SPARC Report No. 5, WCRP-30/2010,WMO/TD-No.40*, 2010. ISSN 1428-345X. URL http://www.sparc-climate.org/publications/sparc-reports/sparc-report-no5/. 136

K. E. Taylor, R. J. Stouffer, and G. A. Meehl. An Overview of CMIP5 and the Experiment Design. *Bulletin of the American Meteorological Society*, 93(4):485–498, 2012. ISSN 0003-0007. doi: 10.1175/BAMS-D-11-00094.1. URL http://journals.ametsoc.org/doi/abs/10.1175/BAMS-D-11-00094.1. 140

E. M. Volodin. The mechanism of multidecadal variability in the Arctic and North Atlantic in climate model INMCM4. *Environmental Research Letters*, 8(3):035038, 2013. ISSN 1748-9326. doi: 10.1088/1748-9326/8/3/035038. URL https://iopscience.iop.org/article/10.1088/1748-9326/8/3/035038. 143

D. N. Walters, K. D. Williams, I. A. Boutle, A. C. Bushell, J. M. Edwards, P. R. Field, A. P. Lock, C. J. Morcrette, R. A. Stratton, J. M. Wilkinson, M. R. Willett, N. Bellouin, A. Bodas-Salcedo, M. E. Brooks, D. Copsey, P. D. Earnshaw, S. C. Hardiman, C. M. Harris, R. C. Levine, C. MacLachlan, J. C. Manners, G. M. Martin, S. F. Milton, M. D. Palmer, M. J. Roberts, J. M. Rodríguez, W. J. Tennant, and P. L. Vidale. The Met Office Unified Model Global Atmosphere 4.0 and JULES Global Land 4.0 configurations. *Geoscientific Model Development*, 7(1):361–386, 2014. ISSN 1991-9603. doi: 10.5194/gmd-7-361-2014. URL https://www.geosci-model-dev.net/7/361/2014/. 140

S. Webster, A. R. Brown, D. R. Cameron, and C. P.Jones. Improvements to the representation of orography in the Met Office Unified Model. *Quarterly Journal of the Royal Meteorological Society*, 129(591):1989–2010, 2003. ISSN 1477870X. doi: 10.1256/qj.02.133. URL http://doi.wiley.com/10.1256/qj.02.133. 140

K. D. Williams, D. Copsey, E. W. Blockley, A. Bodas-Salcedo, D. Calvert, R. Comer, P. Davis, T. Graham, H. T. Hewitt, R. Hill, P. Hyder, S. Ineson, T. C. Johns, A. B. Keen, R. W. Lee, A. Megann, S. F. Milton, J. G. L. Rae, M. J. Roberts, A. A. Scaife, R. Schiemann, D. Storkey, L. Thorpe, I. G. Watterson, D. N. Walters, A. West, R. A. Wood, T. Woollings, and P. K. Xavier. The Met Office Global Coupled Model 3.0 and 3.1 (GC3.0 and GC3.1) Configurations. *Journal of Advances in Modeling Earth*

Systems, 10(2):357–380, 2018. ISSN 1942-2466. doi: 10.1002/2017MS001115. URL https://onlinelibrary.wiley.com/doi/abs/10.1002/2017MS001115. 143

Chapter 4

The utility of indirect measures of the stratospheric residual circulation

Authors: **Andreas Chrysanthou, Amanda C. Maycock and Martyn P. Chipperfield**

Manuscript in preparation for Atmospheric Science Letters

Abstract

The stratospheric residual circulation cannot be directly measured and hence various observable proxies have been used to indirectly quantify changes in the residual circulation on various timescales. However, the extent to which these proxies are successful in capturing the behaviour of the residual circulation is an open question. Here, we use an ensemble of hindcast simulations between $1979-2013$ from the Community Earth System Model version 1 Whole Atmosphere Community Climate Model (CESM1-WACCM) to compare observation-based proxies with direct measures of the residual circulation in a self-consistent manner. The proxies are measures of the contrast in lower stratospheric temperatures between the tropics and pole and ozone concentrations in the tropical lower stratosphere. The temperature-based measure exhibits robust correlations with tropical lower stratospheric upwelling on interannual timescales and a good year-round

correlation between their monthly trends over 1998 – 2013. However, its value in constraining features of the seasonal cycle is limited owing to the details of its calculation. We find that tropical mean ozone at 50 hPa lags tropical upwelling at 70 hPa by 2 months. After accounting for this lag, ozone closely mirrors tropical upwelling variability on seasonal, interannual and long-term trends, especially for the 1998 – 2013 period. On interannual timescales both the tropical mean ozone and temperature-based indices are strongly (anti-)correlated with tropical upwelling ($|r| \sim 0.9$), indicating these are good proxies for the residual circulation in CESM1-WACCM. In terms of multi-year trends, tropical ozone shows the highest anti-correlation across months with tropical upwelling ($r = -0.82$) followed by the temperature-based index. The correlations of monthly trends are consistently smaller during the ozone depletion era (1979 – 1997) than during the era of ozone recovery onset (1998 – 2013).

4.1 Introduction

The Brewer-Dobson circulation (BDC) in the stratosphere can be described as two hemispheric cells with air ascending in the tropics through the tropical tropopause layer (TTL; Fueglistaler et al., 2009), meridional flow towards the poles, and descent in the midlatitudes and extratropics (e.g. Butchart, 2014 and references therein). The BDC modulates the distribution of trace gases in the stratosphere, including methane, nitrous oxide, water vapour and ozone. These gases play an important role in the radiative balance of the stratosphere and troposphere and changes in their distributions can affect radiative forcing and surface temperature trends (e.g. Forster and Shine, 1997, 1999), stratospheric temperature trends (e.g. Maycock et al., 2014, 2018), and regional surface climate via stratosphere-troposphere coupling (e.g. Polvani et al., 2011; Maycock et al., 2013). It is therefore important to understand past and future changes in the BDC.

The BDC is comprised of two parts: slow global-scale advective transport known as the residual circulation and relatively fast quasi-horizontal mixing which occurs mainly in the subtropics (e.g. Plumb, 2002; Shepherd, 2007). The residual circulation can be further separated into two branches, the shallow branch in the lowermost stratosphere and the deep branch in the middle to upper stratosphere (Birner and Bönisch, 2011).

Age-of-air (AoA) is a measure of the stratospheric mass transport that accounts for the effects of both the residual circulation and quasi-horizontal mixing (Kida, 1983; Hall and Plumb, 1994; Plumb, 2002). AoA can be inferred from long-lived stratospheric tracers (e.g. SF_6, CO_2) allowing an assessment of observed BDC changes. However, it is challenging to separate the relative importance of the residual circulation and mixing for estimated variability and trends in AoA (e.g. Stiller et al., 2012; Garny et al., 2014; Ploeger et al., 2015a,b; Eichinger et al., 2019; Šácha et al., 2019).

Chemistry-climate models and general circulation models robustly project a strengthening of the BDC in the lowermost stratosphere since the late 1970s (e.g. Butchart and Scaife, 2001; Butchart et al., 2006, 2010, 2011; Garcia and Randel, 2008; Li et al., 2008; Calvo and Garcia, 2009; McLandress and Shepherd, 2009; Oman et al., 2009; Shepherd and McLandress, 2011; Lin and Fu, 2013). This has been attributed to the effects of ozone depleting substances (ODS), primarily affecting austral spring and summer through the formation of the ozone hole (e.g. Aquila et al., 2016; Polvani et al., 2019, 2017, 2018; Abalos et al., 2019), as well as to rising greenhouse gas concentrations (e.g. Rind et al., 1990, 1998; Sigmond et al., 2004; Butchart et al., 2006, 2010; Fomichev et al., 2007; Olsen et al., 2007; Garcia and Randel, 2008; Li et al., 2008; Calvo and Garcia, 2009; McLandress and Shepherd, 2009; Oman et al., 2009; SPARC, 2010; Shepherd and McLandress, 2011; Garny et al., 2011; Lin and Fu, 2013; Hardiman et al., 2014). In contrast, AoA estimates inferred from in-situ and satellite observations of stratospheric tracers over the satellite era exhibit significant discrepancies with the projected BDC acceleration simulated by climate models (Stiller et al., 2012; Haenel et al., 2015; Engel et al., 2017; Karpechko and Maycock, 2018). These discrepancies may be, in part, associated with the fact that long-term multi-decadal observed AoA trends rely on relatively sparse (in space and time) data (e.g. Engel et al., 2009, 2017). Furthermore, on decadal timescales the residual circulation is strongly affected by internal variability (Hardiman et al., 2017), making it challenging to identify forced trends in satellite datasets with higher spatiotemporal coverage but covering shorter periods (e.g. Stiller et al., 2012). These factors present a challenge for comparing modelled and observed estimates of BDC strength and variability (Garcia et al., 2011).

Since the residual circulation cannot be directly measured, various observable quantities have been used in the literature to indirectly infer changes in its behaviour on interannual to multi-decadal timescales. This includes stratospheric composition, such as lower stratospheric ozone (Randel et al., 2006; Fu et al., 2010), and stratospheric temperatures (e.g. Fu et al., 2010; Young et al., 2012; Ossó et al., 2015).

Stratospheric ozone in the tropical lower stratosphere is strongly controlled by vertical advection and thus ozone changes in this region are closely linked with the BDC over the annual cycle (Randel et al., 2007; Abalos et al., 2013a), on interannual timescales (Randel et al., 2006; Calvo et al., 2010; Oman et al., 2013) and decadal trends (Lamarque and Solomon, 2010; Randel et al., 2007). Nevertheless, in-mixing and photochemical production also play a role in the ozone budget in the tropical lower stratosphere (e.g. Abalos et al., 2013a; Meul et al., 2014), which affects how representative tropical lower stratospheric ozone anomalies are of changes in the residual circulation.

Several studies have used the observed anti-correlation between low and high latitude stratospheric temperatures over the annual cycle (Yulaeva et al., 1994) as a proxy for changes in BDC strength (Ossó et al., 2015; Ueyama and Wallace, 2010; Young et al., 2011, 2012). In the absence of diabatic processes, the effect of an accelerated BDC on lower stratospheric temperatures is manifested as a cooling in the tropics and a warming in high latitudes, as evident in multiple observational studies (Fu et al., 2010, 2015; Johanson and Fu, 2007; Lin et al., 2009; Rosenlof and Reid, 2008; Thompson and Solomon, 2009). Young et al. (2012) used temperature data from the Microwave Sounding Unit channel 4 (MSU4) and Stratospheric Sounding Unit (SSU) to define an empirical residual circulation index and inferred trends between $1979-2005$ throughout the depth of the stratosphere. Conversely, Ossó et al. (2015) concluded that long-term trends derived using the temperature-based residual circulation index were not statistically significant due to contamination from sources of variability such as the El Niño Southern Oscillation (ENSO) and the quasi-biennial oscillation (QBO), highlighting the potential limitations of using temperature-based proxies.

The above discussion serves to highlight the challenges of quantifying observed changes in the stratospheric residual circulation. This is further compounded by the fact that

residual circulation estimates from reanalysis datasets contain substantial discrepancies between the measures used (including uncertainties in the reanalyses; Abalos et al., 2015), presenting a barrier to their use for characterising long-term variability and trends. The extent to which indirect proxy measures are successful in capturing the behaviour of the residual circulation, given that they may be influenced by other unrelated processes, remains as an open question. Since this question cannot be comprehensively addressed using observations, the approach adopted in this study is to use a modelling framework where the residual circulation and observation-based proxy measures can be diagnosed in a self-consistent manner. This enables an assessment of the extent to which proxies are able to capture the behaviour of the residual circulation on different timescales, assuming that the model resolves sufficiently all related processes. The remainder of this paper is structured as follows: Section 4.2 describes the model simulations and measures of the residual circulation used, Section 4.3 presents our results and Section 4.4 summarises our main findings.

4.2 Data and methods

4.2.1 Model description

We use the Community Earth System Model version 1 (CESM1) Whole Atmosphere Community Climate Model (WACCM) run with an interactive chemistry scheme (Garcia et al., 2007; Marsh et al., 2013). We analyse three ensemble members of the free-running hindcast simulations (REF-C1) covering the period 1979 to 2013, performed for the Chemistry-Climate Model Initiative (CCMI; Eyring et al., 2013; Morgenstern et al., 2017). The simulations use prescribed observed sea surface temperatures (SSTs) and sea ice concentrations from the Hadley Centre Ice and Sea Surface Temperature dataset (HadISST; Rayner et al., 2003) and specify observed greenhouse gases (CO_2, N_2O and CH_4), organic halogens, 11-year solar cycle variability and volcanic aerosol surface area densities and heating. Tropical zonal winds over the range $86 - 4\,\mathrm{hPa}$ are nudged toward observations to capture a realistic representation of the QBO. CESM1-WACCM has a horizontal resolution of $1.9° \times 2.5°$ and is run on 66 vertical levels up to an altitude $\sim$ 140 km. In the lower stratosphere, the vertical resolution is $\sim$ 1.2 km near the tropopause increasing to $\sim$ 2 km near the stratopause. An evaluation of

the performance of the free-running simulations of CESM1-WACCM can be found in Froidevaux et al. (2019).

4.2.2 Residual circulation measures

4.2.2.1 Residual vertical velocity

To quantify the residual circulation we use the Transformed Eulerian Mean (TEM; Andrews and McIntyre 1976, 1978; Andrews et al. 1987) residual vertical velocity $\overline{w}^*$ computed as:

$$\overline{w}^* = \overline{w} + \frac{1}{a\cos\phi}\frac{\partial}{\partial\phi}\left[\frac{\overline{v'\theta'}\cos\phi}{\partial\overline{\theta}/\partial z}\right], \tag{4.1}$$

where overbars denote zonal mean quantities and primes the departure from the zonal mean. v and w are the meridional and vertical components of wind, respectively, $z = -H\ln(p/p_s)$ is the log-pressure height, p is pressure, p_s is surface pressure, θ is potential temperature, a is the Earth's radius and ϕ is latitude. We use the 70 hPa level to represent the residual circulation in the lower stratosphere, recognising this captures both the shallow and deep branches of the circulation. $\overline{w}^*$ is averaged between fixed latitude bands (30°S - 30°N), though we have checked the results are similar for other choices of a tropical band (e.g. 20°S - 20°N). This will be referred to as $\overline{w}^*_{trop}$.

To facilitate a comparison with other studies, we use another residual circulation index based on Equation 7 of Ossó et al. (2015), that combines both tropical and extratropical variations in $\overline{w}^*$. This $\mathrm{BDC}_{\overline{w}^*}$ at a given pressure level is defined as:

$$BDC_{\overline{w}^*} = \overline{w}^*_{extr} - \overline{w}^*_{trop}, \tag{4.2}$$

where $\overline{w}^*_{extr}$ is the extratropical ($> 40°N/S$) area-weighted mean $\overline{w}^*$ and $\overline{w}^*_{trop}$ is the tropical (30°S - 30°N) area-weighted mean $\overline{w}^*$. To account for the seasonal cycle in the deep branch of the residual circulation, $\overline{w}^*_{extr}$ is computed for the Northern Hemisphere (NH) between December-May and for the Southern Hemisphere (SH) from June-November. A negative value of $\mathrm{BDC}_{\overline{w}^*}$ indicates an increased overturning circulation; however, as in Ossó et al. (2015), we reverse the sign of $\mathrm{BDC}_{\overline{w}^*}$ to facilitate the comparison with $\overline{w}^*$ and the rest of the proxy measures.

4.2.2.2 Tropical lower stratospheric ozone

For tropical lower stratospheric ozone as a proxy for the residual circulation, we use the zonal mean monthly mean ozone mixing ratio at 50 hPa averaged over 15°S - 15°N. The vertical level is again chosen based on a lagged correlation analysis and selecting the level that shows the highest correlation (see Supplementary Figure S4.1). The altitude identified by this method is broadly consistent with the level at which vertical advection plays the dominant role for the ozone budget in CESM1-WACCM, whereas at higher pressures in-mixing makes a larger relative contribution (Abalos et al., 2013b).

4.2.2.3 Stratospheric temperature indices

We employ the same temperature-based index for the residual circulation as derived from observations by Young et al. (2012) and Ossó et al. (2015). For consistency with those studies, we sample the CESM1-WACCM temperature data using the MSU4 channel weighting function for the upper troposphere/lower stratosphere ($\sim 13-22$ km) (see Supplementary Figure S4.2). The BDC temperature index (BDC_T) is then defined as:

$$BDC_T = T_{extr} - T_{trop}, \tag{4.3}$$

where T_{trop} is the tropical (20°S - 20°N) and T_{extr} is the extratropical ($>$ 40°N/S) mean temperature anomalies for each month. Following Young et al. (2012) and Ossó et al. (2015), we compute BDC_T using T_{extr} in the NH between December-May and in the SH between June-November.

In order to verify that this temperature index captures similar behaviour in the model to that seen in observations, we compute the Pearson correlation coefficient between T_{trop} and T_{extr} for each month (Figure 4.1). We find a statistically significant anti-correlation between T_{trop} and T_{extr} throughout the year across all ensemble members, with the exception of May for just one ensemble member. The correlation is generally largest with the SH in August-September and smallest in December-January and May-June. The individual ensemble members show spread in the correlation coefficient in any one month by up to around 0.3, particularly for months where T_{extr} is taken from the NH; this indicates the important role of internal variability for the relationship between tropical and extratropical lower stratospheric temperatures, which will also affect

observational estimates. With this in mind, Young et al. (2012) and Ossó et al. (2015) did not include calculations for May as the anti-correlation between tropical and extratropical temperatures was found to be weaker than in other months and not statistically significant. However, in CESM1-WACCM the anti-correlation between T_{trop} and T_{extr} is present across all months and in all ensemble members. For this reason we calculate BDC_T for all months.

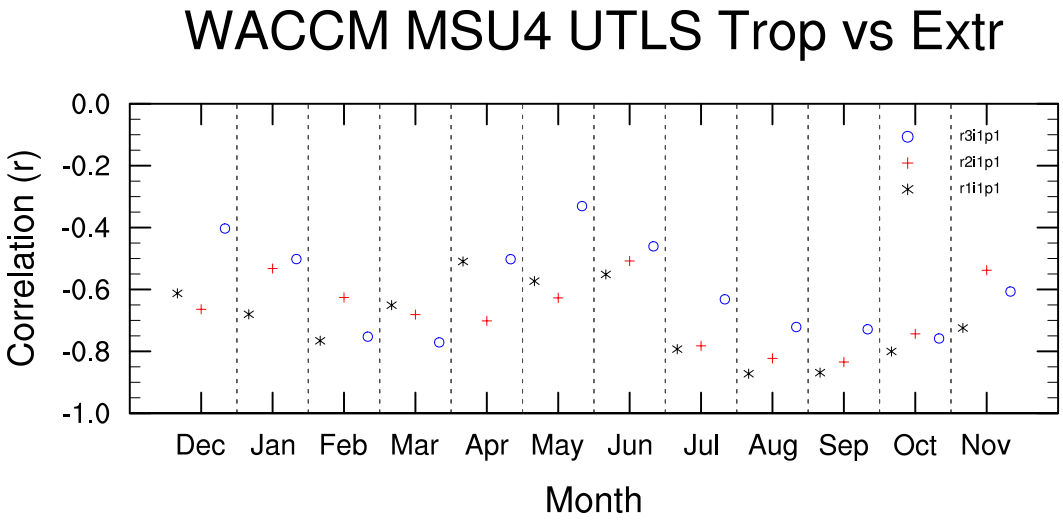

Figure 4.1: Pearson correlation coefficient between the MSU4 weighted CESM1-WACCM tropical mean (20° S - 20° N) and extratropical mean temperature anomalies over 1979-2013. The latter is taken from the Northern Hemisphere between December-May (> 40° N) and from Southern Hemisphere between June-November (> 40° S). Markers (star, cross and open circle) in black, red and blue denote the three ensemble members, respectively. All correlations are statistically significant at the 95% confidence level apart from in May in the third ensemble member (r3i1p1).

4.2.3 Statistical analysis

The relationships between the indices introduced in Section 4.2.2 are quantified using the Pearson linear correlation coefficient. All metrics are standardised to facilitate their intercomparison. We performed lagged correlations between indices and quote results for the lag at which the correlation is a maximum. For the calculation of interannual

variability, all monthly mean data are first detrended and the 10-year running mean is subtracted from the timeseries to remove decadal variability. Long-term trends are calculated using linear least squares regression applied to the raw timeseries.

4.3 Results

4.3.1 Seasonal cycle

Figure 4.2 shows the ensemble mean long-term seasonal cycle of the residual circulation related measures considered in this study. As expected, $\overline{w}^*_{trop}$ exhibits a strong seasonal cycle with a minimum in June and a maximum in boreal winter (December-January) associated with the stronger planetary wave forcing of the residual circulation in NH winter compared to the SH (Rosenlof, 1995). $\mathrm{BDC}_{\overline{w}^*}$ exhibits similar features during boreal winter/spring months though with a larger gradient and minimising a month earlier (May) than $\overline{w}^*_{trop}$; however, during austral winter and spring it exhibits a markedly different behaviour. There is a 'step' in the timeseries between May and June at the switch of hemisphere for $\overline{w}^*_{extr}$, and thereafter $\mathrm{BDC}_{\overline{w}^*}$ remains roughly constant while $\overline{w}^*_{trop}$ shows an increase in upwelling into boreal autumn and winter. Although $\mathrm{BDC}_{\overline{w}^*}$ is based partly on the same information ($\overline{w}^*_{trop}$), between June and November $\mathrm{BDC}_{\overline{w}^*}$ is computed based on the SH extratropics. During austral spring the relative increase in $\overline{w}^*_{trop}$ is offset by a reduction in $\overline{w}^*_{extr}$ associated with the break-down of the Antarctic polar vortex which means $\mathrm{BDC}_{\overline{w}^*}$ shows little variation over these months (not shown).

The seasonal cycle of BDC_T was not evaluated in Young et al. (2012) or Ossó et al. (2015), hence there is no indication what it should look like. BDC_T shows a very different behaviour to $\overline{w}^*_{trop}$ between December - May when it is computed using NH extratropical temperatures. Instead of showing a reduction between boreal winter and spring, as is the case for $\overline{w}^*_{trop}$, it shows an increase due to a more rapid increase in the extratropics compared to the tropics during these months. There is another 'jump' between May and June when the calculation of the BDC_T switches from the NH to the SH cell. The overall minimum of the BDC_T seasonal cycle occurs in July compared to June for $\overline{w}^*_{trop}$. Between July and November, when the SH extratropics are used for the calculation, the BDC_T exhibits an increase that is qualitatively consistent with the seasonal cycle of $\overline{w}^*_{trop}$. Overall, BDC_T exhibits a statistically significant year-round

correlation ($r = 0.47 \pm 0.15$) albeit not fully capturing the shape of the tropical upwelling seasonal cycle.

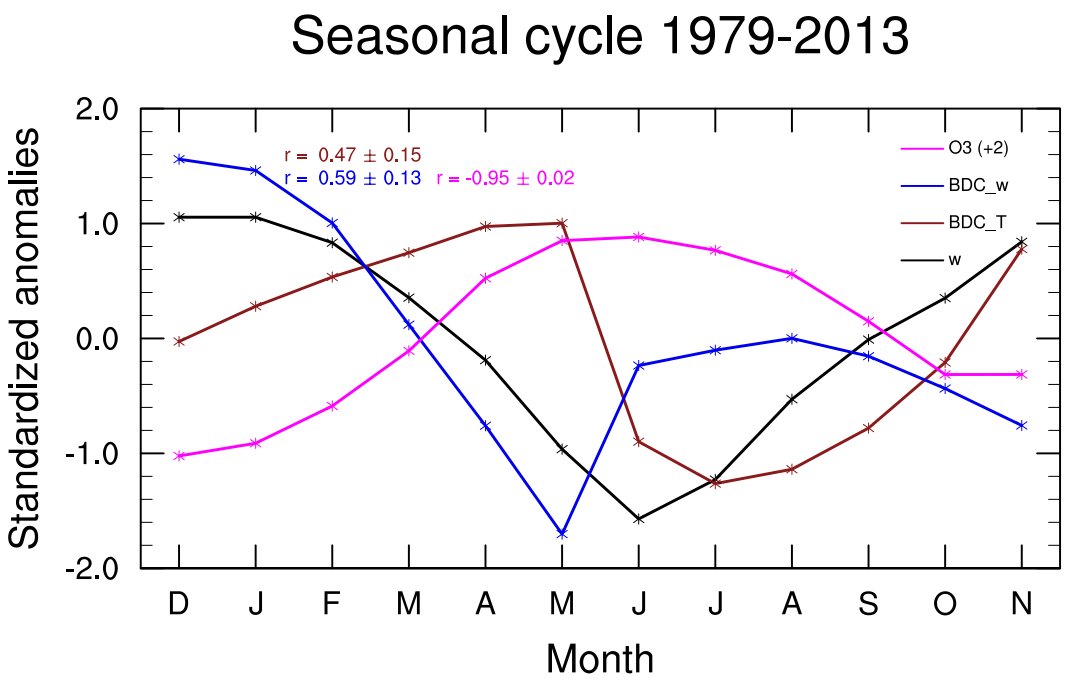

Figure 4.2: Long-term (1979 – 2013) ensemble mean seasonal cycle of $\overline{w}^*_{trop}$ (black), BDC_T (red), $\mathrm{BDC}_{\overline{w}^*}$ (blue) and 50 hPa ozone averaged between 15°S - 15°N (magenta). Ozone timeseries are lagged by +2 months. The year-round correlation coefficient of each index with $\overline{w}^*_{trop}$ is shown along with its associated error. It should be noted that the year-round correlation between $\overline{w}^*_{trop}$ and BDC_T index is not statistically significant ($p > 0.05$). The sign of $\mathrm{BDC}_{\overline{w}^*}$ has been reversed to facilitate a comparison with the other metrics.

Both $\mathrm{BDC}_{\overline{w}^*}$ and BDC_T show spurious behaviour at the time the indices switch hemispheres. Hence their value in constraining features of the seasonal cycle is limited. Furthermore, within the periods when a given hemisphere is used $\mathrm{BDC}_{\overline{w}^*}$ does not resemble $\overline{w}^*_{trop}$ during austral winter and spring and BDC_T does not resemble $\overline{w}^*_{trop}$ during boreal winter and spring. Hence neither appears to be a good proxy for the behaviour of $\overline{w}^*_{trop}$ over the seasonal cycle.

In terms of the stratospheric tracer composition, tropical O_3 at 50 hPa exhibits an almost mirrored seasonal cycle compared to $\overline{w}^*_{trop}$, with a high anti-correlation ($r = 0.95 \pm 0.02$; regression slope of -0.71 $ppm/mm\ s^{-1}$) similar to the observational study of Randel et al. (2007). The anti-correlation between $\overline{w}^*_{trop}$ and O_3 maximises at a lag of +2 months. The lag could be explained due to the long-relaxation timescale of odd oxygen and the cold temperatures in the lower stratosphere (Marsh and Garcia, 2007). Overall, the year-round correlations between $\overline{w}^*_{trop}$ and the residual circulation proxies were similar across the three CESM1-WACCM ensemble members (not shown).

4.3.2 Interannual variability

Figure 4.3 shows the annual mean standardised anomalies of the indices described in Section 4.2.2. The correlation of each index with $\overline{w}^*_{trop}$ is shown in Table 4.1 for each ensemble member (r_i), across all members (r_a) and the ensemble mean (r_{em}), which captures the externally forced variations from the imposed SSTs and the nudged QBO that are consistent amongst ensemble members. BDC_T and $BDC_{\overline{w}^*}$ both exhibit remarkably similar interannual variability as compared to $\overline{w}^*_{trop}$ in terms of the peak-to-peak amplitude and temporal structure. For $BDC_{\overline{w}^*}$, this simply means that the inclusion of information on $\overline{w}^*_{extr}$ does not deteriorate the correlation substantially ($r > 0.93$) and therefore that interannual variability in $\overline{w}^*_{extr}$ and $\overline{w}^*_{trop}$ are strongly correlated, as assumed in the formulation of $BDC_{\overline{w}^*}$. For BDC_T, the strong agreement with $\overline{w}^*_{trop}$ on interannual timescales holds for all three ensemble members with $r > 0.77$ (ensemble mean regression slope is 1.15 $K/mm\ s^{-1}$). This is despite the fact that the MSU4 weighting function includes part of the upper troposphere. Note that we include years with major tropical volcanic eruptions (e.g. El Chichón in 1982 and Mount Pinatubo in 1991), which cause major temperature variations as well as affecting the BDC strength (Fueglistaler et al., 2011), but based on the timeseries in Figure 4.3 these events do not appear to strongly affect the correlations between metrics.

Tropical mean O_3 at 50 hPa exhibits a statistically significant anti-correlation with $\overline{w}^*_{trop}$ on interannual timescales ($r < -0.83$), with relatively small variation across ensemble members and the highest regression slope across all timescales considered in the study (-1.54 $ppm/mm\ s^{-1}$). The differences between the annual mean interannual O_3 vs $\overline{w}^*_{trop}$ regression slope compared to the seasonal cycle, suggest a different relationship

across timescales, potentially associated with QBO-induced variability including a shift of subtropical barriers in the former (e.g. Baldwin et al., 2001; Ploeger et al., 2015b). The results show that over a multi-decadal period in CESM1-WACCM, BDC_T and O_3 at 50 hPa are indeed very good proxies for interannual variability in $\overline{w}^*_{trop}$ and $BDC_{\overline{w}^*}$.

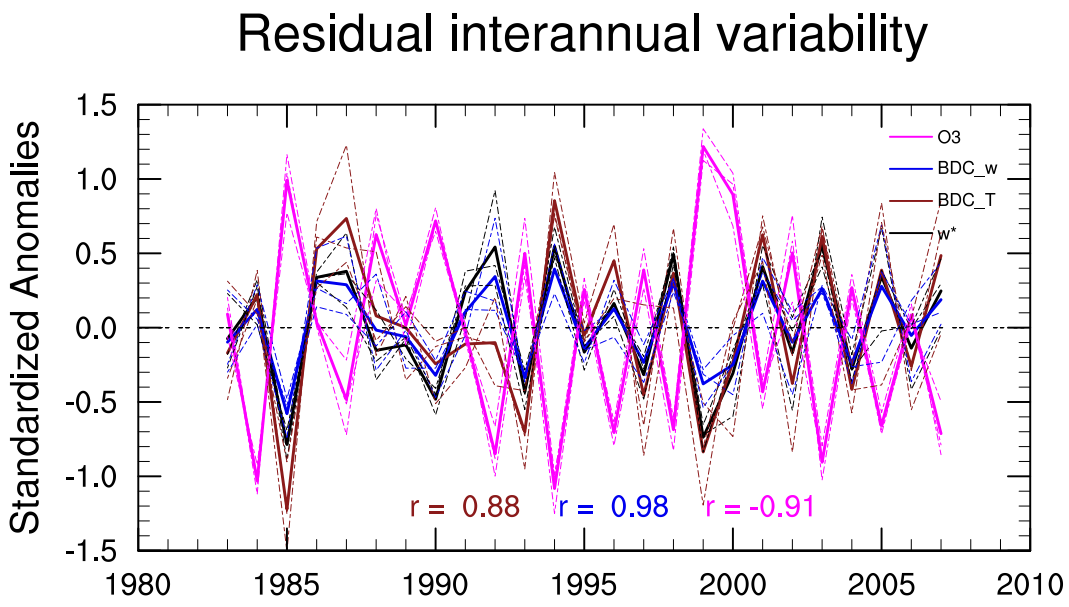

Figure 4.3: Annual mean standardised anomalies of $\overline{w}^*_{trop}$ (black), BDC_T (red), $BDC_{\overline{w}^*}$ (blue) and 50 hPa tropical average (15°S - 15°N) ozone (magenta). The timeseries are deviations from a 10-year running mean. The ensemble mean timeseries are shown in thick lines while the ensemble members in thin dashed lines. The correlation coefficients between $\overline{w}^*_{trop}$ and each metric are shown in the legend for the ensemble mean coloured, respectively. The correlations for individual ensemble members are given in Table 4.1

We next analyse the interannual variability of the metrics by season. Recall that BDC_T and $BDC_{\overline{w}^*}$ are computed using the NH extratropics for December - May and the SH extratropics for June - November; hence our choice of seasons (DJF, MAM, JJA, SON) avoids averaging across the inter-hemispheric 'jumps' described in Section 4.3.1. Figure 4.4 shows timeseries of standardised anomalies of each metric by season. The corresponding correlation coefficients for individual ensemble members are shown in Table 4.2.

Metric	r1i1p1	r2i1p1	r3i1p1	all	ens. mean
BDC$_{\overline{w}^*}$	$\mathbf{r_1 = 0.93}$	$\mathbf{r_2 = 0.96}$	$\mathbf{r_3 = 0.93}$	$\mathbf{r_a = 0.94}$	$\mathbf{r_{em} = 0.98}$
BDC$_T$	$\mathbf{r_1 = 0.92}$	$\mathbf{r_2 = 0.86}$	$\mathbf{r_3 = 0.77}$	$\mathbf{r_a = 0.86}$	$\mathbf{r_{em} = 0.88}$
O$_3$	$\mathbf{r_1 = -0.86}$	$\mathbf{r_2 = -0.91}$	$\mathbf{r_3 = -0.83}$	$\mathbf{r_a = -0.87}$	$\mathbf{r_{em} = -0.91}$

Table 4.1: Correlation between $\overline{w}^*_{trop}$ and BDC$_{\overline{w}^*}$, BDC$_T$ and tropical average (15°S - 15°N) ozone at 50 hPa. r_1, r_2 and r_3 denote the correlations for each ensemble member (r1i1p1, r2i1p1 and r3i1p1, respectively) while r$_a$ and r$_{em}$ denote the correlation for the concatenated and ensemble mean timeseries. Correlations in bold are statistically significant at the 95% confidence level.

The correlation between BDC$_T$ and $\overline{w}^*_{trop}$ is significant year-round and in all ensemble members (see Table 4.2). For a given season, the ensemble spread in the correlation coefficient is generally larger than the difference in the correlation coefficient for all members (r$_a$) between seasons, indicating that BDC$_T$ explains a similar proportion of variance in $\overline{w}^*_{trop}$ over the whole year. The regression slope between BDC$_T$ and $\overline{w}^*_{trop}$ ranges between $0.5 - 0.82\ K/mm\ s^{-1}$ across seasons (for the ensemble mean), considerably lower than for the annual mean. It should be noted that the regression slope estimate between BDC$_T$ and $\overline{w}^*_{trop}$ for JJA and SON seasonal means is not significantly different from the annual mean where BDC$_T$ is computed from the SH extratropics, due to SH extratropical temperature variability not being associated as strongly with $\overline{w}^*_{trop}$ as in other seasons or the annual mean on interannual timescales. The seasonal correlations of BDC$_T$ are, however, systematically lower ($r = 0.64 - 0.70$) than for the annual mean in Figure 4.3 ($r = 0.88$). As expected, BDC$_{\overline{w}^*}$ exhibits a high correlation with $\overline{w}^*_{trop}$ throughout the year; however, the correlations in seasons where the NH extratropics are used are systematically lower by up to 0.09 (e.g. in MAM) than for seasons where the SH extratropics are used. Interestingly, the ensemble mean correlation for BDC$_T$ and BDC$_{\overline{w}^*}$ in MAM and for BDC$_T$ in DJF is consistently higher than for any individual member, indicating that internal variability plays an important role in these seasons. This will affect observed correlations since only one realisation exists.

Compared to the relatively high seasonal correlations for BDC$_T$ and BDC$_{\overline{w}^*}$, 50 hPa O$_3$ exhibits a weaker but statistically significant anti-correlation with $\overline{w}^*_{trop}$ across all

seasons and ensemble members. The anti-correlation with 50 hPa O_3 is stronger in JJA ($r_a = -0.69$) and weaker in MAM potentially associated with stronger mixing tendencies ($r_a = -0.36$), with similar behaviours in DJF and SON ($r_a = -0.57$ and -0.55, respectively). The correlation of the ensemble mean is substantially more negative in DJF ($r_{em} = -0.73$; regression slope of -0.87 $ppm/mm\ s^{-1}$) than for the individual members ($r_i = -0.56$ to -0.58), indicating a relatively larger role for internal variability in this season and a tighter relationship between O_3 and $\overline{w}^*_{trop}$ when the upwelling is stronger.

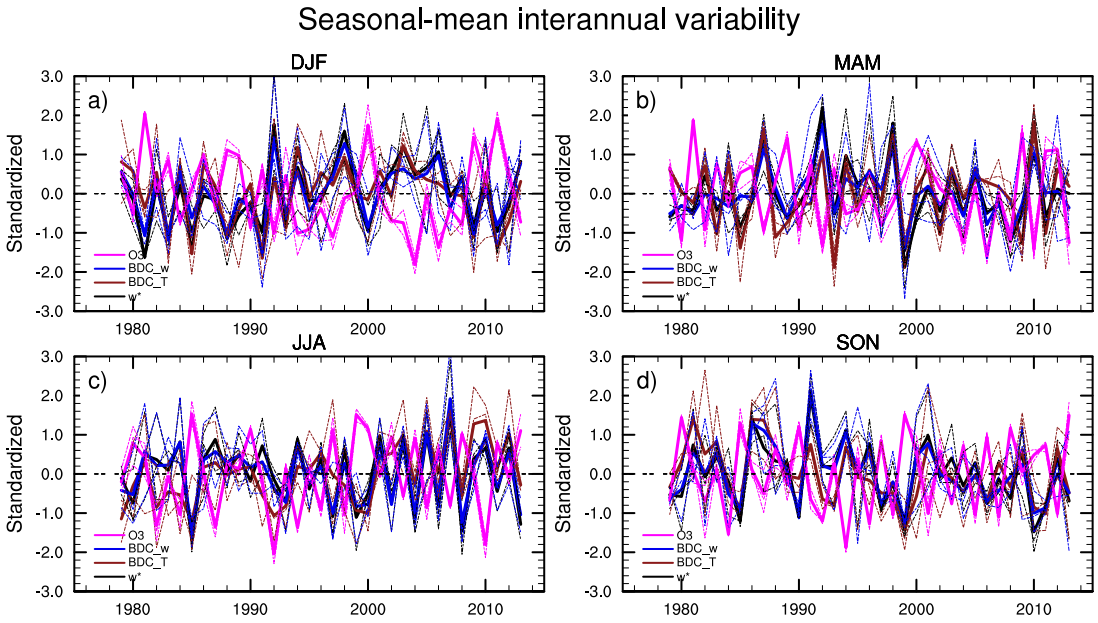

Figure 4.4: Standardised anomalies of the $\overline{w}^*_{trop}$ (black), BDC_T (red), $BDC_{\overline{w}^*}$ (blue) and 50 hPa tropical average (15°S - 15°N) ozone (magenta) for a) DJF, b) MAM, c) JJA and d) SON seasonal means. Thick lines denote the ensemble means while the thin dashed lines the ensemble members. The correlations for individual ensemble members and the concatenated timeseries are given in Table 4.2.

In summary, BDC_T captures a significant fraction of the year-to-year variation in $\overline{w}^*_{trop}$ ($44 - 49\%$) on seasonal timescales, while O_3 at 50 hPa generally captures less of the variance ($13 - 48\%$).

Metric	DJF	MAM	JJA	SON
$BDC_{\overline{w}^*}$	$\mathbf{r_1 = 0.9}$	$\mathbf{r_1 = 0.86}$	$\mathbf{r_1 = 0.98}$	$\mathbf{r_1 = 0.94}$
	$\mathbf{r_2 = 0.95}$	$\mathbf{r_2 = 0.87}$	$\mathbf{r_2 = 0.97}$	$\mathbf{r_2 = 0.94}$
	$\mathbf{r_3 = 0.93}$	$\mathbf{r_3 = 0.83}$	$\mathbf{r_3 = 0.96}$	$\mathbf{r_3 = 0.95}$
	$\mathbf{r_a = 0.93}$	$\mathbf{r_a = 0.85}$	$\mathbf{r_a = 0.97}$	$\mathbf{r_a = 0.94}$
	$\mathbf{r_{em} = 0.94}$	$\mathbf{r_{em} = 0.92}$	$\mathbf{r_{em} = 0.97}$	$\mathbf{r_{em} = 0.94}$
BDC_T	$\mathbf{r_1 = 0.62}$	$\mathbf{r_1 = 0.61}$	$\mathbf{r_1 = 0.64}$	$\mathbf{r_1 = 0.82}$
	$\mathbf{r_2 = 0.68}$	$\mathbf{r_2 = 0.73}$	$\mathbf{r_2 = 0.68}$	$\mathbf{r_2 = 0.65}$
	$\mathbf{r_3 = 0.68}$	$\mathbf{r_3 = 0.66}$	$\mathbf{r_3 = 0.58}$	$\mathbf{r_3 = 0.65}$
	$\mathbf{r_a = 0.66}$	$\mathbf{r_a = 0.67}$	$\mathbf{r_a = 0.64}$	$\mathbf{r_a = 0.7}$
	$\mathbf{r_{em} = 0.75}$	$\mathbf{r_{em} = 0.76}$	$\mathbf{r_{em} = 0.57}$	$\mathbf{r_{em} = 0.74}$
O_3	$\mathbf{r_1 = -0.57}$	$\mathbf{r_1 = -0.4}$	$\mathbf{r_1 = -0.71}$	$\mathbf{r_1 = -0.47}$
	$\mathbf{r_2 = -0.56}$	$\mathbf{r_2 = -0.4}$	$\mathbf{r_2 = -0.75}$	$\mathbf{r_2 = -0.67}$
	$\mathbf{r_3 = -0.58}$	$r_3 = -0.27$	$\mathbf{r_3 = -0.6}$	$\mathbf{r_3 = -0.5}$
	$\mathbf{r_a = -0.57}$	$\mathbf{r_a = -0.36}$	$\mathbf{r_a = -0.69}$	$\mathbf{r_a = -0.55}$
	$\mathbf{r_{em} = -0.73}$	$\mathbf{r_{em} = -0.37}$	$\mathbf{r_{em} = -0.75}$	$\mathbf{r_{em} = -0.6}$

Table 4.2: Correlation between the 1979-2013 $\overline{w}^*_{trop}$ and $BDC_{\overline{w}^*}$, BDC_T and tropical average (15°S - 15°N) ozone at 50 hPa for each season. r_1, r_2 and r_3 denote the correlations for each ensemble member (r1i1p1, r2i1p1 and r3i1p1, respectively) while r_a for the concatenated ensembles and r_{em} for the ensemble mean. Correlations in bold are statistically significant at the 95% confidence level.

4.3.3 Multi-decadal trends

To evaluate linear trends of the residual circulation proxies, we split the $1979 - 2013$ period into two intervals to account for the changing behaviour of ODSs following the implementation of the Montreal Protocol and its amendments. The first period $(1979 - 1997)$ is characterised by increasing concentrations of ODSs causing increasing ozone depletion and a well-documented global lower stratospheric cooling (see recent review in WMO, 2018). The second period between $1998 - 2013$ is associated with a reduction in ODSs (and ozone depletion) while concentrations of other greenhouse gases (GHGs) continued to increase. The motivation for considering these periods separately lies with the fact the tropical lower stratosphere exhibited a global mean cooling trend over $1979 - 1997$, which has been attributed to ozone depletion (e.g. Forster et al., 2007; Polvani and Solomon, 2012) with a smaller role for increasing GHGs (e.g. Maycock, 2016). The cooling of the global lower stratosphere ceased around the mid-1990s (e.g. Maycock et al., 2018). In addition to the changing global mean temperature trend in

the lower stratosphere, recent modelling studies have found that ODSs were the dominant driver of an accelerated BDC since the 1970s (e.g. Polvani et al., 2019, 2018; Abalos et al., 2019). These studies also report that in the future the decrease in ODSs counteracts the GHG-driven acceleration of the BDC, hence we separate these two time periods as they have been characterised by distinct residual circulation trends (Fu et al., 2019). The fact that we do not analyse the whole time period $1979-2013$, differentiates our study from Young et al. (2012) and Ossó et al. (2015) who analysed monthly trends for the observed BDC_T and modelled $\mathrm{BDC}_{\overline{w}^*}$ between $1979-2005$.

Figures 4.5 and 4.6 show monthly trends in the residual circulation indices analysed over $1979-1997$ and $1998-2013$, respectively. The units are arbitrary but the sign of the $\mathrm{BDC}_{\overline{w}^*}$ trends is reversed to facilitate the comparison with $\overline{w}^*_{trop}$. This means that, as plotted, a positive trend in $\overline{w}^*_{trop}$, BDC_T and $\mathrm{BDC}_{\overline{w}^*}$ indicates a strengthening of the BDC. One common feature is that all residual circulation proxies exhibit larger uncertainties over the second period ($1998-2013$; Figure 4.6), which may be partly a consequence of it being a shorter time interval (16 years compared to 20 years). Consistent with this, it was shown that dynamical variability can mask upwelling trends on multi-decadal timescales (Hardiman et al., 2017).

Over the first period $1979-1997$, $\overline{w}^*_{trop}$ shows a statistically significant positive trend in around half of the months consistent with a strengthening of the BDC during the period of ozone depletion (Abalos et al., 2015). Interestingly, in contrast to some previous studies we find a significant positive trend in $\overline{w}^*_{trop}$ in November-December, but no trend in January-February. There is a smaller but statistically significant positive trend in MAM and August-September. The $\mathrm{BDC}_{\overline{w}^*}$ monthly trends are more uncertain, exhibiting significantly larger confidence intervals compared to the rest of the residual circulation proxies, associated with the larger extratropical variability during DJF coming from the NH and SON in the SH. $\mathrm{BDC}_{\overline{w}^*}$ shows a pronounced strengthening of the residual circulation in December and January associated with enhanced downwelling over the NH extratropics. While some months show statistically significant positive trends that qualitatively match the $\overline{w}^*_{trop}$ trend, there are months with significant negative $\mathrm{BDC}_{\overline{w}^*}$ trends (February, July) when $\overline{w}^*_{trop}$ shows no trend. Hence, the overall year-round correlation between $\overline{w}^*_{trop}$ and $\mathrm{BDC}_{\overline{w}^*}$ trends is non-significant ($r_{em} = 0.15$).

The BDC_T trends do not show a good agreement with the sign of the $\overline{w}^*_{trop}$ trends across most months, manifested as a fairly weak year-round correlation ($r_{em} = 0.36$). There are some notable exceptions where the sign of the BDC_T trends and $\overline{w}^*_{trop}$ do not match (e.g. November) while only half of the time, their monthly trends lie consistently within the confidence intervals of the other. Tropical O_3 exhibits negative trends across all months with a year-round anti-correlation with $\overline{w}^*_{trop}$ of $r = -0.50$. However, it must be borne in mind that chemical ozone loss could have contributed to a decrease in tropical ozone over this period. One way to test this would be to examine a simulation with fixed ODS levels, however, given the evidence from models that ODSs forced most of the residual circulation trend over this period, this would not provide a clean comparison with the results in Figure 4.5.

The second period $1998 - 2013$ exhibits distinct differences in the trends of all proxy measures compared to the first period where ODSs were increasing. $\overline{w}^*_{trop}$ shows a statistically significant positive trend in austral winter and a negative trend between September-December. It should be noted that the annual mean tropical upward mass flux trends at 70 hPa starting around the turn of the 21st century were not positive across most of the CCMI REF-C1 simulations (including CESM1-WACCM) evaluated in Chrysanthou et al. (2019). The correlation of $\mathrm{BDC}_{\overline{w}^*}$ trends with $\overline{w}^*_{trop}$ is as similarly low in this period as for $1979 - 1997$. Conversely, BDC_T trends more closely follow the $\overline{w}^*_{trop}$ trends with a substantially higher (compared to $1979 - 1997$) and statistically significant year-round correlation of $r_{em} = 0.73$, characterised by the highest, albeit statistically uncertain regression slope across all timescales considered here ($1.51\ K/mm\ s^{-1}$). It is unclear why BDC_T would better capture $\overline{w}^*_{trop}$ trends in the second period, but this could potentially be due to a pronounced role of increasing GHGs in the temperatures of the UTLS.

The tropical ozone trends are also different in the 1998-2013 period, with positive trends during NH autumn/winter (October, November and December) and a negative trend from April to August, especially in JJA. The year-round anti-correlation is stronger between $\overline{w}^*_{trop}$ and tropical O_3 in this period as compared to over 1979-1997 ($r = -0.82$) as well as statistically significant (regression slope is $-1.3\ ppm/mm\ s^{-1}$).

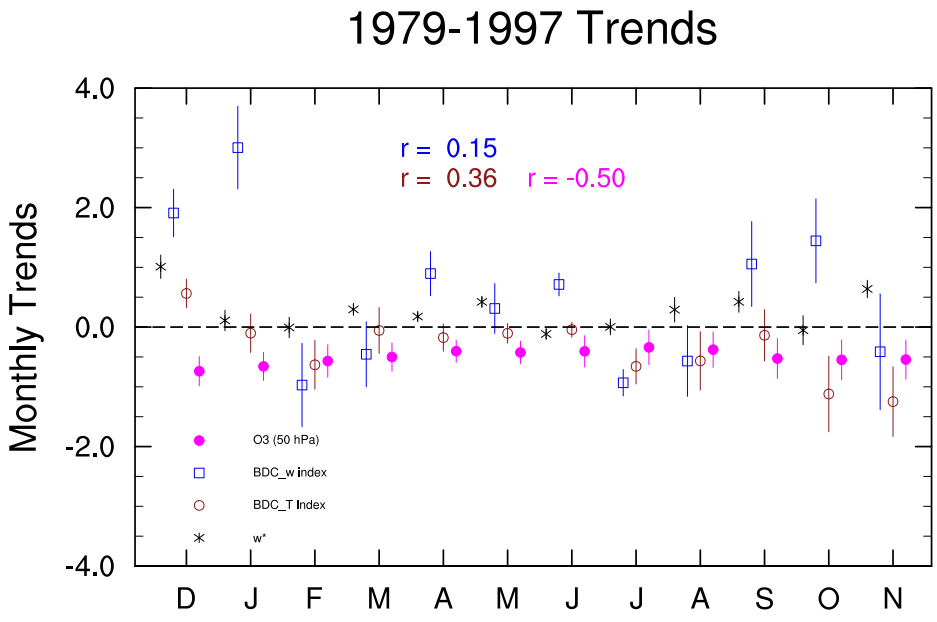

Figure 4.5: Monthly trends of the ensemble mean CESM1-WACCM REF-C1 over 1979–1997 for the $\overline{w}^*_{trop}$ (black), BDC$_T$ (red), BDC$_{\overline{w}^*}$ (blue) and tropical average (15° S - 15° N) O_3 at 50 hPa (magenta). A 7-year running mean was computed prior to the calculation of the trends. The trends units are in $km\ year^{-1}\ dec^{-1}$ for $\overline{w}^*_{trop}$ and BDC$_{\overline{w}^*}$, $K\ dec^{-1}$ for BDC$_T$ and $10 \times\ ppm\ dec^{-1}$ for O_3. The whiskers denote the range of the 95 % confidence level of the trends. The year-round linear cross-correlation coefficients between $\overline{w}^*_{trop}$ and each other metric is shown in the upper centre part of the figure, coloured with the colour of each metric, respectively. The sign of the BDC$_{\overline{w}^*}$ trends is reversed in order to facilitate the intercomparison.

It should be noted that attributing the drivers of the above trends over such short periods may be problematic as the signal to noise ratio can be relatively low over a short time period. Moreover, different trend analysis methods have the potential to exhibit different results hence other approaches were explored in this study. A multiple linear regression (MLR) analysis was also applied for the monthly trends of all metrics considered in this study accounting for known natural drivers of tropical lower stratospheric variability; the El Niño-Southern Oscillation (ENSO), major volcanic eruptions and quasi-biennial oscillation, similar to Chrysanthou et al. (2019), albeit without considering a linear trend regressor. Additionally, a lag for the ENSO signal in the MLR

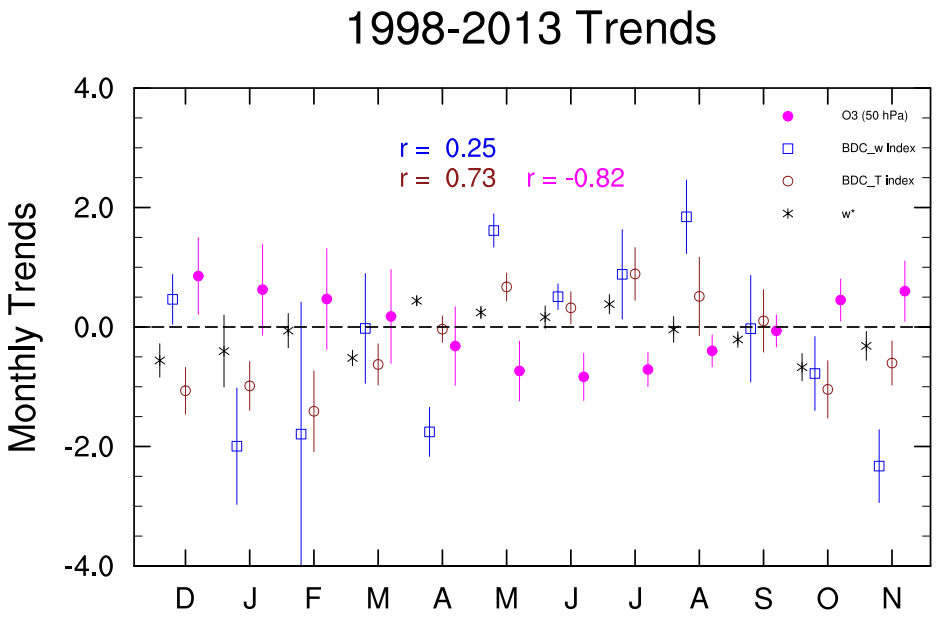

Figure 4.6: As in Figure 4.5 but for 1998 – 2013.

was also considered as this process is not expected to be instantaneous; it would take time for a regressor to drive the tropical lower stratospheric variability of all proxies considered in this study (Marsh and Garcia, 2007). However, $\overline{w}^*_{trop}$, tropical O_3 at 50 hPa and ENSO signal were not found to exhibit strong correlations between them in the lower stratosphere (100-50 hPa) under a range of different lags considered, hence a lag in the ENSO regressor was not used. Subsequently applying a linear trend analysis on the residuals between the original and reconstructed monthly timeseries of all MLR proxies revealed that most of the monthly trends were not statistically significant while the year-round correlations between the tropical upwelling and the rest of the proxies were also adversely affected, hence are not shown.

4.4 Summary and conclusions

Quantifying variability and trends in the stratospheric residual circulation is hampered by a lack of observational constraints and discrepancies amongst reanalysis datasets. We have performed an intercomparison of indirect proxy measures of the residual circulation

in the lower stratosphere based on observable quantities within a modelling framework. We used an ensemble of free-running historical simulations from the CESM1-WACCM model covering the period 1979 – 2013. We used the tropical average $\overline{w}^*$ ($\overline{w}^*_{trop}$) at 70 hPa as the reference measure of the residual circulation. Additionally, for the sake of completeness, we use a slightly modified version of $\mathrm{BDC}_{\overline{w}^*}$ at 70 hPa from Ossó et al. (2015), which incorporates information on $\overline{w}^*$ from the tropics and extratropics. As observation-based measures, we use a temperature-based measure of the residual circulation (BDC_T) in the lower stratosphere, originally defined by Young et al. (2012). We also include the tropical average ozone at the 50 hPa level as a tracer that is controlled by the residual circulation through vertical advection.

For the mean seasonal cycle, the strongest anti-correlation with $\overline{w}^*_{trop}$ was for tropical O_3 at 50 hPa lagged by 2 months, similar to the result of Randel et al. (2007). The temperature-based measure, BDC_T, captured the general behaviour of an increasing residual circulation during austral spring, but did not capture the behaviour in boreal winter and did not reproduce a realistic seasonal cycle. This is in part because of the way the index is calculated using opposite hemispheres for the extratropics in different months.

On interannual timescales, the annual-mean BDC_T and tropical O_3 exhibit excellent agreement ($|r| \sim 0.9$ for the ensemble mean) with $\overline{w}^*_{trop}$. Hence BDC_T and tropical O_3 at 50 hPa are useful indices for representing annual mean variability in tropical upwelling (cf. Weber et al., 2011). For the seasonal means, BDC_T and tropical O_3 are still significantly correlated with $\overline{w}^*_{trop}$ but to a lesser extent than for the annual mean.

We further considered long-term trends in the indices over 1979 – 1997 and 1998 – 2013. The first period is characterised by increasing concentrations of ODSs, while the second period experiences decreasing ODSs. All residual circulation measures exhibit statistically significant trends across some months in both periods, with larger uncertainties over 1998 – 2013 compared to the first period. The year-round correlation of the monthly BDC_T trends with the $\overline{w}^*_{trop}$ trends is $r_{em} = 0.73$ in the second period but 0.36 in the first period. Ossó et al. (2015) considered the correlation between trends in BDC_T and $\mathrm{BDC}_{\overline{w}^*}$ (excluding May) over 1979 – 2005 and found a correlation of 0.71. Our

results show this finding may be sensitive to the time period considered. Tropical mean 50 hPa O_3 trends are negative over $1979-1997$ and are anti-correlated with $\overline{w}^*_{trop}$ trends ($r_{em} = -0.5$). For the period $1998-2013$, the anti-correlation increases ($r_{em} = -0.82$) though caution must be taken as we have not separated the role of chemical loss from transport in determining the ozone trends.

Of the proxy measures considered here, the BDC_T appears to be a good proxy for the residual circulation on shorter timescales, but its representativity for long-term trends may depend on the time period. This should be borne in mind for other studies using this measure to approximate observed residual circulation trends (e.g. Fu et al., 2010, 2015, 2019; Young et al., 2012). Owing to limitations of the model data, we have not considered all methods for estimating the residual circulation in the tropical lower stratosphere, for example using the advection of the water vapour tape recorder (e.g. Minschwaner et al., 2016) or the behaviour of the QBO (Kawatani and Hamilton, 2013). These areas would be ripe for future investigation.

4.5 Supplementary material

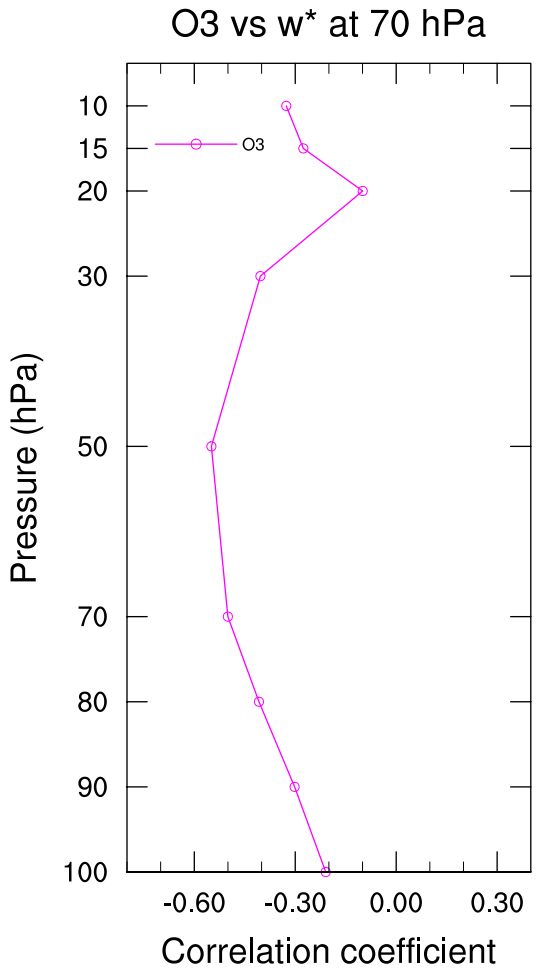

Figure S4.1: Vertical lagged correlation analysis between $\overline{w}^*_{trop}$ and tropical (15°S - 15°N) average O_3 denoted magenta colour. The lag corresponding to each pressure level on the Y axis is 2, 2, 2, 2, 2, 1, 1, 13, 9 months for O_3 at 50 hPa. The maximum anti-correlation value is found for O_3 at 50 hPa for +2 months.

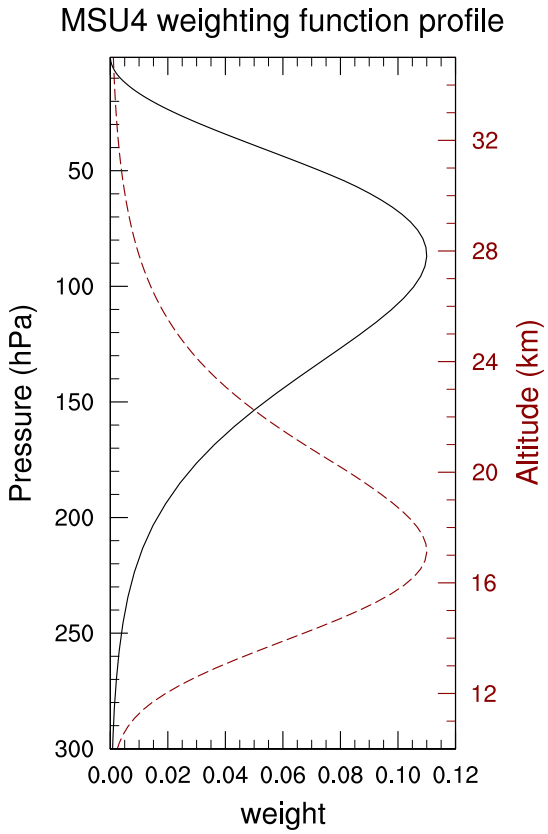

Figure S4.2: Vertical profile of the MSU4 channel weighting function. Left Y axis denotes the pressure range corresponding to the black line and right Y axis the altitude range corresponding to the red dashed line. The values of left and right Y axes are not reflecting each other.

References

M. Abalos, F. Ploeger, P. Konopka, W. J. Randel, and E. Serrano. Ozone seasonality above the tropical tropopause: Reconciling the Eulerian and Lagrangian perspectives of transport processes. *Atmospheric Chemistry and Physics*, 13(21):10787–10794, 2013a. ISSN 16807316. doi: 10.5194/acp-13-10787-2013. 189

M. Abalos, W. J. Randel, D. E. Kinnison, and E. Serrano. Quantifying tracer transport in the tropical lower stratosphere using WACCM. *Atmospheric Chem-*

istry and Physics, 13(21):10591–10607, 2013b. ISSN 16807316. doi: 10.5194/acp-13-10591-2013. URL http://www.atmos-chem-phys.net/13/10591/2013/. 192

M. Abalos, B. Legras, F. Ploeger, and W. J. Randel. Evaluating the advective Brewer-Dobson circulation in three reanalyses for the period 1979–2012. *Journal of Geophysical Research: Atmospheres*, 120(15):7534–7554, 2015. ISSN 2169-897X. doi: 10.1002/2015JD023182. URL https://onlinelibrary.wiley.com/doi/abs/10.1002/2015JD023182. 190, 201

M. Abalos, L. Polvani, N. Calvo, D. Kinnison, F. Ploeger, W. Randel, and S. Solomon. New Insights on the Impact of Ozone-Depleting Substances on the Brewer-Dobson Circulation. *Journal of Geophysical Research: Atmospheres*, 124(5):2435–2451, 2019. ISSN 2169-897X. doi: 10.1029/2018JD029301. URL https://onlinelibrary.wiley.com/doi/abs/10.1029/2018JD029301. 188, 201

D. G. Andrews and M. E. McIntyre. Planetary Waves in Horizontal and Vertical Shear: The Generalized Eliassen-Palm Relation and the Mean Zonal Acceleration. *Journal of the Atmospheric Sciences*, 33(11):2031–2048, 1976. ISSN 0022-4928. doi: 10.1175/1520-0469(1976)033<2031:PWIHAV>2.0.CO;2. URL http://journals.ametsoc.org/doi/abs/10.1175/1520-0469{%}281976{%}29033{%}3C2031{%}3APWIHAV{%}3E2.0.CO{%}3B2. 191

D. G. Andrews and M. E. McIntyre. An exact theory of nonlinear waves on a Lagrangian-mean flow. *Journal of Fluid Mechanics*, 89(4):609–646, 1978. ISSN 0022-1120. doi: 10.1017/S0022112078002773. URL https://www.cambridge.org/core/product/identifier/S0022112078002773/type/journal{_}article. 191

D. G. Andrews, C. B. Leovy, J. R. Holton, and C. B. Leovy. *Middle Atmosphere Dynamics*. Academic press, 1987. 191

V. Aquila, W. H. Swartz, D. W. Waugh, P. R. Colarco, S. Pawson, L. M. Polvani, and R. S. Stolarski. Isolating the roles of different forcing agents in global stratospheric temperature changes using model integrations with incrementally added single forcings. *Journal of Geophysical Research*, 121(13):8067–8082, 2016. ISSN 21562202. doi: 10.1002/2015JD023841. URL http://doi.wiley.com/10.1002/2015JD023841. 188

M. P. Baldwin, L. J. Gray, T. J. Dunkerton, K. Hamilton, P. H. Haynes, W. J. Randel, J. R. Holton, M. J. Alexander, I. Hirota, T. Horinouchi, D. B. A. Jones, J. S. Kinnersley, C. Marquardt, K. Sato, and M. Takahashi. The quasi-biennial oscillation. *Reviews of Geophysics*, 39(2):179–229, 2001. ISSN 87551209. doi: 10.1029/1999RG000073. URL http://doi.wiley.com/10.1029/1999RG000073. 197

T. Birner and H. Bönisch. Residual circulation trajectories and transit times into the extratropical lowermost stratosphere. *Atmospheric Chemistry and Physics*, 11(2): 817–827, 2011. ISSN 1680-7324. doi: 10.5194/acp-11-817-2011. URL https://www.atmos-chem-phys.net/11/817/2011/. 187

N. Butchart. The Brewer-Dobson circulation. *Reviews of Geophysics*, 52(2):157–184, 2014. ISSN 87551209. doi: 10.1002/2013RG000448. URL http://doi.wiley.com/10.1002/2013RG000448. 187

N. Butchart and A. A. Scaife. Removal of chlorofluorocarbons by increased mass exchange between the stratosphere and troposphere in a changing climate. *Nature*, 410(6830):799–802, 2001. ISSN 0028-0836. doi: 10.1038/35071047. URL http://www.nature.com/articles/35071047. 188

N. Butchart, A. A. Scaife, M. Bourqui, J. de Grandpré, S. H. E. Hare, J. Kettleborough, U. Langematz, E. Manzini, F. Sassi, K. Shibata, D. Shindell, and M. Sigmond. Simulations of anthropogenic change in the strength of the Brewer–Dobson circulation. *Climate Dynamics*, 27(7-8):727–741, 2006. ISSN 0930-7575. doi: 10.1007/s00382-006-0162-4. URL http://link.springer.com/10.1007/s00382-006-0162-4. 188

N. Butchart, I. Cionni, V. Eyring, T. G. Shepherd, D. W. Waugh, H. Akiyoshi, J. Austin, C. Brühl, M. P. Chipperfield, E. Cordero, M. Dameris, R. Deckert, S. Dhomse, S. M. Frith, R. R. Garcia, A. Gettelman, M. A. Giorgetta, D. E. Kinnison, F. Li, E. Mancini, C. McLandress, S. Pawson, G. Pitari, D. A. Plummer, E. Rozanov, F. Sassi, J. F. Scinocca, K. Shibata, B. Steil, and W. Tian. Chemistry–Climate Model Simulations of Twenty-First Century Stratospheric Climate and Circulation Changes. *Journal of Climate*, 23(20):5349–5374, 2010. ISSN 0894-8755. doi: 10.1175/2010JCLI3404.1. URL http://journals.ametsoc.org/doi/10.1175/2010JCLI3404.1. 188

N. Butchart, A. J. Charlton-Perez, I. Cionni, S. C. Hardiman, P. H. Haynes, K. Krüger, P. J. Kushner, P. A. Newman, S. M. Osprey, J. Perlwitz, M. Sigmond, L. Wang, H. Akiyoshi, J. Austin, S. Bekki, A. Baumgaertner, P. Braesicke, C. Brühl, M. Chipperfield, M. Dameris, S. Dhomse, V. Eyring, R. Garcia, H. Garny, P. Jöckel, J.-F. Lamarque, M. Marchand, M. Michou, O. Morgenstern, T. Nakamura, S. Pawson, D. Plummer, J. Pyle, E. Rozanov, J. Scinocca, T. G. Shepherd, K. Shibata, D. Smale, H. Teyssèdre, W. Tian, D. Waugh, and Y. Yamashita. Multimodel climate and variability of the stratosphere. *Journal of Geophysical Research*, 116(D5):D05102, 2011. ISSN 0148-0227. doi: 10.1029/2010JD014995. URL http://doi.wiley.com/10.1029/2010JD014995. 188

N. Calvo and R. R. Garcia. Wave Forcing of the Tropical Upwelling in the Lower Stratosphere under Increasing Concentrations of Greenhouse Gases. *Journal of the Atmospheric Sciences*, 66(10):3184–3196, 2009. ISSN 0022-4928. doi: 10.1175/2009jas3085.1. URL http://journals.ametsoc.org/doi/abs/10.1175/2009JAS3085.1. 188

N. Calvo, R. R. Garcia, W. J. Randel, and D. R. Marsh. Dynamical Mechanism for the Increase in Tropical Upwelling in the Lowermost Tropical Stratosphere during Warm ENSO Events. *Journal of the Atmospheric Sciences*, 67(7):2331–2340, 2010. ISSN 0022-4928. doi: 10.1175/2010JAS3433.1. URL http://journals.ametsoc.org/doi/10.1175/2010JAS3433.1. 189

A. Chrysanthou, A. C. Maycock, M. P. Chipperfield, S. Dhomse, H. Garny, D. Kinnison, H. Akiyoshi, M. Deushi, R. R. Garcia, P. Jöckel, O. Kirner, G. Pitari, D. A. Plummer, L. Revell, E. Rozanov, A. Stenke, T. Y. Tanaka, D. Visioni, and Y. Yamashita. The effect of atmospheric nudging on the stratospheric residual circulation in chemistry–climate models. *Atmospheric Chemistry and Physics*, 19 (17):11559–11586, 2019. ISSN 1680-7324. doi: 10.5194/acp-19-11559-2019. URL https://www.atmos-chem-phys.net/19/11559/2019/. 202, 203

R. Eichinger, S. Dietmüller, H. Garny, P. Šácha, T. Birner, H. Bönisch, G. Pitari, D. Visioni, A. Stenke, E. Rozanov, L. Revell, D. A. Plummer, P. Jöckel, L. Oman, M. Deushi, D. E. Kinnison, R. Garcia, O. Morgenstern, G. Zeng, K. A. Stone, and R. Schofield. The influence of mixing on the stratospheric age of air changes in the

21st century. *Atmospheric Chemistry and Physics*, 19(2):921–940, 2019. ISSN 1680-7324. doi: 10.5194/acp-19-921-2019. URL https://www.atmos-chem-phys.net/19/921/2019/. 188

A. Engel, T. Möbius, H. Bönisch, U. Schmidt, R. Heinz, I. Levin, E. Atlas, S. Aoki, T. Nakazawa, S. Sugawara, F. Moore, D. Hurst, J. Elkins, S. Schauffler, A. Andrews, and K. Boering. Age of stratospheric air unchanged within uncertainties over the past 30 years. *Nature Geoscience*, 2(1):28–31, 2009. ISSN 1752-0894. doi: 10.1038/ngeo388. URL http://www.nature.com/articles/ngeo388. 188

A. Engel, H. Bönisch, M. Ullrich, R. Sitals, O. Membrive, F. Danis, and C. Crevoisier. Mean age of stratospheric air derived from AirCore observations. *Atmospheric Chemistry and Physics*, 17(11):6825–6838, 2017. ISSN 1680-7324. doi: 10.5194/acp-17-6825-2017. URL https://www.atmos-chem-phys.net/17/6825/2017/. 188

V. Eyring, J.-F. Lamarque, I. Cionni, B. Duncan, A. Fiore, A. Gettel-Man, M. Hegglin, P. Hess, T. Nagashima, T. Ryerson, T. Shepherd, D. Shindell, D. Waugh, and P. Young. Report on the IGAC/SPARC Chemistry-Climate Model Initiative (CCMI) 2013 Science Workshop. Technical report, 2013. URL www.sparc-climate.org/publications/newsletter/. 190

V. I. Fomichev, A. I. Jonsson, J. de Grandpré, S. R. Beagley, C. McLandress, K. Semeniuk, and T. G. Shepherd. Response of the Middle Atmosphere to CO2 Doubling: Results from the Canadian Middle Atmosphere Model. *Journal of Climate*, 20(7):1121–1144, 2007. ISSN 0894-8755. doi: 10.1175/JCLI4030.1. URL http://journals.ametsoc.org/doi/10.1175/JCLI4030.1. 188

P. M. Forster, G. Bodeker, R. Schofield, S. Solomon, and D. Thompson. Effects of ozone cooling in the tropical lower stratosphere and upper troposphere. *Geophysical Research Letters*, 34(23):1–5, 2007. ISSN 00948276. doi: 10.1029/2007GL031994. 200

P. M. F. Forster and K. P. Shine. Radiative forcing and temperature trends from stratospheric ozone changes. *Journal of Geophysical Research: Atmospheres*, 102 (D9):10841–10855, 1997. ISSN 01480227. doi: 10.1029/96JD03510. URL http://doi.wiley.com/10.1029/96JD03510. 187

P. M. F. Forster and K. P. Shine. Stratospheric water vapour changes as a possible contributor to observed stratospheric cooling. *Geophysical Research Letters*, 26(21): 3309–3312, 1999. ISSN 00948276. doi: 10.1029/1999GL010487. URL http://doi.wiley.com/10.1029/1999GL010487. 187

L. Froidevaux, D. E. Kinnison, R. Wang, J. Anderson, and R. A. Fuller. Evaluation of CESM1 (WACCM) free-running and specified dynamics atmospheric composition simulations using global multispecies satellite data records. *Atmospheric Chemistry and Physics*, 19(7):4783–4821, 2019. ISSN 1680-7324. doi: 10.5194/acp-19-4783-2019. URL https://www.atmos-chem-phys.net/19/4783/2019/. 191

Q. Fu, S. Solomon, and P. Lin. On the seasonal dependence of tropical lower-stratospheric temperature trends. *Atmospheric Chemistry and Physics*, 10(6): 2643–2653, 2010. ISSN 16807324. doi: 10.5194/acp-10-2643-2010. URL www.atmos-chem-phys.net/10/2643/2010/. 189, 206

Q. Fu, P. Lin, S. Solomon, and D. L. Hartmann. Observational evidence of strengthening of the brewer-dobson circulation since 1980. *Journal of Geophysical Research*, 120 (19):10214–10228, 2015. ISSN 21562202. doi: 10.1002/2015JD023657. URL http://doi.wiley.com/10.1002/2015JD023657. 189, 206

Q. Fu, S. Solomon, H. Pahlavan, and P. Lin. Observed changes in Brewer-Dobson circulation for 1980-2018. *Environmental Research Letters*, 2019. ISSN 1748-9326. doi: 10.1088/1748-9326/ab4de7. 201, 206

S. Fueglistaler, A. E. Dessler, T. J. Dunkerton, I. Folkins, Q. Fu, and P. W. Mote. Tropical tropopause layer. *Reviews of Geophysics*, 47(1):RG1004, 2009. ISSN 87551209. doi: 10.1029/2008RG000267. URL http://doi.wiley.com/10.1029/2008RG000267. 187

S. Fueglistaler, P. H. Haynes, and P. M. Forster. The annual cycle in lower stratospheric temperatures revisited. *Atmospheric Chemistry and Physics*, 11(8):3701–3711, 2011. ISSN 16807316. doi: 10.5194/acp-11-3701-2011. 196

R. R. Garcia and W. J. Randel. Acceleration of the Brewer–Dobson Circulation due to Increases in Greenhouse Gases. *Journal of the Atmospheric Sciences*, 65(8):2731–

2739, 2008. ISSN 0022-4928. doi: 10.1175/2008JAS2712.1. URL http://journals.ametsoc.org/doi/10.1175/2008JAS2712.1. 188

R. R. Garcia, D. R. Marsh, D. E. Kinnison, B. A. Boville, and F. Sassi. Simulation of secular trends in the middle atmosphere, 1950–2003. *Journal of Geophysical Research*, 112(D9):D09301, 2007. ISSN 0148-0227. doi: 10.1029/2006JD007485. URL http://doi.wiley.com/10.1029/2006JD007485. 190

R. R. Garcia, W. J. Randel, and D. E. Kinnison. On the Determination of Age of Air Trends from Atmospheric Trace Species. *Journal of the Atmospheric Sciences*, 68(1):139–154, 2011. ISSN 0022-4928. doi: 10.1175/2010JAS3527.1. URL http://journals.ametsoc.org/doi/10.1175/2010JAS3527.1. 188

H. Garny, M. Dameris, W. Randel, G. E. Bodeker, and R. Deckert. Dynamically Forced Increase of Tropical Upwelling in the Lower Stratosphere. *Journal of the Atmospheric Sciences*, 68(6):1214–1233, 2011. ISSN 0022-4928. doi: 10.1175/2011JAS3701.1. URL http://journals.ametsoc.org/doi/10.1175/2011JAS3701.1. 188

H. Garny, T. Birner, H. Bönisch, and F. Bunzel. The effects of mixing on age of air. *Journal of Geophysical Research: Atmospheres*, 119(12):7015–7034, 2014. ISSN 2169897X. doi: 10.1002/2013JD021417. URL http://doi.wiley.com/10.1002/2013JD021417. 188

F. J. Haenel, G. P. Stiller, T. von Clarmann, B. Funke, E. Eckert, N. Glatthor, U. Grabowski, S. Kellmann, M. Kiefer, A. Linden, and T. Reddmann. Reassessment of MIPAS age of air trends and variability. *Atmospheric Chemistry and Physics*, 15 (22):13161–13176, 2015. ISSN 1680-7324. doi: 10.5194/acp-15-13161-2015. URL https://www.atmos-chem-phys.net/15/13161/2015/. 188

T. M. Hall and R. A. Plumb. Age as a diagnostic of stratospheric transport. *Journal of Geophysical Research: Atmospheres*, 99(D1):1059–1070, 1994. ISSN 0148-0227. doi: 10.1029/93JD03192. URL https://doi.org/10.1029/93JD03192. 188

S. C. Hardiman, N. Butchart, and N. Calvo. The morphology of the Brewer-Dobson circulation and its response to climate change in CMIP5 simulations. *Quarterly Journal of the Royal Meteorological Society*, 140(683):1958–1965, 2014. ISSN 00359009. doi: 10.1002/qj.2258. URL http://doi.wiley.com/10.1002/qj.2258. 188

S. C. Hardiman, P. Lin, A. A. Scaife, N. J. Dunstone, and H.-L. Ren. The influence of dynamical variability on the observed Brewer-Dobson circulation trend. *Geophysical Research Letters*, 44(6):2885–2892, 2017. ISSN 00948276. doi: 10.1002/2017GL072706. URL http://doi.wiley.com/10.1002/2017GL072706. 188, 201

C. M. Johanson and Q. Fu. Antarctic atmospheric temperature trend patterns from satellite observations. *Geophysical Research Letters*, 34(12):1–5, 2007. ISSN 00948276. doi: 10.1029/2006GL029108. 189

A. Karpechko and A. C. Maycock. Karpechko, A.Yu and Maycock A.C. (Lead Authors), M. Abalos, H. Akiyoshi, J.M. Arblaster, C.I. Garfinkel, K.H. Rosenlof and M. Sigmond , Stratospheric Ozone Changes and Climate, Chapter 5 in Scientific Assessment of Ozone Depletion: 2018, Global Ozone Rese. Technical report, 2018. 188

Y. Kawatani and K. Hamilton. Weakened stratospheric quasibiennial oscillation driven by increased tropical mean upwelling. *Nature*, 497(7450):478–481, 2013. ISSN 14764687. doi: 10.1038/nature12140. 206

H. Kida. General Circulation of Air Parcels and Transport Characteristics Derived from a hemispheric GCM- Part 1. A Determination of Advective Mass Flow in the Lower Stratosphere. *Journal of the Meteorological Society of Japan. Ser. II*, 61(2):171–187, 1983. ISSN 0026-1165. doi: 10.2151/jmsj1965.61.2_171. URL https://www.jstage.jst.go.jp/article/jmsj1965/61/2/61{_}2{_}171/{_}article. 188

J. F. Lamarque and S. Solomon. Impact of changes in climate and halocarbons on recent lower stratosphere ozone and temperature trends. *Journal of Climate*, 23(10): 2599–2611, 2010. ISSN 08948755. doi: 10.1175/2010JCLI3179.1. 189

F. Li, J. Austin, and J. Wilson. The Strength of the Brewer–Dobson Circulation in a Changing Climate: Coupled Chemistry–Climate Model Simulations. *Journal of Climate*, 21(1):40–57, 2008. ISSN 0894-8755. doi: 10.1175/2007JCLI1663.1. URL http://journals.ametsoc.org/doi/10.1175/2007JCLI1663.1. 188

P. Lin and Q. Fu. Changes in various branches of the Brewer-Dobson circulation from an ensemble of chemistry climate models. *Journal of Geophysical Research: Atmospheres*, 118(1):73–84, 2013. ISSN 2169897X. doi: 10.1029/2012JD018813. URL http://doi.wiley.com/10.1029/2012JD018813. 188

P. Lin, Q. Fu, S. Solomon, and J. M. Wallace. Temperature trend patterns in Southern Hemisphere high latitudes: Novel indicators of stratospheric change. *Journal of Climate*, 22(23):6325–6341, 2009. ISSN 08948755. doi: 10.1175/2009JCLI2971.1. 189

D. R. Marsh and R. R. Garcia. Attribution of decadal variability in lower-stratospheric tropical ozone. *Geophysical Research Letters*, 34(21):L21807, 2007. ISSN 0094-8276. doi: 10.1029/2007GL030935. URL http://doi.wiley.com/10.1029/2007GL030935. 196, 204

D. R. Marsh, M. J. Mills, D. E. Kinnison, J.-F. Lamarque, N. Calvo, and L. M. Polvani. Climate Change from 1850 to 2005 Simulated in CESM1(WACCM). *Journal of Climate*, 26(19):7372–7391, 2013. ISSN 0894-8755. doi: 10.1175/JCLI-D-12-00558.1. URL http://journals.ametsoc.org/doi/10.1175/JCLI-D-12-00558.1. 190

A. C. Maycock. The contribution of ozone to future stratospheric temperature trends. *Geophysical Research Letters*, 43(9):4609–4616, 2016. ISSN 00948276. doi: 10.1002/2016GL068511. URL http://doi.wiley.com/10.1002/2016GL068511. 200

A. C. Maycock, M. M. Joshi, K. P. Shine, and A. A. Scaife. The circulation response to idealized changes in stratospheric water vapor. *Journal of Climate*, 26(2):545–561, 2013. ISSN 08948755. doi: 10.1175/JCLI-D-12-00155.1. 187

A. C. Maycock, M. M. Joshi, K. P. Shine, S. M. Davis, and K. H. Rosenlof. The potential impact of changes in lower stratospheric water vapour on stratospheric temperatures over the past 30 years. *Quarterly Journal of the Royal Meteorological Society*, 140 (684):2176–2185, 2014. ISSN 1477870X. doi: 10.1002/qj.2287. 187

A. C. Maycock, W. J. Randel, A. K. Steiner, A. Y. Karpechko, J. Christy, R. Saunders, D. W. J. Thompson, C.-Z. Zou, A. Chrysanthou, N. Luke Abraham, H. Akiyoshi, A. T. Archibald, N. Butchart, M. Chipperfield, M. Dameris, M. Deushi, S. Dhomse, G. Di Genova, P. Jöckel, D. E. Kinnison, O. Kirner, F. Ladstädter, M. Michou, O. Morgenstern, F. O'Connor, L. Oman, G. Pitari, D. A. Plummer, L. E. Revell, E. Rozanov, A. Stenke, D. Visioni, Y. Yamashita, and G. Zeng. Revisiting the Mystery of Recent Stratospheric Temperature Trends. *Geophysical Research Letters*, 45(18):9919–9933, 2018. ISSN 00948276. doi: 10.1029/2018GL078035. URL http://doi.wiley.com/10.1029/2018GL078035. 187, 200

C. McLandress and T. G. Shepherd. Simulated Anthropogenic Changes in the Brewer–Dobson Circulation, Including Its Extension to High Latitudes. *Journal of Climate*, 22(6):1516–1540, 2009. ISSN 0894-8755. doi: 10.1175/2008JCLI2679.1. URL http://journals.ametsoc.org/doi/10.1175/2008JCLI2679.1. 188

S. Meul, U. Langematz, S. Oberländer, H. Garny, and P. Jöckel. Chemical contribution to future tropical ozone change in the lower stratosphere. *Atmospheric Chemistry and Physics*, 14(6):2959–2971, 2014. ISSN 16807324. doi: 10.5194/acp-14-2959-2014. 189

K. Minschwaner, H. Su, and J. H. Jiang. The upward branch of the Brewer-Dobson circulation quantified by tropical stratospheric water vapor and carbon monoxide measurements from the Aura Microwave Limb Sounder. *Journal of Geophysical Research: Atmospheres*, 121(6):2790–2804, 2016. ISSN 2169897X. doi: 10.1002/2015JD023961. URL http://doi.wiley.com/10.1002/2015JD023961. 206

O. Morgenstern, M. I. Hegglin, E. Rozanov, F. M. O'Connor, N. L. Abraham, H. Akiyoshi, A. T. Archibald, S. Bekki, N. Butchart, M. P. Chipperfield, M. Deushi, S. S. Dhomse, R. R. Garcia, S. C. Hardiman, L. W. Horowitz, P. Jöckel, B. Josse, D. Kinnison, M. Lin, E. Mancini, M. E. Manyin, M. Marchand, V. Maréchal, M. Michou, L. D. Oman, G. Pitari, D. A. Plummer, L. E. Revell, D. Saint-Martin, R. Schofield, A. Stenke, K. Stone, K. Sudo, T. Y. Tanaka, S. Tilmes, Y. Yamashita, K. Yoshida, and G. Zeng. Review of the global models used within phase 1 of the Chemistry–Climate Model Initiative (CCMI). *Geoscientific Model Development*, 10(2):639–671, 2017. ISSN 1991-9603. doi: 10.5194/gmd-10-639-2017. URL https://www.geosci-model-dev.net/10/639/2017/. 190

M. A. Olsen, M. R. Schoeberl, and J. E. Nielsen. Response of stratospheric circulation and stratosphere-troposphere exchange to changing sea surface temperatures. *Journal of Geophysical Research*, 112(D16):D16104, 2007. ISSN 0148-0227. doi: 10.1029/2006JD008012. URL http://doi.wiley.com/10.1029/2006JD008012. 188

L. Oman, D. W. Waugh, S. Pawson, R. S. Stolarski, and P. A. Newman. On the influence of anthropogenic forcings on changes in the stratospheric mean age. *Journal of Geophysical Research*, 114(D3):D03105, 2009. ISSN 0148-0227. doi: 10.1029/2008JD010378. URL http://doi.wiley.com/10.1029/2008JD010378. 188

L. D. Oman, A. R. Douglass, J. R. Ziemke, J. M. Rodriguez, D. W. Waugh, and J. E. Nielsen. The ozone response to ENSO in Aura satellite measurements and a chemistry-climate simulation. *Journal of Geophysical Research: Atmospheres*, 118 (2):965–976, 2013. ISSN 2169897X. doi: 10.1029/2012JD018546. URL http://doi.wiley.com/10.1029/2012JD018546. 189

A. Ossó, Y. Sola, K. Rosenlof, B. Hassler, J. Bech, and J. Lorente. How robust are trends in the Brewer-Dobson circulation derived from observed stratospheric temperatures? *Journal of Climate*, 28(8):3024–3040, 2015. ISSN 08948755. doi: 10.1175/JCLI-D-14-00295.1. 189, 191, 192, 193, 194, 201, 205

F. Ploeger, M. Abalos, T. Birner, P. Konopka, B. Legras, R. Müller, and M. Riese. Quantifying the effects of mixing and residual circulation on trends of stratospheric mean age of air. *Geophysical Research Letters*, 42(6):2047–2054, 2015a. ISSN 00948276. doi: 10.1002/2014GL062927. URL http://doi.wiley.com/10.1002/2014GL062927. 188

F. Ploeger, M. Riese, F. Haenel, P. Konopka, R. Müller, and G. Stiller. Variability of stratospheric mean age of air and of the local effects of residual circulation and eddy mixing. *Journal of Geophysical Research: Atmospheres*, 120(2):716–733, 2015b. ISSN 2169897X. doi: 10.1002/2014JD022468. URL http://doi.wiley.com/10.1002/2014JD022468. 188, 197

R. A. Plumb. Stratospheric Transport. *Journal of the Meteorological Society of Japan. Ser. II*, 80(4B):793–809, 2002. ISSN 0026-1165. doi: 10.2151/jmsj.80.793. URL https://www.jstage.jst.go.jp/article/jmsj/80/4B/80{_}4B{_}793/{_}article. 187, 188

L. Polvani, L. Wang, M. Abalos, N. Butchart, M. Chipperfield, M. Dameris, M. Deushi, S. Dhomse, P. Jöckel, D. Kinnison, M. Michou, O. Morgenstern, L. Oman, D. Plummer, and K. Stone. Large impacts, past and future, of ozone-depleting substances on Brewer-Dobson circulation trends: A multi-model assessment. *Journal of Geophysical Research: Atmospheres*, page 2018JD029516, 2019. ISSN 2169-897X. doi: 10.1029/2018JD029516. URL https://onlinelibrary.wiley.com/doi/abs/10.1029/2018JD029516. 188, 201

L. M. Polvani and S. Solomon. The signature of ozone depletion on tropical temperature trends, as revealed by their seasonal cycle in model integrations with single forcings. *Journal of Geophysical Research Atmospheres*, 117(17):1–8, 2012. ISSN 01480227. doi: 10.1029/2012JD017719. 200

L. M. Polvani, D. W. Waugh, G. J. Correa, and S. W. Son. Stratospheric ozone depletion: The main driver of twentieth-century atmospheric circulation changes in the Southern Hemisphere. *Journal of Climate*, 24(3):795–812, 2011. ISSN 08948755. doi: 10.1175/2010JCLI3772.1. 187

L. M. Polvani, L. Wang, V. Aquila, and D. W. Waugh. The impact of ozone-depleting substances on tropical upwelling, as revealed by the absence of lower-stratospheric cooling since the late 1990s. *Journal of Climate*, 30(7):2523–2534, 2017. ISSN 08948755. doi: 10.1175/JCLI-D-16-0532.1. URL http://journals.ametsoc.org/doi/10.1175/JCLI-D-16-0532.1. 188

L. M. Polvani, M. Abalos, R. Garcia, D. Kinnison, and W. J. Randel. Significant Weakening of Brewer-Dobson Circulation Trends Over the 21st Century as a Consequence of the Montreal Protocol. *Geophysical Research Letters*, 45(1):401–409, 2018. ISSN 00948276. doi: 10.1002/2017GL075345. URL http://doi.wiley.com/10.1002/2017GL075345. 188, 201

W. J. Randel, F. Wu, H. Vömel, G. E. Nedoluha, and P. Forster. Decreases in stratospheric water vapor after 2001: Links to changes in the tropical tropopause and the Brewer-Dobson circulation. *Journal of Geophysical Research Atmospheres*, 111(12): 1–11, 2006. ISSN 01480227. doi: 10.1029/2005JD006744. 189

W. J. Randel, M. Park, F. Wu, and N. Livesey. A large annual cycle in ozone above the tropical tropopause linked to the Brewer-Dobson circulation. *Journal of the Atmospheric Sciences*, 64(12):4479–4488, 2007. ISSN 00224928. doi: 10.1175/2007JAS2409.1. 189, 196, 205

N. A. Rayner, D. E. Parker, E. B. Horton, C. K. Folland, L. V. Alexander, D. P. Rowell, E. C. Kent, and A. Kaplan. Global analyses of sea surface temperature, sea ice, and night marine air temperature since the late nineteenth century. *Journal of Geophysical*

Research: Atmospheres, 108(14), 2003. ISSN 01480227. doi: 10.1029/2002jd002670. 190

D. Rind, R. Suozzo, N. K. Balachandran, and M. J. Prather. Climate Change and the Middle Atmosphere. Part I: The Doubled CO2 Climate. *Journal of the Atmospheric Sciences*, 47(4):475–494, 1990. ISSN 0022-4928. doi: 10.1175/1520-0469(1990)047<0475:CCATMA>2.0.CO;2. URL http://journals.ametsoc.org/doi/abs/10.1175/1520-0469{%}281990{%}29047{%}3C0475{%}3ACCATMA{%}3E2.0.CO{%}3B2. 188

D. Rind, D. Shindell, P. Lonergan, and N. K. Balachandran. Climate change and the middle atmosphere. Part III: the doubled CO2 climate revisited. *Journal of Climate*, 11(5):876–894, 1998. ISSN 08948755. doi: 10.1175/1520-0442(1998)011<0876:CCATMA>2.0.CO;2. 188

K. H. Rosenlof. Seasonal cycle of the residual mean meridional circulation in the stratosphere. *Journal of Geophysical Research*, 100(D3):5173, 1995. ISSN 0148-0227. doi: 10.1029/94JD03122. URL http://doi.wiley.com/10.1029/94JD03122. 194

K. H. Rosenlof and G. C. Reid. Trends in the temperature and water vapor content of the tropical lower stratosphere: Sea surface connection. *Journal of Geophysical Research Atmospheres*, 113(6):1–15, 2008. ISSN 01480227. doi: 10.1029/2007JD009109. 189

P. Šácha, R. Eichinger, H. Garny, P. Pišoft, S. Dietmüller, L. de la Torre, D. A. Plummer, P. Jöckel, O. Morgenstern, G. Zeng, N. Butchart, and J. A. Añel. Extratropical age of air trends and causative factors in climate projection simulations. *Atmospheric Chemistry and Physics*, 19(11):7627–7647, 2019. ISSN 1680-7324. doi: 10.5194/acp-19-7627-2019. URL https://www.atmos-chem-phys.net/19/7627/2019/. 188

T. G. Shepherd. Transport in the Middle Atmosphere. *Journal of the Meteorological Society of Japan. Ser. II*, 85B(0):165–191, 2007. ISSN 0026-1165. doi: 10.2151/jmsj.85b.165. URL https://www.jstage.jst.go.jp/article/jmsj/85B/0/85B{_}0{_}165/{_}article. 187

T. G. Shepherd and C. McLandress. A Robust Mechanism for Strengthening of the Brewer–Dobson Circulation in Response to Climate Change: Critical-Layer Control of Subtropical Wave Breaking. *Journal of the Atmospheric Sciences*, 68

(4):784–797, 2011. ISSN 0022-4928. doi: 10.1175/2010JAS3608.1. URL http://journals.ametsoc.org/doi/10.1175/2010JAS3608.1. 188

M. Sigmond, P. C. Siegmund, E. Manzini, and H. Kelder. A Simulation of the Separate Climate Effects of Middle-Atmospheric and Tropospheric CO 2 Doubling. *Journal of Climate*, 17(12):2352–2367, 2004. ISSN 0894-8755. doi: 10.1175/1520-0442(2004)017<2352:ASOTSC>2.0.CO;2. URL http://journals.ametsoc.org/doi/abs/10.1175/1520-0442{%}282004{%}29017{%}3C2352{%}3AASOTSC{%}3E2.0.CO{%}3B2. 188

SPARC. SPARC CCMVal Report on the Evaluation of Chemistry-Climate Models. V. Eyring, T. Shepherd and D. Waugh (Eds.). *SPARC Report No. 5, WCRP-30/2010, WMO/TD-No.40*, 2010. ISSN 1428-345X. URL http://www.sparc-climate.org/publications/sparc-reports/sparc-report-no5/. 188

G. P. Stiller, T. von Clarmann, F. Haenel, B. Funke, N. Glatthor, U. Grabowski, S. Kellmann, M. Kiefer, A. Linden, S. Lossow, and M. López-Puertas. Observed temporal evolution of global mean age of stratospheric air for the 2002 to 2010 period. *Atmospheric Chemistry and Physics*, 12(7):3311–3331, 2012. ISSN 1680-7324. doi: 10.5194/acp-12-3311-2012. URL https://www.atmos-chem-phys.net/12/3311/2012/. 188

D. W. Thompson and S. Solomon. Understanding recent stratospheric climate change. *Journal of Climate*, 22(8):1934–1943, 2009. ISSN 08948755. doi: 10.1175/2008JCLI2482.1. 189

R. Ueyama and J. M. Wallace. To What Extent Does High-Latitude Wave Forcing Drive Tropical Upwelling in the Brewer–Dobson Circulation? *Journal of the Atmospheric Sciences*, 67(4):1232–1246, 2010. ISSN 0022-4928. doi: 10.1175/2009JAS3216.1. URL http://journals.ametsoc.org/doi/10.1175/2009JAS3216.1. 189

M. Weber, S. Dikty, J. P. Burrows, H. Garny, M. Dameris, A. Kubin, J. Abalichin, and U. Langematz. The Brewer-Dobson circulation and total ozone from seasonal to decadal time scales. *Atmospheric Chemistry and Physics*, 11(21):11221–11235, 2011. ISSN 1680-7324. doi: 10.5194/acp-11-11221-2011. URL https://www.atmos-chem-phys.net/11/11221/2011/. 205

WMO. (World Meteorological Organization), Scientific Assessment of Ozone Depletion: 2018, Global Ozone Research and Monitoring Project – Report No. 58. Technical report, Geneva, Switzerland, 2018. 200

P. J. Young, D. W. Thompson, K. H. Rosenlof, S. Solomon, and J. F. Lamarque. The seasonal cycle and interannual variability in stratospheric temperatures and links to the Brewer-Dobson circulation: An analysis of MSU and SSU data. *Journal of Climate*, 24(23):6243–6258, 2011. ISSN 08948755. doi: 10.1175/JCLI-D-10-05028.1. 189

P. J. Young, K. H. Rosenlof, S. Solomon, S. C. Sherwood, Q. FU, and J. F. Lamarque. Changes in stratospheric temperatures and their implications for changes: In the brewer-dobson circulation, 1979-2005. *Journal of Climate*, 25(5):1759–1772, 2012. ISSN 08948755. doi: 10.1175/2011JCLI4048.1. URL http://journals.ametsoc.org/doi/abs/10.1175/2011JCLI4048.1. 189, 192, 193, 194, 201, 205, 206

E. Yulaeva, J. R. Holton, and J. M. Wallace. On the Cause of the Annual Cycle in Tropical Lower-Stratospheric Temperatures. *Journal of the Atmospheric Sciences*, 51(2):169–174, 1994. ISSN 0022-4928. doi: 10.1175/1520-0469(1994)051<0169:OTCOTA>2.0.CO;2. URL http://journals.ametsoc.org/doi/abs/10.1175/1520-0469{%}281994{%}29051{%}3C0169{%}3AOTCOTA{%}3E2.0.CO{%}3B2. 189

Chapter 5

Conclusions

The Brewer-Dobson circulation (BDC) forms a fundamental part of the global atmospheric circulation and plays important roles in controlling the distribution of trace gases in the stratosphere. While the processes that control the BDC are relatively well understood, there remain gaps in our knowledge of how these processes respond to an evolving climate state and whether global models are able to adequately reproduce them. This thesis has addressed several topics related to our understanding of the stratospheric residual circulation, the advective part of the BDC, and its representation in models under historical and future climates. In this chapter, I summarise the main findings of this thesis before detailing further work that could be conducted motivated by the results from this work.

5.1 Key findings

I first return to the aims of this thesis as set out in Section 1.6. These were set to:

1. Evaluate the representation of the stratospheric residual circulation in a suite of "specified dynamics or nudged" chemistry-climate simulations and assess their performance against free-running simulations and reanalysis datasets.

2. Design and perform climate model simulations to quantify the importance of radiative effects (rapid adjustment), global-average ocean warming and the local patterns of ocean warming for the BDC response to GHG-induced climate change, and assess the extent to which they can be linearly combined to explain the overall response.

3. Investigate the robustness and interchangeability of different observational-based BDC measures within a modelling framework, to determine which measures most closely reproduce the simulated residual circulation and its variability on different timescales.

The work presented in Chapter 2 addressed the first aim using a suite of "specified-dynamics" hindcast simulations recently performed by the World Climate Research Programme (WCRP)/Stratosphere-troposphere Processes And their Role in Climate (SPARC) Chemistry-Climate Model Initiative (CCMI) where models are relaxed towards reanalysis fields of horizontal winds and temperature (or vorticity and divergence). This work was published in Atmospheric Chemistry and Physics (Chrysanthou et al., 2019).

It was found that using nudged meteorology does not constrain the mean strength of the residual circulation. The climatological residual circulation was found to be different in terms of magnitude and structure from both equivalent free-running simulations from the same models and from that estimated in the reanalysis dataset used for nudging. Importantly, nudging leads to a discrepancy between the directly estimated mean circulation and that derived from the total wave forcing via the downward control principle (DCP; Haynes et al., 1991). The addition of a non-physical tendency in the model equations appears to decouple the residual circulation from the wave forcing in the nudged models, violating the steady-state balance between the mean flow and eddy motions (Haynes et al., 1991). The disagreement between the direct residual circulation and the momentum balance estimate was found not to be as strong in the middle stratosphere as in the lower stratosphere, possibly associated with differences in the effect of nudging in the shallow and deep branches of the circulation (Birner and Bönisch, 2011). I posit that the model-specific details of how the nudging is implemented, such as the relaxed variables, the altitude range and timescales that the nudging is applied, are likely to affect the details of this decoupling.

In contrast, nudging was found to tightly constrain the interannual variability of the tropical upward mass flux in the lower stratosphere, associated to the resolved and parameterised wave forcing contributions, despite the fact that the models use different

reanalysis datasets for nudging. The reason why nudging does not constrain the mean strength of the residual circulation while it does constrain the interannual variability in the lower stratosphere is unclear. A potential mismatch between the mean state of the model and the reanalysis driving a continuous spurious forcing via nudging (Miyazaki et al., 2005) could be the reason that nudging affects the mean adversely but tightly constrains the interannual variability; however, a detailed investigation of the nudging effects could not be performed in the context of a multi-model study and further investigation of this point is a topic for future study (see Section 5.2). Recent model-specific sensitivity studies of different specified dynamics schemes evaluated in Davis et al. (2020) have highlighted a promising avenue in tackling the reasons for discrepancies associated with how the nudging is implemented across different models (Orbe et al., 2020a).

Regarding long-term trends, most nudged simulations exhibit a statistically significant positive trend in the lower stratospheric tropical upward mass flux over $1980 - 2009$. However, in many cases this is distinct in amplitude and sign from the reanalysis dataset. Specifically, while the ERA-Interim reanalysis shows a negative residual circulation trend over this period (Abalos et al., 2015), most nudged simulations relaxed towards ERA-Interim show a positive trend. Remarkably, trends starting from the late 1990s up to 2009, are mostly positive in the nudged simulations, disagreeing with a slowdown of the BDC since the turn of the century seen across all reanalysis products associated with the decreasing role of ODSs in driving the stratospheric circulation also seen in models (Abalos et al., 2019; Polvani et al., 2019, 2018). Further investigation of the sensitivity of trends with respect to the time period considered revealed that statistically-significant lower stratospheric tropical upward mass flux trends need at least 12 years (in most cases around 20 years) to emerge in the nudged simulations broadly corroborating the findings of (Hardiman et al., 2017b). The results highlight important limitations of using nudged simulations to study long-term trends of stratospheric tracers.

In summary, the results of Chapter 2 show that nudging in chemistry-climate model simulations indeed affects the residual circulation in the stratosphere without necessarily improving it, similar to the concurrent findings of Orbe et al. (2018) for tropospheric large-scale transport. This showed that the simulated vertical winds are not similar to

the reanalysis and can be far from the free-running simulations. Nevertheless, nudging may be useful in cases where model biases need to be removed (Hardiman et al., 2017a) and/or the temperature-dependent chemistry is of interest (e.g. Froidevaux et al., 2019). Nudging towards anomalies rather than the full fields may improve the simulation of reanalysis trends and preserve the model's climatology (Davis et al., 2020). All things considered, at the present time I would urge caution in drawing quantitative comparisons of stratospheric tracers affected by the residual circulation in nudged simulations against observational data until the mechanistic details of the nudging effects are fully understood.

The second aim of this thesis was addressed in Chapter 3, which used the Hadley Centre Global Environmental Model 3 to quantify the distinct contributions from the radiative effects of CO_2, the global mean SST magnitude and the SST pattern to the projected long-term change in the residual circulation under a $4\times CO_2$ forcing experiment. This work was published in Weather and Climate Dynamics (Chrysanthou et al., 2020). The results show that under the $4\times CO_2$ perturbation, the annual mean mass flux in the tropical lower stratosphere increases by 45%. This arises mainly from the uniform SST warming ($\sim$ 70%) while the contribution from the rapid adjustment was found to be $\sim$ 20%, approximately double that attributed to the effect of the SST pattern. Conversely, in the upper stratosphere, where the deep branch of the BDC resides, the increase in mass transport of the BDC exhibits similar contributions from the uniform SST warming and the rapid adjustment. The importance of the spatially averaged near-surface warming is in agreement with the findings of Lin et al. (2015), while the magnitude of the effect of SST pattern is broadly consistent with the lower stratosphere changes on interannual timescales associated with ENSO (Calvo et al., 2010; Simpson et al., 2011) although the details of the SST pattern are rather different under climate change.

Mechanistically, the increased residual circulation in the lower stratosphere reflects a modulation of the location of the Rossby wave critical layers allowing for an enhanced penetration of Rossby wave activity into the subtropics due to a strengthening of the subtropical jets under increasing GHGs (e.g. Calvo and Garcia, 2009; Shepherd and McLandress, 2011; Hardiman et al., 2014); this feature is largely reproduced from the

uniform SST warming. Nevertheless, in the upper stratosphere the important role of the rapid adjustment associated with stratospheric cooling by CO_2, highlights a drawback in our mechanistic understanding of the controls on wave propagation to higher altitudes in the stratosphere and mesosphere. The radiative cooling in the stratosphere from CO_2 is relatively uniform (Fels et al., 1980) and cannot account for any substantial direct changes in the zonal flow through thermal wind balance. To explain the Eliassen-Palm flux divergence changes induced by the rapid adjustment component of the full $4\times CO_2$ response, I postulate that the reduced static stability associated with the temperature response to CO_2 alters the refractive index, thereby impacting on Rossby wave propagation. The above findings suggest that there are two characteristic timescales in the response of the BDC to increasing CO_2, with the relative importance of each timescale for the long-term response being height dependent. In the shallow branch of the circulation, the tropospheric and ocean warming reflected through changes in the subtropical jets mainly modulates the BDC response, while in the deep branch of the circulation, a slow response due to tropospheric warming acts in tandem with a fast timescale associated with the CO_2 radiative cooling.

Further experiments to investigate the impact of model uncertainty in the global mean SST response to CO_2, as a proxy for climate sensitivity, showed that in the lower stratosphere, the uncertainty in the contribution from uniform SST warming is larger than the absolute contribution from both the rapid adjustment and SST pattern. Conversely, in the upper stratosphere the model spread in the magnitude of global mean SST increase gives an uncertainty that is comparable to the magnitude of the rapid adjustment. In agreement with Hardiman et al. (2014), I derive an approximate relationship between the tropical upward mass flux in the lower stratosphere and on global surface air temperature of $\sim 9\%\ K^{-1}$. However, the estimate of Hardiman et al. (2014) implicitly includes the contributions of the rapid adjustment and SST pattern effects which Chapter 3 explicitly separates.

Neglecting ozone feedbacks is an important caveat of this study, as it was shown that the ozone response to a $4\times CO_2$ perturbation affects the zonal mean extratropical stratospheric circulation (Chiodo and Polvani, 2017). Furthermore, the CO_2 perturbation applied is very high compared to projected CO_2 concentrations during the 21^{st} century.

Smaller perturbations will mean the SST pattern effects will become relatively more important as compared to the rapid adjustment and global mean SST response.

The third and final aim of this thesis was addressed in Chapter 4, which is a manuscript in preparation for Atmospheric Science Letters. This addresses the fact that the residual circulation cannot be directly measured, and as a consequence various indirect observed measures have been used to quantify the circulation. This work focuses on comparing the measures within a self-consistent modelling framework using an ensemble of hindcast simulations with CESM1-WACCM, and evaluating the extent to which they capture the behaviour of the residual circulation in the tropical lower stratosphere on different timescales. The indirect measures used as proxies for the residual circulation may be impacted by unrelated processes and different studies have used different indirect measures making them hard to intercompare. The reference measure for this comparison is the modelled TEM tropical upwelling while the proxies include measures of the contrast in lower stratospheric temperatures between the tropics and extratropics as well as ozone concentrations in the tropical lower stratosphere.

It was found that in the mean seasonal cycle, the tropical O_3 at 50 hPa lagged by 2 months exhibits the strongest anti-correlation with tropical lower stratospheric upwelling. Conversely, the temperature-based measure did not closely reproduce the seasonal cycle in tropical upwelling, as it uses opposite hemispheres for the extratropics in different months. The temperature-based index and tropical mean O_3 at 50 hPa were found to be good proxies for the residual circulation in the lower stratosphere on interannual timescales ($|r| \sim 0.9$ for the ensemble mean). To a lesser degree, the same applied for the seasonal mean, where almost all correlations with the tropical upwelling are statistically significant.

By separating the full time period into two sub-periods, $1979-1997$ and $1998-2013$, characterised by increasing and decreasing concentrations of chlorine-based ODSs reflected on ozone decreases and increases, respectively, the relationship of trends in the proxy measures to that of tropical upwelling were analysed. The temperature-based index and the tropical mean 50 hPa O_3 exhibited statistically significant year-round correlations with tropical upwelling over the $1998-2013$ period ($r_{em} = 0.73$ and

$r_{em} = -0.82$), respectively), which were substantially higher than in the $1979 - 1997$ period. Nevertheless, for the tropical mean 50 hPa O_3 monthly trends, the role of transport associated chemical losses was not quantified, hence caution must be exercised. For the temperature-based index, the year-round correlation with the tropical upwelling indicates a sensitivity to the time period considered, when compared to the findings of Ossó et al. (2015).

Overall, the temperature-based index, originally defined in Young et al. (2012), exhibits encouraging features as a proxy measure of the residual circulation in the tropical lower stratosphere, particularly on interannual timescales. However, for multi-decadal timescales, its close relationship with the residual circulation in the lower stratosphere may be conditional on the time period, a factor that should be taken into consideration when using this measure to infer residual circulation trends based on observations. (e.g. Fu et al., 2010, 2015, 2019; Young et al., 2012; Ossó et al., 2015).

Synthesising the above results, the overarching aim of this PhD was achieved by producing high-quality research that has addressed model uncertainties and/or directly improved the modelling of the stratospheric residual circulation under both historical and future climates. In Chapter 2, I was able to demonstrate that the "specified-dynamics" simulations of a state-of-the-art suite of chemistry-climate models are not currently suited and well understood to be used in order to study the stratospheric composition. This type of simulation is not yet sufficiently optimised and introduces dynamical uncertainties in the model as reflected onto the residual circulation advection processes, bar its control in the interannual variability in the lower stratosphere. Until the errors introduced by this type of simulation onto the mean state are rectified, caution has to be exercised when interpreting stratospheric tracer distributions. Moreover, in Chapter 3, I was able to illustrate that a delineation of the components associated with the modelled response of the BDC to an abrupt-4×CO_2 perturbation, can be approximated to a large extent, without the need to use a coupled-ocean integration. A set of atmosphere-only sensitivity simulations including the separated atmospheric radiative, global ocean and local ocean responses respectively, can be used to approximate the centennial equilibrium full residual circulation response to a quadrupling of CO_2. Mechanistically, I demonstrated the existence of two characteristic timescales in the

residual circulation response acting on different altitudes and these timescales are associated with different components. In the lower stratosphere, the slow response forced by the tropospheric and global ocean warming-induced enhanced planetary wave activity, dominates. In the upper stratosphere, the response is characterised in equal measures by the former slow response and a much faster response associated with the direct atmospheric effects of increased CO_2. Last but not least, in Chapter 4 work, I examined the interchangeability between the modelled residual circulation and observational-based indirect proxy measures in the tropical lower stratosphere, across different timescales. Assuming that the model resolves all necessary processes, I was able to demonstrate the usefulness of a temperature observational-based proxy measure of the residual circulation on interannual timescales within a chemistry-climate model framework. Notably, modelled tropical mean ozone when lagged, captures a remarkably consistent percentage of the residual circulation variability features across multiple timescales, improving our understanding of model processes associated with advection. Overall, this work has progressed our understanding pertaining to mechanistic and diagnostic processes related to the stratospheric residual circulation in numerical simulations.

5.2 Future work

Based on the results of Chapter 2, there are a several unresolved issues relating to the application of nudging in climate models. An important open question is why does the nudging have different effects on the climatological mean circulation in contrast to the interannual variability. A potential way to investigate the mechanistic details of nudging for this question would be a similar approach to Smith et al. (2017) but for the stratosphere. This would entail nudging the model to its free-running version and assessing the error growth rate of the model dynamical fields across various timescales (hourly to multi-decadal) including its effects on diffusion, convection and gravity wave parameterisation schemes in order to pinpoint the timescales where nudging adverse effects emerge. On a technical note, how the choice of nudging parameters affects the simulated stratospheric circulation remains an open question, albeit now partly explored for a single model (Davis et al., 2020; without considering relaxation timescales). A potential way forward would be to study how a diabatic forcing perturbs the residual circulation by imposing tendencies in the thermodynamic equation. Calculation of the

thermodynamic balance estimate of the residual circulation through diabatic heating rates could provide insights of how this process ultimately affects the model dynamics. A further topic for investigation is the extent to which there may be a relationship between model biases and the effect of nudging on the residual circulation. Additionally, the matter of the larger residuals between the direct estimate of tropical upward mass fluxes and the total diagnosed wave forcing quantified using the DCP formulation (Haynes et al., 1991) in the nudged simulations could also be potentially explored. In order to tackle this issue, calculation of the momentum balance estimate of the residual circulation might be key in providing some answers. It is possible that the calculation of the residual circulation based on the thermodynamic and momentum balance for the nudged simulations might result in a whole different behaviour compared to the direct TEM framework used in Chapter 2.

In terms of the response of the residual circulation to climate change, future work could probe the mechanism of how the rapid adjustment affects the residual circulation, which remains less well understood. I postulated that the stratospheric radiative cooling alters the refractive index ultimately affecting the propagation and breaking characteristics of Rossby waves in the stratosphere; however, a detailed investigation of this potential mechanism would be an interesting problem to tackle. Eichinger and Šácha (2020) have highlighted potential technical problems associated with an overestimation of the residual circulation acceleration in climate models due to a shrinking caused by the stratospheric cooling over time. This it turn, affects the transformation assumptions used by models to compute the necessary diagnostics, illustrating the importance of investigating this mechanism in detail. Quantification and attribution of type (transient/stationary and planetary/synoptic) of the resolved waves forcing the BDC under increasing GHGs via a wavenumber-frequency decomposition could also add to the results of Chapter 3. Additionally, investigating the transient behaviour of the BDC response and the characteristics of the different timescales of the responses in abrupt-4×CO_2 simulations with coupled ocean would be insightful. Another interesting research pathway would be to address the influence of ozone-climate feedbacks on the results. To reduce the cost of running climate simulations with interactive chemistry this could make use of novel data science approaches as shown in Nowack et al. (2018) in climate sensitivity simulations. Specifically, Nowack et al. (2018) demonstrated that by

applying a relatively simple temperature-based machine learning algorithm, the ozone distributions in pre-industrial or abrupt-4×CO_2 simulations could be predicted reliably. Hence, this computationally efficient method of including the missing ozone feedbacks on the projected acceleration of the BDC could be applied in a similar fashion in the modelling framework of Chapter 3 in order to evaluate the importance of stratospheric ozone variability compared to a fixed climatology.

Another potential research pathway forward could be partly motivated by the results of Chapter 4. Based on recent observational evidence, lower stratospheric ozone has been declining since 1998 (Ball et al., 2018), in contrary to the expectations of the atmospheric community as ozone exhibits a recovery in the upper stratosphere (e.g. Ball et al., 2017) as well as a total column ozone recovery over Antarctica (Solomon et al., 2016). However, it was shown that nudged chemistry-climate models were not successful in capturing the observed lower stratospheric ozone variations (Ball et al., 2018) attributing this discrepancy to large interannual variability. Conversely, Chipperfield et al. (2018) using a chemistry-transport model, were able to reproduce the observed ozone variability attributed to atmospheric dynamics in the region, corroborated by Wargan et al. (2018) using the the Modern-Era Retrospective Analysis for Research and Applications Version 2 (MERRA-2) reanalysis product. Even more recently, Orbe et al. (2020b) pinpointed the advective residual circulation as the primary driver of these ozone variations using a set of Goddard Earth Observing System (GEOS) general circulation model simulations with a slightly different nudging approach compared to Ball et al. (2018). Nonetheless, Orbe et al. (2020b) also demonstrated that the circulation changes associated with the lower stratospheric ozone variations in both their nudged simulation and MERRA-2 product were outside the range of the internal variability bounds estimated via an ensemble of free-running simulations with the same model. Future work could entail a comprehensive model investigation into the mechanisms associated with the role of the advective residual circulation on the recent lower stratospheric ozone variations as well as any potential reasons for the discrepancies between observations, free-running/nudged models and reanalysis products.

Future work could also take advantage of a relatively new and powerful tool in climate

modelling used to sample more completely the range of internal climate variability, consisting of a large number of ensemble members with identical forcings initiated from slightly different initial conditions. These 'large ensemble' experiments represent climate variations in the model due to random internal variability. They have been used to separate the externally forced response from internal variability, provided that the model can capture the relevant physical processes, hence quantifying the possibility of what could happen in the real world, as in a single realisation (e.g. Deser et al., 2012; Seviour et al., 2017; Maher et al., 2019). Future work could entail investigating the projected strengthening of the BDC under increasing GHG scenarios in such a framework (e.g. Max Planck Institute Grand Ensemble; Maher et al., 2019) that would allow disentangling the forced residual circulation response from internal variability.

Gravity wave effects are very important for the middle atmosphere circulation and they have a substantial impact on the stratospheric tracer distribution (Eichinger et al., 2020); however, there remain large uncertainties in the representation of gravity wave fluxes in models. From a model development point of view, novel data science approaches (e.g. machine learning) could be applied to investigate and potentially improve atmospheric gravity wave sub-grid parameterisations (orographic and non-orographic) in climate models. Another research pathway could be put into the context of studying the implications, based on the quasi-geostrophic theory, related to the compensation between resolved planetary-scale and parameterised wave driving of the BDC in models, manifested both in the climatological mean and wave forcing changes under climate change (Cohen et al., 2013; Sigmond and Shepherd, 2014).

References

M. Abalos, B. Legras, F. Ploeger, and W. J. Randel. Evaluating the advective Brewer-Dobson circulation in three reanalyses for the period 1979–2012. *Journal of Geophysical Research: Atmospheres*, 120(15):7534–7554, 2015. ISSN 2169-897X. doi: 10.1002/2015JD023182. URL https://onlinelibrary.wiley.com/doi/abs/10.1002/2015JD023182. 225

M. Abalos, L. Polvani, N. Calvo, D. Kinnison, F. Ploeger, W. Randel, and S. Solomon. New Insights on the Impact of Ozone-Depleting Substances on the Brewer-Dobson

Circulation. *Journal of Geophysical Research: Atmospheres*, 124(5):2435–2451, 2019. ISSN 2169-897X. doi: 10.1029/2018JD029301. URL https://onlinelibrary.wiley.com/doi/abs/10.1029/2018JD029301. 225

W. T. Ball, J. Alsing, D. J. Mortlock, E. V. Rozanov, F. Tummon, and J. D. Haigh. Reconciling differences in stratospheric ozone composites. *Atmospheric Chemistry and Physics*, 17(20):12269–12302, 2017. ISSN 16807324. doi: 10.5194/acp-17-12269-2017. 232

W. T. Ball, J. Alsing, D. J. Mortlock, J. Staehelin, J. D. Haigh, T. Peter, F. Tummon, R. Stübi, A. Stenke, J. Anderson, A. Bourassa, S. M. Davis, D. Degenstein, S. Frith, L. Froidevaux, C. Roth, V. Sofieva, R. Wang, J. Wild, P. Yu, J. R. Ziemke, and E. V. Rozanov. Evidence for a continuous decline in lower stratospheric ozone offsetting ozone layer recovery. *Atmospheric Chemistry and Physics*, 18(2):1379–1394, 2018. ISSN 1680-7324. doi: 10.5194/acp-18-1379-2018. URL https://www.atmos-chem-phys.net/18/1379/2018/. 232

T. Birner and H. Bönisch. Residual circulation trajectories and transit times into the extratropical lowermost stratosphere. *Atmospheric Chemistry and Physics*, 11(2): 817–827, 2011. ISSN 1680-7324. doi: 10.5194/acp-11-817-2011. URL https://www.atmos-chem-phys.net/11/817/2011/. 224

N. Calvo and R. R. Garcia. Wave Forcing of the Tropical Upwelling in the Lower Stratosphere under Increasing Concentrations of Greenhouse Gases. *Journal of the Atmospheric Sciences*, 66(10):3184–3196, 2009. ISSN 0022-4928. doi: 10.1175/2009jas3085.1. URL http://journals.ametsoc.org/doi/abs/10.1175/2009JAS3085.1. 226

N. Calvo, R. R. Garcia, W. J. Randel, and D. R. Marsh. Dynamical Mechanism for the Increase in Tropical Upwelling in the Lowermost Tropical Stratosphere during Warm ENSO Events. *Journal of the Atmospheric Sciences*, 67(7):2331–2340, 2010. ISSN 0022-4928. doi: 10.1175/2010JAS3433.1. URL http://journals.ametsoc.org/doi/10.1175/2010JAS3433.1. 226

G. Chiodo and L. M. Polvani. Reduced Southern Hemispheric circulation response to quadrupled CO 2 due to stratospheric ozone feedback. *Geophysical Research Letters*,

44(1):465–474, 2017. ISSN 00948276. doi: 10.1002/2016GL071011. URL http://doi.wiley.com/10.1002/2016GL071011. 227

M. P. Chipperfield, S. Dhomse, R. Hossaini, W. Feng, M. L. Santee, M. Weber, J. P. Burrows, J. D. Wild, D. Loyola, and M. Coldewey-Egbers. On the Cause of Recent Variations in Lower Stratospheric Ozone. *Geophysical Research Letters*, 45(11):5718–5726, 2018. ISSN 00948276. doi: 10.1029/2018GL078071. URL http://doi.wiley.com/10.1029/2018GL078071. 232

A. Chrysanthou, A. C. Maycock, M. P. Chipperfield, S. Dhomse, H. Garny, D. Kinnison, H. Akiyoshi, M. Deushi, R. R. Garcia, P. Jöckel, O. Kirner, G. Pitari, D. A. Plummer, L. Revell, E. Rozanov, A. Stenke, T. Y. Tanaka, D. Visioni, and Y. Yamashita. The effect of atmospheric nudging on the stratospheric residual circulation in chemistry–climate models. *Atmospheric Chemistry and Physics*, 19 (17):11559–11586, 2019. ISSN 1680-7324. doi: 10.5194/acp-19-11559-2019. URL https://www.atmos-chem-phys.net/19/11559/2019/. 224

A. Chrysanthou, A. C. Maycock, and M. P. Chipperfield. Decomposing the response of the stratospheric Brewer-Dobson circulation to an abrupt quadrupling in CO2. *Weather and Climate Dynamics*, 1(1):155–174, 2020. ISSN 2698-4016. doi: 10.5194/wcd-1-155-2020. URL http://www.weather-clim-dynam.net/1/155/2020/. 226

N. Y. Cohen, E. P. Gerber, and O. Bühler. Compensation between Resolved and Unresolved Wave Driving in the Stratosphere: Implications for Downward Control. *Journal of the Atmospheric Sciences*, 70(12):3780–3798, 2013. ISSN 0022-4928. doi: 10.1175/JAS-D-12-0346.1. URL http://journals.ametsoc.org/doi/10.1175/JAS-D-12-0346.1. 233

N. A. Davis, S. M. Davis, R. W. Portmann, E. Ray, K. H. Rosenlof, and P. Yu. A comprehensive assessment of tropical stratospheric upwelling in the specified dynamics Community Earth System Model 1.2.2 - Whole Atmosphere Community Climate Model (CESM (WACCM)). *Geoscientific Model Development*, 13(2):717–734, 2020. ISSN 19919603. doi: 10.5194/gmd-13-717-2020. 225, 226, 230

C. Deser, R. Knutti, S. Solomon, and A. S. Phillips. Communication of the role of natural variability in future North American climate. *Nature Climate Change*, 2(11): 775–779, 2012. ISSN 1758678X. doi: 10.1038/nclimate1562. 233

R. Eichinger and P. Šácha. Overestimated acceleration of the advective Brewer-Dobson circulation due to stratospheric cooling . *Quarterly Journal of the Royal Meteorological Society*, (July):1–15, 2020. ISSN 0035-9009. doi: 10.1002/qj.3876. 231

R. Eichinger, H. Garny, P. Šácha, J. Danker, S. Dietmüller, and S. Oberländer-Hayn. Effects of missing gravity waves on stratospheric dynamics; part 1: climatology. *Climate Dynamics*, 54(5-6):3165–3183, 2020. ISSN 14320894. doi: 10.1007/s00382-020-05166-w. URL https://doi.org/10.1007/s00382-020-05166-w. 233

S. B. Fels, J. D. Mahlman, M. D. Schwarzkopf, and R. W. Sinclair. Stratospheric Sensitivity to Perturbations in Ozone and Carbon Dioxide: Radiative and Dynamical Response. *Journal of the Atmospheric Sciences*, 37(10): 2265–2297, 1980. ISSN 0022-4928. doi: 10.1175/1520-0469(1980)037<2265:SSTPIO>2.0.CO;2. URL http://journals.ametsoc.org/doi/abs/10.1175/1520-0469{%}281980{%}29037{%}3C2265{%}3ASSTPIO{%}3E2.0.CO{%}3B2. 227

L. Froidevaux, D. E. Kinnison, R. Wang, J. Anderson, and R. A. Fuller. Evaluation of CESM1 (WACCM) free-running and specified dynamics atmospheric composition simulations using global multispecies satellite data records. *Atmospheric Chemistry and Physics*, 19(7):4783–4821, 2019. ISSN 1680-7324. doi: 10.5194/acp-19-4783-2019. URL https://www.atmos-chem-phys.net/19/4783/2019/. 226

Q. Fu, S. Solomon, and P. Lin. On the seasonal dependence of tropical lower-stratospheric temperature trends. *Atmospheric Chemistry and Physics*, 10(6): 2643–2653, 2010. ISSN 16807324. doi: 10.5194/acp-10-2643-2010. URL www.atmos-chem-phys.net/10/2643/2010/. 229

Q. Fu, P. Lin, S. Solomon, and D. L. Hartmann. Observational evidence of strengthening of the brewer-dobson circulation since 1980. *Journal of Geophysical Research*, 120 (19):10214–10228, 2015. ISSN 21562202. doi: 10.1002/2015JD023657. URL http://doi.wiley.com/10.1002/2015JD023657. 229

Q. Fu, S. Solomon, H. Pahlavan, and P. Lin. Observed changes in Brewer-Dobson circulation for 1980-2018. *Environmental Research Letters*, 2019. ISSN 1748-9326. doi: 10.1088/1748-9326/ab4de7. 229

S. C. Hardiman, N. Butchart, and N. Calvo. The morphology of the Brewer-Dobson circulation and its response to climate change in CMIP5 simulations. *Quarterly Journal of the Royal Meteorological Society*, 140(683):1958–1965, 2014. ISSN 00359009. doi: 10.1002/qj.2258. URL http://doi.wiley.com/10.1002/qj.2258. 226, 227

S. C. Hardiman, N. Butchart, F. M. O'Connor, and S. T. Rumbold. The Met Office HadGEM3-ES chemistry-climate model: evaluation of stratospheric dynamics and its impact on ozone. *Geoscientific Model Development*, 10(3):1209–1232, 2017a. ISSN 1991-9603. doi: 10.5194/gmd-10-1209-2017. URL https://www.geosci-model-dev.net/10/1209/2017/. 226

S. C. Hardiman, P. Lin, A. A. Scaife, N. J. Dunstone, and H.-L. Ren. The influence of dynamical variability on the observed Brewer-Dobson circulation trend. *Geophysical Research Letters*, 44(6):2885–2892, 2017b. ISSN 00948276. doi: 10.1002/2017GL072706. URL http://doi.wiley.com/10.1002/2017GL072706. 225

P. H. Haynes, M. E. McIntyre, T. G. Shepherd, C. J. Marks, and K. P. Shine. On the "Downward Control" of Extratropical Diabatic Circulations by Eddy-Induced Mean Zonal Forces. *Journal of the Atmospheric Sciences*, 48 (4):651–678, 1991. ISSN 0022-4928. doi: 10.1175/1520-0469(1991)048<0651:OTCOED>2.0.CO;2. URL http://journals.ametsoc.org/doi/abs/10.1175/1520-0469{%}281991{%}29048{%}3C0651{%}3AOTCOED{%}3E2.0.CO{%}3B2. 224, 231

P. Lin, Y. Ming, and V. Ramaswamy. Tropical climate change control of the lower stratospheric circulation. *Geophysical Research Letters*, 42(3):941–948, 2015. ISSN 00948276. doi: 10.1002/2014GL062823. URL http://doi.wiley.com/10.1002/2014GL062823. 226

N. Maher, S. Milinski, L. Suarez-Gutierrez, M. Botzet, M. Dobrynin, L. Kornblueh, J. Kröger, Y. Takano, R. Ghosh, C. Hedemann, C. Li, H. Li, E. Manzini, D. Notz, D. Putrasahan, L. Boysen, M. Claussen, T. Ilyina, D. Olonscheck, T. Raddatz, B. Stevens, and J. Marotzke. The Max Planck Institute Grand Ensemble: Enabling

the Exploration of Climate System Variability. *Journal of Advances in Modeling Earth Systems*, 2019. ISSN 19422466. doi: 10.1029/2019MS001639. 233

K. Miyazaki, T. Iwasaki, K. Shibata, M. Deushi, and T. T. Sekiyama. The Impact of Changing Meteorological Variables to Be Assimilated into GCM on Ozone Simulation with MRI CTM. *Journal of the Meteorological Society of Japan*, 83(5):909–918, 2005. ISSN 0026-1165. doi: 10.2151/jmsj.83.909. URL http://joi.jlc.jst.go.jp/JST.JSTAGE/jmsj/83.909?from=CrossRef. 225

P. J. Nowack, N. L. Abraham, P. Braesicke, and J. A. Pyle. The Impact of Stratospheric Ozone Feedbacks on Climate Sensitivity Estimates. *Journal of Geophysical Research: Atmospheres*, 123(9):4630–4641, 2018. ISSN 21698996. doi: 10.1002/2017JD027943. 231

C. Orbe, H. Yang, D. W. Waugh, G. Zeng, O. Morgenstern, D. E. Kinnison, J.-F. Lamarque, S. Tilmes, D. A. Plummer, J. F. Scinocca, B. Josse, V. Marecal, P. Jöckel, L. D. Oman, S. E. Strahan, M. Deushi, T. Y. Tanaka, K. Yoshida, H. Akiyoshi, Y. Yamashita, A. Stenke, L. Revell, T. Sukhodolov, E. Rozanov, G. Pitari, D. Visioni, K. A. Stone, R. Schofield, and A. Banerjee. Large-scale tropospheric transport in the Chemistry–Climate Model Initiative (CCMI) simulations. *Atmospheric Chemistry and Physics*, 18(10):7217–7235, 2018. ISSN 1680-7324. doi: 10.5194/acp-18-7217-2018. URL https://www.atmos-chem-phys.net/18/7217/2018/. 225

C. Orbe, D. A. Plummer, D. W. Waugh, H. Yang, P. Jöckel, D. E. Kinnison, B. Josse, V. Marecal, M. Deushi, N. L. Abraham, A. T. Archibald, M. P. Chipperfield, S. Dhomse, W. Feng, and S. Bekki. Description and Evaluation of the specified-dynamics experiment in the Chemistry-Climate Model Initiative. *Atmospheric Chemistry and Physics*, 20(6):3809–3840, 2020a. ISSN 1680-7324. doi: 10.5194/acp-20-3809-2020. URL https://acp.copernicus.org/articles/20/3809/2020/. 225

C. Orbe, K. Wargan, S. Pawson, and L. D. Oman. Mechanisms Linked to Recent Ozone Decreases in the Northern Hemisphere Lower Stratosphere. *Journal of Geophysical Research: Atmospheres*, 125(9):1–23, 2020b. ISSN 21698996. doi: 10.1029/2019JD031631. 232

A. Ossó, Y. Sola, K. Rosenlof, B. Hassler, J. Bech, and J. Lorente. How robust are trends in the Brewer-Dobson circulation derived from observed stratospheric temperatures? *Journal of Climate*, 28(8):3024–3040, 2015. ISSN 08948755. doi: 10.1175/JCLI-D-14-00295.1. 229

L. Polvani, L. Wang, M. Abalos, N. Butchart, M. Chipperfield, M. Dameris, M. Deushi, S. Dhomse, P. Jöckel, D. Kinnison, M. Michou, O. Morgenstern, L. Oman, D. Plummer, and K. Stone. Large impacts, past and future, of ozone-depleting substances on Brewer-Dobson circulation trends: A multi-model assessment. *Journal of Geophysical Research: Atmospheres*, page 2018JD029516, 2019. ISSN 2169-897X. doi: 10.1029/2018JD029516. URL https://onlinelibrary.wiley.com/doi/abs/10.1029/2018JD029516. 225

L. M. Polvani, M. Abalos, R. Garcia, D. Kinnison, and W. J. Randel. Significant Weakening of Brewer-Dobson Circulation Trends Over the 21st Century as a Consequence of the Montreal Protocol. *Geophysical Research Letters*, 45(1):401–409, 2018. ISSN 00948276. doi: 10.1002/2017GL075345. URL http://doi.wiley.com/10.1002/2017GL075345. 225

W. J. Seviour, D. W. Waugh, L. M. Polvani, G. J. Correa, and C. I. Garfinkel. Robustness of the simulated tropospheric response to ozone depletion. *Journal of Climate*, 30(7):2577–2585, 2017. ISSN 08948755. doi: 10.1175/JCLI-D-16-0817.1. URL http://journals.ametsoc.org/doi/10.1175/JCLI-D-16-0817.1. 233

T. G. Shepherd and C. McLandress. A Robust Mechanism for Strengthening of the Brewer–Dobson Circulation in Response to Climate Change: Critical-Layer Control of Subtropical Wave Breaking. *Journal of the Atmospheric Sciences*, 68 (4):784–797, 2011. ISSN 0022-4928. doi: 10.1175/2010JAS3608.1. URL http://journals.ametsoc.org/doi/10.1175/2010JAS3608.1. 226

M. Sigmond and T. G. Shepherd. Compensation between Resolved Wave Driving and Parameterized Orographic Gravity Wave Driving of the Brewer–Dobson Circulation and Its Response to Climate Change. *Journal of Climate*, 27(14):5601–5610, 2014. ISSN 0894-8755. doi: 10.1175/JCLI-D-13-00644.1. URL http://journals.ametsoc.org/doi/10.1175/JCLI-D-13-00644.1. 233

I. R. Simpson, T. G. Shepherd, and M. Sigmond. Dynamics of the Lower Stratospheric Circulation Response to ENSO. *Journal of the Atmospheric Sciences*, 68(11):2537–2556, 2011. ISSN 0022-4928. doi: 10.1175/JAS-D-11-05.1. URL http://journals.ametsoc.org/doi/10.1175/JAS-D-11-05.1. 226

A. K. Smith, N. M. Pedatella, D. R. Marsh, and T. Matsuo. On the Dynamical Control of the Mesosphere–Lower Thermosphere by the Lower and Middle Atmosphere. *Journal of the Atmospheric Sciences*, 74(3):933–947, 2017. ISSN 0022-4928. doi: 10.1175/JAS-D-16-0226.1. URL http://journals.ametsoc.org/doi/10.1175/JAS-D-16-0226.1. 230

S. Solomon, D. J. Ivy, D. Kinnison, M. J. Mills, R. R. N. Iii, and A. Schmidt. Antarctic ozone layer. *Science*, 353(6296):269–274, 2016. 232

K. Wargan, C. Orbe, S. Pawson, J. R. Ziemke, L. D. Oman, M. A. Olsen, L. Coy, and K. Emma Knowland. Recent Decline in Extratropical Lower Stratospheric Ozone Attributed to Circulation Changes. *Geophysical Research Letters*, 45(10):5166–5176, 2018. ISSN 19448007. doi: 10.1029/2018GL077406. 232

P. J. Young, K. H. Rosenlof, S. Solomon, S. C. Sherwood, Q. FU, and J. F. Lamarque. Changes in stratospheric temperatures and their implications for changes: In the brewer-dobson circulation, 1979-2005. *Journal of Climate*, 25(5):1759–1772, 2012. ISSN 08948755. doi: 10.1175/2011JCLI4048.1. URL http://journals.ametsoc.org/doi/abs/10.1175/2011JCLI4048.1. 229